Rotational Spectra of Weakly Bound H_2S complexes and 'Hydrogen Bond Radius'

A Thesis

Submitted for the Degree of

Doctor of Philosophy

in the Faculty of Science

by

Pankaj Kanti Mandal

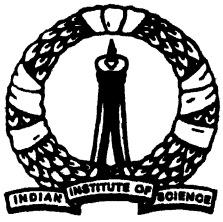

Department of Inorganic and Physical Chemistry

INDIAN INSTITUTE OF SCIENCE

Bangalore - 560 012, India

April, 2005

Dedicated to.....

My Dear Parents

DECLARATION

I hereby declare that the work presented in this thesis entitled "**Rotational Spectra of Weakly Bound H_2S Complexes and Hydrogen Bond Radius**" has been carried out by me at the Department of Inorganic and Physical Chemistry, Indian Institute of Science, Bangalore, India under the supervision of Professor E Arunan

Pankaj Kanti Mandal

Date 25.07.2005

PANKAJ KANTI MANDAL

CERTIFICATE

I hereby certify that the work presented in this thesis entitled "**Rotational Spectra of Weakly Bound H_2S Complexes and Hydrogen Bond Radius**" has been carried out by Mr Pankaj Kanti Mandal at the Department of Inorganic and Physical Chemistry, Indian Institute of Science, Bangalore, India under my supervision

Date 25-7-2005

Professor E. Arunan

(Research Supervisor)

Acknowledgements

I would like to express my profound gratitude towards my research supervisor ***Prof. E. Arunan*** *whose pleasant disposition, invaluable guidance and incessant encouragement enabled me be what I am today It was under his tutelage that I found my feet in scientific research He has been involved actively in every aspect of my work I thank him for giving unforgettable moral support in trying circumstances I have learnt a lot from him, not only in science, but also in life*

I thank Prof P C Mathias of SIF, IISc, for his involvement, guidance and help since the initial stage of the project of building the spectrometer

I thank all my past and present lab mates for their help, cooperation and friendly attitude that made our lab a pleasant ambience to work together I specially thank Tiwari and Biju who contributed most in building the spectrometer, and taught me every detail of the hardware and software Premendar, Utpal, Saket and Dharmendar contributed a lot in modifying the software code to run the spectrometer I specially thank Dharmendar who took care of everything, literally, in the lab during his stay of about four years I thank Sasisankar, Sagarika, Naba, Mausumi and Raghavendra for their cooperation and help in experiments I thank Dr Raja Kumar, Anand, Janardan and Aiswarya for their help and cooperation in the lab I thank all the project students who worked in our lab for short periods Special thanks are due for Ankit who contributed significantly in modifying the codes for running the experiment and fitting the data I specially thank Shivi, who started developing the software code during her MCA project in our lab, for her great friendship, nice behaviour and melodious songs

I thank the Chairmen (present and past) of the Department of Inorganic and Physical chemistry, for providing me the facilities to carry out my research I am grateful to all the faculty, student and staff members of this Department for their helpful and cordial attitude

I thank Prof Sridhar Gadre of University of Pune, for sharing their data and very useful discussions I thank Prof Frank J Lovas of NIST, USA, for sharing their experimental data for $(H_2S)_2$ and H_2O-H_2S

I sincerely thank Prof P K Das for his constant encouragement and very valuable constructive suggestions till today

I thank Prof K L Sebastian, Prof S Umapathy and all other members of the Chemical Dynamics group for their valuable talks and seminars I have learnt a lot of science from the group meetings on every Saturday

I was fortunate to be with Dr Priyodarshi, Dr Dulal and Arpita for many lively moments that I shared with them, during my stay here I thank Suhrit for his encouragement and valuable suggestions at tough times

It is a pleasure to acknowledge all my batch mates, Arindam, Brojo, Girish, Nusrat, Pathik, Prasad, Ritu, Suresh (Late) and Velan, for making IISc a memorable place with their great friendship I thank all my friends for the joyful and fun full time, moments those I've shared with them in this institute Special thanks are due for Praveen and Bani

It is my pleasure to acknowledge my friends, Prodip, Jyotishka, Subholakshmi I still remember the joyful days in Jadavpur University with them Some people come in our life for whom reminiscence becomes a pleasure even after you say good-bye to them Naba, Arindam, Dharu, Udayan are few of those rare findings in my life I owe my deep gratitude to them for encouraging me at difficult situations and bringing out the best in me

I thank Tanmoy & Bappa from the depth of my heart for their company. I cannot forget the affection shown by Tanmoy especially during crucial stages

The attention and care of my family members throughout my academic pursuits, deserves a special mention Without their moral support and encouragement I would not have reached this position I am grateful to my parents for their constant encouragement I specially thank my brother Piyush, sister Swastika, Masi & family whose wishes are always with me I thank my dear wife, Tripti, for constant encouragement and support since I met her

I would like to thank Muktidi , Dadababu, Mam and Anshumanda for being so close and so nice to me

I thank Amresh (Ohio state University) and Dr Sunoj for their company and providing accommodation in Columbus, Ohio

I am grateful to the Supercomputer Education and Research Center (SERC) for the excellent computing facilities accessible any time

I gratefully acknowledge CSIR, DST, INSA and IISc for the financial support for attending the Molecular Spectroscopy symposium in Ohio State University

Finally, I thank the authorities of Indian Institute of Science, for the financial support and access to the Institute facilities for my pleasant stay in the campus

Pankaj Kanti Mandal

Synopsis

The work reported in this Thesis comprises of 1) fabrication of Balle-Flygare microwave spectrometer, 2) rotational spectroscopic and *ab initio* studies of several weakly bound H_2S complexes and 3) definition and determination of 'Hydrogen bond radii' for different H-bond donors A Pulsed Nozzle FT Microwave spectrometer, having a spectral range of 2 0-26.5 GHz, has been fabricated in our laboratory for the studies of weakly bound complexes This spectrometer is not commercially available. The spectrometer consists of a Fabry-Perot cavity, pumping systems for the evacuation of the cavity, and microwave electronics for the polarization of the molecules and detection of the signal The molecules of interest mixed with a carrier gas are expanded supersonically into the cavity to form weakly bound complexes. The microwave circuit is used to detect the transition between rotational energy levels of complexes The typical line width of the spectrum observed in this spectrometer is ~2 8 kHz The spectrometer is sensitive enough to see the ^{18}OCS (natural abundance is 0 2%) signal after averaging only 10 gas pulses This spectrometer is being used routinely to study the rotational spectra of different weakly bound complexes A systematic study on several H_2S complexes has been started in our laboratory, as the experimental data for H_2S complexes are scarce In this work, specifically Ar_2-H_2S and Ar-$(H_2S)_2$ complexes have been investigated Preliminary results on Ar-H_2O-H_2S along with the *ab initio* results of this trimer and the corresponding dimer H_2O-H_2S are also presented

To the best of our knowledge Ar-H_2S is the only complex to show anomalous isotope effect of rotational constant. Ar_3-H_2S shows a normal isotope effect What should be the isotope effect in case of Ar_2-H_2S? To address this question along with some other questions, the rotational spectrum and structure of Ar_2-H_2S complex and its HDS and D_2S isotopomers have been studied The equilibrium structure has heavy-atom C_{2v} symmetry with the two Ar atoms indistinguishable and H_2S freely rotating as evinced by the fact that asymmetric top energy levels with K_p = *odd* levels are missing The rotational constants for the parent isotopomer are: A = 1733 098(1) MHz, B =

1617 6570(5) MHz and C = 830 2755(3) MHz Unlike the Ar-H_2S complex, the Ar_2-H_2S does not show an anomalous isotopic shift in rotational constants on deuterium substitution The Ar-Ar and Ar-c m H_2S distances are determined to be 3 820 Å and 4 105 Å, respectively The A rotational constants for Ar_2-H_2S/HDS/D_2S isotopomers are very close to each other and to the B constant of free Ar_2, indicating that H_2S does not contribute to the moment of inertia about a axis *Ab initio* calculations at MP2 level with aug-cc-pVQZ basis set lead to a C_{2v} minimum structure with the Ar-Ar line perpendicular to the H-H line and the S away from Ar_2 Single point CCSD(T)/aug-cc-pVTZ calculations give a binding energy of 174 cm^{-1} after correcting for both basis set superposition error and zero point energy Potential energy scans point out that the barrier for internal rotation of H_2S about its b axis is only 10 cm^{-1} and it is below the zero point energy (13 5 cm^{-1}) in this torsional degree of freedom Internal rotation of H_2S about its a and c axes also have small barriers of about 50 cm^{-1} only, suggesting that H_2S is extremely floppy within the complex

The second system, studied, is Ar-$(H_2S)_2$ complex Several 'a' and 'b' dipole rotational transitions have been observed for Ar-$(H_2S)_2$ and Ar-$(D_2S)_2$ complexes Only two sets of transitions have been observed The splitting in (A+B)/2 is ~12 3 MHz for the parent isotopomer and only ~45 kHz for Ar-$(D_2S)_2$ However, the difference in B between the two states for $(H_2S)_2$ and $(D_2S)_2$ are 1 2 MHz and 0 887 MHz, respectively For Ar-$(H_2S)_2$, the rotational constants for the lower and upper states are A=1810 410(6) MHz; 1826 18(2) MHz, B = 1596 199(9) MHz, 1605 94(6) MHz and C = 848 814(2) MHz, 847.11(1) MHz. Assuming H_2S to be a sphere, the c m separation between two H_2S units comes out to be 4.05 Å, ~0 07 Å less than that in $(H_2S)_2$ dimer The distance between Ar and c m of $(H_2S)_2$ is 3 55 Å and the Ar-c m (H_2S) distance is 4 09 Å *Ab initio* calculations at MP2 level using different basis sets result in three different minima including a pseudo-linear local minimum At MP2/6-311++G(3df,2p) level of theory, the global mimimum has a structure having Ar along the 'b' axis of $(H_2S)_2$ Previous experiments show a similar two state pattern of the rotational spectrum for $(H_2S)_2$ During the course of this study, two new sets of weaker transitions have been observed

for H_2S-$H_2{}^{34}S$, one for donor $H_2{}^{34}S$ and the other one for acceptor $H_2{}^{34}S$ Some new series of transitions have been observed for the deuteriated isotopomers as well.

H_2O-H_2S is a very important system in the context of hydrogen bonding However it has not been studied extensively H_2O is a good proton donor and a good acceptor as well On the other hand H_2S is neither an efficient proton donor nor an acceptor Which one will be the global minimum of H_2O-H_2S complex, H_2O-HSH or H_2S-HOH? The most recent theoretical calculation determines H_2S-HOH to be more stable, though the energy difference is very less. Zero point vibrational energy was not taken into account in this work *Ab initio* calculations have been done at several levels of theory for H_2S-H_2O dimer and Ar-H_2S-H_2O trimer It has been seen that the zero point energy can play an important role in determining the relative stability of different minima Some rotational transitions for Ar-H_2S-H_2O have been observed Each transition is split into 3/4 lines

Today accurate experimental structural data for many Hydrogen-bonded complexes are available from various advanced spectroscopic methods Experimental hydrogen bond distances, the distance from the bonding atom/center in B (H-bond acceptor) to bonded hydrogen for different B---HX complexes (gas phase) were compiled and analyzed This analysis shows that in hydrogen bonded complexes, hydrogen atom does occupy some space and it is characteristic of the hydrogen-bond donor In the past, B---X distances were analyzed and interpreted, neglecting the hydrogen atom In our analysis, an effective radius of hydrogen in the hydrogen-bonded complexes has been determined and it is defined as "hydrogen bond radius (r_H)" The sum of r_H of a donor (HX) and the radius of a H-bond acceptor (B), r_{ESP}, results in the hydrogen bond distance The r_{ESP} for hydrogen bond acceptor B is taken from the theoretical results of Gadre and Bhadane This is the distance from the bonding center in B to the minimum in the molecular electrostatic potential The r_H values determined for HF, HCl, HBr, HCN, C_2H_2 and H_2O are 0 51±0 09 Å, 0.70±0 10 Å, 0 77±0 13 Å, 0 89±0 12 Å, 1 07±0 08 Å and 0 75±0 09Å respectively The r_H decreases monotonically with the dipole moment of H-X bond, and with the electronegativity difference between H and X In biological system, hydrogen bonds involving C-H and S-H are very important HCCH is treated as

the model system for C-H---B H-bonding, and H_2S is taken as the model system for S-H--B H-bonding However, not much experimental data for H_2S complexes are available to determine its H-bond radius Hence, *ab initio* calculations have been carried out at MP2/6-311++G** level of theory for several H_2S complexes From these theoretical structural data, hydrogen bond radius of H_2S has been determined to be 1 02±0 10 Å Theoretical results at similar levels of calculations have given hydrogen bond radii for HF,HCl and H_2O,in reasonable agreement with the empirical results given above

The Thesis proceeds as follows Chapter I gives a brief introduction about the intermolecular interactions and various experimental techniques used for probing intermolecular interactions As rotational spectroscopy has been studied for weakly bound complexes using pulsed nozzle FT microwave spectrometer in this work, rotational spectroscopy and the technique are introduced as well Chapter II describes the experimental and theoretical methods, used in this work, in detail Experimental and theoretical studies on Ar_2-H_2S and Ar-$(H_2S)_2$ complexes are presented in Chapter III and Chapter IV respectively The *ab initio* studies on H_2O-H_2S and Ar-H_2O-H_2S complexes are discussed in Chapter V Chapter VI deals with the hydrogen bond radius

Contents

Synopsis vi

List of Acronyms xiv

Chapter I **Introduction**

I 1 Intermolecular Interactions van der Waals vs Hydrogen bonding 3

I 2 Different Experimental Methods for Studying van der Waals Complexes 4

I 3 Pulsed Nozzle Fourier Transform Microwave (PNFTMW) Spectrometer 5

I 4 Rotational Spectroscopy 6

I 4.a Linear Molecule 7

I 4 b Symmetric Top Molecule 8

I 4 c Asymmetric Top Molecule 9

I 4 d Nuclear Hyperfine Structure 11

I 5 Present Investigations 12

I 5 a Structure and Dynamics of Ar_2-H_2S 12

I 5 b Rotational Spectra and Structure of Ar-$(H_2S)_2$ 13

I 5 c *Ab Initio* Studies of H_2O-H_2S and Ar-H_2O-H_2S 13

I 5 d. Hydrogen Bond Radius 14

References 15

Chapter II **Experimental and Theoretical Methods**

II 1. Introduction 21

II 2 Design of the Spectrometer 21

II 2 a Mechanical Design 22

II 2 b Electrical design 24

II 3 Performing the Experiment 28

II 4 Operation and Control The Software 31

II 4 a Design of the Program 31
II 4 b Execution of the program 32
II 5 Sample Preparation 34
II 6 Performance of the spectrometer 36
II 7 *Ab Initio* and DFT Calculation 41
References 44

Chapter III **Structure and Dynamics of Ar_2-H_2S complex: Rotational Spectroscopic and ab initio Studies**

III 1 Introduction 49
III 2 Experimental Details 51
III 3 Results And Discussions 51
III 3 a Search and Assignment 51
III 3 b Structure 56
III 3 c *Ab Initio* Calculations 59
III 3 c 1 Structure at MP2/6-311++G** level 60
III 3 c 2 Stabilization Energies at MP2 and CCSD(T) Levels With 6-311++G** Basis Set 63
III 3 c 3 Results With Higher Basis Sets 65
III 3 c 3 a Geometry 65
III 3 c 3 b Interaction energy and barrier energies for internal rotation 66
III 3 c 3 c Vibrational frequencies and centrifugal distortion constants 68
III 4 Conclusions 72
References 79

Chapter IV **Rotational Spectra and Structure of Ar-$(H_2S)_2$ Complex**

IV 1 Introduction 85
IV 2 Background $(H_2S)_2$ Dimer 86

IV 3 Experimental Details 88
IV 4 Experimental Results 89
IV 4 a Search and Assignment of Ar-$(H_2S)_2$ and Ar-$(D_2S)_2$ Spectra 89
IV 4 b Structure 95
IV 5 *Ab Initio* Calculation 97
IV 5 a Geometry optimization 97
IV 5 b Structure 98
IV 5 c Interaction energy 101
IV 5 d Vibrational Frequency 103
IV 6 Discussion 104
IV 7 Conclusions 108
References 124

Chapter V ***Ab Initio* Studies of H_2S-H_2O and Ar-H_2S-H_2O Complexes**
V 1 Introduction 129
V 2 Method of Calculation 130
V 3 H_2O H_2S Dimer 130
V 3 a Optimized Structures 130
V 3 b Interaction Energy and Vibrational Frequency 132
V 4. Ar-H_2O-H_2S Trimer 134
V 4 a Structure 137
V 4 b Interaction Energy and Vibrational Frequency 138
V 5 Preliminary experimental results of Ar-H_2S-H_2O complex 141
V 6 Conclusions 143
References 150

Chapter VI **Hydrogen Bond Radius**
VI 1 Introduction 155
VI 2 Buckingham and Fowler Model 156
VI 3 Gadre and Bhadane Model 157

VI 4 Extension of Gadre and Bhadane Approach 158
VI 4 a r(Z H) vs r(E) 160
VI 4 b [r(Z H) – r(E)] vs r(E) and "Hydrogen Bond Radius" 162
VI 5 "H-bond radius" of H_2S *ab initio* analysis 165
VI 5 a Method of calculation 166
VI 5 b r(Z H) and r(H) 167
VI 6 How does r(H) depend on different properties of the H-bond donor (HX)? 170
VI 7 Distance Criterion for H-bonding 173
VI 8 Conclusions 174
References 211

Chapter VII **Conclusions and Future Directions**
VII 1 Conclusions 219
VII 2 Future Directions 221

List of Acronyms

BSSE	Basis set superposition error
c m	Center of mass
Ch	Channel
CP	Counterpoise
CVI	C for virtual instruments
DFT	Density Functional Theory
ESP	Electrostatic potential
Expt	Experimental
FID	Free induction decay
FP	Fabry Perrot
Freq	Frequency
FT	Fourier Transform
FWHM	Full width at half maximum
GPIB	General purpose interface bus
H-bond	Hydrogen bond
HF	Hartree-Fock
IF	Intermediate frequency
IPS	Intermilecular potential surface
IR	Infra-red
IRM	Image rejection mixer
MESP	Molecular electrostatic potential
MO	Master oscillator
MW	Microwave
NI	National Instruments
OD	Outer diameter
PES	Potential energy surface

PNFTMW	Pulsed nozzle Fourier transform microwave
Res	Residue
RF	Radio frequency
RG	Rare gas/Reagent gas
rms	Root mean square
SCCM	Standard cubic centimeter per minute
SD	Standard Deviation
SLM	Standard litre per minute
SMA	Subminiature (version) A
SPDT	Single pole double through
SSBM	Single side band mixer
TEM	Transverse electromagnetic
UV	Ultraviolet
ZPE	Zero point energy (vibrational)

Chapter I

Introduction

I.1. Intermolecular Interactions: van der Waals vs Hydrogen bonding

The nature of intramolecular interactions is fairly well understood today [1] However, our understanding about the intermolecular interactions is still evolving[2] In the last few decades, there have been a lot of investigations of these relatively weak interactions between molecules [3-6] Intermolecular interaction includes the interaction between any two or more species, which can be atoms, neutral molecules, ions or radicals, without the formation of a chemical bond The energy associated may seem very insignificant compared to the chemical energy, but this weak interaction plays a very significant role in nature Solids and liquids form because of this interaction Most of the biological activities depend on such interactions Probably 'life' would have been very different, rather 'impossible' without intermolecular interactions Hence, it is very important to understand the intermolecular interactions to solve a wide range of problems in Physics, Chemistry and Biology

The interaction energy associated with intermolecular interactions range from a fraction of a kcal/mol to tens of kcal/mol, whereas typical chemical bond energy is in the range of 50-100 kcal/mol Intermolecular interactions have usually been classified as van der Waals and Hydrogen bonding interaction.[7-10] Recently some other interactions have also been discussed, such as Lithium bond,[11-14] improper hydrogen bond[15-18] and halogen bond [19-21] Are all these interactions fundamentally different?

To address this question we need to go to the details of the intermolecular interaction [22,23] Classically the interaction is purely electrostatic, interaction between the electric charges, permanent moments and induced moments of different molecules However, classical physics is not able to explain the nature of attractive forces between neutral molecules without any permanent electric moment, such as the attractive forces between rare gas atoms at large distance According to quantum mechanics there can be an attractive force between molecules having no permanent moments This is known as dispersion or London force, which arises due to the instantaneous quantum mechanical fluctuation of the electron density of the molecule This fluctuation momentarily creates electric moments in molecules and in turn that can induce a moment in the neighboring

molecules Correlation between the instantaneous moments of molecules leads to an attractive force between them

According to Morokuma, the intermolecular interactions can be decomposed to the contributions from electrostatic, induction, dispersion and exchange correlation [24] Electrostatic is the strongest among them and is directional, whereas the dispersion is weak and non-directional In case of stronger intermolecular interactions such as hydrogen bond or halogen bond, electrostatic contributes most However, dispersion is the most dominant part in case of weak van der Waals complexes, e g complex between rare gas atoms Indeed the physical forces of all the intermolecular interactions appear to be same! In hydrogen bond the hydrogen atom is involved and the interaction is through hydrogen In halogen bond it is the halogen atom Considering van der Waals equation, one could argue that all intermolecular interactions are van der Waals However, van der Waals forces are often equated to dispersion in practice For a thorough understanding of intermolecular interactions, it is important to generate reliable experimental data on a large number of systems exhibiting these interactions Often the pair wise potential contributes significantly towards many-body potential Investigation on isolated weakly bound dimers gives an opportunity to develop two-body potential Third body effects need to be included for quantitative agreement between theory and experiment Studies on trimers and tetramers, would help in developing accurate many-body potentials

I.2. Different Experimental Methods for Studying van der Waals Complexes

There are several spectroscopic techniques existing for the study of weakly bound complexes The spectroscopic methods vary in a wide range, and depend on which part of the potential energy surface one is looking at Most of the techniques use the molecular beam method to produce the van der Waals complex of interest

Mass spectroscopy[25] is used to study the structure and reactivity of hydrogen bonded clusters Pure rotational spectroscopy of van der Waals complexes is studied using Molecular Beam Electric Resonance (MBER)[26] spectrometer as well as Pulsed

Nozzle Fourier Transform Microwave (PNFTMW)[27,28] spectrometer Development of far Infrared (THz) lasers opened up a new and important field of study of clusters The intermolecular vibrations are probed by Vibrational Rotational Tunneling (VRT)[29,30] spectroscopy High resolution IR spectroscopy[31-33] of weakly bound clusters reveals the high vibrational region of the PES Time resolved study[34] of infrared photodissociation of weakly bound clusters produce information about the vibrational energy flow High resolution UV spectroscopy[35] of van der Waals clusters is also a powerful tool to study the structure and dynamics Other methods used to study the dynamics of weakly bound complexes include Zero Electron Kinetic Energy (ZEKE)[36] spectroscopy and Resonance Enhanced Multi Photon Ionization (REMPI) [37] Rare gas matrix have also been used to isolate and capture van der Waals complex for spectroscopic studies [38] Nonlinear Raman spectroscopic studies are also done for clusters formed in molecular beam [39] Recently weakly bound clusters are studied in superfluid Helium nano-droplets [40-42] In this work, a pulsed nozzle Fourier transform microwave spectrometer has been used and it is discussed in more detail next

I.3. Pulsed Nozzle Fourier Transform Microwave (PNFTMW) Spectrometer

Microwave spectroscopy with static cell was limited for the gaseous or liquid and solid molecules with a finite vapor pressure However, the development of the pulsed nozzle Fourier transform microwave spectrometer by Balle and Flygare[27] revolutionized the field of microwave spectroscopy, as the spectrometer offers very high resolution and sensitivity simultaneously This technique is the combination of the microwave spectroscopic technique and the supersonic expansion technique [43,44] The gas molecules (back pressure ~1 atm), mixed with a carrier gas, are expanded into a Fabry-Perrot (FP) cavity kept in vacuum (10^{-6} torr) through a supersonic nozzle The supersonic expansion cools the molecules internally and leads to the complex formation Complex can be formed between any two species, which are co-expanded Thus the rotational spectroscopy of the complexes (weakly bound) can be studied Due to internal cooling

only the ground vibrational level and the lower rotational levels are significantly populated, resulting in less congestion in the rotational spectrum

A microwave pulse polarizes the expanded gas molecules inside the FP cavity The polarized molecules then emit radiation, the frequency of which is related to the energy difference between two rotational levels of the molecule This emitted radiation is detected using double super-heterodyne detection technique and digitized for further processing The digitized signal is in time domain and subsequent Fourier transformation gives the frequency domain signal The whole operation consists of a sequence of events and all the events are pulsed

We have fabricated a PNFTMW spectrometer in our laboratory for the rotational spectroscopic studies of the weakly bound complexes The details about the spectrometer and the experimental procedure are discussed in chapter II

I.4. Rotational Spectroscopy

Rotational spectroscopy or microwave spectroscopy[45,46] is basically the measurement of the frequency difference between two rotational energy levels of the molecule of interest Rotational spectrum can be seen only for those species, which have permanent dipole moment The rotational energy levels depend on the moments of inertia (inverse of the rotational constants) of the molecule and hence on the mass distribution From microwave spectra of a molecule the rotational constants are determined, after fitting the observed rotational transitions to a suitable molecular rotational Hamiltonian (distortable rotor) The rotational constants, in turn, give the detailed structural information (bond length, bond angle, etc) of the molecule The distortion constants are also determined from the fit and these contain information about the force field of the molecule about different inertial axes Stark effect measurement directly determines the dipole moment of the molecule

The selection rules and pattern of the rotational spectrum depend on the symmetry of the molecule According to symmetry the molecules are categorized as linear, symmetric top, asymmetric top and spherical top The pure rotational Hamiltonian

depends on the angular momentum operator of the overall rotation and moments of inertia

$$\hat{H} = \frac{L_a^2}{2I_a} + \frac{L_b^2}{2I_b} + \frac{L_c^2}{2I_c}$$

where a, b and c are molecule fixed principal inertial axes, $\boldsymbol{L_a}$, $\boldsymbol{L_b}$ and $\boldsymbol{L_c}$ are the angular momentum about a, b and c respectively, I_a, I_b and I_c are the moments of inertia about a, b and c respectively For any molecule, $\boldsymbol{L}^2$ ($= \boldsymbol{L_a}^2+\boldsymbol{L_b}^2+\boldsymbol{L_c}^2$) and $\boldsymbol{L_Z}$ commute with $\hat{\boldsymbol{H}}$, where $\boldsymbol{L_Z}$ is the angular momentum about a space fixed axis Z. If ψ_{JM} is the common Eigen function of $\boldsymbol{L}^2$ and $\boldsymbol{L_Z}$, it can be written,

$$\boldsymbol{L}^2 \psi_{JM} = J(J+1)\hbar^2 \psi_{JM} \qquad J = 0, 1, 2, 3,$$

$$\boldsymbol{L_Z} \psi_{JM} = M \hbar \psi_{JM} \qquad M = J, J-1, J-2, \quad , -J$$

where, J is the total angular momentum quantum number, and M is the projection of $\boldsymbol{J}$ on the space fixed Z-axis All the J rotational levels are 2J+1 fold degenerate in absence of any external field due to M quantization This degeneracy can be removed by applying an external field

I.4.a. Linear Molecule

The linear molecule has no moment of inertia about the molecular axis and the moments about the two perpendicular axes are identical, i e $I_a = 0$ and $I_b = I_c$ According to the rigid rotor approximation the rotational energy expression is

$$E_J = h[2BJ(J+1)]$$

Rotational constant, $B = h/8\pi^2 I_B$, h is Plank's constant

The selection rule for linear molecule is· $\Delta J = 0, \pm 1$ The energy difference between Jth and $(J+1)^{th}$ level is

$$\Delta E_{J \rightarrow J+1} = h[2B(J+1)]$$

Real molecules are not rigid rotors As the molecules rotate, they will be distorted because of the centrifugal force Taking this centrifugal distortion into account, the energy difference becomes

$$\Delta E_{J \rightarrow J+1} = h\{2B(J+1) - 4D_J(J+1)^3 + H_J(J+1)^3[(J+2)^3 - J^3]\}$$

D_J and H_J are the first and second order centrifugal distortion constants, respectively If the centrifugal distortions are small, we should observe rotational lines at about 2B separation

I.4.b. Symmetric Top Molecule

For a symmetric top, any two of the principal moments of inertia are equal This is due to the symmetry of the system If a molecule contains a rotational symmetry axis of order three or more, it is a symmetric top molecule Symmetric tops can be of two types i) prolate symmetric top, $I_a < I_b = I_c$, and ii) oblate symmetric top, $I_a = I_b < I_c$ For prolate top '*a*' is the symmetry axis whereas for oblate top '*c*' is the symmetry axis The *a*/*c* axis is called the unique axis for prolate/oblate symmetric top In case of a symmetric top $\boldsymbol{L_a}/\boldsymbol{L_c}$ also commutes with the rotational Hamiltonian The projection of the total angular momentum on the symmetry axis or unique axis is also quantized If ψ_{JKM} is the common eigen function of $\boldsymbol{L}^2$, $\boldsymbol{L_{a/c}}$ and $\boldsymbol{L_Z}$, it can be written,

$$\boldsymbol{L}^2 \psi_{JKM} = J(J+1)\hbar^2 \psi_{JKM} \qquad J = 0, 1, 2, 3,$$

$$\boldsymbol{L_{a/c}} \psi_{JKM} = K\hbar \psi_{JKM} \qquad K = 0, \pm1, \pm2, \quad , \pm J$$

$$\boldsymbol{L_Z} \psi_{JKM} = M\hbar \psi_{JKM} \qquad M = J, J-1, J-2, \quad , -J$$

The energy expression for a prolate symmetric top is

$$E_{J,K} = h[BJ(J+1) + (A-B)K^2]$$

After addition of the first order centrifugal distortion terms,

$$E_{J,K} = h[BJ(J+1) + (A-B)K^2 - D_J J^2(J+1)^2 - D_{JK} J(J+1)K^2 + D_K K^4]$$

For oblate top (A-B) of the second term of the above equation becomes (C-B) Every J,K rotational levels, except K = 0, are 2(2J+1) fold degenerate when there is no external field The K degeneracy cannot be split by applying any external field The selection rules for rotational transition for a symmetric top are

$$\Delta J = 0, \pm1 \qquad \Delta K = 0$$

Including the second order centrifugal distortion terms, the frequency for the rotational transition J→J+1, K→K is given by the following equation

$$\nu = 2B(J+1) - 4D_J (J+1)^3 - 2D_{JK} (J+1)K^2 + H_J (J+1)^3[(J+2)^3 - J^3] + 4H_{JK} (J+1)^3 K^2 + 2H_{KJ} (J+1) K^4$$

A typical symmetric top spectrum appears like the one shown in Figure I 1 The K lines for the same J will be separated because of the distortion terms This separation is very small compared to that between two different J The transition frequency depends only on one rotational constant, B Hence for a symmetric top the spectral fittings give only one rotational constant

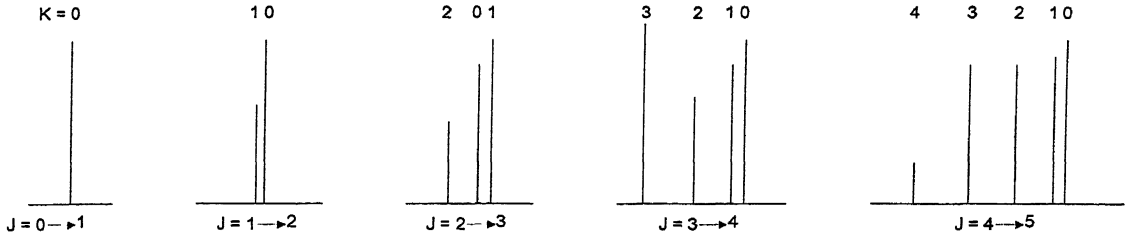

Figure I.1. Symmetric top spectrum. K lines are separated due to distortion

I.4.c. Asymmetric top molecule

For an asymmetric top, all three principal moments of inertia are different ($I_a \neq I_b \neq I_c$) When $I_b \rightarrow I_c$, the prolate symmetric top is approached, and when $I_b \rightarrow I_a$, the oblate symmetric top is approached The behaviour of an asymmetric rotor can be described in terms of the asymmetry parameter, defined as

$$\kappa = \frac{2B - A - C}{A - C}$$

The limiting values for κ, -1 and +1, correspond to the prolate and oblate symmetric tops, respectively The most asymmetric top has $\kappa = 0$

None of $\boldsymbol{L}_a$, $\boldsymbol{L}_b$ or $\boldsymbol{L}_c$ commutes with the rotational Hamiltonian for an asymmetric top rotor Thus K is not a good quantum number for an asymmetric top, only J and M are good quantum numbers The energy levels of an asymmetric rotor are different from the limiting symmetric tops The K degeneracy of symmetric top is split due to asymmetry

and '+K' and '–K' levels are separated Thus an asymmetric rotor has (2J+1) sublevels for every J level The energy levels of the asymmetric top are correlated with that of the limiting prolate ($\kappa = -1$) and oblate ($\kappa = +1$) symmetric tops As K is not a good quantum number, the energy levels are designated using the pseudo-quantum numbers K_{-1} and K_{+1} as $J_{K-1\,K+1}$ (or J_τ; $\tau = K_{-1} - K_{+1}$) K_{-1} is the K value of correlated prolate top level, and K_{+1} is that of the correlated oblate top level The correlation diagram is shown in Figure I 2

Solving the Schrodinger equation for the asymmetric rotor is quite complicated compared to that of linear or symmetric top rotors. The asymmetric rotor wave function can be expressed as a linear combination of the limiting symmetric top wave functions

$$\Psi_{J\tau} = \Sigma\, c_{JKM}\, \Psi_{JKM}$$

where c_{JKM}'s are numerical constants The energies of the asymmetric rotor depend on the asymmetry parameter and can not be expressed as a simple expression

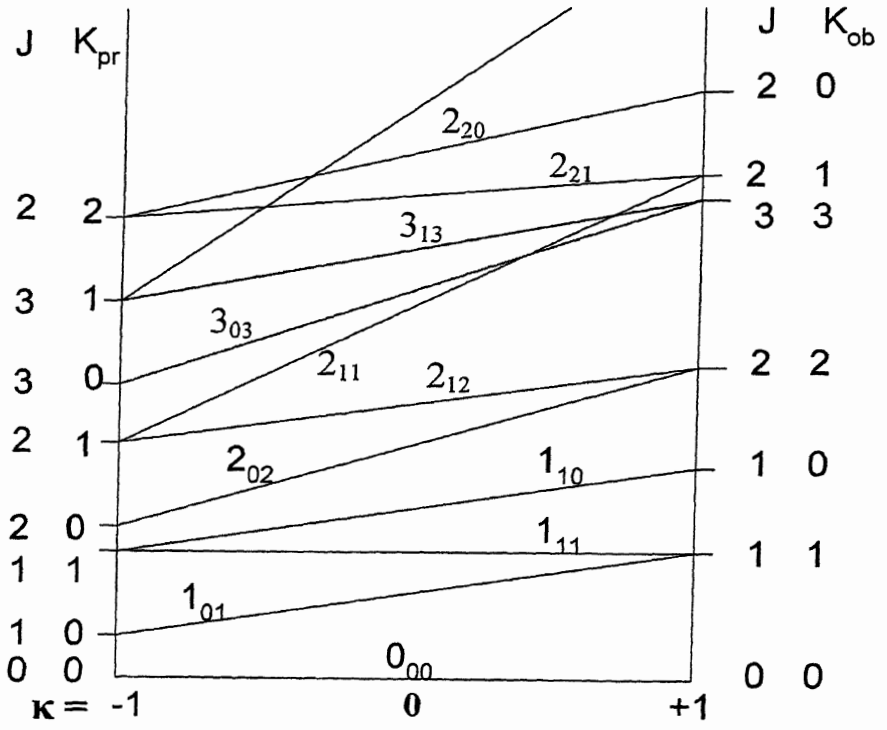

Figure I 2. Correlation of the asymmetric rotor energy levels to those of the limiting prolate and oblate symmetric top

An asymmetric top molecule can have non-vanishing dipole moment components along any of the principal axes The selection rules for rotational transitions depend on the component of dipole moment, which causes the transition Therefore, there can be i) *a*-dipole ($\mu_a \neq 0$), ii) *b*-dipole ($\mu_b \neq 0$) and iii) *c*-dipole ($\mu_c \neq 0$) transitions The selection rules are

$\Delta J = 0, \pm 1$

i) *a*-dipole $\Delta K_{-1} = 0, \pm 2, \pm 4,$ $\Delta K_{+1} = \pm 1, \pm 3,$

ii) *b*-dipole $\Delta K_{-1} = \pm 1, \pm 3,$ $\Delta K_{+1} = \pm 1, \pm 3,$

iii) *c*-dipole $\Delta K_{-1} = \pm 1, \pm 3,$ $\Delta K_{+1} = 0, \pm 2, \pm 4,$.

Thus, a highly asymmetric top spectrum is really complicated without any particular pattern

I.4.d. Nuclear Hyperfine Structure

If one or more number of nuclei in the molecule have nuclear spin, $I \geq 1$, nuclear hyperfine structure is observed in the rotational spectrum The overall spectrum becomes even more complicated However, this hyperfine structure gives useful information about the molecule

The nucleus having spin, $I \geq 1$, will have electric quadruple moment and this moment interacts with the molecular field gradient If either of these is absent, there will be no hyperfine structure in the spectrum The nuclear spin $\boldsymbol{I}$ is coupled to the molecular rotational angular momentum $\boldsymbol{J}$ to form a resultant $\boldsymbol{F}$ $\boldsymbol{F}$ is the total angular momentum, not $\boldsymbol{J}$ The rotational Hamiltonian commutes with $\boldsymbol{F}^2$, $\boldsymbol{J}^2$ and $\boldsymbol{F}_Z$ (projection of F along a space fixed axis) The good quantum numbers are F, M_F, J and I The new angular momentum quantum numbers are

$$F = (J + I), (J + I - 1), (J + I - 2), \quad , |J - I|$$

$$M_F = F, F - 1, F - 2, \quad , -F$$

The Eigen values of $\boldsymbol{F}^2$ and $\boldsymbol{F}_Z$ are

$$\boldsymbol{F}^2 \Psi_{F,MF} = F(F+1)\, \hbar^2 \Psi_{F,MF}$$

$$\boldsymbol{F}_Z \Psi_{F,MF} = M_F \hbar \Psi_{F,MF}$$

The energy levels depend on F, J and I quantum numbers The additional selection rules for rotational transitions are

$$\Delta F = 0, \pm 1 \text{ and } \Delta I = 0$$

Therefore for each rotational transition, there will be a number of lines associated, which arise from the transitions between different F levels

The internal dynamics of the molecules further complicates the spectrum If internal rotation or tunneling motion is present, the rotational levels are split, and different sets of transitions are observed Nuclear spin statistics also plays an important role in spectroscopy The intensities of different transitions depend on the statistical weights of the energy levels involved Due to the symmetry of the nuclear spin function different transitions may be strong, weak or even forbidden

I.5. Present Investigations

I.5.a. Structure and Dynamics of Ar_2-H_2S

As per our knowledge Ar-H_2S is the only species to show anomalous isotope effect in rotational constants [47] The rotational constant of pseudo-diatomic Ar-H_2S is smaller than that of Ar-D_2S Normally the rotational constant for the heavier isotopomer is smaller However, Ar_3-H_2S[48] does not show any anomalous effect What will be the isotope effect of rotational constants for Ar_2-H_2S complex? The rotational spectroscopy of this complex has been studied using PNFTMW spectrometer Several *a*-dipole rotational transitions were observed for Ar_2-H_2S, Ar_2-D_2S and Ar_2-HDS The rotational constants and the centrifugal distortion constants were determined from fitting of the observed transitions It shows a normal isotope effect of rotational constants The nature of the spectrum and the isotopic substitution analysis give geometry with C_{2v} symmetry This vibrationally averaged geometry has both the hydrogen atoms directed towards Ar_2 *Ab initio* calculations have been done at MP2 and CCSD(T) levels, using several large basis sets A potential energy surface scan has been performed to understand the internal dynamics of the complex This work is discussed in chapter III in detail

I.5.b. Rotational Spectra and Structure of Ar-$(H_2S)_2$

Water dimer is probably the most extensively studied hydrogen bonded system both theoretically and experimentally [49-51] The rotational spectrum, rather rovibrational spectrum is highly complicated due to different tunneling motions If we move to the analogous system of the second row hydride, how does the rotational spectrum look like? What is the nature of the tunneling motions? If one Ar atom is added to the $(H_2S)_2$ dimer, how are the structure and tunneling motions affected?

The rotational spectral studies have been done for Ar-$(H_2S)_2$ and Ar-$(D_2S)_2$ Similar to $(H_2S)_2$, two sets of transitions were observed for the trimer, which arise due to tunneling motion Some new sets of transitions of $(H_2S)_2$ were observed during this work, as well The trimer has a T-shaped heavy atom geometry In addition to experiment, *ab initio* calculations were done at several levels of theory to optimize the geometry and calculate the interaction energies The details are presented in chapter IV

I.5.c. *Ab Initio* Studies of H_2O-H_2S and Ar-H_2O-H_2S

H_2O-H_2S is a very important system in the context of hydrogen bonding However, it has not been studied extensively H_2O is a good proton donor and a good acceptor as well On the other hand H_2S is neither an efficient proton donor nor an acceptor Which one will be the global minimum of H_2O-H_2S complex, H_2O-HSH or H_2S-HOH? The most recent theoretical calculation determines H_2S-HOH to be more stable, though the energy difference is very less [52] Zero point vibrational energy was not taken into account in this work *Ab initio* calculations have been done at several levels of theory for H_2S-H_2O dimer and Ar-H_2S-H_2O trimer It has been seen that the zero point energy can play an important role in determining the relative stability of different minima Some rotational transitions for Ar-H_2S-H_2O have been observed Preliminary experimental data for the trimer and the *ab initio* results for both dimer and trimer are reported in chapter V

I.5.d. Hydrogen Bond Radius

Pauling has defined covalent radius, ionic radius, metallic radius and van der Waals radius for different species[1] Is it possible to define 'hydrogen bond radius' for different hydrogen bond donors? The experimental data available for several hydrogen-bonded complexes, B HX (X = F, Cl, Br, CN, OH and C≡CH), were analyzed It is found that for a particular X, the 'hydrogen bond distances' could be expressed as the sum of a constant and r(E) of B [53] The r(E) is the distance from B to the point at which the molecular electrostatic potential is minimum This constant is the contribution of hydrogen atom towards the 'hydrogen bond distance' This effective size of hydrogen is defined as 'hydrogen bond radius' for that particular hydrogen bond donor It shows an inverse correlation with the dipole moment of H-X bond and the electronegativity difference between H and X As the experimental data for H_2S complexes are scarce, *ab initio* and DFT calculations have been performed for several B-H_2S complexes, and from those calculated structural parameters, 'hydrogen bond radius' has been determined for H_2S The same procedure has been followed for HF, HCl and H_2O complexes as well to confirm our analysis Chapter VI presents the details of this work

"HF" has been used to denote 'hydrogen fluoride' and 'Hartree-Fock' throughout the Thesis What is meant should be obvious from the context

References

1 L Pauling, "*The Nature of Chemical Bond and the Structure of Molecules and Crystals An Introduction to Modern Structural Chemistry*", Cornell University Press, Ithaka (1960)

2 B Pullman (ed), "*Intermolecular Interactions from Diatomics to Biopolymers*", Wiley, New York (1978)

3 van der Waals molecules I, special issue, *Chem Rev.* **88** (6), (1988)

4 van der Waals molecules II, special issue, *Chem Rev* **94** (7), (1994)

5 van der Waals molecules III, special issue, *Chem Rev.* **100** (11), (2000)

6 S E Novick, *Bibliography of rotational spectra of weakly bound complexes*, (2004), available at http //www wesleyan edu/chem/faculty/novick/vdw html

7 W M Latimer and W H Rodebush, *J Am Chem Soc* **42**, 1419 (1920)

8 G C Pimentel and A L McClellan, "*The Hydrogen Bond*" W H Freeman and Company (1960)

9 G R Desiraju and T Steiner, "*The Weak Hydrogen Bond*", Oxford University Press Oxford (1999)

10 S Scheiner, "*Hydrogen Bonding, A Theoretical Perspective*", Oxford University Press New York (1997)

11 P A Kollman, J F Liebman and L C Allen, *J Am Chem Soc* **92**, 1142 (1970)

12 B S Ault and G C Pimentel, *J Phys Chem* **79**, 621 (1975)

13 S Scheiner, "*Lithium Chemistry A theoretical and experimental overview*", eds A M Sapse and P von R Schleyer, John Wiley & Sons Inc , New York (1995)

14 Y Feng, L Liu, J Wang, X Li and Q Guo, *Chem Commun* **1**, 88 (2004)

15 P Hobza and Z Havlas, *Chem Rev* **100**, 4253 (2000)

16 P Hobza, V Spirko, Z Havlas, K Buchhold, B Reimann, H D Bart and B Brutschy, *Chem Phys Lett* **299** 180 (1999)

17 S Scheiner and T Kar, *J Phys Chem A*, **106**, 1784 (2002)

18 X Li, L. Liu and H B Schlegel, *J Am Chem Soc* **124**, 9639 (2002)

19 P Metrangalo and G. Resnati, *Chem Eur J* **7**, 2511 (2001)

20 A C Legon, *Angew Chem Int Ed* **38**, 2686 (1999)

21 N K Karan and E Arunan, *J Mol Struct* **688**, 203 (2004)

22 I G Kaplan, "*Theory of Molecular Interaction*", Elsevier Amsterdam (1987)

23 J Israelachvili, "*Intermolecular and Surface Forces*", Second Edition, Academic Press, Amsterdam (2003)

24 H Umeyama and K Morokuma, *J Am Chem Soc* **99**, 1316 (1977)

25 J F Garvey, W J Herron and G Vaidyanathan, *Chem Rev* **94**, 1999 (1994)

26 S J Harris, S E Novick, W Klemperer, *J Chem Phys* **60**, 3208 (1974)

27 T J Balle and W H Flygare, *Rev Sci Instrum.* **52**, 33 (1981)

28 A C. Legon, in "*Atomic and Molecular Beam Methods*" (ed G Scoles), Oxford University Press, New York, Vol 2, 289-308 (1992)

29 R J Saykally, *Acc Chem Res* **22**, 295 (1989)

30 R C Cohen and R J Saykally, *J Phys Chem* **96**, 1024 (1992)

31 D J Nesbitt, *Chem Rev.* **88**, 843 (1988)

32 D J Nesbitt, *Proceedings of SPIE-The International Society for Optical Engineering*, **742**, 16 (1987)

33 D J Nesbitt, *NATO ASI Series, Series-C, Mathematical and Physical Sciences*, **212**, 107 (1987)

34 M P Casassa, *Chem Rev* **88**, 815 (1988)

35 H J. Neusser and K Siglow, *Chem Rev* **100**, 3921 (2000)

36 K Muller-Dethlefs O Dopfer, *Chem Rev* **94**, 1845 (1994)

37 C. E H. Dessent and K Muller-Dethlefs, *Chem Rev* **100**,3999 (2000)

38 P Klaeboe, C J Nielsen, *Analyst*, **117**, 335 (1992)

39 P M Felker, P M Maxtin and M W Schaeffer, *Chem Rev* **94**, 1787 (1994)

40 J P Toennies, A F Vilesov and K B, Whaley, *Physics Today*, (February), 31 (2001)

41 M Hartmann, R E Miller, J. P Toennies and A F Vilesov, *Science*, **272**, 1631 (1996).

42 K Nauta and R E Miller, *Science*, **283**, 1895 (1999)

43 R D Suenram, J-U Grabow, A Zuban and I Leonov, *Rev Sci Instrum* **70**, 2127 (1999)

44 J-U Grabow, W Stahl and H Dreizler, *Rev Sci Instrum* **67**, 4072 (1996)

45 C H Townes and A L Schawlow, "*Microwave Spectroscopy*", McGraw Hill, New York (1955)

46 W Gordy and R L Cook, "*Microwave Molecular Spectra*", Wiley, New York (1984)

47 H S Gutowsky, T Emilsson and E Arunan, *J Chem Phys* **106**, 5309 (1997)

48 E Arunan, T Emilsson, H S Gutowsky and C E Dykstra, *J Chem Phys* **114**, 1242 (2001)

49 G T Fraser, *Int Rev, Phys Chem* **10**, 189 (1991) and the references therein

50 N Goldman, R S Fellers, M G Brown L B Braly, C J Keoshian, C Leforestier and R J Saykally, *J Chem Phys* **116**, 10148 (2002)

51 Y Watanabe, T Taketsugufoot and D J Wales, *J Chem Phys* **120**, 5993 (2004)

52 Y-B Yang, F M Tao and Y K Pan, *Chem Phys Lett* **230**, 480 (1994)

53 S R Gadre and P K Bhadane, *J Chem Phys* **107**, 5625 (1997)

Chapter II

Experimental and Theoretical Methods

II.1. Introduction

Microwave spectroscopy has traditionally been used to determine the structure of small molecules accurately [1,2] Only gaseous molecules or liquids and solids with finite vapour pressure could be studied Hence, unlike spectrometers in other region of the electromagnetic spectrum, microwave spectrometers did not become very popular Commercial microwave spectrometers were available during the 60s and 70s and slowly they disappeared Development of the pulsed nozzle Fourier transform microwave spectrometer by Balle and Flygare[3], expanded the scope of microwave spectroscopy significantly This spectrometer turned out to be almost ideal as it had very high sensitivity and resolution, simultaneously [4] With this, one could look at weakly bound complexes (with non-zero permanent electric dipole moment) formed between virtually any two chemicals, be they atoms, molecules, radicals or ions Several laboratories around the world have built such a spectrometer, mainly in the last two decades [5-14] This spectrometer is primarily a research equipment and hence is not commercially available The PNFTMW spectrometer has been fabricated in our laboratory and this chapter describes the details

II.2. Design of the Spectrometer

The pulsed nozzle Fourier transform microwave spectrometer combines the supersonic expansion technique with the cavity Fourier transform microwave spectrometer It has several components i) a Fabry-Perot cavity made of two highly polished Aluminium mirrors (surface roughness better than microns) one of which is movable, ii) supersonic nozzle source for producing a cold jet/beam of molecules, iii) high vacuum chamber pumped by a 20" diffusion pump housing both i and ii, iv) microwave electrical circuit for polarizing the molecules and for detecting the molecular emission The complete design of the spectrometer is described below in two parts as mechanical and electrical

II.2.a. Mechanical Design

The mechanical design of the vacuum chamber housing the Fabry-Perot cavity is shown in Figure 1 It is a cylindrical chamber made of stainless steel, SS 304 It is 1000 mm long and the diameter is 850 mm The chamber is directly seated on top of the 20" diffusion pump (Vacuum Techniques, Bangalore, India) The pumping speed of the diffusion pump is $\approx$ 10,000 l s^{-1} and it is backed by an oil free roots blower (Boc Edward, EH 250) and a belt-less rotary mechanical pump (Boc Edward, E2M80) The combined pumping speed of the backing pumping system is ~4000 l min^{-1} The chamber can be evacuated to 10^{-6} Torr and a liquid nitrogen trap improves the pumping below 10^{-5} Torr The diffusion pump is water-cooled and a closed circuit water circulation facility includes a water circulation pump, a cooling tower cum water reservoir to keep the water at room temperature and a flow-switch to check the water flow Inside the chamber, two spherical Aluminium mirrors have been mounted co-axially on 3 SS guide rods The mirrors were made from 65 mm thick Aluminium disks with a diameter of 500 mm The radius of curvature of both the mirrors is 800 mm and CNC machining ensured that the surface roughness and the radius were good to 1 micron The distance between the mirrors could be varied in steps of microns between 630 and 730 mm We have opted for a large mirror, so that the low frequency cutoff for the spectrometer is about 3 8 GHz The radius of the mirror (a) and its radius of curvature (R) determine the lower frequency at which the Fresnel number is unity [6]

$$a^2/R\lambda = 1 \qquad (1)$$

Several laboratories have smaller mirrors with a low frequency cutoff near 8 GHz and the frequency range of such spectrometers is typically 6-18 GHz The lower frequency limit is important, if one is interested in looking at larger clusters, which would have many low J transitions below 4 GHz The Fabry-Perot cavity has been tested between 2-26 GHz in our spectrometer

The movable mirror is fixed with a micrometer controlled fine pitch screw rod and it is driven by a synchronized stepper motor (103H8221-5041,Sanyo Denki, Japan) The stepper motor driver (PMM-BA-4803) is controlled by the PC The linear screw rod

has a pitch of 5 mm, which means that the linear distance covered by the mirror for a 360° rotation is 5 mm The stepper motor, in high-resolution mode, takes 4000 steps for a complete rotation and thus the mirror moves in steps of 1 25 μm

This movable mirror has a10 mm hole at the center In addition, the backside of this mirror has a 25 mm cylinder carved out so that a pulsed nozzle (General Valve, USA, Series 9), connected with a stainless steel tube of ¼ inch OD, could be placed The pulsed valve goes through a 4" gate valve and an 'O' ring seal This assembly could also be connected at the top of the chamber through another 4" gate valve The diameter of

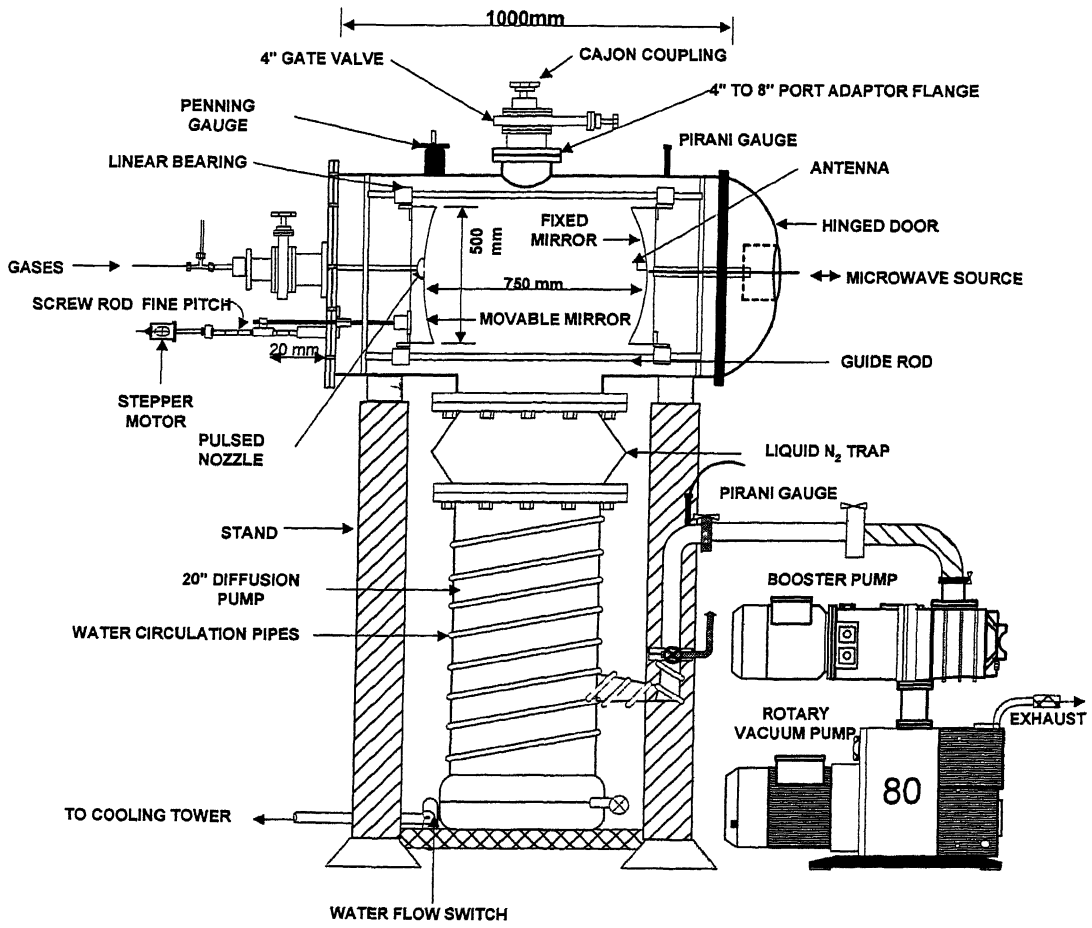

Figure II.1. Mechanical Design of the PNFTMW Spectrometer

the nozzle is 0 8 mm The electrical signal (trigger) to open and close the nozzle is fed through a pin connector, which is sealed with a 'O' ring and a clamp

A coaxial cable runs through the supporting tube with an SMA female connector at the mirror (fixed) end This cable has a hermetically sealed SMA connector at the other end so that the mw power can be coupled in and out of the cavity at vacuum The SMA connector goes through a small hole at the center of the mirror and an antenna (L-shaped bent wire made from the central wire of the coaxial cable) can be placed at the connector. Antennas of different length are used for different frequency range The length (L) of the antenna and the wavelength (λ) of the radiation are related as

$$L \approx \lambda/4 \qquad (2)$$

This is a good enough approximation to make antenna for a particular frequency region having the range extended by few GHz on both side of central frequency corresponding to λ Using 3-4 antennas of different lengths one could cover the entire range of the spectrometer, 2-26 5 GHz

II. 2.b. Electrical design

The microwave/rf circuit used for polarization of the molecules and detection of the molecular signal is shown in Figure II 2 The microwave source is a frequency synthesizer (#1 in Figure II 2, HP 83630L, 13 dBm power), which can generate any frequency between 10 MHz and 26 5 GHz to 1 Hz accuracy The output from the synthesizer (at ν) is routed to a single pole double throw (SPDT) switch (#7, Sierra Microwave Technology, SFD0526-001, Isolation 60 dB), which powers either a single side band generator (#5 Miteq, SM-0226-LC1A) or an image rejection mixer (#11 Miteq, IR-0226-LC1A) The SSBM mixes the synthesizer output at ν with a synchronous 30 MHz signal (Stanford Research Systems DS345) and generates ν+30 MHz signal This signal is amplified by a medium power amplifier (#6, Miteq, JS3-02002600-5-7A) with a gain of 24 dB The amplified signal goes through another SPDT switch (similar to #7) Both switches work synchronously connecting the polarization and detection parts (top and bottom of the SPDT switches in the Figure II 2), alternatively During the

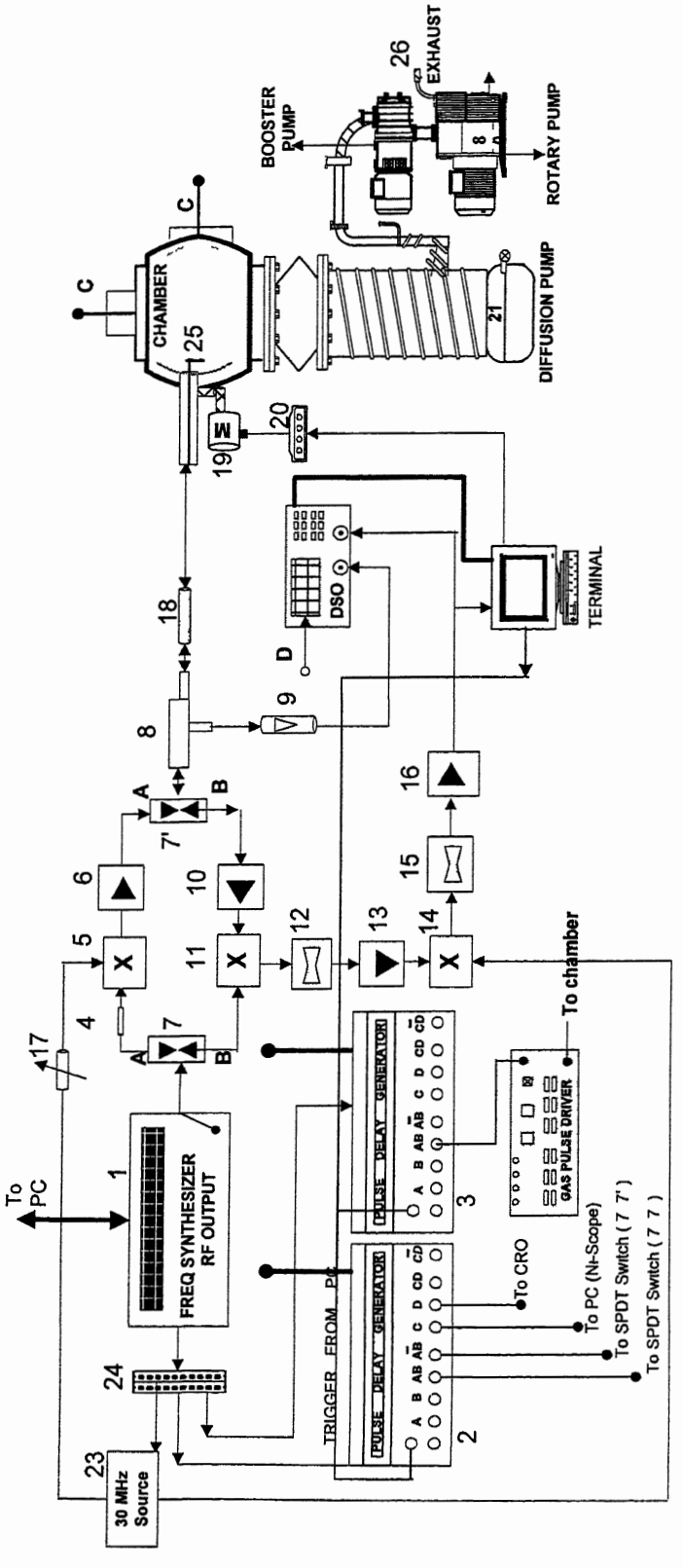

Figure II.2 Electrical design of the spectrometer [(1) Frequency Synthesizer (Hewlett Packard, HP83630L), (2) & (3) Delay generator, (4) Microwave Attenuator (HP, 8493C, 3dB), (5) SSB Mixer (Miteq, SMO-226LC1A), (6) Medium Power Amplifier (Miteq, JS3-02002600-5-7A), (7) MW SPDT Switch (Startra MW, 0 5-26 5 SFD0526-000), (8)Direction Coupler (Narda, 1 7-26 5--4227-16), (9) Diode Detector (Narda, 0 01-26 5--4507), (10) Low noise Amplifier (Miteq, JS4-02002600-3-5P), (11) Image Rejection Mixer (Miteq, IRO-0226LC1A), (12) Band Pass Filter (Mini Circuits, BBP-30), (13) RF Amplifier (Mini Circuits, ZFL-500LN), (14) RF Mixer (Mini Circuits, ZAD-1), (15) Low Pass Filter (Mini Circuits, BLP-5), (16) RF Amplifier (HD Communications Corp , HD 17153BB), (17) Attenuator (Mini Circuits, ZAFT-51020), (18) Blocking Capacitor (HP, 11742A), (19) Stepper motor, (20) Motor Driver, (21) Diffusion Pump, (22) Rotory Pump, (23) 30 MHz Function Generator (Stanford Research System, DS345), (24) Distribution Amplifier (Stanford Research System, FS710), (25) Antenna, (26) Exhaust

polarization pulse, the SPDT output goes through a directional coupler (#8, Narda, 4227-16) and a DC block (#18, HP 11742 A) to the antenna inside the chamber This polarization scheme, along with the detection scheme, is shown in Figure II 3 as a simple schematic, where only the frequencies of the radiations, involved, are shown

As the microwave radiation for the polarization of the molecule enters the cavity through the SPDT switch for a finite time (μs), it will have a bandwidth associated with the central frequency The microwave pulse length of ≈ 1 μs leads to a frequency width of about 1 MHz and if there is an allowed transition within this bandwidth for the molecules/complexes in the cavity, polarization occurs (Figure II 4) The free induction decay (FID) from the polarized molecules is at a frequency of ν+30±Δ, and it lasts for a few hundred microseconds The same antenna couples the molecular signal back to the detection circuit This signal is amplified by a low noise amplifier (#10, Miteq JS4-02002600-3-5P, noise 2 8 dB, gain 28 dB) and mixed with the synthesizer signal at ν in an image rejection mixer (#11, Miteq, IRO-0226-LC1A) The IRM gives only the 30±Δ signal, which passes through a band pass filter (#12, Minicircuits BBP 30) and a low noise amplifier (#13, Minicircuits, ZFL-500LN) The 30±Δ signal is down converted (Figure II 3) to Δ by the RF mixer (#14, Minicircuits ZAD-1) and a low pass filter (#15, Minicircuits, BLP-5) This signal (Δ), generally in kHz range, is amplified and digitized by the virtual scope card (National Instrument, PCI 5112) and transferred to the computer for further processing The 30 MHz signal is from the function generator (#23, SRS DS345) and so we have the option of varying the intermediate frequency (IF) in the mixer This detection scheme is called "Double Super-heterodyne" detection In this way the molecular signal in GHz range is converted to <1 MHz signal, making it easier to digitize In this spectrometer the frequency offset between the polarizing and molecular signal is detected, not the actual molecular frequency Adding or subtracting this offset to the polarizing signal frequency gives the molecular frequency

During the polarization pulse, if the Fabry-Perot cavity is not tuned to the particular frequency ν+30 MHz, most of the mw power is reflected The directional coupler routes 2 5 % of this reflected signal to the oscilloscope (#27, Tektronix, TDS 430A) via a diode detector (#9, Narda, 4507) The moving mirror is moved in steps of

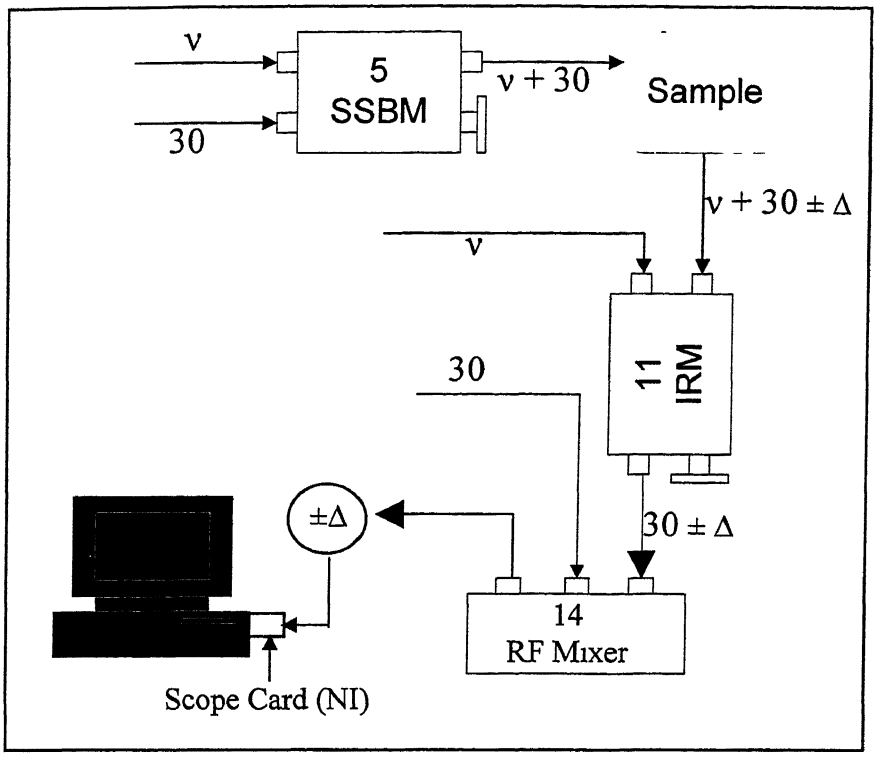

Figure II.3. Polarization and double Super-heterodyne detection of molecular signal

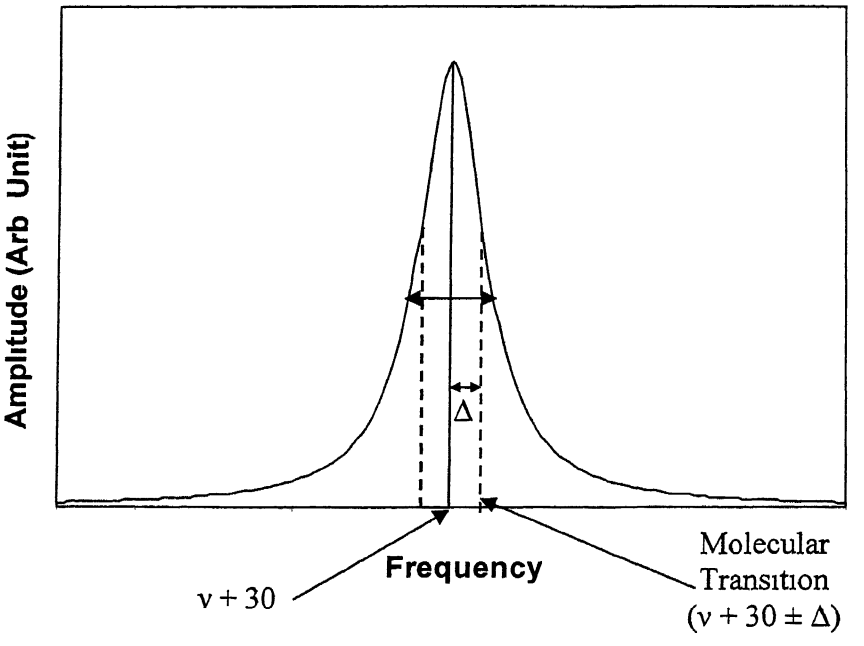

Figure II.4. The bandwidth of the polarizing MW pulse and molecular transition within the bandwidth

micron until the reflected power shows a dip in the scope The resonant frequencies, ν, of Fabry-Perot resonator for the TEM_{mnq} modes are [3]

$$\nu = c/2d\,[(q+1) + (1/\pi)(m+n+1)\cos^{-1}(d/R)] \qquad (3)$$

Here, d is the distance between the mirrors and R is the radius of curvature, m, n and q are the number of nodes in the three perpendicular axes Thus, within the maximum variation of the distance between the mirrors (100 mm), several resonances can be observed for a given frequency As the mirror moves the reflected signal is monitored in the oscilloscope (Figure II 5) It is preferable to do the experiment with the cavity tuned to the TEM_{00q} mode at a particular frequency Most of the laboratories having a PNFTMW spectrometer[5-14] employ 2 antennas, one in each mirror, for tuning and detection This leads to an inherent reduction in the detected signal Using the directional coupler with only one antenna is more advantageous. Only 2 5 % of the signal is used for tuning purpose instead of almost half the signal

All the microwave components used in our setup are ultra-wide band The original spectrometer could be operated only in octave bandwidths and several switches were used for going from one band to another In some cases, the components needed to be physically changed for going from one band to another All the recently built PNFTMW spectrometers[5,6] use one set of components that perform reasonably well throughout the frequency range Our spectrometer can be operated from 2-26 GHz without changing any components

II.3. Performing the Experiment

This is an experiment of pulses with both the molecular sample and the microwave source being pulsed Two delay generators (# 2 and 3, SRS, DG535) generate all the timing sequence (shown in Figure II 6) needed for the experiment The sequence is described below with typical pulse lengths and delays First a microwave pulse is applied to the evacuated chamber and the background response from the chamber is digitized This includes random noise as well as coherent ringing from the cavity The ringing typically lasts for a few microseconds The digitizer is triggered after a delay to

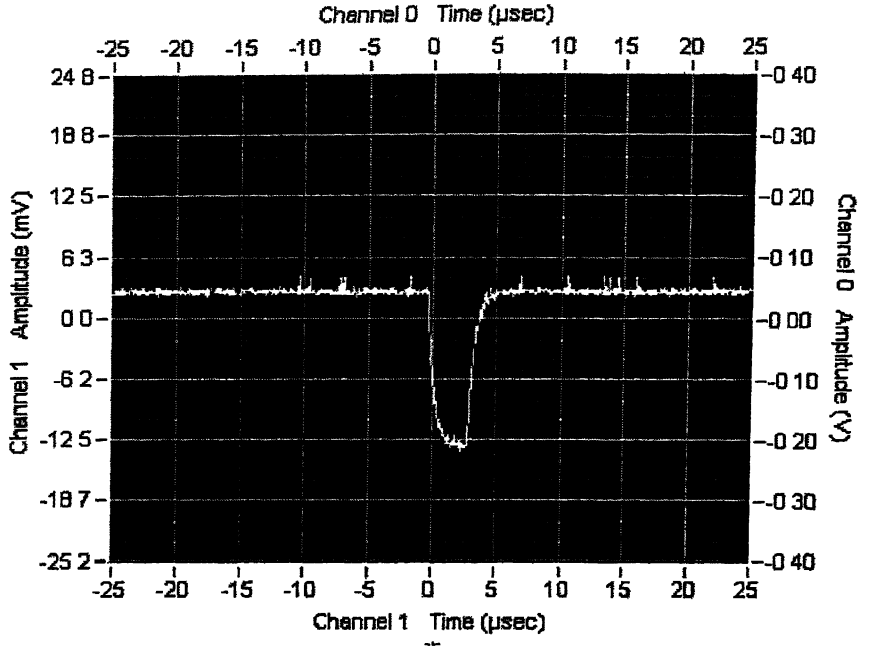

(A)

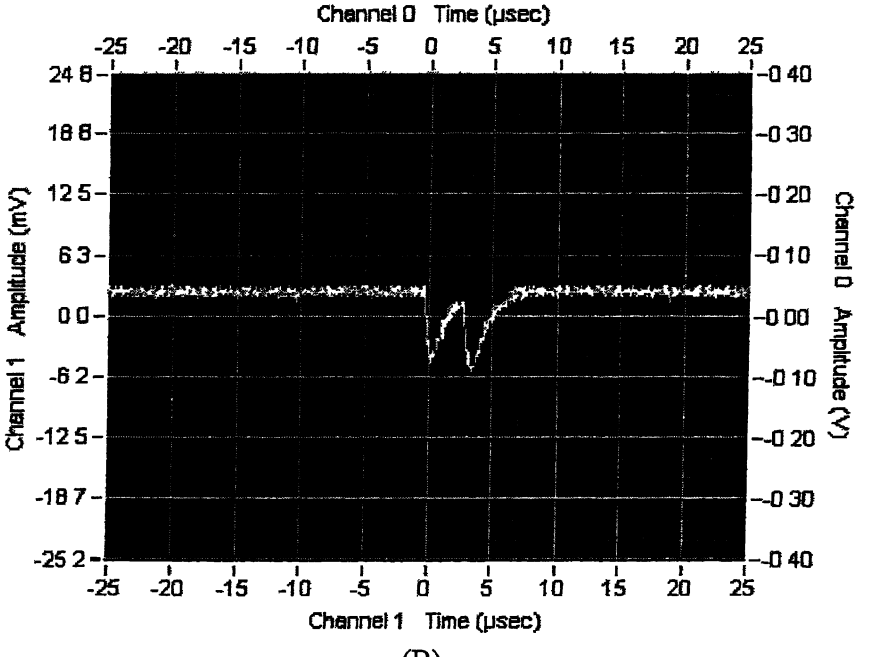

(B)

Figure II.5 Reflected signal from the cavity (A) The amplitude of reflected signal is maximum, the cavity is not in tune (B) The amplitude is minimum, the cavity is in tune

avoid the ringing This delay is called "record delay" The pulsed nozzle is opened for 1 ms After a delay (start delay) of 100 μs for the molecules to reach the center of the cavity, the microwave pulse is applied again The response from the molecules is digitized now and the background collected earlier is subtracted Fourier transformation of this time domain signal gives the frequency domain spectrum As the molecules stay within the cavity for ~2 ms, it is possible to collect up to 20 FIDs per gas pulse by applying as many microwave pulses between two gas pulses The experiment can be repeated for N number of gas pulses to improve the signal-to-noise ratio

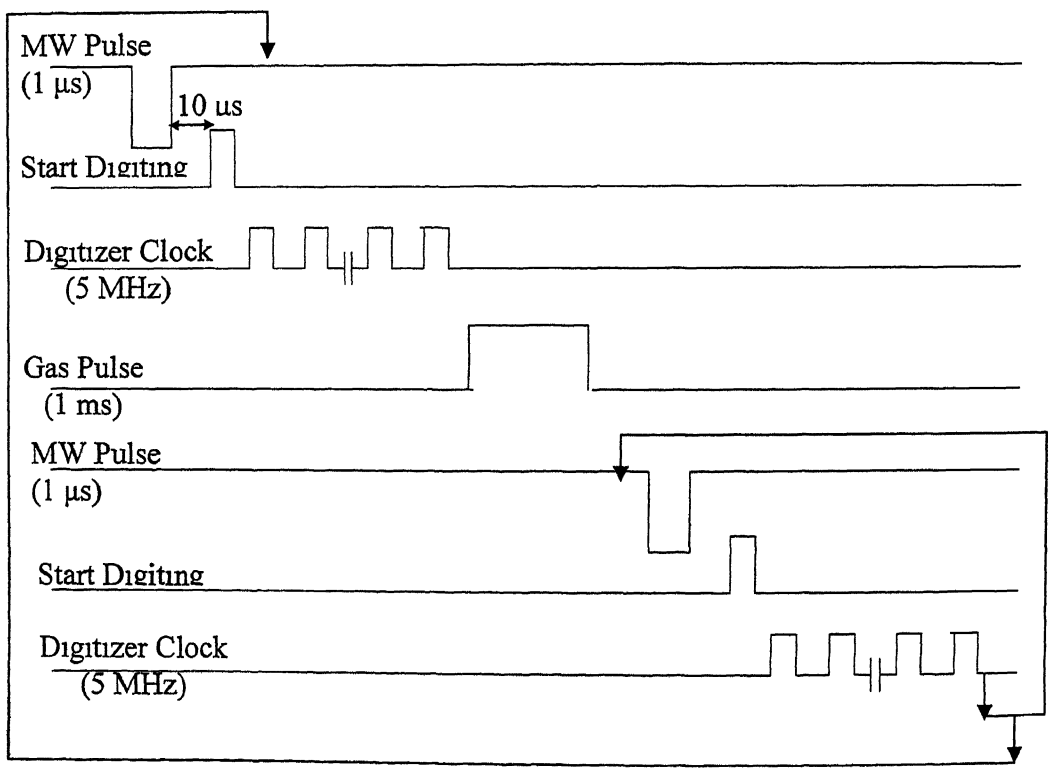

Figure II 6. Pulse Sequence of a typical experiment

II.4. Operation and Control: The Software

The spectrometer operation is fully automated CVI LabWindows (National Instruments) software offers the backbone using which the software has been developed The code is written in C The MW synthesizer, oscilloscope and the delay generators are controlled by a GPIB (NI) interface The stepper motor driver is controlled by the parallel port, which also sends the start trigger for the experiments The time domain FID is digitized using a virtual scope card (NI, PCI 5112), and finally transferred to a PC for averaging and Fourier transformation

II.4.a. Design of the Program

The first step of designing a program like this is making a User Interface, which will communicate between the user and the program The program is written such that the main function calls the User Interface, which serves as a platform for the input and output data The User Interface Panel calls various other functions as and when they are required

'User Interface panel' is a graphical interface, which could be easily made by the LabWindows/CVI User Interface Editor The 'User Interface panels', used for performing the experiment and displaying the saved data, are shown in Figures II 7 and II 8 All the different types of Buttons, Dropdown menus, Input boxes, outputs like graphs, etc can be made These are then related to various call back functions and constants in the program, which provide them the functionality Relating these functions to the program is done automatically by the LabWindows Actually LabWindows assigns each item in the User Interface Panel some number, which serves as its handle Whenever program needs to read or write something then it uses these panel handles The panel numbers are stored in a header file created automatically by LabWindows There are six files required for running this whole program These files are -

1 Library file for functions controlling NiScope digitizer
2 An instrument file used by LabWindows

3 User Interface file which contains the graphical design of the User Interface Panel
4 Source file, containing the code written in C for the program
5 Header file containing different panel handles, which is auto generated by LabWindows This file needs to be included in the source file
6 Another user made file, containing declaration of variables used in the program

II.4.b. Execution of the program

When the project is run, the main program is executed first Main program reads data from a file, which contains all the inputs set when the program was run last time After reading this file, main program calls the user interface function The user interface is displayed on screen The user interface has been designed to control the various equipments/components by virtual buttons and text boxes on screen On pressing these buttons or entering new values in the boxes corresponding functions are called, which will decide the functions of each button.

There are four basic modes of operation provided by the program These do not differ in basic functionality, but differ in some features These modes are 1) Single Shot, 2) Average 3) Average multi-acquisition and 4) Auto scan mode

In single shot mode repetitive data is taken for the same frequency without saving the records In this mode the noise and the signal for a gas pulse are displayed repetitively at the upper and lower 'graph panel' of the 'User Interface panel" shown in Figure II 7 This mode is used to optimize the experimental conditions (back pressure, MW pulse length, relative proportion of the component species, etc) for a particular transition of a complex

In "Averaging" mode data is collected for specified number of times (gas pulses) and averaged at a fixed frequency This mode is used to obtain a good S/N ratio so that the frequency of a particular signal can be measured accurately

"Average multi-acquisition" is same as "Average", except that several FIDs are collected per gas pulse All the FIDs are averaged and it is repeated for a finite number

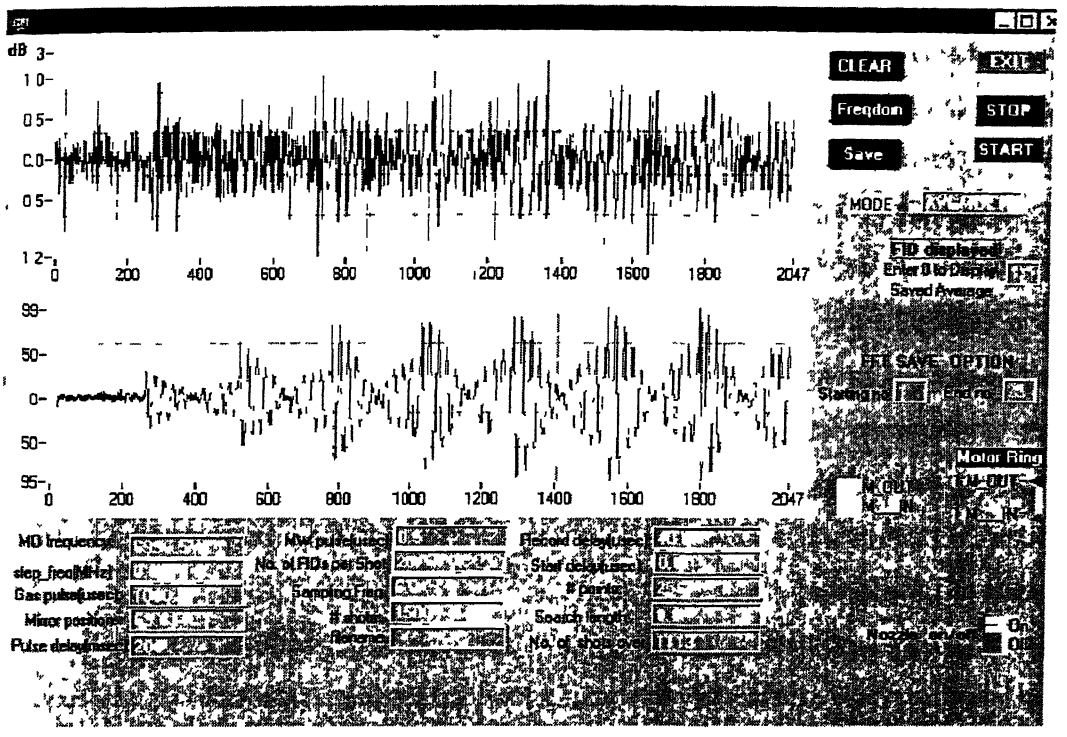

Figure II.7. User Interface panels for performing the experiment

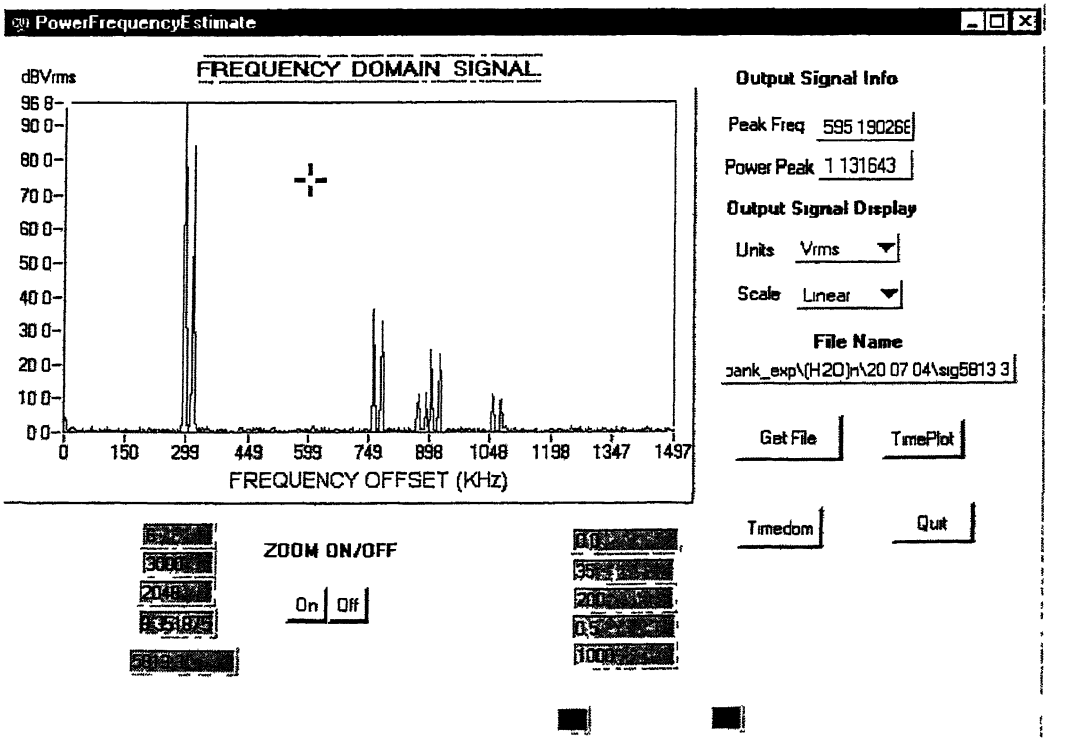

Figure II.8 User Interface panels displaying the saved data

of gas pulses The number of FIDs to be collected and the number of FIDs to be averaged can be specified in the user interface panel Figure II 7 shows a typical experiment in this mode where total 25 FIDs are collected and only the first 8 of them are displayed in the panel

In "Auto Scan" mode, the "Average multi-acquisition" process is carried out for a particular frequency, and the data are saved in a file Then the frequency is changed automatically by the specified step size, and the mirror is moved accordingly to keep the cavity tuned The acquisition and averaging are carried out for this changed frequency This combination of events, i e changing the frequency, adjusting the tuning and collecting the signal, continues till a certain 'search length', specified by the user, is covered This mode is used for scanning a particular frequency range to search the transitions for a system

All the saved data, obtained in "Average", "Average multi-acquisition" or "Auto Scan" mode, can be viewed any time using the user interface panel shown in Figure II 8

II.5. Sample Preparation

A four-channel mass flow controller/reader (MKS Instruments, 647B) and four different mass flow meters (1179A) are used for preparing the gaseous mixture on the fly Two of them are used for the carrier gases (either Helium or Argon) and their range is 0 – 1000 SCCM calibrated for N_2 The other two are used for reagent gas(es) flow and they have a range of 0-20 SCCM The output from all the four flow meters are mixed and taken to the pulsed valve The reagent flow meters are connected to 3-way valves in order to handle gases and liquids The gaseous reagents are directly flown to the mixer and for liquids, the carrier gas is bubbled through a glass reservoir containing the liquid The 3-way valves could be selected either for direct flow or through the liquid bubbler A very flexible 'gas handling arrangement' has been set up (shown in Figure II 9) so that at any time two carrier gases (Ar and He), two reagent gases and two liquid reagents can be used, without changing any hardware The pulsed valve feed through has a 3-way valve as well so that the excess gases can be pumped out with a separate mechanical

pump This bleed line goes through a needle valve to control the outflow so that the back pressure at the nozzle could be maintained at the required level (typically 1-2 atm)

The gas mixture (sample gas and carrier gas) undergoes supersonic expansion on opening the nozzle The nozzle diameter (0 8 mm) is much larger than the mean free path of the gas Hence, there is a huge number of collisions between the molecules Due to the two-body collision the random motion of the molecules is converted to a directed mass flow As a result the translational temperature of the expanded molecules

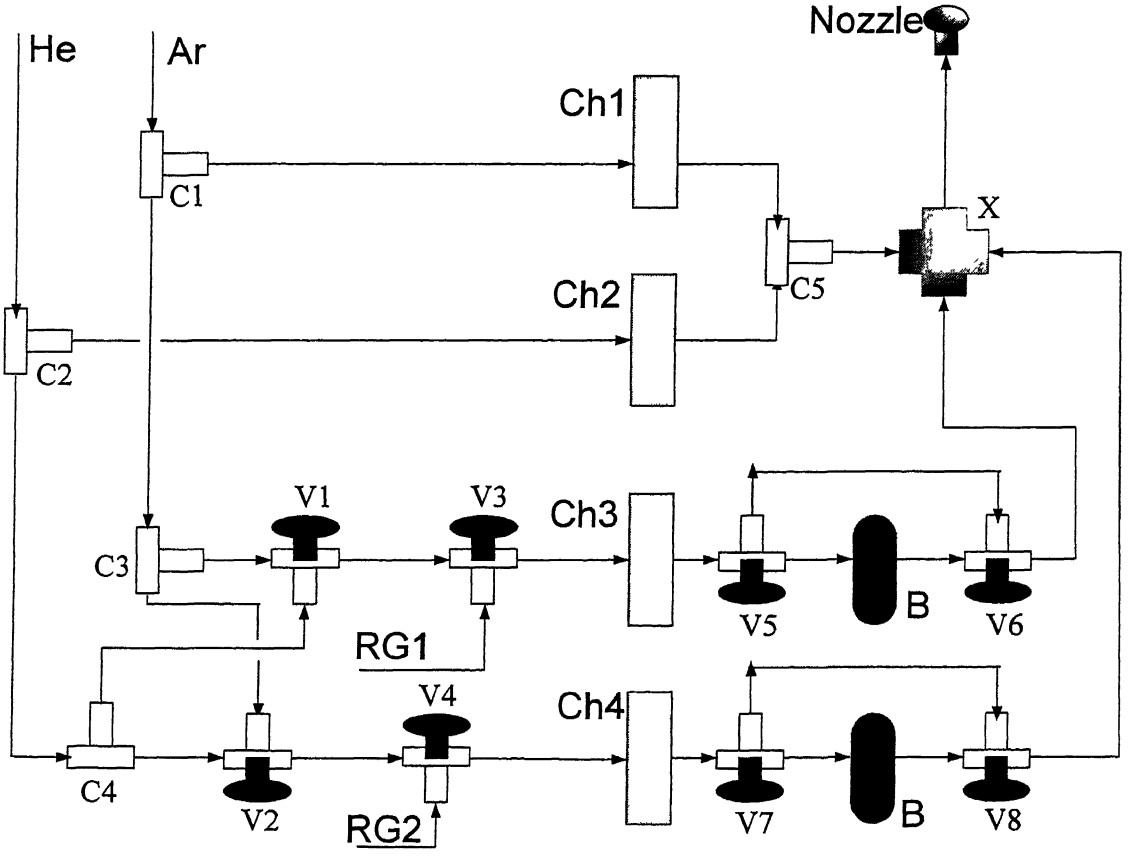

Figure II.9 Gas handling system Ch1 and Ch2 are the MKS mass flow controller having flow range of 0-1000 SCCM, and Ch3 and Ch4 are of 0-20 SCCM B is glass bubbler containing liquid sample V's are three-way valves, C's are three-way connectors and X is a four-way connector

goes down The other degrees of freedom, rotational and vibrational, equilibriate with the translational degree of freedom at slower rates The rotation-translation equilibrium is much faster than the vibration-translation equilibrium Thus the expanded molecules become rotationally very cooled Only few lower rotational levels are populated The rotational temperature, achieved on the expansion, is ~3 K The vibrational cooling is efficient enough to have significant population only in the ground vibrational level The three body collisions lead to complex formation Therefore rotationally and vibrationally cooled weakly bound complexes are formed They are characterized by their rotational spectra

II. 6. Performance of the spectrometer

The time domain signal obtained from the standard OCS is shown in Figure II 10 The frequency domain spectrum shown in Figure II 11 reveals the resolution of the spectrometer The FWHM is only 2 8 kHz The line center could be determined to 0 1 kHz as is typical for the PNFTMW spectrometers The doubling of the signal is due to Doppler effect, which is also typical to such spectrometers The standing wave in the cavity is the super-position of two traveling waves going in opposite directions leading to Doppler doubling Molecular beam is traveling coaxially in one direction The Doppler doubling could be reduced with a skimmer if the pulsed valve is kept on top of the chamber The real molecular frequency, 12162 9789 MHz, is the mean value of the two Doppler peaks The signal from ^{18}OCS at 11409 7097 MHz is shown in Figure II 12 The natural abundance of ^{18}O is only 0 2 % and this signal can be seen by averaging just 10 shots Most of the isotopomers of OCS (OCS, $OC^{34}S$, $OC^{33}S$, $O^{13}CS$, $O^{13}C^{34}S$, ^{18}OCS) have been observed The J = 0 $\rightarrow$1 transition for $O^{13}CS$ is shown in Figure II 13 The line is split by a mere 4 9 kHz but it is well resolved The splitting is due to the spin-rotation interaction, which couples the ^{13}C nuclear spin with the rotation of the molecule

Signals from several weakly bound complexes such as $(Ar)_n$-H_2O, where n = 1-3 (Ref 15-17) have also been observed Several naturally occurring isotopomers of these

complexes could be seen as well The J = 0→1 transitions of the para (I=0) and ortho (I=1) states of Ar-H_2O complexes are shown in Figure II 14 and II 15 Note the well-resolved hyperfine interaction from the I=1 state In order to test the performance of the spectrometer over the frequency range, Ar-H_2S^{18} signals were observed from 3 – 20 GHz Two different antennas were used to cover this frequency range [6]

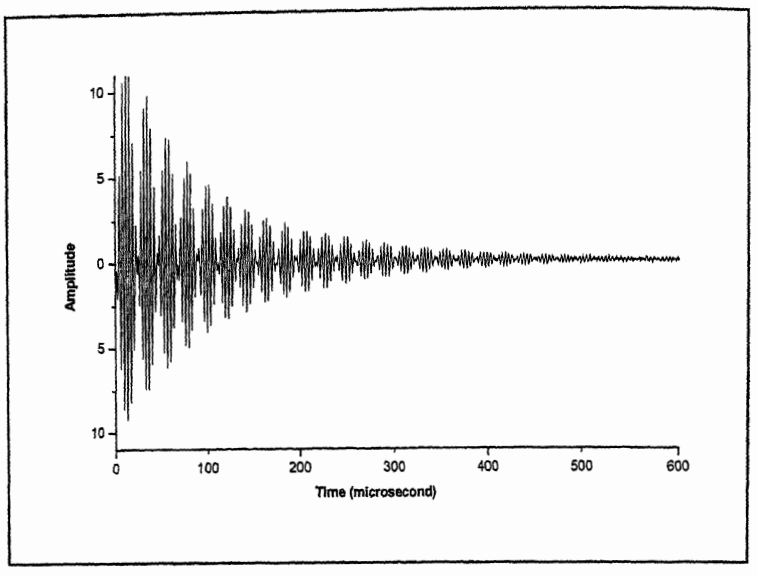

Figure II.10. The FID from the OCS polarized at 12162 7 MHz with a microwave pulse of 0 5 μs The backing pressure was 1 atm. 3 % OCS in Argon was used

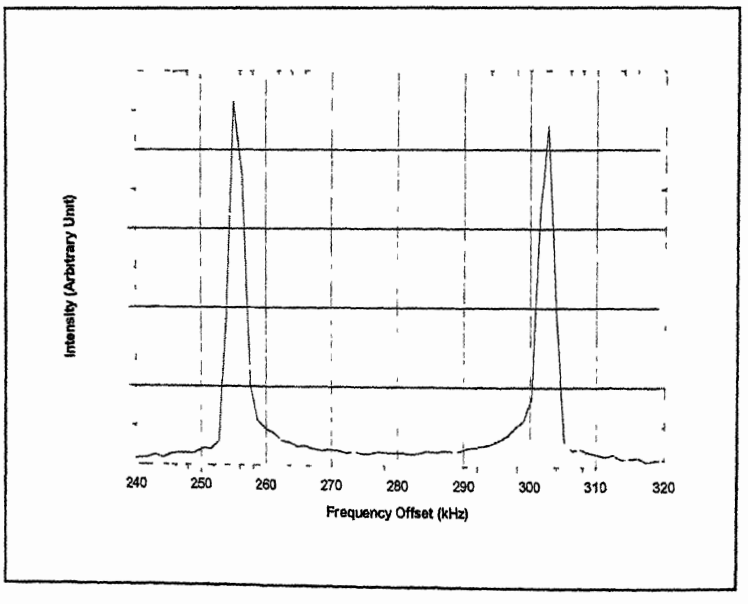

Figure II.11 The frequency domain spectrum of Figure II 10 showing the Doppler doublets of the J = 0→1 transition of OCS at 12162 9789 MHz

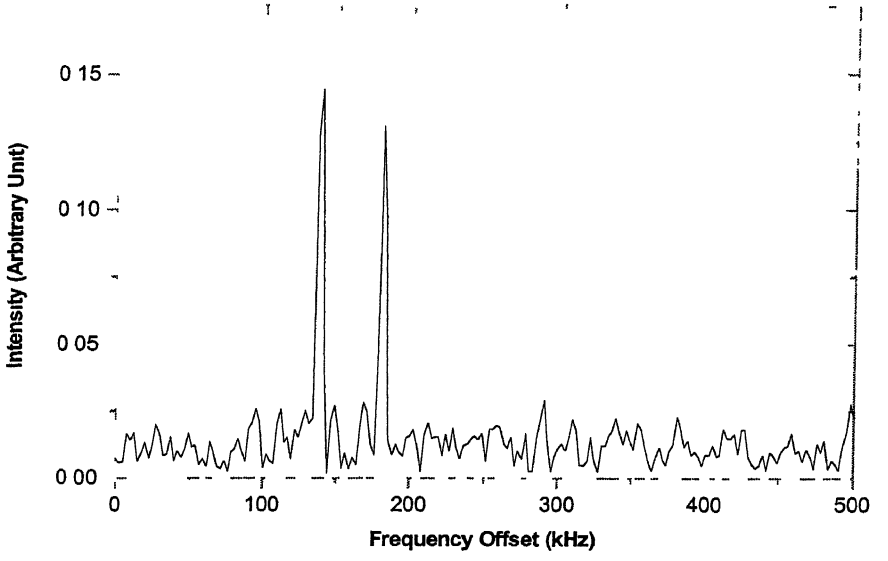

Figure II.12 The J=0→1 transition for the ^{18}OCS observed at 11409 7097 MHz, with the natural sample of OCS The MO frequency was 11409 550 MHz

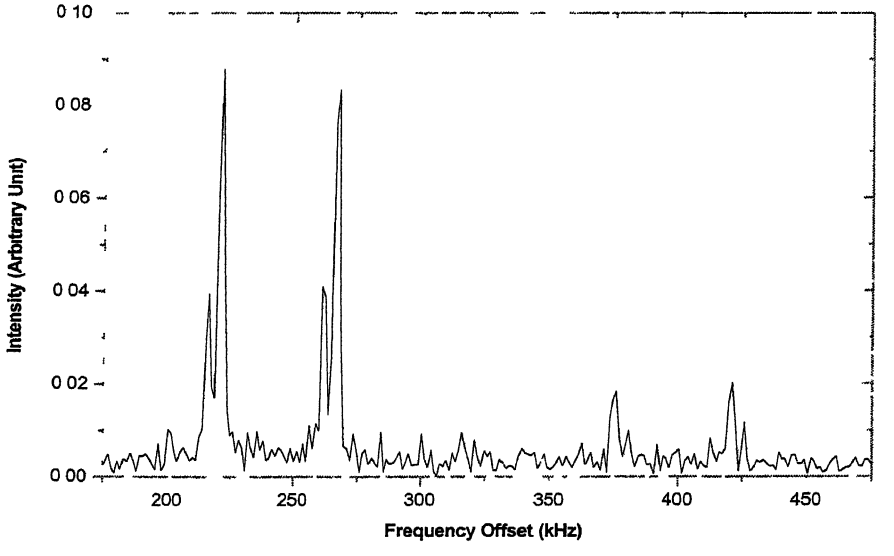

Figure II.13 The J=0→1 transitions for the O^{13}CS observed with the natural sample of OCS at 12123 8388 and 12123 8437 MHz The doubling of the line is due to the spin-rotation interaction from the ^{13}C The MO frequency was 12123 6 MHz

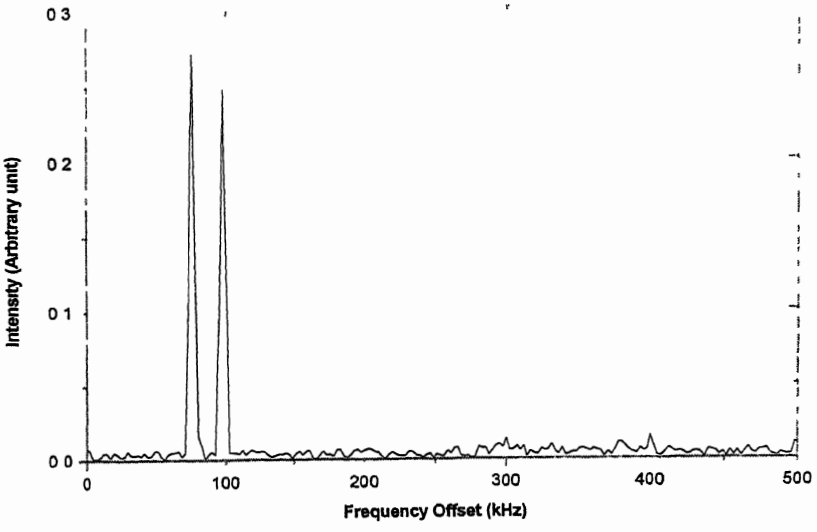

Figure II 14 The J = 0→1 transition of the Ar-H_2O complex with H_2O in the lowest para 0_{00} state showing a sharp singlet at 5976 1866 MHz The MO frequency was 5976 1 MHz

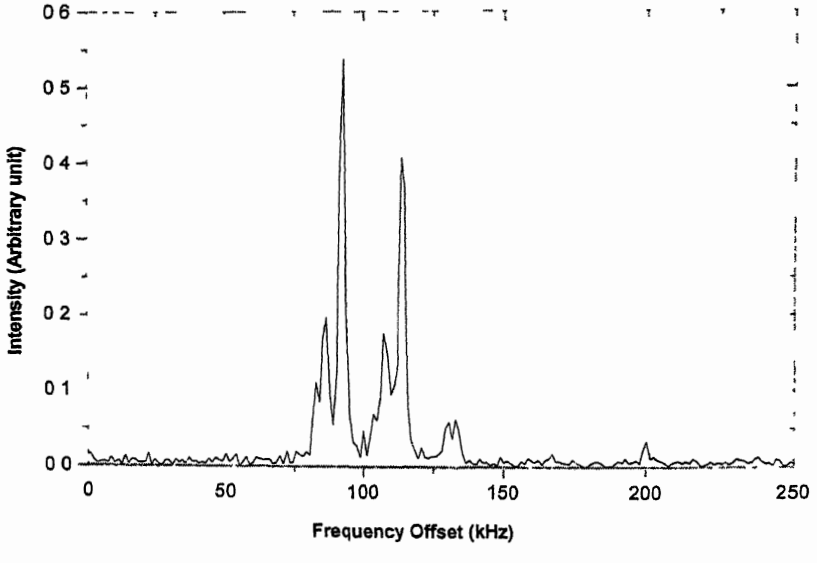

Figure II.15 The J = 0→1 transition of Ar-H_2O complex with H_2O in the lowest ortho 1_{01} state (I=1) showing a triplet at 5824 2430, 5824 2532 and 5824 2700 MHz The MO frequency was 5824 15 MHz

II.7. *Ab Initio* and DFT Calculation

Ab initio and DFT calculations[19-23] were done for the complexes, studied with PNFTMW spectrometer The results of the calculations were used along with the experimental data to understand the structure and dynamics of the complexes of interest The methods used are MP2, CCSD(T) and B3LYP Complex geometries were optimized mainly at MP2 and B3LYP levels For Ar_2-H_2S, $(H_2S)_2$, Ar-$(H_2S)_2$, H_2O-H_2S and Ar-H_2O-H_2S complexes, the equilibrium geometries were optimized at MP2 level using several large basis sets, starting from 6-311++G** up to aug-cc-pVQZ MP2 level is quite efficient for these kind of weakly bound complexes and is used in general Dunning's correlation consistent basis sets (aug-cc-pVnZ) are known to produce the best results for the weakly bound complexes HF and B3LYP methods were tried too for the complexes involving Ar However, the results (structural parameters and interaction energy) are far from reality, and are not included in this thesis For Ar_2-H_2S and Ar-$(H_2S)_2$ complexes, single point energy was calculated at CCSD(T) level, for the MP2 optimized geometries, using the same basis sets For the determination of the 'hydrogen bond radii' for HX (X = F, Cl, OH and SH) from the calculated intermolecular distances, calculations were performed for about sixty B---HX complexes Here MP2 and B3LYP methods were used with 6-311++G** basis set It should be noted here that our main emphasis is on the structural parameters (intermolecular distances) of the complexes Both MP2 and B3LYP methods work reasonably well for these H-bonded complexes For all the calculations GAUSSIAN 98 suite of program[24] was used

The structural parameters are obtained from the optimized geometry Frequency calculation confirms whether the optimization gives a minimum or not. The frequencies of the intermolecular modes and those involved in weak bond formation are of interest Potential Energy Surface (PES) scanning was done whenever needed

The interaction energy or stabilization energy for the complex formation is calculated in supermolecular approach[25] In this approach the interaction energy,

$$\Delta E_C = E_C - \Sigma (E_M) \qquad (4)$$

where E_M is the monomer energy However, this energy is contaminated with a kind of error known as **Basis Set Superposition Error (BSSE)** [26-28] This error arises because of the mismatch of the monomer energies while subtraction The interaction energy of a complex AB formed from its monomers A and B is

$$\Delta E_{AB} = E_{AB}^{\{AB\}} - E_A^{\{A\}} - E_B^{\{B\}} \qquad (5)$$

The monomer energies E_A and E_B are calculated using their own basis sets, i e {A} for A and {B} for B However, the dimer energy E_{AB} is calculated in dimer basis set {AB} which consists of the basis set of both the monomers A and B As the intermolecular distance decreases, the monomers A and B start using the one electron basis set of their partner in the complex A will use the available orbital of the basis set of B, {B}, and vice versa This leads to an additional artificial stabilization that has nothing to do with the interaction energy concerned This error is basically due to the incompleteness of the basis set Using a complete basis set will remove the error

However, in our calculation the BSSE is corrected by using the 'Counterpoise' method of Boys and Bernardi[29-31] According to this method, if the interaction energy has to be obtained in supermolecular approach, all the energies (dimer and monomers) should be evaluated within the same basis of the whole dimer, {AB}

$$\Delta E_{AB}^{(CP)} = E_{AB}^{\{AB\}} - E_A^{\{AB\}} - E_B^{\{AB\}} \qquad (6)$$

Where $E_A^{\{AB\}}$ is the energy of the monomer A evaluated in the dimer basis set {AB} The definition of BSSE according to this method is

$$BSSE = E_A^{\{AB\}} + E_B^{\{AB\}} - E_A^{\{A\}} - E_B^{\{B\}} \qquad (7)$$

Equation (6) and (7), for correcting and determining BSSE respectively, are valid only when the monomer geometry remains intact or nearly so on complex formation If the monomer geometries are distorted in the complex, the energies involved are different The energy associated with the distortion is a part of the interaction energy, and it should be taken into account while correcting for BSSE In such cases, first BSSE uncorrected interaction energy is calculated from equation (5) This uncorrected interaction energy is then corrected for BSSE The BSSE is evaluated as

$$BSSE = [E_A^{*\{A\}} - E_A^{*\{AB\}}] + [E_B^{*\{B\}} - E_B^{*\{AB\}}] \qquad (8)$$

where '*' indicates the monomer geometry to be as it is in the complex The CP corrected interaction energy (ΔE_{AB}^{CP}) is calculated as

$$\Delta E_{AB}^{CP} = \Delta E_{AB} + BSSE \qquad (9)$$

In most of the cases, the CP corrected interaction energy has been corrected for the zero point vibrational energy

References

1 C H Townes and A L Schawlow, *Microwave Spcetroscopy*, McGraw Hill, New York, (1955)

2 W Gordy, and R L Cook, *Microwave Molecular Spectra*, Wiley, New York, (1984)

3 T J Balle, and W H Flygare, *Rev Sci Instrumen* , **52**, 33 (1981)

4 J S Muenter, in *Structure and Dynamics of Weakly Bound Complexes* (Ed Weber, A), Reidel, Dordrecht, 3 (1987)

5 R D Suenram, J-U Grabow, A Zuban, and I. Leonov, *Rev Sci Instrumen* **70**, 2127 (1999)

6 J-U Grabow, W Stahl, and H Dreizler, *Rev Sci Instrumen* **67**, 4072 (1996)

7 J L Alonso, F J Lorenzo, J C Lopez, A Lesarri, S Mata, and H Dreizler, *Chem Phys* **218**, 267 (1997).

8 H E Warner, Y Wang, C Ward, C W Gillies, and L Interrante, *J Phys Chem* , **98**, 12215 (1994)

9 A R Hight Walker, W Chen, S E Novick, B. D Bean, and M D Marshall, *J Chem Phys* **102**, 7298 (1995)

10 M D Harmony, K A Beran, D M Angst, and L Ratzlaff, *Rev Sci Instrumen* **66**, 5196 (1995)

11 M Lida, Y Ohshima, and Y Endo, *J Chem Phys* , **94**, 6989 (1994)

12 A C Legon, in *Atomic and Molecular Beam Methods vol 2* , (Ed Scoles, G) Oxford University Press, New York, 289 (1992)

13 R E Bumgarner, and S G Kukolich, *J Chem Phys* **86**, 1083 (1987)

14 K W Hillig, J Matos, A Scioly, and R L Kuczkowski, *Chem Phys Lett* **133**, 359 (1987)

15 T C Germann, and H S Gutowsky, *J Chem Phys* **98**, 5235 (1993)

16 E Arunan, C E Dykstra, T Emilsson, and H S Gutowsky, *J Chem Phys* **105**, 8495 (1996)

17 E Arunan, T Emilsson, H S Gutowsky, and C E Dykstra, *J Chem Phys* **114**, 1242 (2001)

18 H S Gutowsky, T Emilsson, and E Arunan, *J Chem Phys* **106**, 5309 (1997)

19 Szabo and N S Ostlund, "Modern Quantum Chemistry Introduction to Advanced Electronic Structure Theory", Dover Publications Inc, Mineola, (1996)

20 D R Yarkony (ed), "*ModernElectronic Structure Theory*", Part I & II, World Scientific, Singapore (1995)

21 F Jensen, "*Introduction to Computational Chemistry*", John Wiley & Sons, New York (1999)

22 M Springborg, "*Methods of Electronic Structure Calculations*" John Wiley & Sons, New York (2000)

23 J B Foresman and A E Frisch, "*Exploring Chemistry with Electronic Structure Method*", Gaussian Inc, Pittsburgh (1996)

24 M J Frisch, G W Trucks, H B Schlegel, G E Scuseria, M A Robb, J R Cheeseman, V G Zakrzewski, J A Montgomery, Jr, R E Stratmann, J C Burant, S Dapprich, J M Millam, A D Daniels, K N Kudin, M C Strain, O Farkas, J Tomasi, V Barone, M Cossi, R Cammi, B Mennucci, C Pomelli, C Adamo, S Clifford, J Ochterski, G A Petersson, P Y Ayala, Q Cui, K Morokuma, N Rega, P Salvador, J J Dannenberg, D K Malick, A D Rabuck, K Raghavachari, J B Foresman, J Cioslowski, J V Ortiz, A G Baboul, B B Stefanov, G Liu, A Liashenko, P Piskorz, I Komaromi, R Gomperts, R L Martin, D J Fox, T Keith, M A Al-Laham, C Y Peng, A Nanayakkara, M Challacombe, P M W Gill, B Johnson, W Chen, M W Wong, J L Andres, C Gonzalez, M Head-Gordon, E S Replogle, and J A Pople, Gaussian 98, Revision A 11 3, Gaussian, Inc, Pittsburgh PA, (2002)

25 F. B van Duijneveltd, J G C M van Duijneveltd-van de Rijdt and J H van Lenthe, *Chem Rev* **94**, 1873 (1994)

26 B Liu and A D McLean, *J Chem Phys* **59**, 4557 (1973)

27 M N Szczesniak and S Scheiner, *J Chem Phys* **84**, 6328 (1986)

28 M Gutowski and G Chalasinski, *J Chem Phys* **98**, 5540 (1993)

29 S F Boys and F Bernardi, *Mol Phys* **19**, 55 (1970)

30 S Simon, M Duran and J J Dannenberg, *J Chem Phys* **105**, 11024 (1996)

31 I Alkorta, I Rozas and J Elguero, *Chem Soc Rev* **27**, 163 (1998)

Chapter III

Structure and Dynamics of Ar_2-H_2S complex: Rotational Spectroscopic and Ab Initio Studies

III.1. Introduction

Weakly bound complexes, bound by van der Waals or hydrogen bonding interactions, have attracted enormous interest in the last few decades [1-3] Coupling of molecular beam techniques with various spectroscopic methods has resulted in a wealth of experimental data on such complexes Rotational spectroscopic studies have been revolutionized by the development of the Balle-Flygare Pulsed Nozzle Fourier Transform Microwave (PNFTMW) spectrometer [4] Rotational spectra of these complexes can provide direct information about the ground state structure, which is the starting point towards developing intermolecular potential surfaces (IPS) Accurate IPS, in turn, can lead to detailed understanding of intermolecular interactions

Rare gas (RG)-molecule complexes have found a unique place in this field, starting with the very first report on the PNFTMW spectrometer [5] These complexes are useful as model systems to study the effect of dispersive and inductive forces in intermolecular interactions The RG-HX (X=halogen) complexes are particularly intriguing as all of them have the structure as written with the HX interacting with RG through H This has led Bader to conclude that these are 'hydrogen bonded' complexes[6], though such a view would not be accepted by many Recently, Aquilanti and coworkers have reported scattering studies of RG-H_2O[7] and concluded that the interaction in RG-H_2O attains hydrogen bonding character as the RG is changed from He to Xe Experimental[8] studies on Ar-H_2O complexes show only a small red-shift (1 5 cm^{-1}) in O-H stretching frequency, significantly smaller than what is commonly observed in hydrogen bonded complexes of H_2O However, today there are many examples of hydrogen bonded complexes showing a blue-shift in X-H stretching frequency [9] Wategaonkar and coworkers[10] have recently reported theoretical results that predict a 12 cm^{-1} blue shift in O-H stretching frequency for the 'hydrogen bonded' Ar-hydroquinone complex If hydrogen bonds can have red or blue shift in stretching frequencies, logic demands that there may be hydrogen bonds with no shift in stretching frequencies

It has been pointed out that the binding energies of hydrogen bonded complexes of second row hydrides (HCl and H_2S) have significant contribution from dispersive (van

der Waals?) forces compared to those of first row hydrides [11] With the objective of comparing the weakly bound complexes formed by first and second row hydrides, a systematic investigation on Ar_m-$(H_2O)_n$[12-15] and Ar_m-$(H_2S)_n$[14,16] complexes have been reported earlier This chapter reports results on Ar_2-H_2S complex and completes the series Ar_m-H_2X for *m* up to 3 and X = O and S The experiments on Ar_2-H_2S were particularly interesting given the results for Ar-H_2S[16] and Ar_3-H_2S[14] The Ar-H_2S showed an anomalous isotope effect in rotational constants [16] The rotational constant *B* for Ar-D_2S is larger than that of the Ar-H_2S complex To the best of our knowledge, this is the only example in the literature, showing an increase in rotational constant with increase in mass of an isotope (Imaginary coordinates are observed if the substituted atom is very close to the center of mass such as in N_2O[17] or H_2O-HCl[18] However, Ar-H_2S does not belong to this category The substituted atom is more than 1 Å away from the c m It turned out to be the result of an extremely floppy intermolecular potential surface[19] leading to different zero-point averaged ground state geometries for Ar-H_2S and Ar-D_2S However, an unusual trend in the rotational constants has been observed for Ne-H_2S complex and its deuterated isotopomers, by Jaeger and coworker. Though the rotational constants for Ne-HDS and Ne-D_2S are not higher than that of Ne-H_2S, but they are quite different from what one expect for a rigid structure[20]) However, Ar_3-H_2S showed a normal isotope effect [14] What will be the isotope effect on rotational constants for Ar_2-H_2S complex? What would be the ramifications of a floppy IPS on the rotational spectra of Ar_2-H_2S? How, if at all, does the Ar-H_2S distance vary in going from Ar-H_2S to Ar_3-H_2S? These questions are addressed in this work Rotational spectra for Ar_2-H_2S,/HDS/D_2S isotopomers are reported In addition, results of *ab initio* calculations are reported at MP2 and CCSD(T) levels of theory with sufficiently large basis sets, up to aug-cc-pVQZ basis set The theoretical and experimental results are compared and discussed

Our interest in H_2S complexes is strengthened by another concern Recently, we defined 'hydrogen bond radii' for all the hydrogen halides, HCN, H_2O and C_2H_2[21-23] This definition was based on experimental distances in B•••HX complexes and the electrostatic potential of isolated B[24] Though not as strong and prevalent as OH groups,

SH groups also involve in hydrogen bonding and they are important in the amino-acid cysteine and its derivatives [25,26] Experimental data on H_2S complexes are relatively scarce compared to the other HX listed above Hence, systematic investigations on several H_2S complexes are in progress in our laboratory As Argon is typically used as the carrier gas in these studies, identification and assignment of Ar_m-$(H_2S)_n$ complexes are essential to our larger objective

III.2. Experimental Details

The rotational spectra for Ar_2-H_2S and its isotopomers were observed using our home-built Balle-Flygare pulsed nozzle FT microwave spectrometer (discussed in the previous chapter) The Ar_2-H_2S complex was formed through supersonic expansion of Ar gas seeded with 1 to 2 % of H_2S The D_2S or HDS was formed by flowing H_2S through several bubblers placed sequentially and filled with either D_2O or 1 1 D_2O/H_2O mixture, respectively The back pressure was kept typically at 0 6 atm The optimum microwave pulse was of 2 0 μs duration Typically 1000 to 2000 shots were averaged to obtain a reasonable signal to noise ratio The identity of the complexes was established by confirming the presence of H_2S/D_2S/HDS and Ar No signal was observed without H_2S When He was used as the carrier gas, no signal was observed even though H_2S was present The signal appeared again as a few % of Ar was added to the gas mixture in He All gases were obtained from Bhuruka Gases Ltd and used as supplied, Ar (99 999 %), He (99 999%) and H_2S (99 5 %) D_2O was obtained from Sigma-Aldrich, 99 96 atom % D

III.3. Results And Discussions

III.3.a. Search and Assignment

The geometry of Ar_2-H_2S complex was assumed to be similar to that of Ar_2-H_2O, which is an asymmetric top having a planar structure with C_{2v} symmetry [13] In all the complexes involving Ar_2 moiety, the Ar-Ar distance is very close to 3 821Å, which is the

same as in Ar_2 dimer [23,27] It is observed that Ar/HF systems have rotational constants and rotational spectra very similar to Ar/H_2O systems For example, the rotational constants for Ar_2-H_2O (3383 MHz 1732 MHz and 1145 MHz)[13] and Ar_2-HF (3576 MHz, 1739 MHz, and 1161 MHz)[28] are quite similar The same resemblance is observed between Ar/HCl and Ar/H_2S systems This is because of the similarity in masses between HF and H_2O, and HCl and H_2S and their interactions with Ar_n A search for $2_{02}\rightarrow3_{03}$ transition was started from 5925 MHz downwards, as the corresponding transition for Ar_2-HCl occurs at 5924 MHz [29] It was found soon at 5830 1040 MHz (However, this approach is not always successful as evinced by the case of C_2H_4-H_2S The interaction between HCl and C_2H_4 is significantly stronger than that between H_2S and C_2H_4) [30] The time domain and frequency domain spectra for this particular transition are shown in Figure III 1 More transitions could be predicted readily and observed A total of 22 *a*-dipole transitions were observed for Ar_2-H_2S and 21 transitions were observed for both Ar_2-D_2S and Ar_2-HDS The search for the deuterated species was straightforward as the rigid rotor prediction from the Ar_2-H_2S constants gave rotational constants very close to the experimental values, unlike for Ar-H_2S Table III 1 contains all the observed transitions along with their residues for all three isotopomers The observed transitions were fitted to a distorted asymmetric rotor Hamiltonian using Watson S reduction[31] in I^r representation The fitted parameters and the standard deviations are shown in Table III 2 for all three complexes For Ar_2-H_2S and Ar_2-HDS, rms deviations were ~ 3 kHz However, for Ar_2-D_2S the rms deviation was 8 8 kHz, possibly due to the unresolved hyperfine splitting from D atoms In all these cases, the uncertainties in determining the rotational constants and the centrifugal distortion constants look reasonable The distortion constants show significant variation with isotopomers (H_2S, HDS and D_2S) compared to the variation observed for Ar_2-H_2O isotopomers[13] Such dramatic variation in distortion constants has been noted earlier between C_6H_6-H_2S and C_6H_6-D_2S isotopomers [32] *Ab initio* force field calculations reported later in this chapter do predict the distortion constants reasonably well However, they do not predict the variation observed for the different isotopomers It certainly is a manifestation of the floppy nature of these complexes having several large amplitude vibrations

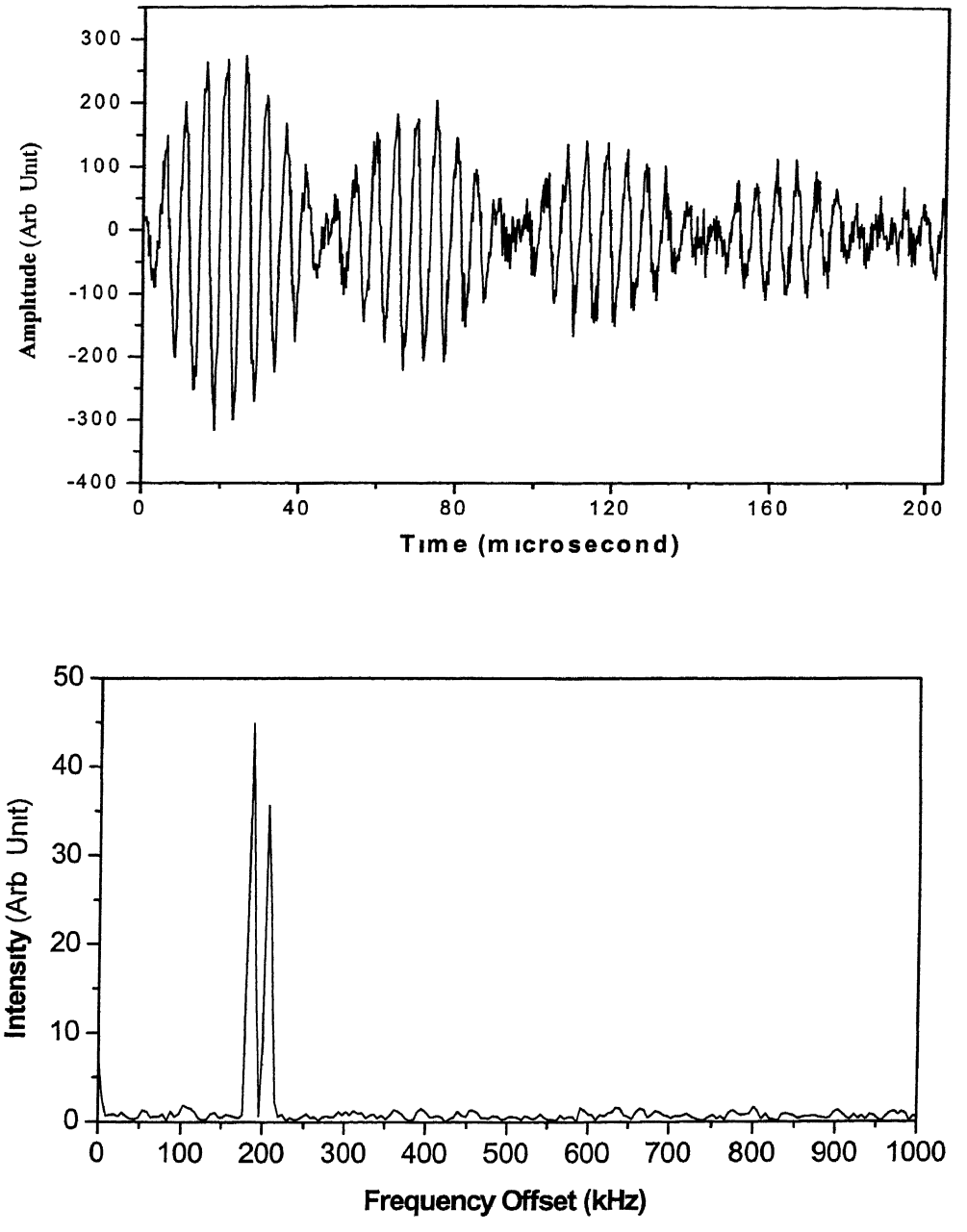

Figure III.1. Time domain and corresponding frequency domain spectra of $2_{02} \rightarrow 3_{03}$ transition of Ar_2-H_2S complex at 5830 1040 MHz The MO frequency was 5830 3 MHz 1000 gas pulses (single FID) have been averaged for this signal

Table III.1. Observed rotational transitions of Ar_2-H_2S, Ar_2-HDS and Ar_2-D_2S complexes

Transitions	Ar_2-H_2S		Ar_2-HDS		Ar_2-D_2S	
	Observed freq (MHz)	Res[a] (kHz)	Observed freq (MHz)	Res (kHz)	Observed freq (MHz)	Res (kHz)
$0_{00} \rightarrow 1_{01}$	2447 8427	-0 9	--	--	--	--
$1_{01} \rightarrow 2_{02}$	4211 9863	1 2	4200 3178	-0 3	4190 3226	-16 7
$2_{02} \rightarrow 3_{03}$	5830 1040	1 5	5808 8030	-1 2	5790 6443	-9 9
$2_{21} \rightarrow 3_{22}$	7341 3208	1 2	7291 2183	-7 9	7250 9890	0 0
$3_{03} \rightarrow 4_{04}$	7484 5311	1 7	7455 4795	0 0	7430 6364	-5 8
$1_{01} \rightarrow 2_{20}$	7614 6752	2 2	7597 6150	1 1	7586 1016	2 8
$2_{20} \rightarrow 3_{21}$	8852 6162	-0 5	8774 4476	1 1	8714 1249	-9 1
$4_{04} \rightarrow 5_{05}$	9143 5875	0 5	9107 9423	-0 4	9077 4039	-2 1
$3_{22} \rightarrow 4_{23}$	9145 6587	1 1	9103 9619	3 8	9070 2738	16 7
$5_{05} \rightarrow 6_{06}$	10802 5295	-0 5	10760 4230	0 3	10724 3530	-0 3
$4_{23} \rightarrow 5_{24}$	10825 8807	-0 6	10782 6017	2 2	10747 0090	14 1
$3_{21} \rightarrow 4_{22}$	11040 3743	-1 0	11001 0151	5 7	10969 1749	10 1
$2_{02} \rightarrow 3_{21}$	12255 3042	-0 4	12171 7410	-1 3	12109 8889	-4 6
$6_{06} \rightarrow 7_{07}$	12460 9390	-1 2	12412 3869	0 4	12370 8844	-0 1
$5_{24} \rightarrow 6_{25}$	12485 4364	-2 2	12436 2299	-0 3	12395 3050	10 7
$4_{22} \rightarrow 5_{23}$	12596 0798	-5 7	12564 6096	-6 3	12537 5096	-4 4
$4_{41} \rightarrow 5_{42}$	13630 5749	-0 6	13503 8280	5 6	13397 2790	9 7
$7_{07} \rightarrow 8_{08}$	14118 7037	-0 8	14063 7115	-0 3	14016 8880	2 3
$6_{25} \rightarrow 7_{26}$	14142 7369	-1 5	14087 0097	0 3	14040 4908	-8 8
$5_{23} \rightarrow 6_{24}$	14180 7909	7 0	14128 7516	-0 9	14084 5128	-11 5
$4_{40} \rightarrow 5_{41}$	14945 3465	0 0	14760 3978	-2 9	14613 1809	-3 8
$8_{08} \rightarrow 9_{09}$	15775 7315	1 4	15714 3046	0 0	15662 2745	-0 2

[a] Residue = Observed - calculated

Table III.2. Fitted rotational constants, centrifugal distortion constants and standard deviations (SD) of the fits for Ar_2-H_2S, Ar_2-HDS and Ar_2-D_2S Number of transitions (#) fitted for each isotopomer is also included

Parameters	Ar_2-H_2S	Ar_2-HDS	Ar_2-D_2S
A (MHz)	1733 098 (1)	1734 213 (1)	1735 405 (4)
B	1617 6570 (5)	1604 4189 (7)	1594 515 (2)
C	830 2755 (3)	827 0251 (3)	824 0730 (9)
d_1 (kHz)	9 269 (5)	8 85 (1)	7 53 (2)
d_2	25 58 (2)	40 28 (3)	81 94 (8)
D_J	22 20 (1)	21 37 (1)	18 20 (4)
D_{JK}	3 34 (4)	33 26 (6)	117 1 (2)
D_K	6 17 (8)	-22 3 (1)	-101 0 (3)
SD (kHz)	2 3	3 1	8 6
#	21	20	20

The vibrationally averaged structure has C_{2v} symmetry as all the transitions observed are between states $J_{Kp,Ko}$, which have K_p and K_o either *even-even* (*ee*) or *even-odd* (*eo*) Transitions corresponding to *oe/oo* levels could not be seen, though they could be predicted accurately The C_2 axis interchanges the two identical spin zero (I=0) Ar nuclei and it happens to be the '*a*' axis for the complex According to nuclear spin statistics, the levels with '*oo*' and '*oe*' will be missing The same is true for Ar_2-HCl complex as well [29] For Ar_2-HF and Ar_2-H_2O complexes the C_2 axis is the '*b*' axis and '*eo*' and '*oe*' levels have zero statistical weights

The sensitivity of the spectrometer below 3 GHz was not good enough to get a good S/N ratio The $0_{00}\rightarrow 1_{01}$ transitions were not observed for –HDS and –D_2S complexes and in the higher J transitions, the nuclear hyperfine splitting due to D atom(s) could not be resolved Hence, quadrupole coupling constants could not be determined Based on the experimental results for Ar-H_2S[16] and Ar_2-H_2O[13], two sets of transitions were expected for Ar_2-H_2S/D_2S, corresponding to the internal rotor/tunneling states

involving different spin states of H_2S/D_2S However, so far even after extensive searches both above and below the observed lines, no transitions could be unambiguously assigned to a second state As Ar and H_2S have similar masses, it is suspected that several transitions of Ar-$(H_2S)_2$ also occur in the same region Many transitions have been assigned for Ar-$(H_2S)_2$ now (see chapter IV) and it is hoped that unambiguous conclusions about internal rotors states of Ar_2-H_2S will emerge However, for both Ar_3-H_2S and Ar_3-H_2O complexes also, only one state has been found [14] Our attempts to look for Ar_2-$H_2{}^{34}S$ were not successful either

III.3.b. Structure

The fact that '*oo*' and '*oe*' levels are missing also indicates that H_2S undergoes large amplitude internal motion within the complex If H_2S were to be rigid and symmetrically bound to Ar_2 (as in Figure 1), the spin statistics would be similar to that of C_2H_2 and all rotational levels should be present If it was rigid but not symmetrically bound, the complex could not have a C_2 axis The rotational constant A for Ar_2-H_2S is 1733 115(1) MHz, which is very close to that of free Ar_2 dimer [27] For the –HDS and –D_2S complexes, A is within 1-2 MHz of the above value A rigid structure will have significantly different A for the three complexes The A rotational constants for Ar_2-H_2S and Ar_2-HDS differ by 4-6 MHz for rigid structures and for Ar_2-D_2S and Ar_2-H_2S, this difference is about 10 MHz Clearly, the H_2S unit is not contributing to the A rotational constant of the complex This, again, happens due to the large amplitude internal rotation of H_2S monomer within the complex

The intermolecular separation can be determined using the following inertial equations As H_2S does not contribute to the moments about the a axis, it was assumed to be spherical in this analysis

$$I_a = I(Ar_2) = \tfrac{1}{2}\, mr^2 \qquad (1)$$

$$I_b = \mu_c R^2 \qquad (2)$$

$$I_c = \tfrac{1}{2}\, mr^2 + \mu_c R^2 \qquad (3)$$

Here 'm' is the mass of Ar, 'r' is the Ar-Ar- distance, 'R' is the distance between center of masses of H_2S and Ar_2 unit and 'μ_c' is the reduced mass of the complex The structural parameters 'r' and 'R' and the inertial axis system are defined in Figure III 2 From equation (1), using the Ar_2-H_2S rotational constants, the 'r' value comes out to be 3 820 Å, which is almost identical to the Ar-Ar distance in free Ar_2, 3 821 Å The Ar_2-HDS and Ar_2-D_2S constants give this value as 3 819 Å and 3 818 Å, respectively Equation (2) and (3) lead to 'R' values of 3 620 Å and 3 646 Å respectively for Ar_2-H_2S and it is taken as 3 633 Å From these results, the distance between the c m of complex and the c m (H_2S) is determined to be 2 549 Å These values also correspond to the Ar-c m (H_2S) distances, R_1, of 4 093 Å and 4 116 Å, respectively, giving an average value of 4 105 Å The R_1 for Ar-H_2S and Ar_3-H_2S are 4 013 Å and 4 112 Å, respectively Thus, R_1 for Ar_2-H_2S appears to be very close to those of Ar-H_2S and Ar_3-H_2S and lie in between these values For comparison, Ar_2-D_2S rotational constants lead to 4 052 Å and 4 077 Å for R_1, from Equations 2 and 3, respectively The experimental inertial defect is

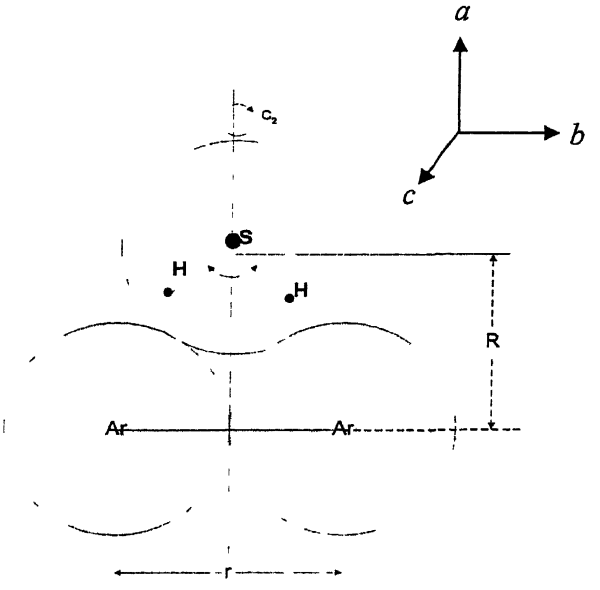

Figure III.2. Experimentally observed, vibrationally averaged geometry of Ar_2-H_2S The H_2S orientation cannot be determined accurately with the experimental data and so a sphere is shown R is the distance between the centers of masses of H_2S and Ar_2 r is the Ar-Ar distance

4 650 a m u Å^2 This large and positive value supports an effectively planar structure for this complex This, again, is similar to Ar_2-H_2O complex,[13] which has an inertial defect of 3 52 a m u Å^2

The above structural analysis gives mainly the distances between the three monomers in Ar_2-H_2S Qualitative information about the orientation of H_2S can be obtained using the rotational constants of the three isotopomers, Ar_2-H_2S/HDS/D_2S It is qualitative because of the floppy nature of the complex and also the fact that the substituted atoms are H/D The distance of the substituted atom from the c m is given by[33]

$$|r| = \left[\left(\frac{1}{2\mu}\right)(\Delta I_a + \Delta I_b + \Delta I_c)\right]^{\frac{1}{2}} \qquad (4)$$

Here μ is the reduced mass for substitution, MΔm/(M+Δm) The distances for the two hydrogens are determined to be 1 547 Å and 1 401 Å These distances may be contrasted with the results from C_2H_4-H_2S complex [30] It is a very floppy complex as well, with both C_2H_4 and H_2S exhibiting large amplitude motions within the complex A similar substitution analysis led to distances of 1 034 Å and 2 163 Å, clearly indicating that only one hydrogen is pointing towards the π center in C_2H_4 [30] It appears that, in Ar_2-H_2S both hydrogens of H_2S are pointing towards Ar_2 It is also consistent with the distance between

Table III.3. The structural parameters for Ar_2-H_2S obtained from different levels of theory and experiment The parameters are defined in figure III 2 & III 3 The distances are given in Å and the inertial defects are given in amu Å^2

Parameters[a]	6-311++G**		6-311++G (3df,2p)	6-311++G (3df,3pd)	aug-cc-pVDZ	aug-cc-pVTZ	aug-cc-pVQZ	Expt
	A	B						
R	3 584	3 730	3 625	3 559	3 638	3 507	3 487	3 633
r	4 064	4 051	3 820	3 816	3 882	3 743	3 730	3 820
R_1	4 120	4 244	4 097	4 038	4 123	3 975	3 954	4 105
Δ(=I_c-I_a-I_b)	-3 7	-1 31	-3 8	-3 7	-3 8	-3 8	-3 8	4 7

c m (Ar_2-H_2S)-c m (H_2S) from the inertial analysis (2 549 Å) reported above The orientation of H_2S can not be determined any more accurately with the experimental data presented here and hence Figure III 2 shows a sphere around H_2S All the structural parameters including inertial defects (Δ) for Ar_2-H_2S are given in Table III 3 along with results from *ab initio* calculations, which are discussed next

III.3.c. *Ab Initio* Calculations

The *ab initio* calculations were done to determine the optimized geometry and the stabilization energies for Ar_2-H_2S In addition Potential Energy Surface (PES) was scanned to determine the barrier for internal rotation of H_2S within the complex Gaussian 98 software package[34] and PC-GAMESS[35] were used for calculations Frequency calculations were done to ascertain the nature of the stationary points The vibrational force field from the PC-GAMESS calculations were also used to estimate the centrifugal distortion constants using FCONV/VIBCA codes available through the PROSPE data base [36]

Initially, geometry optimization was done at MP2/6-311++G** level with single point energy calculations at CCSD(T)/6-311++G** level of theory It led to two different minima as shown in Figure 3 (a) and (b) The transition state connecting these minima was identified as well However, it was noted that the BSSE (Basis Set Superposition Error) corrections to the stabilization energies resulted in artificial positive energy Later on, calculations were done with larger basis sets such as aug-cc-pVTZ and aug-cc-pVQZ The complete list of structural parameters for all the optimized geometries is given in Table III A and III B The absolute energies of the complex and the fragments are given in Table III C to Table III F The rotational constants corresponding to each optimized structure are tabulated in Table III G Tables III A to III G are collectively given at the end of this chapter The results of all these calculations are presented and discussed next

III.3.c.1. Structure at MP2/6-311++G** level

The initial geometry for optimization was given as a planar C_{2v} symmetric structure However, optimization at MP2/6-311++G** level of theory led to a non-planar geometry with C_1 symmetry as shown in Figure III 3 (A) Frequency calculation confirmed it to be a true minimum This structure is very close to a C_{2v} symmetric geometry having H_2S plane perpendicular to the Ar-Ar bond Both hydrogen atoms are pointing towards the Ar atoms and the S is away from them The Ar-Ar distance, r, is 4 038 Å and the distance between the centers of masses of H_2S and Ar_2, R, is 3 609 Å The

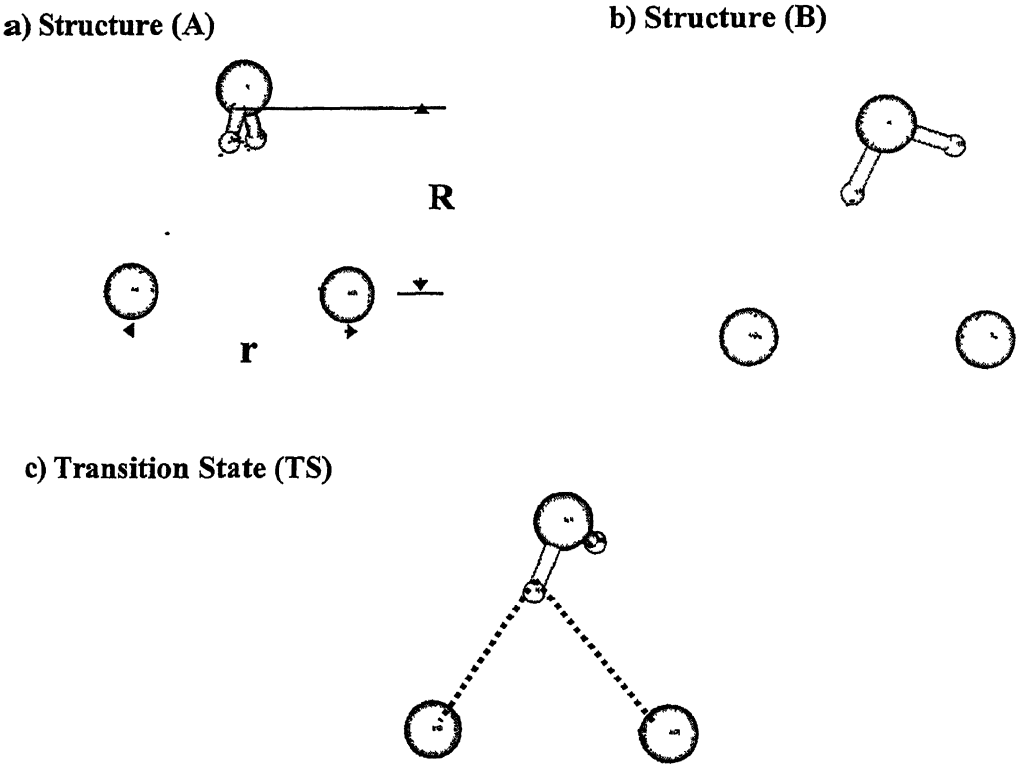

Figure III.3. (a) Optimized structure of Ar_2-H_2S in the MP2/6-311++G** level of theory The H_2S plane is perpendicular to the Ar-Ar bond Both the hydrogens are pointed towards Ar atoms (b) Optimized structure of the minimum B, found in the PES scan, at the same level of theory (c) Transition state between structure A and B See Figure III 4 for the HSArAr dihedral angle for the three structures

distance from Ar to the H_2S center of mass is 4 135 Å, slightly larger than the experimental value

Experimental results indicate that the H_2S is exhibiting large amplitude internal motion within the complex Hence, it was decided to do a PES scan to determine the barrier for internal rotation of H_2S Scanning was done starting from the MP2 optimized geometry (structure A) at the same level of theory (MP2/6-311++G**) In this scan the dihedral angle between H_2S plane and the Ar-Ar-S plane was intended to vary by 10 0 degrees per step Specifically, d_{HSArAr} was varied in steps of 10 degrees Except for the Ar-S-Ar angle, all parameters were allowed to relax and hence the scanning did not correspond to a simple rotation of H_2S about its *b* axis The main reason for doing the scanning in this manner was the fact that the initial optimization corresponding to the planar structure did not yield any stationary points, minimum or a saddle point of any order Hence, for each value of d_{HSArAr}, all other parameters were optimized The initial value of the dihedral angle was –64 88° and it was varied in both directions, 90° in each,

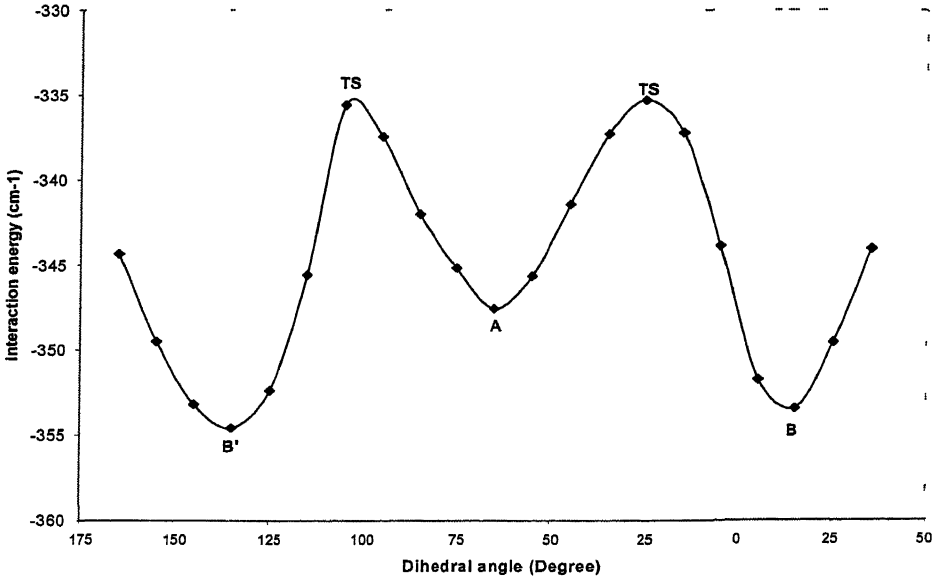

Figure III.4. Potential energy surface scan The reaction coordinate is the dihedral angle d_{HSArAr} (see Figure III 3) The y-axis is the difference in energy between the complex and its components ($\Delta E = E_{complex} - 2E_{Ar} - E_{H2S}$)

to complete a total of 180° rotation The result of the scan is shown in Figure III 4 Two equivalent minima were found on either side of the structure 'A' These two minima are labeled as 'B' and 'B'' These structures had only one hydrogen pointing towards the Ar-Ar bond, asymmetrically i e H is close to one Ar (3 03 Å) than the other (3 50 Å) These were fully optimized again at the same level of theory (MP2/6-311++G**) to obtain more accurate geometry and energies This second minimum (B or B') is ~8 0 cm^{-1} lower in energy compared to A The dihedral angles d_{HSArAr} are 11 78° and −135 16° for B and B', respectively The Ar-Ar distance is almost the same as that in Structure A, 4 05 Å However, the H_2S unit is slightly away from Ar_2 compared to A The distance between centers of masses of Ar_2 and H_2S, R, is 3 73 Å and Ar-c m (H_2S) is 4 24 Å Figure III 3(b) shows the optimized geometry of structure B and the Figure III 3(c) shows the transition state connecting structures A and B The transition state has also been optimized at the same level of theory In the transition-state, one hydrogen is directed towards the Ar_2 and the d_{HSArAr} dihedral angle is in between those in the two minima, i e −26 11° The energy barrier (ΔE_B) going from structure A to B is only 11 5 cm^{-1} at MP2

Table III.4. The vibrational frequencies for all the minima and transition states, calculated at MP2/6-311++G** level of theory All values are in cm^{-1}

Normal modes	MP2/6-311++G**				
	A	B	B'	TS1	TS2
Intermolecular stretching (Ar-Ar)	20	20	20	20	19
Intermolecular stretching (Ar-H_2S)	28	29	29	29	28
Intermolecular stretching (Ar_2-H_2S)	38	39	39	42	41
Torsion about 'b' of H_2S*	40	47	47	-40	-36
Torsion about 'a' of H_2S	49	75	75	49	50
Torsion about 'c' of H_2S	97	106	105	87	93
H_2S bending	1230	1237	1237	1231	1232
H_2S symmetric stretch	2818	2820	2820	2819	2818
H_2S asymmetric stretch	2837	2840	2840	2839	2838

*Reaction coordinate for A → B conversion

level calculation Single point calculations of the stationary points at CCSD(T) level yielded a value very close to that at MP2 level, 11 8 cm^{-1}

For all the optimized geometries (three minima and one transition state), the vibrational frequencies have been calculated and are given in Table III 4 All minima had only positive Eigen values in the Hessian However, as expected, the two transition states had one negative value in Hessian The vibrational motion corresponding to this imaginary frequency was confirmed to be the reaction coordinate for going from structure A to B The vibrational frequencies for all three stationary points (Table III 4) indicate that the zero point level is significantly above the barrier This supports the experimental observation that H_2S undergoes large amplitude motions within the complex However, the nature of the PES with two different minima (A and B) suggests that the large amplitude motion is unlikely to be simple internal rotation of H_2S about its C_2 axis

III.3.c.2. Stabilization Energies at MP2 and CCSD(T) Levels with 6-311++G** Basis Set

The interaction energy has been calculated using the super-molecule approach According to this approach the interaction energy is evaluated as

$$\Delta E = E_{complex} - E_{Ar} - E_{Ar} - E_{H2S} \qquad (5)$$

Table III 5 shows the interaction energies calculated for all five stationary points for MP2 and CCSD(T) methods using 6-311++G** basis set These values were corrected for Basis Set Superposition Error (BSSE) using the Counterpoise method [37-39] The BSSE is calculated as

$$BSSE = [E_{Ar1}^*(M) + E_{Ar2}^*(M) + E_{H2S}^*(M)] - [E_{Ar1}^*(C) + E_{Ar2}^*(C) + E_{H2S}^*(C)] \qquad (6)$$

where '*' indicates that the monomer geometry is distorted and is same as in the complex, (M) and (C) indicate whether the energies are calculated in monomer or complex basis set respectively The CP corrected interaction energy is,

$$\Delta E^{CP} = \Delta E + BSSE \qquad (7)$$

Usually, the CP corrected interaction energy is given as[11]

$$\Delta E^{CP} = E_{complex} - E_{Ar1}^{*}(C) - E_{Ar2}^{*}(C) - E_{H2S}^{*}(C) \quad (8)$$

According to Eq (8),

$$BSSE = [E_{Ar1}(M) + E_{Ar2}(M) + E_{H2S}(M)] - [E_{Ar1}^{*}(C) + E_{Ar2}^{*}(C) + E_{H2S}^{*}(C)] \quad (9)$$

The BSSE calculated from Equations (6) and (9) will be significantly different, if the monomer geometries are distorted on complex formation It is important for hydrogen bonded complexes of HF and H_2O, for instance [40] For the Ar_2-H_2S complex, the difference in BSSE calculated between Equations (6) and (9), is only 0 5 cm^{-1} at MP2/6-311++G** level calculations In any case, in this work, BSSE has been reported using Equation 6 only.

ΔE^{ZPE} is the interaction energy after zero-point vibrational energy correction over ΔE^{CP} For structure A, the stabilization energy of 347 6 cm^{-1} is obtained with MP2 method without BSSE correction The CCSD(T) value is again close to the MP2 result and it is 353 6 cm^{-1} For structure B the stabilization energies, without BSSE correction, are 355 4 cm^{-1} and 362 7 cm^{-1} with MP2 and CCSD(T) methods, respectively

Table III.5. Interaction energies for all five stationary points (three minima and two transition states) calculated at MP2 and CCSD(T) method using 6-311++G** basis set

Energy	MP2/6-311++G**					CCSD(T)/6-311++G**				
(cm^{-1})	A	B	B'	TS1	TS2	A	B	B'	TS1	TS2
ΔE	-347 5	-355 4	-355 4	-336 1	-335 6	-353 6	-362 5	-362 5	-341 7	-341 7
BSSE	394 2	395 3	395 4	376 4	368 3	407 9	413 5	413 5	391 7	383 1
ΔE^{CP}	46 8	39 9	40 0	40 3	32 7	54 3	51 0	51 0	50 0	41 4
ΔE^{ZPE}	181 9	203 7	203 4	156 5	148 4	190 0	214 8	214 4	166 2	157 1

Employing the BSSE correction using counterpoise method leads to artificial positive stabilization energies for all cases This is due to incompleteness of the basis set used The BSSE can be reduced significantly to obtain a reliable interaction energy using

higher basis sets (approach to complete basis set limit) Hence the calculations have been performed at MP2 method using higher basis sets, 6-311++G(3df,2p), 6-311++G(3df,dpd), aug-cc-pVDZ, aug-cc-pVTZ and aug-cc-pVQZ and these are discussed next

III.3.c.3. Results With Higher Basis Sets

III.3.c.3.a. Geometry

Structure A has been optimized at MP2 level using all the above basis sets All calculations resulted in a true minimum with all positive eigen values in the Hessian except for the calculation with aug-cc-pVDZ basis set, which resulted in a saddle point of order 2 Further, CCSD(T) single point energy calculations were done for all MP2 optimized geometries (except aug-cc-pVQZ) using the same basis set that was used for optimization However, Structure B and B' could not be optimized using any of the higher basis sets The optimizations never converged The geometry, optimized at MP2/6-311++G(3df,2p) level is shown in Figure III 5 The figure also shows the axis system of both the Ar_2-H_2S complex and H_2S monomer in the complex The axis system denoted as '*a, b, c*' is for the complex and the axis system denoted as '*a', b', c'*' is for H_2S monomer All the structural parameters for the optimized geometries using these basis sets are listed in Table III 3 along with the experimental and lower basis set values

The Ar-Ar and Ar-c m (H_2S) distances both reduce with increasing basis size The distances calculated at MP2/6-311++G(3df,2p) are fortuitously close to the experimental values Particularly, the Ar-Ar distance calculated at this level (3 820 Å) is very close to the R_0 for Ar_2 dimer[27], 3 822(2) Å However, the R_e for Ar_2 is less at 3 763 Å[27], and not surprisingly, higher basis sets give better agreement The structural parameters do show some convergence and the basis sets used, appear to be large enough It is evident from the theoretical stabilization energies as well and they are discussed next

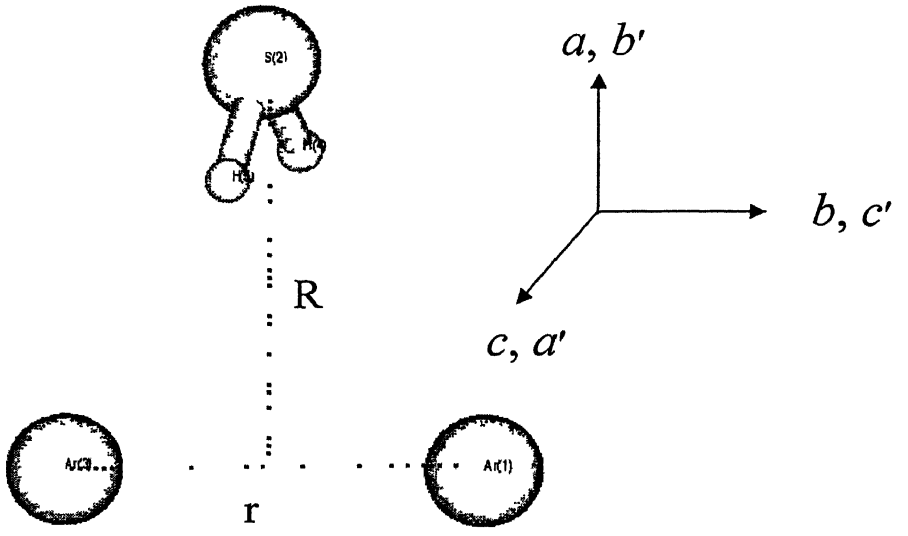

Figure III.5. Optimized structure of Ar_2-H_2S at MP2/6-311++G(3df,2p) level of theory This is exactly C_{2v} symmetric structure with all the structural parameters very close to experimental ones *a, b, c* is the axis system of the complex whereas *a', b', c'* is that of H_2S monomer R is the distance between the centers of masses of H_2S and Ar_2, r is the Ar-Ar distance, and R_1 (not shown) is the distance between Ar and c m (H_2S)

III.3.c.3.b. Interaction energy and barrier energies for internal rotation

Table III 6 shows the interaction energies calculated at MP2 and CCSD(T) level calculations with various basis sets The BSSE is significant (394 cm^{-1}) at MP2 level with 6-311++G** basis set and in fact it is larger than the absolute value of interaction energy (-348 cm^{-1}), leading to net 'destabilization' It is interesting to note that single point calculations at CCSD(T) level with this small basis set, increases both ΔE (-354 cm^{-1}) and BSSE (408 cm^{-1}) As the increase in BSSE is more than that of ΔE, the results look worse at CCSD(T) level than at MP2 level As the basis size is increased to 6-311++G(3df,2p), ΔE increases and BSSE reduces by more than half, leading to a net stabilization of -263 cm^{-1} As the basis size is increased to aug-cc-pVQZ, the BSSE reduces to 70 cm^{-1} only, ~ 15 % of the interaction energy of - 471 1 cm^{-1} The ZPE correction increased from 103 cm^{-1} with 6-311++G (3df,2p) basis set to 117 cm^{-1} with

aug-cc-pVTZ basis set This increase could be due to the over-estimation of intermolecular vibrational frequencies and it appears that these frequencies should be scaled by 0 7, see next section The stabilization energy calculated at MP2 level calculations with aug-cc-pVDZ/pVTZ/pVQZ were used to extrapolate to CBS limit [41] At this limit, the binding energy of Ar_2-H_2S is 507 cm^{-1} and 418 cm^{-1}, respectively without and with ZPE corrections

Table III.6. The interaction energies obtained from *ab initio* calculations [a] The values are in cm^{-1}

Energy	6-311++G**		6-311++G(3df,2p)		aug-cc-pVDZ		aug-cc-pVTZ		aug-cc-pVQZ	CBS
	MP2	CCSD(T)	MP2	CCSD(T)	MP2	CCSD(T)	MP2	CCSD(T)	MP2	MP2
ΔE	-347 7	-353 6	-418 3	-364 3	-393 4	-352 0	-484 1	-421 5	-471 1	--
ΔE^{CP}	46 2	54 3	-263 0	-197 9	-242 4	-188 7	-350 9	-290 9	-401 1	-507 1
ΔE^{ZPE}	181 9	190 0	-159 8	-94 7	-125 1[b]	-71 4[b]	-233 6	-173 6	-283 8[b]	-418 2
BSSE	394 2	407 9	155 3	166 3	151 0	163 3	133 2	130 6	70 0	--

[a] ΔE^{ZPE} is the interaction energy after zero-point vibrational energy correction over ΔE^{CP} CBS extrapolation was done using the aug-cc-pVnZ results (Ref 41)

[b] Zero point energy corrections used vibrational frequencies calculated at MP2/ aug-cc-pVTZ level

As discussed in the previous section, experimental results do indicate that the H_2S is quite floppy within the complex Hence, it was decided to determine the barriers for internal rotation of H_2S about its principal axes, within the complex by doing potential energy scans Energies were calculated by varying the corresponding angles by 10 degrees every step, keeping the other structural parameters fixed To simplify the

calculations, S was held fixed The results of MP2/6-311++G(3df,2p) calculations are shown in Figure III 6 Not surprisingly, internal rotation about the *b* axis of H_2S has the lowest barrier of only 10 cm^{-1} It is less than the zero point energy along this torsional coordinate (13 5 cm^{-1}) The barrier for rotation about *a* and *c* axes are also small, 53 and 47 cm^{-1}, respectively The corresponding torsional frequencies are 49 and 43 cm^{-1}, respectively It is clear that the H_2S can exhibit very large amplitude motions within the complex

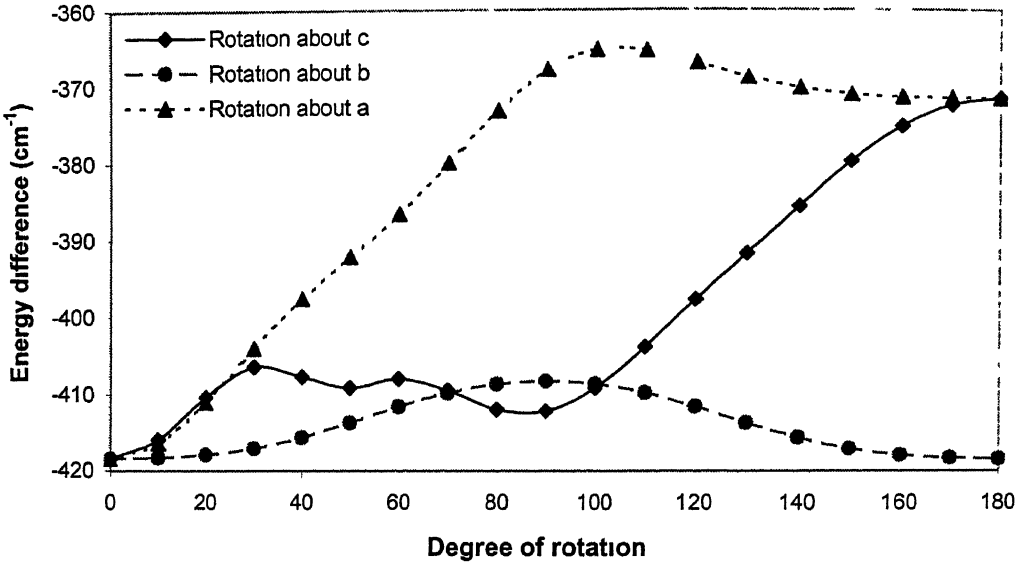

Figure III.6. PES scan for H_2S internal rotation about its inertial axes *a*, *b* and *c* All other coordinates have been kept unchanged during the scan The 'y' axis is the difference between the energies of the complex and its constituting monomers.

III.3.c.3.c. Vibrational frequencies and centrifugal distortion constants

The vibrational frequencies calculated at MP2/6-311++G(3df,2p) and MP2/aug-cc-pVTZ levels of theory are given in Table III 7 The only experimental result available for comparison is that of Ar-Ar stretching, observed in the free Ar_2 dimer[27], which is 30 68 cm^{-1} It is predicted to be 26 cm^{-1} in Ar_2-H_2S, which seems reasonable A more stringent test would be the comparison of centrifugal distortion constants from this *ab*

initio force field with the experimental values Kisiel and coworkers[42] have carried out such analysis for Ar_2-HF/HCl/HBr and a similar analysis was done here for Ar_2-H_2S The FCONV/VIBCA codes were used to determine the centrifugal distortion constants from the *ab initio* force field Table III 8 gives the centrifugal distortion constants and the harmonic vibration-rotation contribution to the inertial defect, determined from the force field with and without scaling (It should be remembered that the equilibrium inertial defect from the calculations (see Table III 3) is about -3 8 a m u Å^2, as the out of plane protons do contribute in the equilibrium structure In this Table, it has been assumed to be zero as the H_2S appears to be nearly spherical in the complex) A frequency scaling factor of 0 7 gives a reasonable agreement for three of the five distortion constants (D_J, D_{JK} and D_K) The other two constants (d_1 and d_2) are of smaller magnitude in comparison They are predicted to be of the right order of magnitude but wrong signs For Ar_2 -HBr and Ar_2-HCl, Kisiel and coworkers found that a frequency

Table III.7. All the vibrational frequencies of Ar_2-H_2S, bending and stretching frequencies of H_2S in H_2S-H_2S (both H-bond donor and acceptor) and free H_2S The values are calculated at the MP2 level using 6-311++G(3df,2p) and aug-cc-pVTZ basis sets. All the values are given in cm^{-1}

Vibrational Modes	MP2/6-311++G(3df,2p)			MP2/aug-cc-pVTZ		
	Ar_2-H_2S	H_2S-H_2S*	H_2S	Ar_2-H_2S	H_2S-H_2S*	H_2S
Intermolecular bending	26	--	--	32	--	--
Intermolecular stretching (Ar-Ar)	26	--	--	26	--	--
Torsion about 'b' of H_2S	27	--	--	19	--	--
Intermolecular stretching (Ar_2-H_2S)	37	--	--	45	--	--
Torsion about 'c' of H_2S	43	--	--	43	--	--
Torsion about 'a' of H_2S	49	--	--	63	--	--
H-S-H bending	1214	1223/1215	1217	1209	1216/1209	1212
S-H symmetric stretch	2776	2741/2773	2776	2773	2729/2769	2771
S-H asymmetric stretch	2794	2786/2792	2795	2792	2783/2789	2791

*First entry is for the donor H_2S and the second entry is for acceptor H_2S

scaling factor of 0 8 works better [42] Though, the scaling improves the agreement with centrifugal distortion constants, it is obvious that the Ar-Ar stretching frequency would become even smaller However, this appears to be a general trend with Ar_2-HX clusters as this frequency is estimated to be 21 cm^{-1}, 24 cm^{-1} and 23 cm^{-1} for Ar_2-HCl[43], Ar_2-OCS[44] and Ar_2-N_2O[45] by analyzing the respective centrifugal distortion constants

Table III.8. Distortion constants (kHz) and inertial defects[a] (a m u Å^2) from experiment and *ab initio* force field

Distortion constants	Experiment	MP2/6-311++G(3df,3pd)		MP2/aug-cc-pVTZ	
Frequency Scaling factor	1 0	1 0	0 7	1 0	0 7
d_1	-2 26 (2)	3 14	6 29	3 74	7 49
d_2	2 565 (5)	-0 91	-1 81	-0 80	-1 60
D_J	41 34 (2)	19 09	38 17	20 15	40 30
D_{JK}	-69 47 (6)	-31 35	-62 69	-32 87	-65 74
D_K	31 79 (4)	13 95	27 89	14 53	29 05
δI_a	-	-1 835	- 2 595	- 1 582	-2 237
δI_b	-	-1 735	- 2 454	- 1 667	-2 358
δI_c	-	-0 708	- 1 002	- 0 497	-0 703
Δ	4 650	2 862	4 047	2 751	3 891

[a] Harmonic vibration-rotation contribution to inertial defect, defined as $I_\alpha = (I_o)_\alpha - \delta I\alpha$

Despite the reasonable agreement between the experimental centrifugal distortion constants and those derived from a scaled *ab initio* force field, there are at least two experimental observations that point to the inadequacy of the *ab initio* force field 1) The distortion constants for Ar_2-HDS and Ar_2-D_2S are predicted to be very similar to those of Ar_2-H_2S (within 5%) Experimental distortion constants (see Table III 2) for the three isotopomers vary by 60-70 % 2) The inertial defect calculated from the harmonic vibration-rotation contribution is 4 047/3 891 a m u Å^2 with 6-311++G(3df,2pd) and aug-cc-pVTZ basis sets, compared to the experimental value of 4 650 a m u Å^2 In comparison, for Ar_2-HF/HCl/HBr Kisiel and coworkers[42] found much better agreement

between the experimental inertial defect and that calculated from the harmonic vibration-rotation contribution at MP2/aug-cc-pVDZ calculations These observations highlight the fact that the IPS for Ar_2-H_2S is floppier than the IPS for the relatively strongly bound Ar_2-HX systems It is hoped that the experimental results reported in this manuscript would stimulate development of more accurate IPS for Rg-H_2S complexes

In the Introduction, we commented about the shift in vibrational frequencies observed following complex formation Table III 7 compares the intra-molecular vibrational frequencies involving H_2S for Ar_2-H_2S, H_2S-H_2S, and free H_2S, as well The S-H stretching frequencies calculated for Ar_2-H_2S are both within 2 cm^{-1} of those corresponding to free H_2S AT MP2/6-311++G(3df, 2p) level, there is a 1 cm^{-1} red shift and at MP2/aug-cc-pVTZ level there is a 1-2 cm^{-1} blue shift These results suggest that one needs to exercise caution in interpreting small blue shifts Interestingly, the S-H stretching frequencies calculated for the acceptor H_2S in $(H_2S)_2$ show a red-shift of 2-3 cm^{-1} compared to the monomer values The stretching frequency for donor H_2S in $(H_2S)_2$ shows a red-shift of 42 cm^{-1} For comparison, the red-shift observed in OH stretching frequency[46] for the strongly hydrogen bonded $(H_2O)_2$ is significantly higher at 226 cm^{-1} From the vibrational frequency shifts observed, $(H_2S)_2$ could easily be classified as a hydrogen bonded complex However, the same can not be concluded about Ar-H_2O (1 5 cm^{-1} red-shift)[8] or Ar-H_2S complex Considering Aquilanti et al 's recent work on Rg-H_2O complexes[7], it may be expected that the frequency shifts observed in Rg-H_2O and Rg-H_2S would be more pronounced as Rg is changed from He to Xe

III.4. Conclusions

The rotational spectra for Ar_2-H_2S and its isotopomers have been observed using PNFTMW spectrometer It exhibits normal isotope effect unlike Ar-H_2S dimer Again, unlike Ar-H_2S, only one set of transitions has been observed The experimental rotational constants are consistent with a vibrationally averaged heavy-atom C_{2v} symmetric structure with both hydrogen atoms pointing towards Ar_2 The Ar-Ar and Ar-H_2S distances are determined to be 3 820 Å and 4 105 Å, respectively The Ar-H_2S distance falls in between those determined for Ar-H_2S dimer (4 013 Å) and Ar_3-H_2S tetramer (4 112 Å) *Ab initio* calculations have also been reported at MP2 and CCSD(T) levels with large basis sets up to aug-cc-pVQZ MP2 results give a minimum energy structure, which is non-planar with C_{2v} symmetry where H_2S plane is perpendicular to the Ar-Ar bond and both hydrogens are pointing towards Ar_2 The CBS extrapolation for binding energy of this complex is about 507 cm^{-1} The vibrational force field from *ab initio* calculations could reasonably reproduce the experimental centrifugal distortion constants for the parent isotopomer, but they do not predict the changes on D substitution The harmonic-vibration-rotation contribution to the inertial defect is significantly below the experimental inertial defect, unlike that of Ar_2-HX (X=F,Cl and Br)

Table III.A. Optimized structural parameters of different minima and transition states of Ar_2-H_2S system at MP2/6-311++G** level of theory

Parameters	6-311++G**				
	A	B	B'	TS1	TS2
R(1,2)	4 1675	4 3294	4 3289	4 3054	4 3156
R(1,3)	4 0644	4 0512	4 0513	4 0591	4 0732
R(1,4)	3 5238	4 7882	3 0296	4 2713	3 1242
R(1,5)	3 5203	3 0298	4 7879	3 1071	4 2840
R(2,3)	4 1682	4 1588	4 1588	4 1740	4 1961
R(2,4)	1 3334	1 3335	1 3332	1 3335	1 3334
R(2,5)	1 3334	1 3332	1 3335	1 3332	1 3336
R(3,4)	3 5231	3 6217	3 5030	3 5607	3 5391
R(3,5)	3 5244	3 5016	3 6211	3 5219	3 5592
A(4,1,5)	17 5	11 6	11 6	24 2	24 1
A(4,2,5)	92 1	92 1	92 1	92 0	91 9
A(4,3,5)	31 6	31 2	31 2	31 4	31 3
D(4,2,3,1)	64 9	135 1	-11 9	101 6	26 8
D(5,2,3,1)	-64 7	11 8	-135 2	-26 1	-102 7

Ar 1 S 2 Ar 3 H4 H5

Table III.B. Optimized structural parameters of different minima and transition states of Ar_2-H_2S system at different levels of theory

Parameters	6-311++G(3df,2p)	6-311++G(3df,3pd)	Aug-cc-pVDZ	aug-cc-pVTZ	aug-cc-pVQZ
R(1,2)	4 146	4 0364	4 1234	4 0124	4 0033
R(1,3)	3 8203	3 8166	3 8824	3 7432	3 7301
R(1,4)	3 4868	3 3824	3 4661	3 3608	3 3530
R(1,5)	3 4868	3 3824	3 4661	3 3608	3 3530
R(2,3)	4 1460	4 0387	4 1234	4 0124	4 0033
R(2,4)	1 3336	1 3322	1 3497	1 3365	1 3344
R(2,5)	1 3336	1 3322	1 3497	1 3365	1 3344
R(3,4)	3 4868	3 3982	3 4661	3 3608	3 353
R(3,5)	3 4868	3 3982	3 4661	3 3608	3 353
A(4,1,5)	31 9	32 9	32 5837	33 2	33 2
A(4,2,5)	92 1	92 0	92 1803	91 9	92 0
A(4,3,5)	31 9	32 9	32 5837	33 2	33 2
D(4,2,3,1)	66 0	65 0	65 6	65 7	65 7
D(5,2,3,1)	-66 0	-65 0	-65 6	-65 7	-65 7

Ar 1 S 2 Ar 3 H4 H5

Table III.C. Energies of three minima and two transition states of Ar_2-H_2S, along with their monomer energies calculated at monomer and complex basis sets All energy values are calculated at MP2/6-311++G** level of theory '*' indicates the monomer geometry in complex (C) and (M) signify whether the energy is evaluated using complex or monomer basis set, respectively

Energy	MP2/6-311++G**				
	A	B	B'	TS1	TS2
E_{com}	-1452 7586484	-1452 7586841	-1452 7586841	-1452 758596	-1452 7585947
E_{Ar1}*(C)	-526 9550407	-526 9552551	-526 955255	-526 9551746	-526 9551613
E_{Ar2}*(C)	-526 9550401	-526 9550361	-526 9550359	-526 9550345	-526 9550263
E_{H2S}*(C)	-398 8487803	-398 8485748	-398 8485753	-398 8485706	-398 8485551
E_{Ar1}*(M)	-526 9546706	-526 9546706	-526 9546706	-526 9546706	-526 9546706
E_{Ar2}*(M)	-526 9546706	-526 9546706	-526 9546706	-526 9546706	-526 9546706
E_{H2S}*(M)	-398 8477236	-398 8477235	-398 8477235	-398 8477234	-398 8477232

Table III.D. Energy values calculated at CCSD(T)/6-311++G** level of theory

Energy	CCSD(T)/6-311++G**				
	A	B	B'	TS1	TS2
E_{com}	-1452 8115663	-1452 8116074	-1452 8116072	-1452 8115126	-1452 8115122
E_{Ar1}*(C)	-526 9686784	-526 9689052	-526 9689051	-526 9688189	-526 9688048
E_{Ar2}*(C)	-526 9686778	-526 968674	-526 9686738	-526 9686723	-526 9686638
E_{H2S}*(C)	-398 8744592	-398 8742605	-398 8742609	-398 8742496	-398 8742344
E_{Ar1}*(M)	-526 9682924	-526 9682924	-526 9682924	-526 9682924	-526 9682924
E_{Ar2}*(M)	-526 9682924	-526 9682924	-526 9682924	-526 9682924	-526 9682924
E_{H2S}*(M)	-398 8733719	-398 873371	-398 8733709	-398 8733711	-398 8733726

Table III.E. Energy of the optimized geometries of Ar_2-H_2S and the constituent monomers using different basis sets at MP2 level The monomer energies are evaluated at both monomer and complex basis sets to calculate the BSSE

Energy (h)	6-311++G(3df,2p)	aug-cc-pVDZ	aug-cc-pVTZ	aug-cc-pVQZ
E_{com}	-1452 9184184	-1452 765609	-1452 9595903	-1453 0265779
E_{Ar1}*(C)	-527 0117816	-526 9555517	-527 0245168	-527 0490743
E_{Ar2}*(C)	-527 0117816	-526 9555517	-527 0245168	-527 0490743
E_{H2S}*(C)	-398 8936559	-398 8534004	-398 9089564	-398 9265992
E_{Ar1}*(M)	-527 0115495	-526 9552989	-527 0242833	-527 0489519
E_{Ar2}*(M)	-527 0115495	-526 9552989	-527 0242833	-527 0489519
E_{H2S}*(M)	-398 8934129	-398 853217	-398 9088164	-398 9265253
E_{Ar}(M)	-527 0115495	-526 9552989	-527 0242833	-527 0489519
E_{H2S}(M)	-398 8934133	-398 8532189	-398 9088178	-398 9265264

Table III.F. Energy of the MP2 optimized geometries of Ar_2-H_2S and the constituent monomers using different basis sets at CCSD(T) level The monomer energies are evaluated at both monomer and complex basis sets to calculate the BSSE

Energy (h)	CCSD(T)/6-311++G(3df,2p)	CCSD(T)/aug-cc-pVDZ	CCSD(T)/aug-cc-pVTZ
E_{com}	-1453 00047	-1452 8217852	-1453 040242
E_{Ar1}*(C)	-527 0368457	-526 9699581	-527 048988
E_{Ar2}*(C)	-527 0368457	-526 9699581	-527 048988
E_{H2S}*(C)	-398 9258759	-398 8810069	-398 9409355
E_{Ar1}*(M)	-527 0365992	-526 9696846	-527 0487584
E_{Ar2}*(M)	-527 0365992	-526 9696846	-527 0487584
E_{H2S}*(M)	-398 925611	-398 8808099	-398 9407998
E_{Ar}(M)	-527 0365992	-526 9696846	-527 0487584
E_{H2S}(M)	-398 9256116	-398 8808119	-398 9408049

Table III.G. Rotational constants of the optimized structures (minima) of Ar_2-H_2S at different levels of theory

Constants	Experiment	6-311++G**		6-311++G(3df, 2p)	6-311++G(3df, 3pd)	aug-cc-pVDZ	aug-cc-pVTZ	aug-cc-pVQZ
		A	B					
A	1733 098	1631 4	1626 9	1730 5	1724 5	1667 5	1793 2	1805 7
B	1617 6570	1522 6	1461 9	1596 2	1705 0	1632 4	1715 2	1721 9
C	830 2755	792 1	771 5	820 0	862 8	830 0	882 4	887 2

References

1) van der Waals molecules-I, Special issue, *Chem Rev* 1988, **88(6)**
2) van der Waals molecules-II, Special issue, *Chem Rev* 1994, **94(7)**
3) van der Waals molecules-III, Special issue, *Chem Rev* 2000, **100(11)**
4) T J Balle and W H Flygare, *Rev Sci Instrum* 1981, **52**, 33.
5) T J Balle, E J Campbell, M R Keenan, and W H Flygare, *J Chem Phys* , 1979, **71**, 2723
6) R F W Bader, *Atoms in Molecule A quantum Theory*, Clarendon Press, Oxford, 1990, 302
7) V Aquilanti, E Cornicchi, M M Teixidor, N Saendig, F Pirani, and D Cappelletti, *Angew Chem Int Ed* 2005, **44**, 2356
8) R Lascola and D J Nesbitt, *J Chem Phys* 1991, **95**, 7917
9) P Hobza and Z Havlas, *Chem Rev* 2000, **100**, 4253
10) P S Meenakshi, N Biswas and S J Wategaonkar, *J Chem Phys* 2003, **118**, 9963
11) S Scheiner, *Hydrogen Bonding, A Theoretical Perspective*, Oxford University Press, New York, 1997, 24
12) E Arunan, T. Emilsson and H S Gutowsky, *J Am Chem Soc* 1994, **116**, 8418
13) E Arunan, C E Dykstra, T Emilsson and H S Gutowsky, *J Chem Phys* 1996, **105**, 8495
14) E Arunan, T Emilsson, H S Gutowsky and C E Dykstra, *J Chem Phys* 2001, **114**, 1242
15) E Arunan, T Emilsson and H S Gutowsky, *J Chem Phys* 2002, **116**, 4886
16) H S Gutowsky, T Emilsson and E Arunan, *J Chem Phys* 1997, **106**, 5309
17) C H Townes and A L Schawlow, *Microwave Spectroscopy*, McGraw Hill, New York, 1955
18) Z Kisiel, B A Pietrewicz, P W Fowler, A C Legon, and E Steiner, *J Phys Chem A* 2000, **104**, 6970
19) G. de Oliveira and C E Dykstra, *J Chem Phys* 1997, **106**, 5316

20) Y Liu and W Jaeger, *Mol Phys* **100**, 611 (2002)

21) P K Mandal and E Arunan, *J Chem Phys* 2001, **114**, 3880

22) E Arunan, A P Tiwari, P K Mandal and P C Mathias, *Curr Sci* 2002, **82**, 533

23) E Arunan, S Dev and P K Mandal, *Appl Spec Rev* 2004, **39**, 131

24) S R Gadre and P. K Bhadane, *J Chem Phys* 1997, **107**, 5625

25) G R Desiraju and T Steiner, *The Weak Hydrogen Bond In Structural Chemistry and Biology*, Oxford University Press, Oxford 1999

26) G A Jeffrey and W Saenger, *Hydrogen Bonding in Biological Structures*, Springer Verlog, Berlin 1991

27) P R Herman, P E LaRoucque and B P Stoicheff, *J Chem Phys* 1988, **89**, 4535

28) H S Gutowsky, T D Klots, C Chuang, C A Schmuttenmaer, and T Emilsson, *J Chem Phys* 1986, **86**, 569

29) T D Klots, C Chuang, R S Ruoff, T Emilsson and H S Gutowsky, *J Chem Phys* 1987, **86**, 5315

30) M Goswami, P K Mandal, D Ramdass and E Arunan, *Chem Phys Lett* 2004, **393**, 22

31) J. K G Watson, in *Vibrational Spectra and Structure*, Ed J R During, Elsevier, Amsterdam, 1977, **6**, 1 We thank G T Fraser for providing us with the program ASYM82 by A G Maki which was used in the fitting Ankit Jain added a feature that enables the program to remove one line from the fitting at a time and compare the rms deviation with the full fitting It is helpful in identifying a wrong assignment

32) E Arunan, T Emilsson, H S Gutowsky, G T Fraser, G de Oliveira, and C E Dykstra, *J Chem Phys* 2002, **117**, 9766

33) W Gordy and R L Cook, *Microwave Molecular Spectra*, John Wiley & Sons, 1984, p 663

34) M J Frisch, G W Trucks, H B Schlegel, G E Scuseria, M A Robb, J R Cheeseman, V G Zakrzewski, J A Montgomery, Jr, R E Stratmann, J C

Burant, S Dapprich, J M Millam, A D Daniels, K N Kudin, M C Strain, O Farkas, J Tomasi, V Barone, M Cossi, R Cammi, B Mennucci, C Pomelli, C Adamo, S Clifford, J Ochterski, G A Petersson, P Y Ayala, Q. Cui, K Morokuma, N Rega, P Salvador, J J Dannenberg, D K Malick, A D Rabuck, K Raghavachari, J B Foresman, J Cioslowski, J V Ortiz, A G Baboul, B B Stefanov, G Liu, A Liashenko, P Piskorz, I Komaromi, R Gomperts, R L Martin, D J Fox, T Keith, M A Al-Laham, C Y Peng, A Nanayakkara, M Challacombe, P M W Gill, B Johnson, W Chen, M W. Wong, J L Andres, C Gonzalez, M Head-Gordon, E S Replogle, and J A Pople, Gaussian 98, Revision A 11 3, Gaussian, Inc , Pittsburgh PA, 2002

35) Alex A Granowsky, http //classic chem msu su/gran/gamess/index html

36) Z Kisiel, PROSPE – Programs for ROtational Spectroscopy, http //info ifpan edu pl/ ~kisiel/prospe htm

37) S F Boys and F Bernardi, *Mol Phys* 1970, **19**, 55

38) S Simon, M Duran, and J J Dannenberg, *J Chem Phys* 1996, **105**, 11024

39) I Alkorta, I Rozas, and J Elguero, *Chem Soc Rev* 1998, **27**, 163

40) B Raghavendra and E Arunan, *unpublished results*

41) C J Cramer, *Essentials of Computational Chemistry* John Wiley and Sons, New York 2002

42) Z Kisiel, B A Pietrewicz, and L Pszczólkowski, *J Chem Phys* 2002, **117**, 8248

43) T D Klots and H S Gutowsky, *J Chem Phys* 1989, **91**, 63

44) Y Xu, M C L Gerry, J P Connelly and B J Howard, *J Chem Phys* 1993, **98**, 2735

45) M S Ngaří and W Jager, *J Chem Phys* 1999, **111**, 3919

46) Z S Huang and R E Miller, *J Chem Phys* 1989, **91**, 6613

Chapter IV

Rotational Spectra and Structure of Ar-$(H_2S)_2$ Complex

IV.1. Introduction

Water dimer is probably the most extensively studied Hydrogen bonded system [1-11] It has a C_S symmetric equilibrium geometry similar to that shown in Figure IV 1 for $(H_2S)_2$ Water dimer undergoes several tunneling motions that involve the interchange of identical nuclei There are mainly two types of tunneling motions The first type involves a simple two-fold rotations of either or both of the two H_2O molecules about its C_2 symmetry axis, giving permutation such as (12) (donor tunneling), (34) (acceptor tunneling) or (12)(34) (donor-acceptor tunneling) The other type, donor-acceptor interchange tunneling, interchanges the proton donor and proton acceptor roles in the dimer by permutations such as (ab)(13)(24) in Figure IV 1 As a result of these tunneling motions, the rotational energy levels are split into six sublevels[1] Two of them are doubly degenerate and the rest four are non-degenerate The acceptor tunneling splitting is ~200 GHz in $(H_2O)_2$ and ~9 GHz in $(D_2O)_2$ The donor-acceptor interchange tunneling splitting is ~20 GHz for $(H_2O)_2$ and ~1 GHz for $(D_2O)_2$ Only the doubly degenerate E states of $(H_2O)_2$ give rigid rotor type rotational spectra The other states give rotational tunneling spectra The rotational spectra of Ar-$(H_2O)_2$ have also been studied [12,13] It has a T-shaped heavy atom geometry, where Ar approaches towards $(H_2O)_2$ along its *b* inertial axis The O-O distance in Ar-$(H_2O)_2$ trimer is 2.945 Å, which is 0 035 Å shorter than that in $(H_2O)_2$ dimer. The trimer also undergoes several tunneling motions similar to the dimer The rotational energy levels of Ar-$(H_2O)_2$ could be correlated with those of $(H_2O)_2$ As the addition of Ar generates a dipole moment that does not invert on donor-acceptor interchange tunneling, A, B and E states give rigid rotor spectra The donor-acceptor interchange tunneling was determined to be ~106 MHz for Ar-$(D_2O)_2$, which is about $1/10^{th}$ of the $(D_2O)_2$ value (~1GHz)

As mentioned in the previous chapter, systematic studies of several weakly bound H_2S complexes have been started in our laboratory The main goal in this study is understanding weak intermolecular interactions involving second row hydrides This chapter reports the rotational spectral and *ab initio* studies of Ar-$(H_2S)_2$ complex Though $(H_2O)_2$ has been investigated extensively, the second row analogue $(H_2S)_2$ has

not received as much attention The rotational spectrum of $(H_2S)_2$ and several isotopomers has been investigated by Lovas [14] Some other experimental and theoretical investigations have also been published [15-21] During the course of our investigation on Ar-$(H_2S)_2$ some new transitions have been assigned for some isotopomers of $(H_2S)_2$ These are presented in this chapter along with some new theoretical results Rotational spectrum for Ar-$(H_2S)_2$ is reported for the first time The spectra and the structure of Ar-$(H_2S)_2$ are compared with that of $(H_2S)_2$ to gain maximum insight about the weakly bound Ar-$(H_2S)_2$ trimer

IV.2. Background: $(H_2S)_2$ Dimer

The theoretical studies[15-19] predict the linear H-bonded structure to be the global minimum, similar to that of $(H_2O)_2$ Experimentally, it has been studied by IR spectroscopy in matrix [20,21] The rotational spectra also have been recorded by Lovas [14] He has observed rotational spectra for several isotopomers of the dimer, including H_2S-$H_2{}^{34}S$ and the deuterated isotopomers The pure rotational spectra correspond to a pseudo-diatomic molecular complex For $(H_2S)_2$ a two state pattern has been observed in the rotational spectrum These are probably two tunneling states of $(H_2S)_2$ Hydrogen sulphide dimer is expected to undergo several tunneling motions similar to $(H_2O)_2$ As

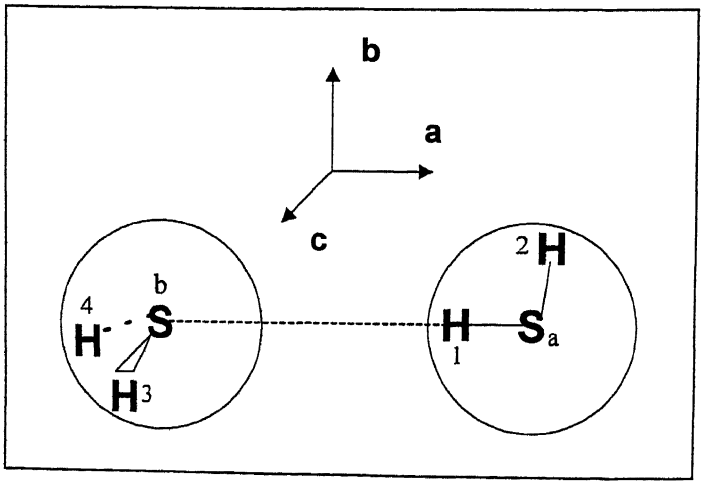

Figure IV 1. Structure of $(H_2S)_2$

Table IV.1. List of rotational and distortion constants for different isotopomers of $(H_2S)_2$ [14]

Species	Upper State		Lower State	
	B^0 (MHz)	D_J (kHz)	B^0 (MHz)	D_J (kHz)
$H_2{}^{32}S$-$H_2{}^{32}S$	1749 3088 (5)	14 937 (9)	1748 1088 (5)	15 247 (9)
$H_2{}^{32}S$-$H_2{}^{34}S$	1701 1578 (2)	14 016 (6)	*1700 3210	14 41 (1)
$H_2{}^{34}S$-$H_2{}^{32}S$	1700 553 (3)	14 24 (6)	*1699 468 (1)	14 52 (4)
$D_2{}^{32}S$-$D_2{}^{32}S$	1645 295 (2)	13 653 (3)	1644 408 (1)	13 41 (2)
D_2S-DSH/ HDS-D_2S	1678 747 (2)	13 06 (6)	1677 990 (1)	12 90 (5)
H_2S/D_2S/HDS	1730 8232 (2)	12 846 (6)	1728 3983 (3)	12.342 (6)
H_2S/D_2S/HDS	1690 3701 (7)	11 12 (3)	1689 8311	12 36
H_2S/D_2S/HDS	1693 203 (1)	12 17 (3)	--	--
H_2S/D_2S/HDS	1701 6852 (2)	13 972 (7)	--	--
*H_2S/D_2S/HDS	1705 579 (5)	14 6 (2)	--	--

* Present work

Table IV.2. List of rotational transitions observed for the new deuterated species and the weaker states of H_2S-$H_2{}^{34}S$

J	J'	H_2S-$H^{34}SH$ / $H_2{}^{34}S$-HSH	Res (kHz)	H_2S-$H^{34}SH$ / $H_2{}^{34}S$-HSH	Res (kHz)	D_2S/HDS	Res
0	1	--	--	--	--	3411 1263	26 9
1	2	6800 8262	3 4	6797 4062	-2 4	6821 8393	-10 1
2	3	10200 3679	-1 7	10195 2443	2 7	10231 8929	-7 7
3	4	13598 8770	-1 7	13592 0281	-0 9	13640.9079	4 1
4	5	16996 0055	1 0	--	--	--	--

the intermolecular potential energy surface is expected to be shallow, the barriers for these motions may be significantly smaller than those of $(H_2O)_2$ However, in microwave region, no other state has been found The rotational and distortion constants for different isotopomers are given in Table IV 1 One more set of transitions for a deuterated species and two new weaker states have been observed for H_2S-$H_2{}^{34}S$, one for donor $H_2{}^{34}S$ and the other for acceptor $H_2{}^{34}S$

The splitting in B rotational constant between the Upper and Lower states of $(H_2S)_2$ is 1 2 MHz whereas for the two $H_2{}^{34}S$-H_2S isotopomers, it is ~0 84 MHz and 1 09 MHz For $(D_2S)_2$ the splitting is ~0 89 MHz From the $(H_2S)_2$ rotational constants for Upper and Lower states, the vibrationally averaged c m separation between two H_2S sub-units is calculated to be 4 123 Å and 4 125 Å respectively

In addition to this experimental and theoretical information, some *ab initio* calculations have been performed for the dimer at MP2 method using higher basis sets The geometry was optimized using different basis sets The vibrational frequencies and interaction energy are calculated for the optimized geometry, and these will be discussed in the latter sections With this knowledge about the $(H_2S)_2$ dimer, the studies for the Ar-$(H_2S)_2$ trimer have been carried out

IV.3. Experimental Details

The rotational spectra for Ar-$(H_2S)_2$ and Ar-$(D_2S)_2$ were observed using our home-built Balle-Flygare pulsed nozzle FT microwave spectrometer [22] The Ar-$(H_2S)_2$ complex was formed through supersonic expansion of Ar gas seeded with 2 to 3 % of H_2S The D_2S was formed by flowing H_2S through several bubblers placed sequentially and filled with D_2O The back-pressure was kept typically at 0 6 atm The optimum microwave pulse was of 0 5 μs duration Typically 1000 to 2000 shots were averaged to obtain a reasonable signal to noise ratio The identity of the complexes was established by confirming the presence of H_2S/D_2S and Ar No signal was observed without H_2S When He was used as the carrier gas, no signal was observed even though H_2S was present. The signal appeared again as a few % of Ar was added to the gas mixture in He

During the search for Ar-$(H_2S)_2$ two new sets of transitions for H_2S-$H_2{}^{34}S$ and a set of transitions for a deuterated isotopomer of $(H_2S)_2$ were observed For the dimer the optimum back-pressure was 0 5 atm and the optimum microwave pulse length was 0 5 μs The ^{34}S signal was observed from natural abundance of isotope All gases were obtained from Bhuruka Gases Ltd and used as supplied, Ar (99 999 %), He (99 999%) and H_2S (99 5 %) D_2O was obtained from Sigma-Aldrich, 99 96 atom % D

IV.4. Experimental Results

IV.4.a. Search and Assignment of Ar-$(H_2S)_2$ and Ar-$(D_2S)_2$ Spectra

A symmetric T-shaped heavy atom geometry has been assumed for Ar-$(H_2S)_2$ complex as a similar structure has been determined for Ar-$(H_2O)_2$ complex [13] In the assumed geometry, which is an asymmetric top, the distance between two H_2S units was taken to be the same as that in $(H_2S)_2$ The Ar atom was placed equidistant from both the H_2S units such that the Ar-c m (H_2S) distance is similar to that in Ar-H_2S complex [23] The rotational transitions, both *a* and *b*-dipoles, were predicted for this assumed geometry As the principal inertial axis parallel to the S-S bond is *b* axis for this geometry, the *b*-dipole transitions were expected to be stronger Hence, scanning was started for the *b*-dipole transition $2_{02} \rightarrow 3_{13}$ which was predicted to occur at ~ 6025 MHz Two strong lines were readily found at 5964 1340 MHz and 5971 5046 MHz along with two other weaker lines at 5959 3882 MHz and 5966 6796 MHz The line at 5964 1340 MHz was assigned as $2_{02} \rightarrow 3_{13}$ transition and the weaker line at 5959 3882 MHz was assigned as *a*-dipole $2_{02} \rightarrow 3_{03}$ transition for Ar-$(H_2S)_2$ On the basis of these assignments, the other *a* and *b*-dipole transitions were predicted and found easily Total 40 *a* and *b*-dipole transitions have been observed for Ar-$(H_2S)_2$

Even after the complete assignment of these transitions, many lines were left unassigned (e g 5971 5046 MHz and 5966 6796 MHz) Most of them are very close to the assigned transitions for Ar-$(H_2S)_2$ and need similar optimum conditions to be observed These lines could be fitted as another set of transitions where the lines at 5971 5046 MHz and 5966 6796 MHz are assigned as $2_{02} \rightarrow 3_{13}$ and $2_{02} \rightarrow 3_{03}$ transitions

respectively A total of 32 *a* and *b*-dipole transitions have been observed and assigned for this series of transitions Both sets of transitions are listed in Table IV 3 along with the residues from the fit These two sets of transitions correspond to two different tunneling/internal rotor states of Ar-$(H_2S)_2$ and are designated as the Lower and Upper states The Upper state transition frequencies are higher than the corresponding Lower state transition A similar two state pattern in rotational spectra has been observed for $(H_2S)_2$ dimer also (discussed in previous section) No other set of transitions was observed even after extensive search in both directions

Table IV.3. List of rotational transitions observed for both Lower and Upper states for Ar-$(H_2S)_2$ The residues of the fits are also included

Transitions	Lower		Upper	
	Obs Freq (MHz)	Res (kHz)	Obs Freq (MHz)	Res (kHz)
$2_{12} \rightarrow 3_{03}$	5919 5143	10 4	--	--
$2_{12} \rightarrow 3_{13}$	5924 2629	10 5	--	--
$2_{02} \rightarrow 3_{03}$	5959 3882	-5 1	5966 6796	-9 9
$2_{02} \rightarrow 3_{13}$	5964 1340	-7 8	5971 5046	11 1
$2_{21} \rightarrow 3_{12}$	7142 7020	-3 0	7136 2504	0 8
$3_{13} \rightarrow 4_{04}$	7635 8962	11 7	7642 0509	-19 6
$3_{13} \rightarrow 4_{14}$	7636 3661	12 9	7642 5010	2 9
$3_{03} \rightarrow 4_{04}$	7640 6394	6 4	7646 8630	-11 5
$3_{03} \rightarrow 4_{14}$	7641 1092	7 5	7647 3053	3 2
$2_{11} \rightarrow 3_{22}$	7976 1100	-7 4	7996 1130	3 0
$3_{22} \rightarrow 4_{13}$	9229 0356	-1 5	--	--
$3_{22} \rightarrow 4_{23}$	9261 5525	-0 2	--	--
$4_{14} \rightarrow 5_{05}$	9335 2010	-3 2	9341 8420	-12 2
$4_{14} \rightarrow 5_{15}$	9335 2426	-3 6	9341 8820	-1 6
$4_{04} \rightarrow 5_{05}$	9335 6683	-4 7	9342 2920	10 3

Table IV 3 continued

$4_{04} \rightarrow 5_{15}$	9335 7076	-7 4	9342 3290	17 9
$3_{12} \rightarrow 4_{13}$	9419 9420	-0 8	9429 0690	-1 6
$3_{12} \rightarrow 4_{23}$	9452 4774	18 9	9461 9275	-4 3
$2_{20} \rightarrow 3_{31}$	9986 1125	-2 1	9998 9205	0 6
$4_{23} \rightarrow 5_{14}$	11015 9524	2 6	--	--
$4_{23} \rightarrow 5_{24}$	11020 1115	7 9	11024 9062	1 6
$5_{15} \rightarrow 6_{06}$	11032 3329	-10 1	11039 8235	-0 2
$5_{15} \rightarrow 6_{16}$	11032 3329	-13 6	11039 8235	-1 4
$5_{05} \rightarrow 6_{06}$	11032 3745	-10 5	11039 8664	13 3
$5_{05} \rightarrow 6_{16}$	11032 3745	-14 0	11039 8664	12 1
$4_{13} \rightarrow 5_{14}$	11048 4680	2 5	--	--
$4_{13} \rightarrow 5_{24}$	11052 6015	-17 7	--	--
$3_{21} \rightarrow 4_{32}$	11702 6670	0 3	--	--
$6_{16} \rightarrow 7_{07}$	12729 0515	1 0	12737 5490	-2 1
$6_{16} \rightarrow 7_{17}$	12729 0515	0 8	12737 5490	-2 0
$6_{06} \rightarrow 7_{07}$	12729 0515	-2 4	12737 5490	-3 3
$6_{06} \rightarrow 7_{17}$	12729 0515	-2 8	12737 5490	-3 2
$7_{17} \rightarrow 8_{08}$	14425 4752	13 1	14435 0073	-3 2
$7_{17} \rightarrow 8_{18}$	14425 4752	13 0	14435 0073	-3 2
$7_{07} \rightarrow 8_{08}$	14425 4752	12 8	14435 0073	-3 1
$7_{07} \rightarrow 8_{18}$	14425 4752	12 8	14435 0073	-3 1
$8_{18} \rightarrow 9_{09}$	16121 5749	-5 3	16132 1660	1 6
$8_{18} \rightarrow 9_{19}$	16121 5749	-5 3	16132 1660	1 6
$8_{08} \rightarrow 9_{09}$	16121 5749	-5 3	16132 1660	1 6
$8_{08} \rightarrow 9_{19}$	16121 5749	-5 3	16132 1660	1 6

Residue = Observed - Calculated

The search for the Ar-$(D_2S)_2$ spectra was quiet straightforward as the rigid rotor prediction from the Ar-$(H_2S)_2$ rotational constants gave rotational constants very close to the experimental values A total of 41 transitions, *a* and *b*-dipole, have been observed for each tunneling/internal rotor state of Ar-$(D_2S)_2$ For this isotopomer both the states are very close to each other and could be seen in a single window The observed transitions and their residues are listed in Table IV 4 The quadrupole hyperfine splitting due to four D nuclei could not be resolved to obtain the quadrupole coupling constants

Table: IV.4. Observed transitions and their corresponding residues for both Lower and Upper states for Ar-$(D_2S)_2$

Transitions	Lower		Upper	
	Obs Freq (MHz)	Res (kHz)	Obs Freq (MHz)	Res (kHz)
$2_{12} \rightarrow 3_{03}$	5764 0315	-2 4	5764 0640	-4 3
$2_{12} \rightarrow 3_{13}$	5766 1600	-5 2	5766 1930	-5 2
$2_{02} \rightarrow 3_{03}$	--	--	--	--
$2_{02} \rightarrow 3_{13}$	5789 2690	-6 3	5789 2990	-1 1
$3_{13} \rightarrow 4_{04}$	7428 3615	18 8	7428 3886	14 7
$3_{13} \rightarrow 4_{14}$	7428 5175	11 2	7428 5461	8 8
$3_{03} \rightarrow 4_{04}$	7430 4981	24 2	7430 5244	20 7
$3_{03} \rightarrow 4_{14}$	7430 6523	14 7	7430 6799	12 7
$2_{11} \rightarrow 3_{22}$	7656 1790	-1 8	7656 2180	0 4
$3_{22} \rightarrow 4_{13}$	9001 5100	3 4	9001 5550	0 2
$3_{22} \rightarrow 4_{23}$	9016 2330	-9 4	9016 284	-3 1
$4_{14} \rightarrow 5_{05}$	9082 4446	-3 6	9082 4785	-3 5
$4_{14} \rightarrow 5_{15}$	9082 4446	-15 1	9082 4785	-14 9
$4_{04} \rightarrow 5_{05}$	9082 6086	-3 3	9082 6429	-2 6
$4_{04} \rightarrow 5_{15}$	9082 6086	-14 8	9082 6429	-14 0

Table IV 4 continued

$3_{12} \rightarrow 4_{13}$	9113 9930	0 9	9114 0160	-9 6
$3_{12} \rightarrow 4_{23}$	9128 7280	0 0	9128 7600	2 1
$2_{20} \rightarrow 3_{31}$	9522 5860	-0 2	9522 6550	0 3
$4_{23} \rightarrow 5_{14}$	10706 4090	0 0	10706 4500	2 3
$4_{23} \rightarrow 5_{24}$	10707 8705	0 5	10707 9135	5 4
$4_{13} \rightarrow 5_{14}$	10721 1480	3 3	10721 182	2 0
$4_{13} \rightarrow 5_{24}$	10722 6070	1 2	10722 6410	5 5
$5_{15} \rightarrow 6_{06}$	10735 4942	-1 8	10735 5324	-2 4
$5_{15} \rightarrow 6_{16}$	10735 4942	-2 5	10735 5324	-3 2
$5_{05} \rightarrow 6_{06}$	10735 4942	-13 3	10735 5324	-13 9
$5_{05} \rightarrow 6_{16}$	10735 4942	-14 0	10735 5324	-14 7
$5_{24} \rightarrow 6_{15}$	12364 8730	3 5	12364 9170	1 3
$5_{24} \rightarrow 6_{25}$	12364 9910	-3 6	12365 0390	-1 8
$5_{14} \rightarrow 6_{15}$	12366 3325	1 9	12366 3775	1 3
$5_{14} \rightarrow 6_{25}$	12366 4540	-1 7	12366 4980	-3 2
$6_{16} \rightarrow 7_{07}$	12388 2940	6 3	12388 3420	9 0
$6_{16} \rightarrow 7_{17}$	12388 2940	6 3	12388 3420	8 9
$6_{06} \rightarrow 7_{07}$	12388 2940	5 6	12388 3420	8 2
$6_{06} \rightarrow 7_{17}$	12388 2940	5 5	12388 3420	8 2
$7_{17} \rightarrow 8_{08}$	14040 8390	-1 8	14040 8920	-1 4
$7_{17} \rightarrow 8_{18}$	14040 8390	-1 8	14040 8920	-1 4
$7_{07} \rightarrow 8_{08}$	14040 8390	-1 9	14040 8920	-1 4
$7_{07} \rightarrow 8_{18}$	14040 8390	-1 9	14040 8920	-1 4
$8_{18} \rightarrow 9_{09}$	15693 1205	1 0	15693 1790	-0 2
$8_{18} \rightarrow 9_{19}$	15693 1205	1 0	15693 1790	-0 2
$8_{08} \rightarrow 9_{09}$	15693 1205	1 0	15693 1790	-0 2
$8_{08} \rightarrow 9_{19}$	15693 1205	1 0	15693 1790	-0 2

For both isotopomers, the *b*-dipole transitions are stronger than the *a*-dipole ones This indicates that the dipole moment component along the *b* inertial axis of the complex is higher than that on the *a* axis Both sets of transitions for Ar-$(H_2S)_2$ and Ar-$(D_2S)_2$ have been fitted independently to the Watson Hamiltonian[24] for distorted asymmetric rotor with A reduction The fitted rotational and distortion constants are shown in Table IV 5 along with the standard deviations of the fits For all four series of transitions the standard deviations are within 7-9 kHz However, for Ar-$(H_2S)_2$ total six distortion terms are used in the fit, H_J being the only sextet term, whereas using five first order distortion terms gives a reasonably good fit for Ar-$(D_2S)_2$ The uncertainties associated with the fitted parameters are quite reasonable The distortion constants for Lower and Upper states of Ar-$(H_2S)_2$ have same sign However, the values for the Upper state are about an order higher than the corresponding Lower state distortion constants For Ar-$(D_2S)_2$ both the states have very similar distortion constants

Table IV.5. Fitted rotational constants and distortion constants for Ar-$(H_2S)_2$ and Ar-$(D_2S)_2$ The standard deviation (SD) and the number of transitions (#) fitted are included too

Parameters	Ar-$(H_2S)_2$		Ar-$(D_2S)_2$	
	Lower	Upper	Lower	Upper
A (MHz)	1810 410 (6)	1826 18 (2)	1725 49 (1)	1725 52 (1)
B	1596 199 (9)	1605 94 (6)	1566 26 (2)	1566 32 (2)
C	848 814 (2)	847 11 (1)	826 818 (3)	826 814 (3)
Δ_J (kHz)	20 4 (4)	323 (2)	9 5 (7)	11 1 (7)
Δ_{JK}	-32 (1)	-399 (6)	-12 (2)	-15 (2)
Δ_K	82 4 (7)	1045 (4)	26 (1)	28 (1)
δ_J	8 4 (2)	153 (1)	4 1 (4)	4 8 (4)
δ_K	38 9 (4)	746 (4)	6 3 (9)	8 3 (8)
H_J (Hz)	4 2 (1)	41 2 (6)	--	--
SD (kHz)	8 7	7 4	7 8	7 4
#	40	32	41	41

IV.4.b. Structure

The rotational spectra observed and the fitted rotational constants of Ar-$(H_2S)_2$ match very well with the assumed asymmetric top geometry, a T-shaped heavy atom geometry The vibrationally averaged structure, along with its principal inertial axis

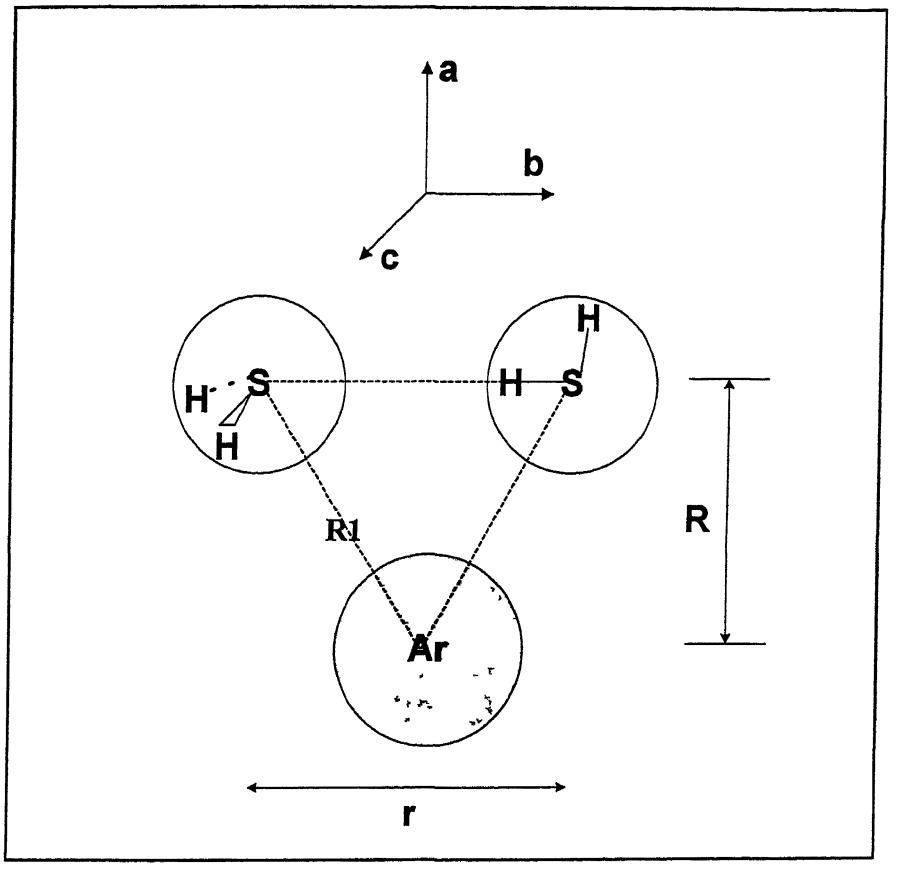

Figure IV 2. Vibrationally averaged geometry of Ar-$(H_2S)_2$ obtained from spectroscopic constants 'r' is the c m distance between two H_2S units and 'R' is the distance between Ar and c m of $(H_2S)_2$ moiety R1 is the distance between Ar and c m of (H_2S)

system, is shown in Figure IV 2 Ar-$(H_2S)_2$ is a weakly bound complex and the H_2S units undergo large amplitude internal motions in the complex As a result the H_2S molecules

become effectively spherical Hence, taking H_2S to be spherical, the intermolecular separations can be determined applying the following inertial equations

$$I_a = \frac{1}{2} m_{H2S} r^2 \quad (1)$$

$$I_b = \mu_c R^2 \quad (2)$$

Here m_{H2S} is the mass of H_2S unit, 'r' is the c m distance between the two H_2S units, μ_c is the reduced mass $[2m_{H2S}*m_{Ar} / (2m_{H2S} + m_{Ar})]$ of the complex and 'R' is distance between Ar and c m of $(H_2S)_2$ moiety From equation (1), using the Lower state rotational constants of Ar-$(H_2S)_2$, the 'r' value is determined to be 4 053 Å The Upper state constants give rise to a value of 4 035 Å whereas the Ar-$(D_2S)_2$ constants (both Lower and Upper states) give a value of 4 034 Å Equation (2) leads to 'R' values of 3 547 Å and 3 536 Å respectively for the Lower and Upper states of Ar-$(H_2S)_2$ The rotational constants for the deuterated isotopomer give an 'R' value of 3 543 Å These values correspond to a Ar-c m (H_2S) (R1) distances of 4 085 Å, 4 071 Å and 4 077 Å respectively All the structural parameters obtained including inertial defects (Δ) for both the states of Ar-$(H_2S)_2$ and Ar-$(D_2S)_2$ are given in Table IV 6 The inertial defects for the Lower and Upper states of both the isotopomers give a very important insight about the structure of the complex in its different tunneling/internal rotor states For Ar-$(H_2S)_2$ the

Table IV.6. The structural parameters determined from the experimental rotational constants for Lower and Upper states of Ar-$(H_2S)_2$ and Ar-$(D_2S)_2$ The inertial defects are also included The parameters are defined in figure IV 2 The distances are given in Å and the inertial defects are given in amu Å^2

Parameters	Ar-$(H_2S)_2$		Ar-$(D_2S)_2$		Ar-H_2S	$(H_2S)_2$
	Lower	Upper	Lower	Upper		
r	4 053	4 035	4 034	4 034	--	4 12
R	3 547	3 536	3 543	3 543	--	--
R1	4 085	4 071	4 077	4 077	4 01	--
Δ (=I_c-I_a-I_b)	-0 37	5 16	-4 32	-4 30	--	--

Lower state has a very small negative inertial defect, whereas the Upper state has a large positive value This indicates that probably the structure and dynamics of Ar-$(H_2S)_2$ are very different in these states Both the states of the per-deuterated species have a large negative Δ (-4 3) Probably, the increased mass of the out of plane nuclei accounts for it

IV.5. *Ab Initio* Calculation

Ab initio calculations were performed at different levels of theory to optimize the Ar-$(H_2S)_2$ geometry and to determine the interaction energy These *ab initio* results are combined with the rotational spectral studies to understand the system in more detail The computation was started with the $(H_2S)_2$, the precursor of Ar-$(H_2S)_2$ The global minimum of $(H_2S)_2$ has been optimized at MP2 level using different basis sets An Ar atom can approach towards $(H_2S)_2$ from several orientations to form the trimer, Ar-$(H_2S)_2$ Here all possible approaches have been considered to find the global minimum and any other local minima at MP2 level using different basis sets Frequency calculations were performed to confirm the nature of the stationary points found CCSD(T) single point energies were calculated for all the MP2 optimized geometries using the same basis set All the calculations were performed using Gaussian 98 software package[25] The optimized structural parameters, the absolute energies, and the vibrational frequencies, calculated at different level, for H_2S, $(H_2S)_2$ and Ar-$(H_2S)_2$ are tabulated in Tables IV A to IV P at the end of this chapter

IV.5.a. Geometry Optimization

Hydrogen sulphide dimer has been optimized at MP2 level using 6-311++G**, 6-311++G(3df,2p), aug-cc-pVTZ and aug-cc-pVQZ basis sets The global minimum has a linear Hydrogen bonded structure as shown in Figure IV 3 The Ar atom can approach towards $(H_2S)_2$ along its *a*, *b* or *c* axis to form Ar-$(H_2S)_2$ There are two ways for Ar atom to approach to $(H_2S)_2$ along its *b* inertial axis, from the top or bottom Approach from the top produced a saddle point with one imaginary frequency However approach from

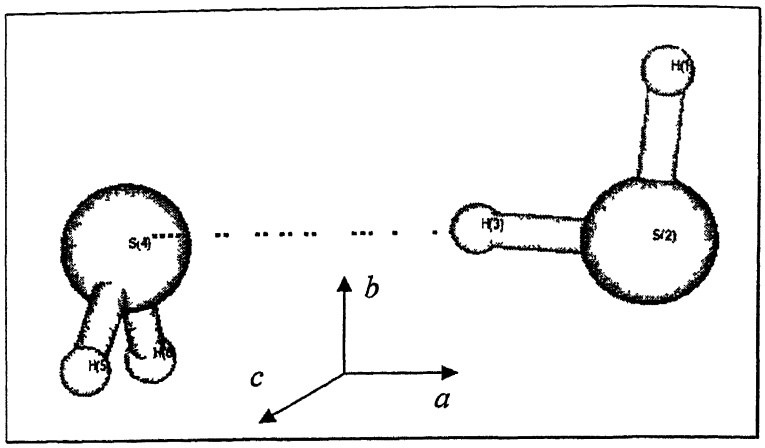

Figure IV.3. Optimized geometry of $(H_2S)_2$ at MP2/aug-cc-pVTZ level of theory

bottom resulted in a minimum (Structure A) at MP2/6-311++G(3df,2p) and MP2/aug-cc-pVTZ levels of theory However at MP2/6-311++G** level, this geometry was not optimized even after 100 steps starting from the initial geometry Another geometry (Structure B) could be optimized where Ar lies along the *c* inertial axis of $(H_2S)_2$ Structure B could not be optimized at MP2/aug-cc-pVQZ level of theory because of the limited allotted run time of the computers Ar approaching along *a* axis of $(H_2S)_2$ has again two possibilities There is no minimum where Ar is interacting with the H-bond acceptor H_2S However, a real pseudo-linear local minimum (Structure C) has been found, where Ar interacts with the H-bond donor H_2S moiety

IV.5.b. Structure

All three minima optimized at MP2/aug-cc-pVTZ level of theory are shown in Figure IV 4 The structural parameters calculated at different levels for all three minima are given in Table IV 7 In structure 'A', two hydrogens of the acceptor H_2S subunit are directed towards the Ar Ar is closer to the donor H_2S compared to the acceptor H_2S, the Ar-S distances being 3 6581 Å (R1) and 3 9727 Å (R2) respectively at MP2/aug-cc-pVTZ

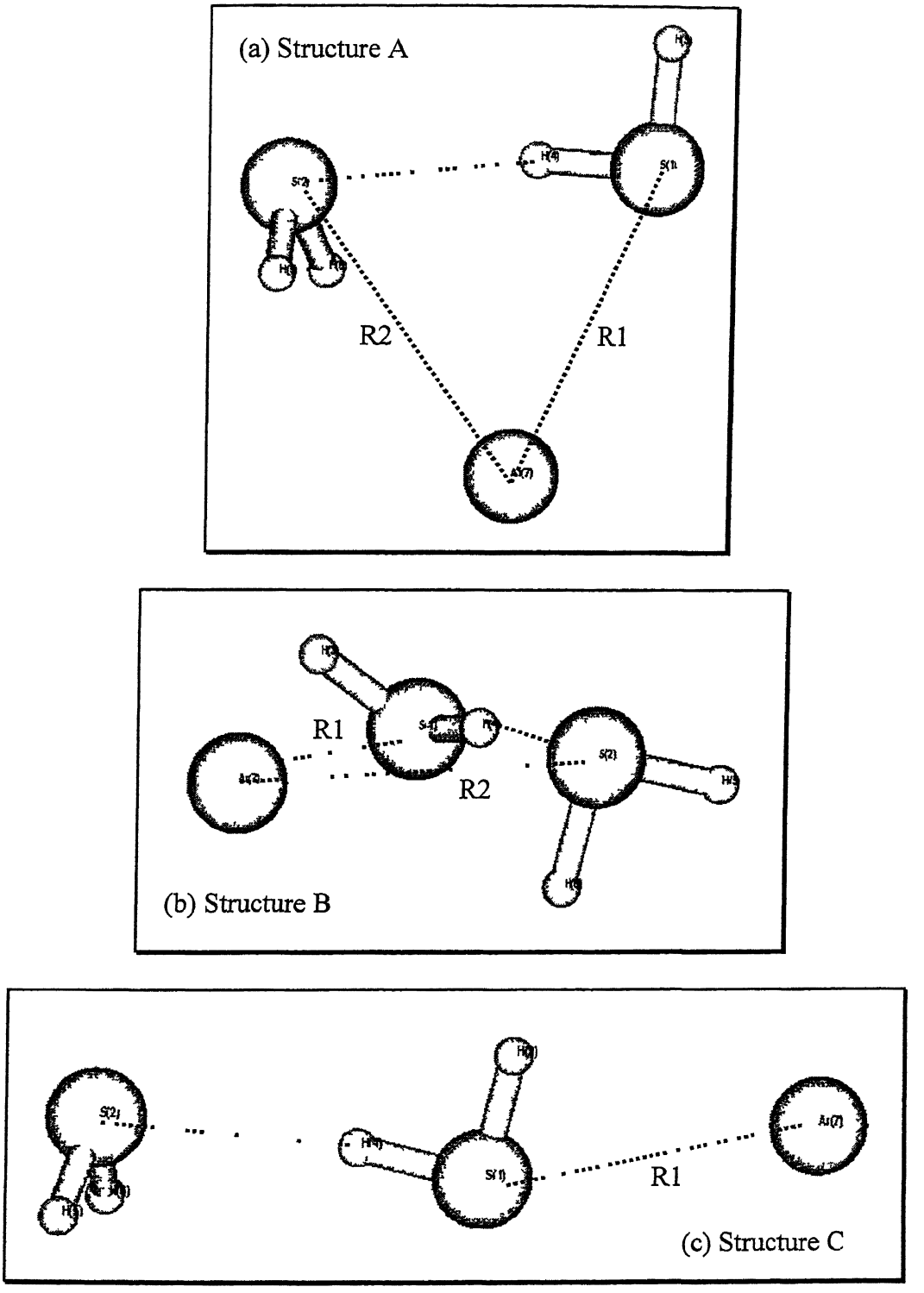

Figure IV 4. Geometries of three minima optimized at MP2/aug-cc-pVTZ level of theory

level of theory In contrast to the structure 'A', Ar is closer to the acceptor H_2S subunit in structure 'B' At MP2/aug-cc-pVTZ level the Ar-S distances R1 and R2 are 4 0543 Å and 3 6340 Å respectively In pseudo-linear local minimum, 'C', the Ar atom interacts with the donor H_2S subunit, and the Ar-S distance R1 is 3 6643 Å at MP2/aug-cc-pVTZ level of theory In both geometries 'A' and 'C', the $(H_2S)_2$ unit is not distorted much due to interaction with Ar However, the distortion is more in 'B' Relative orientation of two H_2S sub units is changed in presence of Ar in 'B' The free (non H-bonded) H of the donor H_2S moiety is inclined towards Ar in 'B', as evident from Figures IV 3 and IV.4 (b) The separation between two H_2S sub units (r) is similar for all three minima, the values being 4 0686 Å, 4 0683 Å and 4 0775 Å for A, B and C respectively at MP2/aug-cc-pVTZ level of theory The structural parameters have similar trend at each level of theory considered However, the intermolecular distances become shorter on increasing the basis set

Table IV.7. The structural parameters (intermolecular distances) and the inertial defects for three minima optimized at different levels of theory The structural parameters are defined in Figure IV 4 The distances are in Å and inertial defects are in amu Å^2

		6-311++G**	6-311++G(3df,2p)	aug-cc-pVTZ	aug-cc-pVQZ
Structure A	r	--	4 1164	4 0686	4 0664
	R1	--	3 6946	3 6581	3 6565
	R2	--	4 0651	3 9727	3 9709
	Δ	--	-3 73	-3 74	-3 68
Structure B	r	4 1668	4 1159	4 0683	--
	R1	4 1848	4 1344	4 05435	--
	R2	3 8208	3 6883	3 6340	--
	Δ	-4 71	-4 71	-4 04	--
Structure C	r	4 1745	4 1256	4 0775	4 0840
	R1	3 8470	3 6941	3 6643	3 6456
	Δ	-4 57	-4 31	-3 75	-3 77
r in $(H_2S)_2$		4 1725	4 1272	4 0765	4 0751

Table IV.8. Rotational constants (in MHz) for three minima optimized at different levels of theory

		6-311++G**	6-311++G(3df,2p)	aug-cc-pVTZ	aug-cc-pVQZ	Experiment
Structure A	A	--	1959 80	1994 59	1996 43	1810 410
	B	--	1646 92	1720 96	1722 66	1596 199
	C	--	900 85	930 21	931 09	848 814
Structure B	A	1845 47	1971 72	2023 66	--	
	B	1566 47	1600 42	1663 89	--	
	C	854 03	890 72	919 83	--	
Structure C	A	50227 41	68620 26	43894 38	44729 35	
	B	429 94	451 39	467 37	468 63	
	C	427 94	450 16	464 04	465 38	

The rotational constants for all three geometries at different levels of theory, along with the experimentally obtained ones, are shown in Table IV 8 The experimental rotational constants can be correlated to those of structure A and B However, the values of the calculated rotational constants should not be compared quantitatively with the experimental ones The calculation gives the rotational constants for the equilibrium geometry at a particular level, whereas rotational constants of a vibrationally averaged structure are obtained in experiment

IV.5.c. Interaction energy

The interaction energies (ΔE) are calculated using super-molecule approach The interaction energies are corrected for Basis Set Superposition Error (BSSE) using counterpoise method[26-28] to give the CP corrected interaction energies (ΔE^{CP}) The interaction energies for all three minima calculated at different levels of theory are given in Table IV 9 Single point energy was calculated at CCSD(T) level for all three minima,

optimized at MP2 level using 6-311++G(3f,2p) and aug-cc-pVTZ basis sets, using the same basis sets Though the interaction energies for all three minima are comparable, the CP corrected interaction energy for structure A is more than that for B and C at every level of calculations However, the zero point energy corrected interaction energy at higher basis set (aug-cc-pVTZ) for minimum B is marginally (10 5 cm^{-1}) higher than that for A This is due to the lower zero point vibrational energy of B than that of A at this

Table IV.9. Interaction energies of all the minimum structures optimized at different levels of theory for Ar-$(H_2S)_2$ ΔE^{CP} is the interaction energy after BSSE correction in Counterpoise method ΔE^{ZPE} is the interaction energy after correcting for zero point vibrational energy over ΔE^{CP}. All the energy values are in cm^{-1}

Structure	Energy	6-311++G**	6-311++G(3df,2p)		aug-cc-pVTZ		aug-cc-pVQZ
		MP2	MP2	CCSD(T)	MP2	CCSD(T)	MP2
A	ΔE	--	-1042 3	-902 4	-1161 2	-1007 3	-1112 2
	BSSE	--	297 3	314 8	234 3	223 8	118 9
	ΔE^{CP}	--	-745 0	-587 6	-926 8	-783 4	-993 3
	ΔE^{ZPE}	--	-335 8	-178 4	-486 2	-342 8	-552 6
B	ΔE	-1056 3	-1028.3	-891 9	-1122 7	-965 3	--
	BSSE	783 4	304 3	321 8	230 8	220 3	--
	ΔE^{CP}	-272 8	-724 0	-570 1	-891 9	-745 0	--
	ΔE^{ZPE}	241 3	-304 3	-150 4	-496 7	-349 8	--
C	ΔE	-909 4	-898 9	-786 9	-979 3	-853 4	-965 3
	BSSE	612 1	255 3	269 3	192 4	181 9	94 4
	ΔE^{CP}	-297 3	-640 0	-517 6	-786 9	-671 5	-839 4
	ΔE^{ZPE}	143.4	-262 3	-139 9	-391 7	-276 3	-444 2

particular level of calculation The CCSD(T) interaction energies are ~140 cm^{-1} smaller than the corresponding MP2 values The stabilization energies (ΔE^{ZPE}) for structures A, B and C are –342 8 cm^{-1}, -349 8 cm^{-1} and –276 3 cm^{-1} at CCSD(T)/aug-cc-pVTZ level of calculation The BSSE decreases drastically on increasing the basis set For the structure C at MP2 level, BSSE goes down from a value of 612 1 cm^{-1} for 6-311++G** basis set to a value of 94 4 cm^{-1} for aug-cc-pVQZ basis set

IV.5.d. Vibrational Frequency

Frequency calculation was performed for all optimized geometries to confirm the nature of the stationary points All minima had only positive Eigen values in the Hessian. The frequencies involving only the vibrations of H_2S units for all three geometries, calculated at MP2/aug-cc-pVTZ level, are listed in Table IV 10 The corresponding vibrational frequencies of $(H_2S)_2$ dimer and the free monomer, calculated at the same level of theory, are also included in the Table In $(H_2S)_2$ dimer the symmetric S-H stretch of the donor H_2S sub-unit undergoes a red-shift of ~42 cm^{-1}

Table IV.10. Intramolecular H_2S vibrational frequencies for three minima (A, B, and C) for Ar-$(H_2S)_2$ along with the $(H_2S)_2$ dimer and free H_2S monomer frequencies calculated at MP2/aug-cc-pVTZ level All values are in cm^{-1}.

Modes	H_2S	$(H_2S)_2$	Ar-$(H_2S)_2$		
			A	B	C
Acceptor bend	1212	1209	1208	1208	1209
Donor bend		1216	1215	1215	1215
Donor symmetric stretch	2771	2729	2726	2730	2728
Acceptor symmetric stretch		2769	2768	2769	2769
Donor asymmetric stretch	2791	2783	2782	2784	2784
Acceptor asymmetric stretch		2789	2788	2790	2789

In previous IR spectroscopic study of $(H_2S)_2$ in matrix, a shift of ~50 cm^{-1} was observed [19] In Ar-$(H_2S)_2$ for B and C geometries there is a similar red shift in the same mode, whereas the structure A undergoes a slightly higher shift, ~47 cm^{-1} This shift is quite significant compared to the other weakly bound complex of H_2S, Ar_2-H_2S, discussed in the previous chapter There is practically no shift in the H_2S vibrational modes in Ar_2-H_2S In the view of this fact, both $(H_2S)_2$ and Ar-$(H_2S)_2$ can be classified as weak H-bonded complex The donor asymmetric stretch also undergoes a little red shift for both $(H_2S)_2$ and Ar-$(H_2S)_2$ The bending modes and the acceptor stretching modes are almost unperturbed

IV.6. Discussion

The rotational spectra observed for Ar-$(H_2S)_2$ and Ar-$(D_2S)_2$ could be matched with both minima A and B Both of them have a T-shaped heavy atom geometry It is not possible to comment anything about the nature of the global minimum from the experimental data On vibrational averaging H_2S becomes effectively spherical, and both 'A' and 'B' will be identical However, pseudo-linear minimum could be ruled out as it will have totally different spectrum

The C rotational constants for Lower and Upper states are almost identical for both the isotopomers The difference observed in (A+B)/2 between the two states for Ar-$(H_2S)_2$ is 12 29 MHz, whereas the same is only 45 kHz for Ar-$(D_2S)_2$ This is in contrast to the very similar difference observed in B rotational constants between the two states for $(H_2S)_2$ (1 20 MHz) and $(D_2S)_2$ (0 89 MHz) This difference in rotational constants between the two tunneling/internal rotor states is not the real 'tunneling/internal rotor splitting However it is directly related to the real 'splitting' due to tunneling/internal rotation This can be understood qualitatively from Figure IV 5 The ground vibrational/torsional mode (can not be defined unambiguously for Ar-$(H_2S)_2$), shown in the Figure, is split into two sub levels, v_0 and v_0' due to tunneling/internal rotation There is independent set of rotational energy levels corresponding to each of v_0 and v_0' Transitions between the rotational levels of v_0 and that of v_0' are not observed for

Ar-$(H_2S)_2$ and Ar-$(D_2S)_2$ These transitions may not be allowed due to symmetry I they are allowed, they fall certainly out of the range of our spectrometer However, transitions between the rotational levels of a particular tunneling/internal rotation state are allowed, and that is what is observed in the experiment Hence both the sets of transitions observed could be fitted independently into a semi-rigid rotor Hamiltonian The vibrationally averaged geometries at these two levels are different Hence the rotational constants observed for the two states are different As the real tunneling splitting (Δ) between v_0 and v_0' increases, the difference in average geometry for these states will be more, and thus the difference in rotational constants The real tunneling splitting is much more for Ar-$(H_2S)_2$ compared to that in Ar-$(D_2S)_2$ The states v_0 and v_0' are very close to each other for Ar-$(D_2S)_2$, and virtually there is no difference in averaged geometries for these two states As a result the difference in (A+B)/2 is very small here, 45 kHz, than that for Ar-$(H_2S)_2$ (12 29 MHz) If transitions between the rotational levels

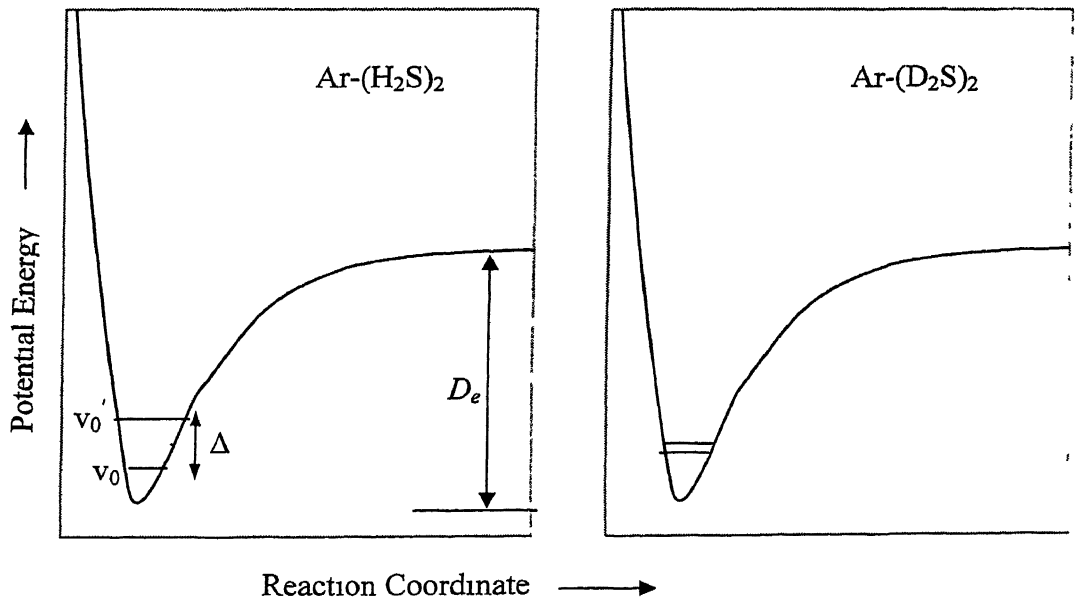

Figure IV.5. Schematic (cartoon) potential energy diagram for Ar-$(H_2S)_2$ and Ar-$(D_2S)_2$ showing the splitting (Δ) of ground state of some vibrational mode due to tunneling/internal rotation From the experimental findings the x-axis could not be defined for Ar-$(H_2S)_2$

of v_0 and that of v_0' are allowed, the tunneling rotational spectra would be observed, where each rotational transition would be split into two lines These spectra can not be fitted independently into a semi-rigid rotor Hamiltonian In turn, the mean of the two lines corresponding to each rotational transition can be fitted in to a semi-rigid rotor Hamiltonian The splitting of each rotational line is the actual splitting due to tunneling/internal rotation

The tunneling splitting is expected to decrease going from $(H_2S)_2$ dimer to Ar-$(H_2S)_2$ trimer, as observed in case of $(H_2O)_2$ and Ar-$(H_2O)_2$ However, here it is ~10 times more in the trimer compared to the dimer In the dimer the splitting for $(D_2S)_2$ is reduced by ~26 % of the $(H_2S)_2$ value However, for the trimer the reduction is ~273 times more. This anomalous difference in the splitting between the dimer and the trimer can not be explained from the present observations Also it is not possible to infer the nature of the coordinate along which the tunneling/internal rotation occurs, and whether there are any other such states or not, from the experimental data

It is also likely that the two states observed for the trimer do not have 1 1 correspondence with the dimer states The splitting depends directly on the reduced barrier height s, defined as [29]

$$s = V/C\,F \qquad (3)$$

where V is the actual barrier height, C is a constant, and F is the reduced rotational constant of the top and the framework F is given as

$$F = A\,(Top) + A\,(Frame) \qquad (4)$$

If Ar is involved in the tunneling/internal rotation of Ar-$(H_2S)_2$, 'F' for the trimer becomes much smaller than that for the dimer, regardless of Ar being a part of the top or the frame If the actual barrier height 'V' for the trimer does not differ much from that of the dimer, 's' should be much higher for the trimer Hence, the splitting in the trimer is expected to be smaller than that in $(H_2S)_2$ dimer If Ar is not involved in tunneling/internal rotation, and the barrier height goes up for the trimer, the splitting would again be smaller in trimer than in the dimer

It is possible that the splitting observed in $(H_2S)_2$ is too small in the trimer to be resolved, and the splitting observed in Ar-$(H_2S)_2$ spectra is too large in the dimer to be

observed in microwave region Experiments in THz range will help in more clear understanding of dynamic nature of $(H_2S)_2$ and Ar-$(H_2S)_2$ complexes

The c m separation between two H_2S sub units, r, is 4 053 Å for Ar-$(H_2S)_2$ and 4 123 Å for $(H_2S)_2$ (Table IV 6). It should be noted here that the H_2S units come closer in presence of a third moiety, Ar The distance between two units reduces by 0 07 Å This could be attributed as the third body effect A similar reduction in the intermolecular distance is observed in case of $(H_2O)_2$ and Ar-$(H_2O)_2$ also This result is supported by the *ab initio* calculation, though the reduction is much smaller At MP2/aug-cc-pVTZ level of theory, the S-S distance is reduced by ~0 01 Å in Ar-$(H_2S)_2$ (Structure A) compared to $(H_2S)_2$ (Table IV 7)

It is difficult to rationalize the huge differences between the distortion constants for two states of Ar-$(H_2S)_2$, where the distortion constants for both the states of Ar-$(D_2S)_2$ are very similar More work, both theory and experiments in different spectral range, is needed to address the unsolved questions for the weakly bound complex Ar-$(H_2S)_2$

IV.7. Conclusions

The rotational spectra for Ar-$(H_2S)_2$ and Ar-$(D_2S)_2$ have been observed Ar-$(H_2S)_2$ is an asymmetric top in the oblate limit, having the asymmetry parameter $\kappa = 0.55$ Similar to $(H_2S)_2$, a two state pattern has been observed for the trimer The splitting in (A+B)/2 between the two states is 12.3 MHz for Ar-$(H_2S)_2$ and 45 kHz for Ar-$(D_2S)_2$ The spectra and the rotational constants are consistent with a T-shaped heavy atom vibrationally averaged geometry The distance between two H_2S units in Ar-$(H_2S)_2$ is determined to be 4.053 Å, which is 0.07 Å smaller than that in $(H_2S)_2$ The Ar-c m(H_2S) distance is 4.085 Å, almost the same as that in Ar_2-H_2S complex *Ab initio* calculations at MP2 and CCSD(T) level have also been performed using 6-311++G**, 6-311++G(3df,2p), aug-cc-pVTZ an aug-cc-pVQZ basis sets Calculation gives three minima. In these three minima Ar approaches towards $(H_2S)_2$ along its *a*, *b* and *c* axis Ar being along the *a* axis is a pseudo-linear geometry and has least stabilization energy The other two minima have a T-shaped heavy atom geometry The spectra, observed, are consistent with either of these two minima At CCSD(T)/aug-cc-pVTZ level the minimum having Ar along *b* axis has a CP corrected stabilization energy of 769.5 cm^{-1} The vibrational frequency shift of donor H_2S indicates that Ar-$(H_2S)_2$ is weak H-bonded complex

Table IV.A. Optimized parameters of H_2S at different levels of theory.

Parameters	MP2/6-311++G**	MP2/6-311G(3df,2p)	MP2/aug-cc-pVTZ	MP2/aug-cc-pVQZ
R(1,2)	1 3333	1 3335	1 3366	1 3343
R(2,3)	1 3333	1 3335	1 3366	1 3343
A(1,2,3)	92 1	92 3	92 3	92 3
1H	2S	3H		

Table IV.B. Optimized parameters of $(H_2S)_2$ at different levels of theory

Parameters	MP2/6-311++G**	MP2/6-311G(3df,2p)	MP2/aug-cc-pVTZ	MP2/aug-cc-pVQZ
R(1,2)	1 3337	1 3336	1 3364	1 3341
R(2,3)	1 3349	1 3369	1 3405	1 3384
R(3,4)	2 8382	2 7965	2 7432	2 744
R(3,5)	3 5385	3 2032	3 1000	3 0991
R(3,6)	3 5433	3.2000	3.0949	3 0945
R(4,5)	1 3336	1 3339	1 3369	1 3347
R(4,6)	1 3336	1 3339	1 3369	1 3347
A(1,2,3)	92 3	92 4	92 4	92 4
A(2,3,4)	177 8	173 3	172 7	172 7
A(2,3,5)	157 9	150 6	149 1	149 1
A(2,3,6)	158 1	150 3	148 9	148 9
A(5,3,6)	31 5	35 0	36 3	36 2
A(5,4,6)	92 3	92 4	92 3	92 3
D(1,2,3,4)	-179 8	179 9	-179 9	-179 9
D(1,2,3,5)	-134 9	-141 4	-141 6	-141 7
D(1,2,3,6)	132 2	143 4	144 0	144 0
1H	2S	3H	4S	5H	6H

Table IV.C. Optimized structural parameters of structure "A" of $Ar-(H_2S)_2$ at different levels of theory

Parameters	MP2/6-311G(3df,2p)	MP2/aug-cc-pVTZ	MP2/aug-cc-pVQZ
R(1,3)	1 3338	1 3366	1 3344
R(1,4)	1 3371	1 3408	1 3387
R(1,7)	3 6946	3 6581	3 6565
R(2,4)	2 7907	2 7397	2 7397
R(2,5)	1 3340	1 3370	1 3349
R(2,6)	1 3340	1 3370	1 3349
R(2,7)	4 0651	3 9727	3 9709
R(4,5)	3 1315	2 9984	2 9986
R(4,6)	3 1363	3 0007	3 0008
R(4,7)	3 4403	3 3890	3 3881
R(5,7)	3 4879	3 3366	3 3365
R(6,7)	3 509	3.344	3 3438
A(3,1,4)	92 5	92 4	92 4
A(3,1,7)	161 1	160 3	160 3
A(5,2,6)	92 3	92 2	92 2
A(1,4,2)	170 9	170 7	170 6
A(1,4,5)	147 7	146 4	146 4
A(1,4,6)	148 0	146 5	146 5
A(5,4,6)	35 8	37 5	37 4
A(1,7,2)	63 9	64 3	64 3
A(1,7,5)	73 9	73 3	73 3
A(1,7,6)	73 8	73.3	73 2
A(5,7,6)	31 9	33 5	33 5
D(3,1,4,2)	-179 1	-179 5	-179 6
D(3,1,4,5)	-145 0	-144 5	-144 5
D(3,1,4,6)	144 5	144 5	144 5
D(3,1,7,2)	-0 3	0 1	0 2
D(3,1,7,5)	-16 8	-17 4	-17 4
D(3,1,7,6)	16 4	17 6	17 6

1S 2S 3H 4H 5H 6H 7Ar

Table IV.D. Optimized structural parameters of structure "B" of Ar-$(H_2S)_2$ at different levels of theory

Parameters	MP2/6-311++G**	MP2/6-311G(3df,2p)	MP2/aug-cc-pVTZ
R(1,3)	1 3337	1 3337	1 3364
R(1,4)	1 3350	1 3370	1 3405
R(1,7)	4 1848	4 1344	4 0543
R(2,4)	2 8326	2 7867	2 7440
R(2,5)	1 3337	1 3342	1 3370
R(2,6)	1 3336	1 3341	1 3370
R(2,7)	3 8208	3 6883	3 6340
R(3,7)	3 7902	3 5401	3 2652
R(4,5)	3 5312	3 3432	3 2960
R(4,6)	3 5244	3 1050	2 9460
R(4,7)	3 5473	3 5401	3 5057
R(6,7)	3 6338	3 5187	3 4348
A(3,1,4)	92 3	92 4	92 3
A(5,2,6)	92 3	92 4	92 4
A(5,2,7)	157 1	159 2	159 0
A(1,4,2)	177 6	172 5	169 1
A(1,4,5)	156 9	156 3	156 5
A(1,4,6)	159 1	147 0	142 4
A(5,4,6)	31 6	34 5	35 5
A(5,4,7)	91 6	92 1	92 3
A(1,7,2)	62 5	63 2	63 6
A(1,7,6)	75 3	67.6	65 6
A(2,7,3)	71 7	75 3	77 5
A(3,7,4)	30 2	31 6	32 9
A(3,7,6)	88 2	83 7	82 2
D(3,1,4,2)	-159 4	110 0	88 2
D(3,1,4,5)	-150 9	-174 3	164 9
D(3,1,4,6)	115 7	110 4	96 1
D(5,2,7,1)	-77 1	-52 9	-51 8
D(5,2,7,3)	-94 5	-67 1	-62 4
D(5,4,7,3)	155 0	164 8	174 0

1S 2S 3H 4H 5H 6H 7Ar

Table IV.E. Optimized structural parameters of structure "C" of Ar-$(H_2S)_2$ at different levels of theory

Parameters	MP2/6-311++G**	MP2/6-311G(3df,2p)	MP2/aug-cc-pVTZ	MP2/aug-cc-pVQZ
R(1,3)	1 3337	1 3337	1 3363	1 3342
R(1,4)	1 3349	1 3371	1 3407	1 3387
R(1,7)	3 8470	3 6941	3 6643	3 6455
R(2,4)	2 8433	2 7995	2 7439	2 7527
R(2,5)	1 3336	1 3339	1 3368	1 3347
R(2,6)	1 3341	1 3339	1 3368	1 3347
R(3,7)	3 6743	3 5285	3 3262	3 3104
R(4,5)	3 5363	3 1630	3 0964	3 1012
R(4,6)	3.5466	3 2207	3 1058	3 1135
A(3,1,4)	92 7	92 5	92 5	92 5
A(4,1,7)	162 4	164 7	157 4	157 5
A(5,2,6)	92 3	92 4	92 3	92 3
A(1,4,2)	174 8	171 1	172 8	172 6
A(1,4,5)	155 6	147 1	148 9	148 7
A(1,4,6)	155 9	150 4	149.3	149 4
A(5,4,6)	31 5	35 1	36 2	36 1
D(3,1,4,2)	-169 9	-155 2	-174 2	-174 3
D(3,1,4,5)	-129 5	-131 6	-138 8	-140 1
D(3,1,4,6)	147 7	157 5	146 6	145 7
D(7,1,4,2)	-137 7	-145 3	-173.3	-173 2
D(7,1,4,5)	-97 2	-121 7	-137 9	-139 0
D(7,1,4,6)	179 9	167 4	147 6	146 9

1S 2S 3H 4H 5H 6H 7Ar

Table IV.F. Energies of H_2S-H_2S

Energy	MP2/6-311++G(3df,2p)	MP2/aug-cc-pVTZ	MP2/aug-cc-pVQZ
E_{com} (h)	-797 7899331	-797 8210235	-797 8562629
$E_{H2S}1$(C)*	-398 8938573	-398 9092309	-398 9267238
$E_{H2S}2$(C)*	-398 8937231	-398 9089928	-398 9266107
$E_{H2S}1$(M)*	-398 8934125	-398 9088172	-398 9265259
$E_{H2S}2$(M)*	-398 8934058	-398 9088075	-398 9265162
E_{H2S} (M)	-398 8934133	-398 9088177	-398 9265264
ΔE (kcal/M)	-1 9494	-2 1261	-2 0144
BSSE	0 4782	0 3759	0 1835
ΔE^{CP}	-1 4712	-1 7502	-1 8309

Table IV.G. Energies of three minima of Ar-$(H_2S)_2$ at MP2/6-311++G** and MP2/aug-cc-pVQZ levels of theory

Energy	Structure A	Structure B	Structure C (Pseudo-linear)	
	aug-cc-pVQZ	6-311++G**	6-311++G**	aug-cc-pVQZ
Ecom (h)	-1324 9070702	-1324 6549282	-1324 6542634	-1324 9062567
$E_{H2S}1(C)$*	-398 9267597	-398 8496655	-398 8492982	-398 9267248
$E_{H2S}2(C)$*	-398 9266399	-398 8487843	-398 8485092	-398 9266379
E_{Ar} (C)*	-527 049127	-526 9552308	-526 9550842	-527 04906
$E_{H2S}1(M)$*	-398 9265259	-398 8477225	-398 8477217	-398 9265258
$E_{H2S}2(M)$*	-398 9265146	-398 8477213	-398 8477119	-398 9265138
E_{Ar} (M)*	-527 0489519	-526 9546706	-526 9546706	-527 0489519
E_{H2S} (M)	-398 9265264	-398 8477235	-398 8477235	-398 9265264
E_{Ar} (M)	-527 0489519	-526 9546706	-526 9546706	-527 0489519
ΔE (kcal/mol)	-3 18	-3 02	-2 60	-2 67
BSSE	0 34	2 24	1 75	0 27
ΔE^{CP}	-2 84	-0 78	-0 85	-2 40
ΔE^{ZPE}	-1 58	0 69	0 41	-1 27

Table IV H Energies for Structure A of Ar-$(H_2S)_2$ at different levels using 6-311++G(3df,2p)_basis set

Energy	MP2	MP3	MP4D	MP4DQ	MP4SDQ	CCSD	CCSD(T)
E_{com} (h)	-1324 8031287	-1324 8674823	-1324 8829635	-1324 8676769	-1324 8695659	-1324 8688265	-1324 8919374
$E_{H2S}1$(C)*	-398 8939584	-398 9170902	-398 9229394	-398 9177331	-398 9185573	-398 9183915	-398 9261911
$E_{H2S}2$(C)*	-398 8938583	-398 9169987	-398 9228505	-398 9176464	-398 9184727	-398 9183089	-398 926106
E_{Ar} (C)*	-527 0119068	-527 0309733	-527 0348765	-527 0302752	-527.0304565	-527 0300832	-527 036982
$E_{H2S}1$(M)*	-398 8934129	-398 9165373	-398.9223783	-398 9171903	-398 9180154	-398 9178511	-398 9256175
$E_{H2S}2$(M)*	-398 8934042	-398 9165366	-398 9223832	-398 917193	-398 9180196	-398 9178568	-398 9256271
E_{Ar} (M)*	-527 0115495	-527 0305977	-527 0344954	-527 0299064	-527 0300926	-527 029721	-527 0365992
E_{H2S} (M)	-398 8934133	-398 9165356	-398 9223744	-398 9171878	-398 9180123	-398 9178474	-398 9256116
E_{Ar} (M)	-527 0115495	-527 0305977	-527 0344954	-527 0299064	-527 0300926	-527 029721	-527 0365992
ΔE (kcal/mol)	-2 98	-2 39	-2 33	-2 13	-2 16	-2 14	-2 58
BSSE	0 85	0 87	0 89	0 86	0 85	0 85	0 90
ΔE^{CP}	-2 13	-1 52	-1 45	-1 27	-1 31	-1 29	-1 68
ΔE^{ZPE}	-0 96	-0 34	-0 27	-0 10	-0 14	-0 11	-0 51

Table IV I Energies for Structure A of Ar-$(H_2S)_2$ at different levels using aug-cc-pVTZ basis set

Energy	MP2	MP3	MP4D	MP4DQ	MP4SDQ	CCSD	CCSD(T)
E_{com} (h)	-1324 8472145	-1324 9103315	-1324 9256079	-1324 9088174	-1324 9105552	-1324 9095906	-1324 9349529
$E_{H2S}1$(C)*	-398 909291	-398 9320885	-398 9379317	-398 9321684	-398 9329277	-398 932681	-398 941245
$E_{H2S}2$(C)*	-398 9090661	-398 9318972	-398 9377466	-398 9319881	-398 9327507	-398 9325042	-398 9410628
E_{Ar} (C)*	-527 0246242	-527 0432008	-527 0468875	-527 0420115	-527 0421471	-527 0417307	-527 0490944
$E_{H2S}1$(M)*	-398 9088174	-398 931664	-398 9375069	-398 9317612	-398 932522	-398 9322729	-398 9408084
$E_{H2S}2$(M)*	-398 9088061	-398 9316619	-398 9375115	-398 9317631	-398 9325253	-398 932278	-398 9408179
E_{Ar} (M)*	-527 0242833	-527 0428734	-527 0465594	-527 041692	-527 0418281	-527 0414106	-527 0487584
E_{H2S} (M)	-398 9088177	-398 9316641	-398 9375053	-398 9317617	-398 9325219	-398 9322724	-398 9408049
E_{Ar} (M)	-527 0242833	-527 0428734	-527 0465594	-527 041692	-527 0418281	-527 0414106	-527 0487584
ΔE (kcal/mol)	-3 32	-2 59	-2 53	-2 26	-2 31	-2 28	-2 88
BSSE	0 67	0 62	0 62	0 60	0 60	0 60	0 64
ΔE^{CP}	-2 65	-1 97	-1 91	-1 66	-1 72	-1 68	-2 24
ΔE^{ZPT}	-1 39	-0 71	-0 65	-0 40	-0 45	-0 42	-0 98

Table IV J Energies for Structure B of Ar-$(H_2S)_2$ at different levels using 6-311++G(3df,2p)_basis set

Energy	MP2	MP3	MP4D	MP4DQ	MP4SDQ	CCSD	CCSD(T)
E_{com} (h)	-1324 8030562	-1324 8674334	-1324 8829176	-1324 867634	-1324 8695206	-1324 8687805	-1324 8918817
$E_{H2S}1$(C)*	-398.8940171	-398 917154	-398 9230044	-398 9177958	-398 9186193	-398 9184536	-398 9262551
$E_{H2S}2$(C)*	-398 8938444	-398 9169802	-398 9228312	-398 9176276	-398 9184553	-398 9182918	-398 9260899
E_{Ar} (C)*	-527 011896	-527 0309618	-527 0348649	-527 0302639	-527 0304453	-527 0300721	-527 0369701
$E_{H2S}1$(M)*	-398 8934119	-398 9165381	-398 9223793	-398 9171923	-398 9180174	-398 9178531	-398 9256183
$E_{H2S}2$(M)*	-398 8934061	-398 9165366	-398 9223828	-398 9171919	-398 9180185	-398 9178555	-398 9256266
E_{Ar} (M)*	-527 0115495	-527 0305977	-527 0344954	-527 0299064	-527 0300926	-527 029721	-527 0365992
E_{H2S} (M)	-398 8934133	-398 9165356	-398 9223744	-398 9171878	-398 9180123	-398 9178474	-398 9256116
E_{Ar} (M)	-527 0115495	-527 0305977	-527 0344954	-527 0299064	-527 0300926	-527 029721	-527 0365992
ΔE (kcal/mol)	-2 94	-2 36	-2 31	-2 10	-2 14	-2 11	-2 55
BSSE	0 87	0 89	0 91	0 88	0 87	0 87	0 92
ΔE^{CP}	-2 07	-1 47	-1 40	-1 23	-1 26	-1 24	-1 62
ΔE^{ZPE}	-0 87	-0 28	-0 21	-0 03	-0 07	-0 05	-0 43

Table IV.K Energies for Structure B of Ar-$(H_2S)_2$ at different levels using aug-cc-pVTZ basis set

Energy	MP2	MP3	MP4D	MP4DQ	MP4SDQ	CCSD	CCSD(T)
E_{com} (h)	-1324 8470374	-1324 9101803	-1324 9254542	-1324 9086751	-1324 9104018	-1324 9094351	-1324 9347692
$E_{H2S}1$(C)*	-398 9093143	-398 9321094	-398 9379508	-398 9321898	-398 9329486	-398 9327023	-398 9412644
$E_{H2S}2$(C)*	-398 9090552	-398 9318863	-398 9377345	-398 9319765	-398 9327388	-398 9324916	-398 9410488
E_{Ar} (C)*	-527 0245938	-527 0431714	-527 0468579	-527 0419826	-527 0421183	-527 0417018	-527 0490643
$E_{H2S}1$(M)*	-398 908816	-398 9316653	-398 937507	-398 9317646	-398 9325248	-398 9322755	-398 9408066
$E_{H2S}2$(M)*	-398 9088087	-398 9316619	-398 9375105	-398 9317618	-398 9325238	-398 9322762	-398 9408164
E_{Ar} (M)*	-527 0242833	-527 0428734	-527 0465594	-527 041692	-527 0418281	-527 0414106	-527 0487584
E_{H2S} (M)	-398 9088177	-398 9316641	-398 9375053	-398 9317617	-398 9325219	-398 9322724	-398 9408049
E_{Ar} (M)	-527 0242833	-527 0428734	-527 0465594	-527 041692	-527 0418281	-527 0414106	-527 0487584
ΔE (kcal/mol)	-3 21	-2 50	-2 44	-2 17	-2 22	-2 18	-2 76
BSSE	0 66	0 61	0 61	0 58	0 58	0 59	0 63
ΔE^{CP}	-2 55	-1 89	-1 83	-1 59	-1 63	-1 60	-2 14
ΔE^{ZPE}	-1 14	-0 76	-0 70	-0 45	-0 50	-0 46	-1 00

Table IV.L. Energies for Structure C (Pseudo-linear) of Ar-$(H_2S)_2$ at different levels using 6-311++G(3df,2p)_basis set

Energy	MP2	MP3	MP4D	MP4DQ	MP4SDQ	CCSD	CCSD(T)
E_{com} (h)	-1324 8024651	-1324 8670489	-1324 8825335	-1324 8672929	-1324 8691672	-1324 8684245	-1324 8914051
$E_{H2S}1$(C)*	-398 8938678	-398 9169977	-398 9228448	-398 9176428	-398 9184671	-398 9183016	-398 9260914
$E_{H2S}2$(C)*	-398 8938607	-398 917	-398 922851	-398 9176477	-398 9184741	-398 9183104	-398 9261069
E_{Ar} (C)*	-527 0118048	-527 0308654	-527 0347672	-527 0301693	-527 0303522	-527 0299794	-527 0368726
$E_{H2S}1$(M)*	-398 8934126	-398 9165376	-398 9223781	-398 9171911	-398 918016	-398 9178516	-398 9256167
$E_{H2S}2$(M)*	-398 8934038	-398 9165362	-398 9223824	-398 9171928	-398 9180192	-398 9178563	-398 9256257
E_{Ar} (M)*	-527 0115495	-527 0305977	-527 0344954	-527 0299064	-527 0300926	-527 029721	-527 0365992
E_{H2S} (M)	-398 8934133	-398 9165356	-398 9223744	-398 9171878	-398 9180123	-398 9178474	-398 9256116
E_{Ar} (M)	-527 0115495	-527 0305977	-527 0344954	-527 0299064	-527 0300926	-527 029721	-527 0365992
ΔE (kcal/mol)	-2 57	-2 12	-2 06	-1 89	-1 91	-1 89	-2 25
BSSE	0 73	0 75	0 76	0 73	0 73	0 73	0 77
ΔE^{CP}	-1 83	-1 37	-1 30	-1 16	-1 18	-1 16	-1 48
ΔE^{ZPE}	-0 75	-0 29	-0 22	-0 07	-0 10	-0 08	-0 40

Table IV.M. Energies for Structure C (Pseudo-lineal) of Ar-$(H_2S)_2$ at different levels using aug-cc-pVTZ basis set

Energy	MP2	MP3	MP4D	MP4DQ	MP4SDQ	CCSD	CCSD(T)
E_{com} (h)	-1324 8463765	-1324 9097956	-1324 92507	-1324 9083506	-1324 9100563	-1324 9090897	-1324 9342548
$E_{H2S}1$(C)*	-398 9092399	-398 9320418	-398 9378834	-398 9321243	-398 9328833	-398 9326366	-398 9411942
$E_{H2S}2$(C)*	-398 9090645	-398 9318957	-398 9377441	-398 9319868	-398 9327492	-398 9325025	-398 9410592
E_{Ar} (C)*	-527 024482	-527 0430643	-527 0467506	-527 0418781	-527 0420138	-527 041597	-527 0489543
$E_{H2S}1$(M)*	-398 9088173	-398 9316651	-398 9375072	-398 9317634	-398 9325238	-398 9322745	-398 9408074
$E_{H2S}2$(M)*	-398 9088055	-398 9316616	-398 9375104	-398 9317632	-398 9325251	-398 9322776	-398 9408158
E_{Ar} (M)*	-527 0242833	-527 0428734	-527 0465594	-527 041692	-527 0418281	-527 0414106	-527 0487584
E_{H2S} (M)	-398 9088177	-398 9316641	-398 9375053	-398 9317617	-398 9325219	-398 9322724	-398 9408049
E_{Ar} (M)	-527 0242833	-527 0428734	-527 0465594	-527 041692	-527 0418281	-527 0414106	-527 0487584
ΔE (kcal/mol)	-2 80	-2 26	-2 20	-1 97	-2 00	-1 97	-2 44
BSSE	0 55	0 50	0 50	0 48	0 48	0 49	0 52
ΔE^{CP}	-2 25	-1 75	-1 69	-1 48	-1 52	-1 48	-1 92
ΔE^{ZPF}	-1 12	-0 63	-0 57	-0 36	-0 39	-0 36	-0 79

Table IV.N. Frequencies of free H_2S monomer at different levels of theory

Modes	MP2/6-311++G**	MP2/6-311++G(3df,2p)	MP2/aug-cc-pVTZ	MP2/aug-cc-pVQZ
Bend	1233	1217	1211	1214
Symm stretch	2818	2776	2771	2774
Asym Stretch	2837	2795	2791	2794
ZPE (kcal/mol)	9 85	9 71	9 68	9 70

Table IV.O. Frequencies of $(H_2S)_2$ at different levels of theory

Modes	MP2/6-311++G**	MP2/6-311++G(3df,2p)	MP2/aug-cc-pVTZ
Intermolecular vibrations	50	40	40
	68	66	66
	76	75	78
	122	86	83
	232	165	165
	272	271	292
Acceptor bending	1230	1215	1209
Donor bending	1257	1223	1216
Donor sym stretch	2806	2741	2729
Acceptor sym stretch	2817	2773	2769
Donor asym stretch	2830	2786	2783
Acceptor asym stretch	2836	2792	2789
ZPE (kcal/mol)	20 87	20 35	20 33

Table IV.P. Vibrational frequencies of different minima for Ar-$(H_2S)_2$ calculated at different levels of theory

Modes	MP2/6-311++G**	MP2/6-311++G(3df,2p)	MP2/aug-cc-pVTZ
		Structure A	
Intermolecular vibrations	--	31	40
	--	33	40
	--	42	43
	--	69	73
	--	76	85
	--	93	97
	--	95	98
	--	169	175
	--	272	292
Acceptor bending	--	1212	1208
Donor bending	--	1220	1215
Donor sym stretch	--	2738	2726
Acceptor sym stretch	--	2772	2768
Donor asym. stretch	--	2784	2781
Acceptor asym stretch	--	2791	2788
ZPE (kcal/mol)	--	20 59	20 63
		Structure B	
Intermolecular vibrations	27	28	6
	36	36	31
	55	41	43
	70	67	61
	75	69	65
	106	90	82
	135	103	100
	219	172	168
	311	281	289
Acceptor bending	1230	1214	1208
Donor bending	1255	1222	1215

Table IV P continued

Donor sym stretch	2806	2740	2729
Acceptor sym stretch	2817	2771	2769
Donor asym stretch	2829	2786	2783
Acceptor asym stretch	2836	2791	2789
ZPE (kcal/mol)	21 17	20 60	20 50
Structure C (Pseudo-linear)			
Intermolecular vibrations	1	10	11
	21	12	15
	30	35	37
	31	46	53
	71	70	71
	86	83	85
	132	93	94
	232	171	171
	286	286	303
Acceptor bending	1230	1215	1209
Donor bending	1255	1222	1215
Donor sym stretch	2806	2740	2728
Acceptor sym stretch	2815	2772	2769
Donor asym stretch	2830	2786	2784
Acceptor asym stretch	2835	2792	2789
ZPE (kcal/mol)	20 96	20 49	20 49

References

1 G T Fraser, *Intl Rev Phys Chem* 10, 189 (1991)

2 T R Dyke and J S Muenter, *J Chem Phys* **60**, 2929 (1974)

3 T R Dyke, *J Chem Phys* **66**, 492 (1977)

4 L H Coudert, F J Lovas, R D Suenram and J T Hougen, *J Chem Phys* **87**, 6290 (1987)

5 J A Odutola, T A Hu, D Prinslow, S E O'dell and T R Dyke, *J Chem Phys* **88**, 5352 (1988)

6 K L Busarow, R C Cohen, G A Blake, K B Laughlin, Y T Lee and R J Saykally, *J Chem Phys* **90**, 3937 (1989)

7 G T Fraser, R D Suenram and L H Coudert, *J Chem Phys* **90**, 6077 (1989)

8 L H Coudert and J T Hougen, *J Mol Spectrosc* **139**, 259 (1990)

9 R S Fellers, L B Braly, R J Saykally and C Leforestier, *J Chem Phys* **110**, 6306 (1999)

10 N Goldman, R S Fellers, M G Brown, L B Braly, C J Keoshian, C Leforestier and R J Saykally, *J Chem Phys* **116**, 10148 (2002)

11 Y Watanabe, T Taketsugufoot and D J Wales, *J Chem Phys* **120**, 5993 (2004)

12 E Arunan, T Emilsson and H S Gutowsky, *J Am Chem Soc* **116**, 8418 (1994)

13 E Arunan, T Emilsson and H S Gutowsky, *J Chem Phys* **116**, 4886 (2002)

14 F J Lovas, private commn

15 J R Sabin, *J Am Chem Soc* **93**, 3613 (1971)

16 R C Kerns and L C Allen, *J Am Chem Soc* **100**, 6587 (1978)

17 M J Frisch, J A Pople and J E Del Bene, *J Phys Chem* **89**, 3664 (1985)

18 G de Oliviera and C E Dykstra, *Chem Phys Lett* **243**, 158 (1995)

19 G de Oliviera and C E Dykstra, *J Mo Struct (Theochem)*, **362**, 275 (1996)

20 E L Woodbridge, T Tso, M P McGrath, W J Hehre and E K C Lee, *J Chem Phys* **85**, 6991 (1986)

21 H. Tsuji, K Takizawa and S Koda, *Chem Phys* **285**, 319 (2002)

22 Chapter II of this thesis

23 H S Gutowsky, T Emilsson and E Arunan, *J Chem Phys* **106**, 5309 (1997)

24 J K G Watson, in *Vibrational Spectra and Structure*, Ed J R During (Elsevier, Amsterdam, **6**, 1 (1977) We thank G T Fraser for providing us with the program ASYM82 by A G Maki which was used in the fitting

25 M J Frisch, G W Trucks, H B Schlegel, G E Scuseria, M A Robb, J R Cheeseman, V G Zakrzewski, J A Montgomery, Jr, R E Stratmann, J C Burant, S Dapprich, J M Millam, A D Daniels, K N Kudin, M C Strain, O Farkas, J Tomasi, V Barone, M Cossi, R Cammi, B Mennucci, C Pomelli, C Adamo, S Clifford, J Ochterski, G A Petersson, P Y. Ayala, Q Cui, K Morokuma, N Rega, P Salvador, J J Dannenberg, D K Malick, A D Rabuck, K Raghavachari, J B Foresman, J Cioslowski, J V Ortiz, A G Baboul, B B Stefanov, G Liu, A Liashenko, P Piskorz, I Komaromi, R Gomperts, R L. Martin, D J Fox, T Keith, M A Al-Laham, C Y Peng, A Nanayakkara, M Challacombe, P M W Gill, B Johnson, W Chen, M W Wong, J L Andres, C Gonzalez, M Head-Gordon, E S Replogle, and J A Pople, Gaussian 98, Revision A 11 3, Gaussian, Inc , Pittsburgh PA, (2002)

26 S F. Boys and F Bernardi, *Mol Phys* **19**, 55 (1970)

27 S Simon, M Duran and J J Dannenberg, *J Chem Phys* **105**, 11024 (1996)

28 I Alkorta, I Rozas and J Elguero, *Chem Soc Rev* **27**, 163 (1998)

29 A P Cox, *J Mol Struct* **97**, 61 (1983)

Chapter V

Ab Initio Studies of H_2S-H_2O and Ar-H_2S-H_2O Complexes

V.1. Introduction

Hydrogen bonding is a very important phenomenon [1,2] Hydrogen bonding is defined as a non-covalent interaction between a proton donor X-H and a proton acceptor Y and it is denoted as X-H Y [3] Both X and Y are typically electronegative atoms The strength of H-bond depends on the proton donating efficiency of the donor and the proton accepting capability of the acceptor However, which is more dominating between the two? There have been many theoretical and experimental efforts to unravel the relative importance of the proton donor and acceptor in hydrogen bond formation H_2O-H_2S is a very suitable and interesting hydrogen bonded system in this context Depending on the mode of participation of each monomer in hydrogen bond formation there can be two geometries as shown in Figure V 1(A) and (B) One is H_2S HOH, (structure A H_2O is proton donor and H_2S is the acceptor) and the other one is H_2O· HSH (structure B H_2S is donor and H_2O acts as proton acceptor) H_2O is a good proton donor as well as an efficient proton acceptor, whereas H_2S is much weaker as both donor and acceptor Which one will be the global minimum for H_2O-H_2S complex, structure 'A' or 'B'?

Both structures have been observed in vibrational spectroscopic studies in matrix.[4,5] However, the global minimum could not be determined from these experiments Lovas has recorded the rotational spectra for H_2O-H_2S complex [6] From this spectrum for a vibrationally averaged geometry, it is not possible to comment on the nature of the minimum observed There are several theoretical papers as well on this particular hydrogen bonded complex [7-10] All the previous calculations at SCF level predict structure B to be more stable [8-10] However, the most recent theoretical paper of Wang *et al* on this system shows structure 'A' to be the global minimum [11] They optimized both the structures at MP2 level with 6-311++G(3d1f,3p1d) basis set and calculated the energy at several other correlated methods up to CCSD(T) They determined the structure 'A' to be more stable than B by ~0 27 kcal/mol In their analysis it was assumed that the zero point vibrational energy would not alter the relative stability of the two minima, and it was concluded that proton donor plays a more dominant role in hydrogen bond interaction

Our interest in this particular dimer is natural As discussed in the previous chapters, a systematic study on hydrogen bonded complexes of H_2O and H_2S is in progress in our laboratory It is hoped that experimental results on a series of H_2S complexes would be valuable in understanding hydrogen bonding Detailed investigation on H_2O-H_2S dimer is inevitable During the search for Ar_2-H_2S and Ar-$(H_2S)_2$, a series of lines were observed which are likely to be Ar-H_2O-H_2S trimer Though their assignment is preliminary as of now, a detailed look at H_2O-H_2S becomes imperative This chapter reports detailed theoretical investigations on H_2O-H_2S and Ar-H_2O-H_2S complexes and preliminary observations of the rotational spectrum of Ar-H_2O-H_2S

V.2. Method of Calculation

Different possible minima for both the dimer and the trimer were optimized at MP2 level of theory using 6-311++G(3df,2p) and aug-cc-pVTZ basis sets Frequency calculations were done for all the optimized geometries to confirm the nature of the stationary point All minima had only positive Eigen values in the Hessian The interaction energy was calculated following supermolecule approach and the energies were corrected for the Basis Set Superposition Error (BSSE) using Counterpoise method [12-14] Zero point corrections were done to test the assumption of Wang *et al* All the calculations were performed using Gaussian 98 software package [15]

V.3. H_2O···H_2S Dimer

V.3.a. Optimized Structures

The optimized structures are shown in Figure V 1 and are consistent with the previous reports Structure 'A' has H_2S as proton acceptor and H_2O as proton donor whereas in structure 'B' the donor and acceptor are interchanged The optimized

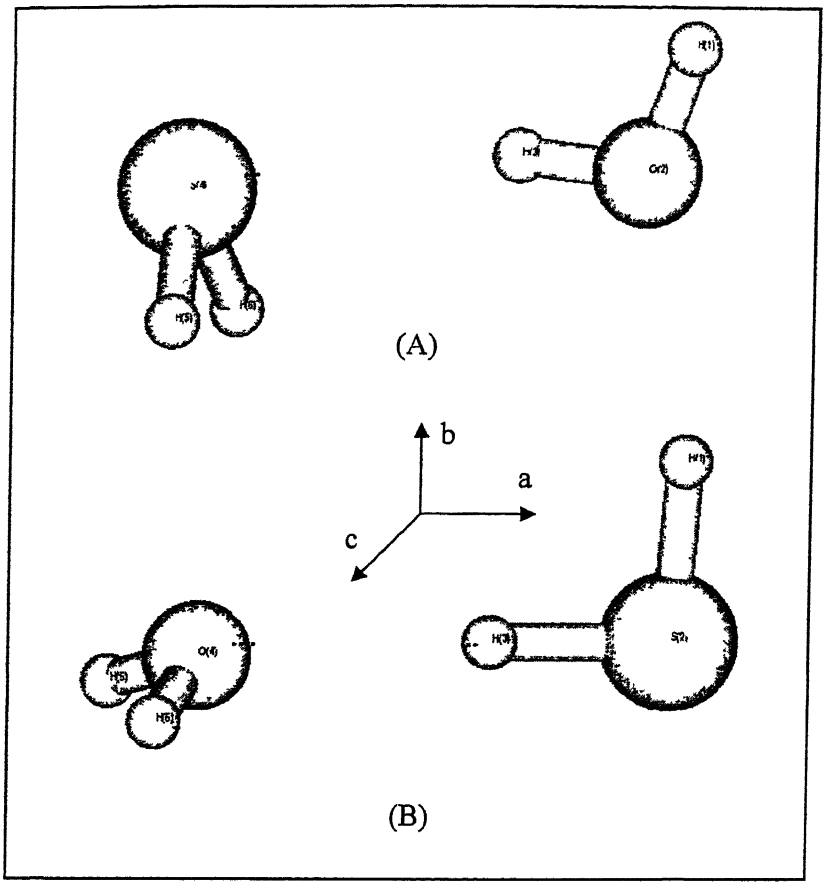

Figure V.1. Optimized structures of H_2O-H_2S complex (A) H_2O is proton donor and H_2S is proton acceptor, (B) H_2O is acceptor and H_2S is donor

Table V.1. Optimized structural parameters of H_2S-HOH and H_2O-HSH Δr is the change in O-H/S-H distance of H_2O/H_2S on hydrogen bond formation

Parameters	H_2S-HOH (A)		H_2O-HSH (B)	
	6-311++G(3df,2p)	aug-cc-pVTZ	6-311++G(3df,2p)	aug-cc-pVTZ
R(O-S)	3 4748	3 4607	3 5266	3 5238
R(XH1)	0 9585	0 9611	1 3333	1 3360
R(XH2)	0 9634	0 9662	1 3382	1 3410
A(X1-H-X2)	167.2	167 2	177 8	177 4
Δr	0.0047	0 0048	0 0047	0.0044

structural parameters are given in Table V 1 Both structures have C_s symmetry In structure 'A' the interacting monomers are slightly closer than in structure 'B' At MP2/aug-cc-pVTZ level, the O-S distances are 3 4607 Å and 3 5238 Å for structure 'A' and 'B' respectively However, the hydrogen bond is more linear in structure 'B' The angle in question is ~167° in 'A' and ~177° in 'B' at both level of theory The H_2S plane in structure A is almost perpendicular to hydrogen bond axis (intermolecular) The change in X-H bond length (Δr) is almost identical (0 005 Å) for both structures

V.3.b. Interaction Energy and Vibrational Frequency

The interaction energies are calculated following supermolecule approach The interaction energies are corrected for BSSE using counterpoise method The CP corrected interaction energy has been corrected for the zero point vibrational energy, as well The interaction energies calculated at both levels for both structures are listed in Table V 2 At both levels, uncorrected stabilization energy for structure 'A' is more than that of structure 'B'. The values are –3 30 kcal/mol and –2.98 kcal/mol at MP2/aug-cc-pVTZ level for 'A' and 'B' respectively Though the BSSE is comparatively less for structure 'B' at both levels, the CP corrected interaction energy is higher for structure 'A' The difference in CP corrected stabilization energy between the two structures is 0 18 kcal/mol at MP2/aug-cc-pVTZ level This difference is only 0 09 kcal/mol, using the lower basis set However, correcting for zero point vibrational energy over ΔE^{CP} leads to an interesting finding The zero point energy corrected interaction energy predicts the structure 'B' to be more stable than 'A' At MP2/aug-cc-pVTZ level of theory the stabilization energy of structure 'B' (1 44 kcal/mol) is 0 08 kcal/mol higher than that of A (1 36 kcal/mol) The difference is very similar at MP2/6-311++G(3df,2p) level also This is contradictory to the assumption made by Wang *et al.* on the relative stability of the two structures [11] This alteration in relative stability of structure 'A' and 'B' is the result of the difference in zero point vibrational energies for the two structures At MP2/aug-cc-pVTZ level, structure 'B' has zero point vibrational energy of 24 32 kcal/mol, which is 0 26 kcal/mol less than that of structure 'A'

Table V.2. Interaction energies of H_2S-HOH (A) and H_2O-HSH (B) at MP2 level using 6-311++G(3df,2p) and aug-cc-pVTZ basis sets

Energy (kcal/mol)	H_2S-HOH (A)		H_2O-HSH (B)	
	6-311++G(3df,2p)	aug-cc-pVTZ	6-311++G(3df,2p)	aug-cc-pVTZ
ΔE	-3 14	-3 30	-2 98	-2 98
BSSE	0 55	0 48	0 48	0 34
ΔE^{CP}	-2 59	-2 82	-2 50	-2 64
ΔE^{ZPE}	-1 13	-1 36	-1 22	-1 44
ZPE	24 72	24 58	24 54	24 32

This difference in zero point vibrational energy between the two structures results from the differences in frequencies of some intermolecular vibrational modes All the vibrational frequencies, calculated at both levels, for 'A' and 'B' are shown in Table V 3 Four intermolecular vibrational modes, marked in the Table V 3, have lower frequencies for structure 'B' than that for structure 'A' The red shifts of the donor X-H (X = O,S) stretching modes are given in the parenthesis in Table V 3 H_2O as donor undergoes a arger red shift than H_2S as donor At the highest level of theory considered here, the symmetric and asymmetric O-H stretches are red shifted by ~68 cm^{-1} and ~34 cm^{-1} espectively for structure 'A' At the same level for structure 'B' the S-H symmetric and asymmetric stretches are shifted by ~40 cm^{-1} and ~5 cm^{-1} respectively

Without zero point vibrational energy correction, structure 'A' is lower in energy, whereas with correction structure 'B' is more stable With and without zero point correction the interaction energies for the two structures differ by only ~30 cm^{-1} and ~60 cm^{-1} respectively Hence it is not possible to determine the global minimum unambiguously

Table V.3. Vibrational frequencies of structures A and B of H_2S-H_2O at MP2 level using 6-311++G(3df,2p) and aug-cc-pVTZ basis sets The values are in cm^{-1} The values in the parenthesis are the shift of the corresponding modes at respective levels of theory

Modes	H_2S-HOH		H_2O-HSH	
	6-311++G(3df,2p)	aug-cc-pVTZ	6-311++G(3df,2p)	aug-cc-pVTZ
Intermolecular vibrations	61	57	81	66
	96	95	106	93
	122	115	110	101
	124	131	111	109
	278	283	168	153
	448	446	383	368
H_2S bend	1214	1209	1227	1219
H_2O bend	1634	1635	1624	1627
H_2S sym stretch	2771	2769	2734 (42)	2731 (40)
H_2S asym stretch	2790	2788	2788 (7)	2786 (5)
H_2O sym stretch	3797 (64)	3754 (68)	3851	3815
H_2O asym stretch	3957 (33)	3914 (34)	3979	3940

V.4. Ar-H_2O-H_2S Trimer

Ar can approach towards H_2S-H_2O dimer from different orientation to form Ar-H_2S-H_2O trimer It can add to either structure 'A' or structure 'B' of H_2S-H_2O to produce different structures for the trimer Geometry optimization was carried out at MP2 method using both 6-311++G(3df,2p) and aug-cc-pVTZ basis sets Starting with the structure 'A' of the dimer, three minima have been found for the trimer These three minima differ in the relative position of Ar with respect to the H_2S-HOH dimer Ar is along *c*, *b* or *a* principal inertial axis of H_2S-HOH to produce the structures 'C', 'D' and 'E' respectively as shown in Figure V 2 (optimized at MP2/aug-cc-pVTZ level) Approaching Ar along '*b*' axis could have two possibilities either from the donor H side or from the acceptor H side However only the latter one could be optimized Again Ar

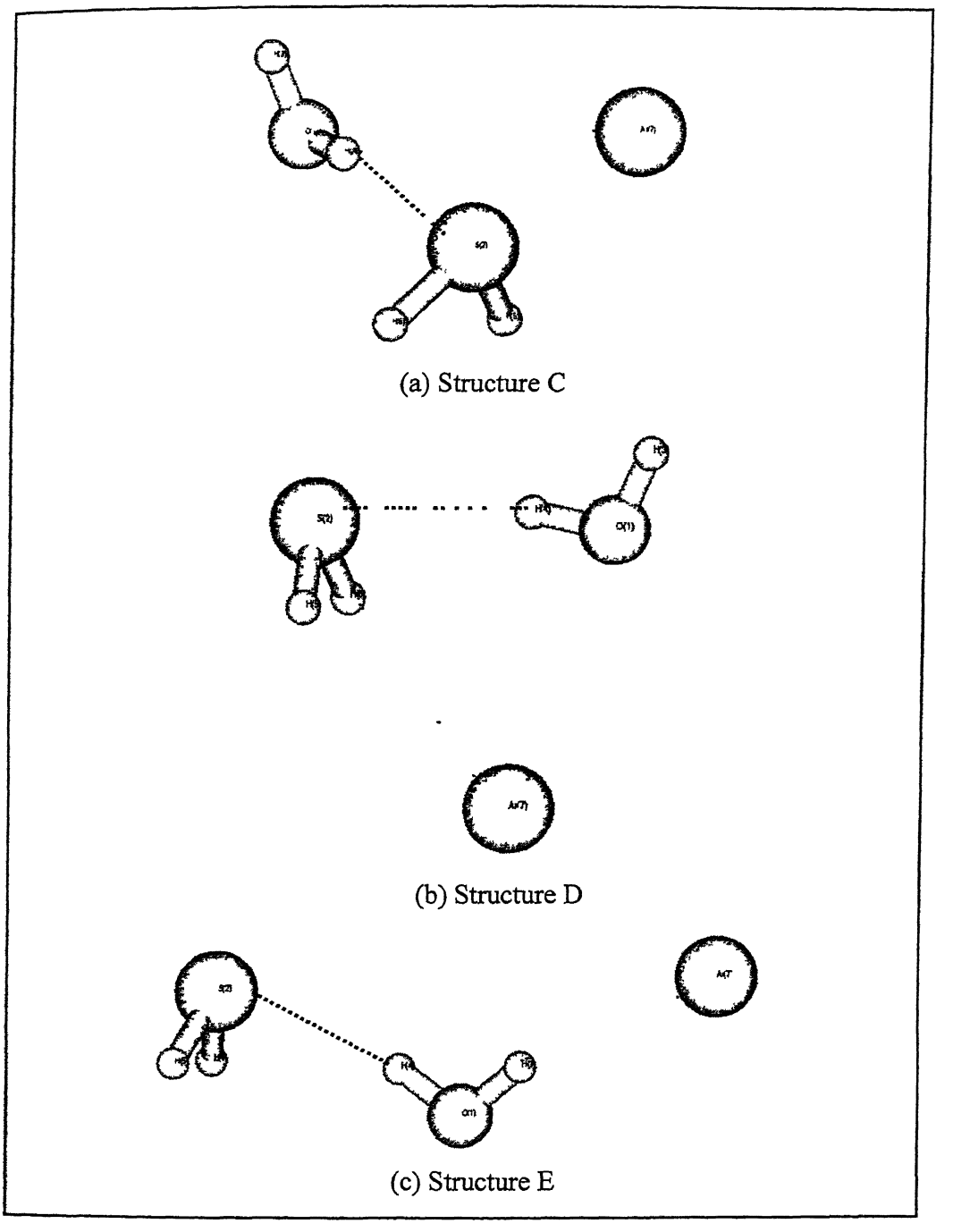

Figure V.2. Optimized structures of Ar-H_2S-HOH trimer where Ar interacts with structure **A** of H_2S-H_2O, at MP2/aug-cc-pVTZ level (a) Structure C Ar along 'c' axis, (b) Structure D Ar along '*b*' axis and (c) Structure E Ar along '*a*' axis of H_2S-HOH

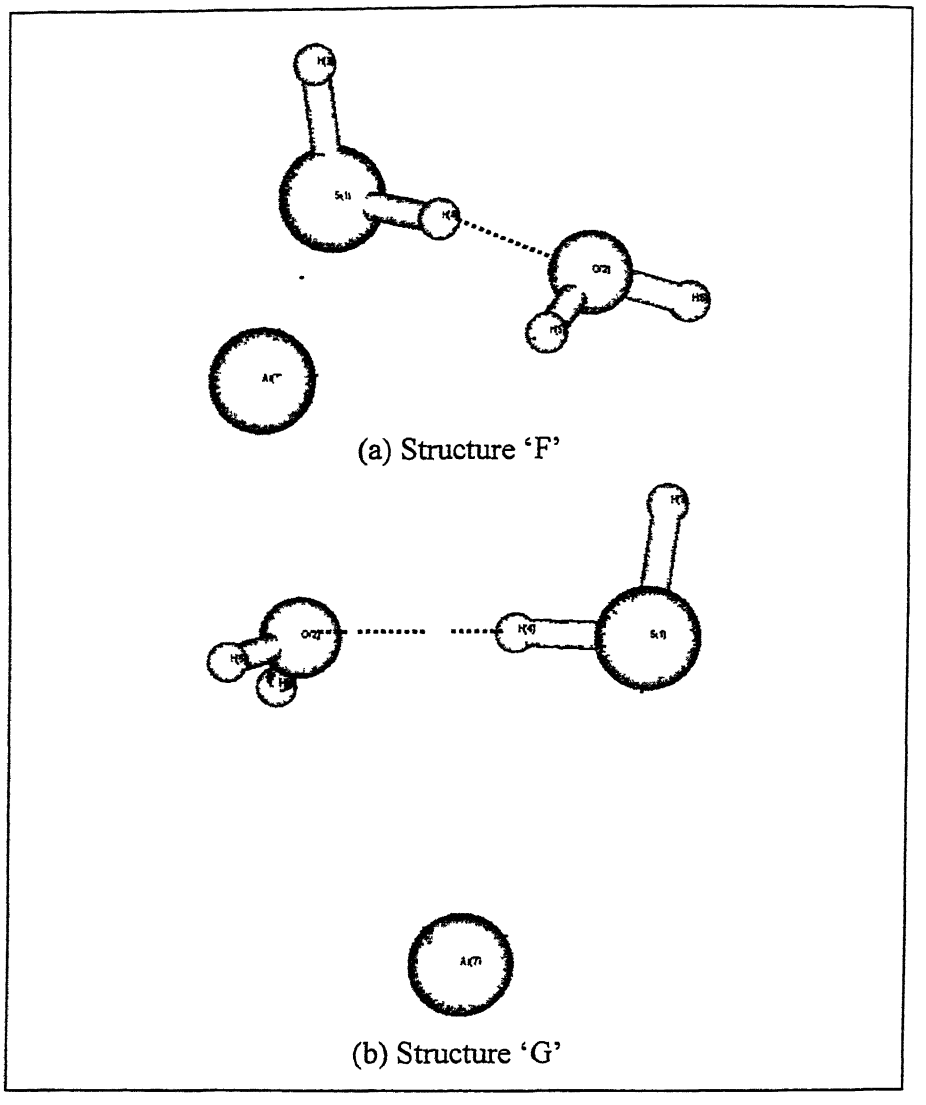

Figure V 3. Optimized structures of Ar-H_2O-HSH, where Ar interacts with structure B of H_2O-H_2S, at MP2/aug-cc-pVTZ level (a) Structure 'F' Ar along '*c*' axis and (b) Structure 'G' Ar along '*b*' axis

approaching along '*a*' axis of H_2S-HOH has two possibilities too Only one structure could be optimized where Ar interacts with the donor H_2O Starting from structure 'B', i e H_2O-HSH, only two minima have been optimized These minima are analogous to structures 'C'(F) and 'D'(G), and the optimized geometries at MP2/aug-cc-pVTZ level

are shown in Figure V 3 (a) and (b), respectively No minimum analogous to the structure 'E' could be optimized

V.4.a. Structure

Structures 'C' and 'F' have Ar along the '*c*' axis of the dimer In both these structures the dimer is slightly distorted The relative orientation of H_2S and H_2O is altered in the presence of Ar In 'C' all three heavy atoms and one H of acceptor, H_2S, are almost coplanar However, in 'F' all three heavy atoms and both H atoms of the acceptor, H_2O, are coplanar Structures 'D' and 'G' have Ar along the '*b*' axis of H_2O-H_2S dimer In both structures, the H_2S-H_2O unit retains its Cs symmetry and the symmetry of the trimer is also C_S In the structure 'E', Ar interacts only with the donor H_2O, to be specific, with one H of H_2O In this structure one H of H_2O is hydrogen bonded to H_2S and the other one is directed towards Ar The structural parameters for structures 'C', 'D' and 'E' are given in Table V 4 and those for structures 'F' and 'G' are listed in Table V 5

Table V.5. Structural parameters of three minima of Ar-H_2S-HOH ('C', 'D' and 'E') calculated at MP2 level using 6-311++G(3df,2p) and aug-cc-pVTZ basis sets Δr is the change in O-H distance of H_2O on hydrogen bond formation

Parameters	MP2/6-311++G(3df,2p)			MP2/aug-cc-pVTZ		
	C	D	E	C	D	E
R(O-S)	3 4667	3 4708	3 4726	3 4473	3 4553	3 4581
R(Ar-O)	3 8118	3 4609	3 6723	3 7475	3 4024	3 6454
R(Ar-S)	3 7123	4 0308	--	3 6916	3 9442	--
R(O-H3)	0 9586	0 9588	0 9586	0 9612	0 9614	0 9613
R(O-H4)	0 9635	0 9637	0 9634	0 9664	0 9666	0 9662
∠O-H4-S	166 3	166 9	166 7	164 1	165 8	165 7
Δr	0 0048	0 0050	0 0047	0.0050	0 0052	0 0048

Table V.6. Structural parameters of three minima of Ar-H_2O-HSH ('F' and 'G') calculated at MP2 level using 6-311++G(3df,2p) and aug-cc-pVTZ basis sets Δr is the change in S-H distance of H_2S on hydrogen bond formation

Parameters	MP2/6-311++G(3df,2p)		MP2/aug-cc-pVTZ	
	F	G	F	G
R(O-S)	3 5230	3 5277	3 5135	3 5256
R(Ar-O)	3 4924	3 7297	3 4693	3 7284
R(Ar-S)	4 1309	3 7056	4 0940	3 6507
R(S-H3)	1 3333	1 3335	1 3361	1 3362
R(S-H4)	1 3382	1 3384	1 3411	1 3412
∠O-H4-S	177 7	176 4	171 2	176 3
Δr	0 0049	0 0051	0 0045	0 0046

The O-S distances are very similar for all three minima (C, D and E) of Ar-H_2S-HOH At MP2/aug-cc-pVTZ levels, the values are 3 4473 Å, 3 4553 Å and 3 4581 Å for structures C, D and E respectively The O-S distances for both structures of Ar-H_2O-HSH (F and G) are also very similar, but slightly higher than those for Ar-H_2S-HOH. The distances at MP2/aug-cc-pVTZ are 3 5135 Å and 3 5256 Å These distances are almost identical to that in the corresponding dimer structure The change in the length of the hydrogen bonded X-H bond on hydrogen bond formation (Δr) is almost identical to that in the corresponding dimers

V.4.b. Interaction Energy and Vibrational Frequency

The interaction energies for the three minima of Ar-H_2S-HOH (structures C, D and E) and the two minima of Ar-H_2O-HSH (structures F and G), calculated at MP2 level using 6-311++G(3df,2p) basis set are tabulated in Table V 7 and those calculated at MP2/aug-cc-pVTZ level, are listed in Table V 8 The pseudo-linear structure (E) is the least stable among all of them in both levels The CP corrected and the CP and zero point

energy corrected interaction energies are –3 14 kcal/mol and –1 43 kcal/mol respectively at MP2/aug-cc-pVTZ level of theory The CP corrected interaction energies predict the other two minima of Ar-H_2S-HOH (structure C and D) to be more stable than the two minima (structures F and G) of Ar-H_2O-HSH at both levels The CP corrected interaction energies for structures C, D, F and G are –3 47 kcal/mol, -3 59 kcal/mol, -3 29 kcal/mol and –3 30 kcal/mol respectively at MP2/aug-cc-pVTZ level However, on correcting for the zero point vibrational energy over the CP corrected interaction energy leads to a similar result as in case of H_2S-H_2O dimer At MP2/aug-cc-pVTZ level of theory, both minima (F and G) of Ar-H_2O-HSH are more stable than the minima C and D of Ar-H_2S-HOH However, the structures D and F have almost identical stabilization energies, the values are –1 84 kcal/mol and –1 85 kcal/mol respectively Among the three minima of Ar-H_2S-HOH system the structure D is most stable, whereas the structure G is most stable (-1 92 kcal/mol) among all five minima at MP2/aug-cc-pVTZ level However, the lower level results do not exactly support this At MP2/6-311++G(3df,2p) level of theory, the structure F is most stable (-1 56 kcal/mol) among all five minima As the differences in stabilization energies for the five minima are marginal and different levels of calculations lead to different relative stability of the minima, it is not possible to determine the global minimum unambiguously for Ar-H_2O-H_2S system

Table V.7. Interaction energies for the three minima of Ar-H_2S-HOH (structures C, D and E) and the two for Ar-H_2O-HSH (structures F, G) calculated at MP2/6-311++G(3df,2p) level of theory All the values are in kcal/mol.

Energy	C	D	E	F	G
ΔE	-3 96	-4 04	-3 60	-3 82	-3 87
BSSE	0 91	0 88	0.78	0 81	0 89
ΔE^{CP}	-3 05	-3 16	-2 82	-3 01	-2 98
ΔE^{ZPE}	-1 39	-1 45	-1 24	-1 56	-1 39
ZPE	24 92	24 97	24 84	24 71	24 82

Table V.8. Interaction energies for three minima of Ar-H_2S-HOH (structures C, D and E) and the two for Ar-H_2O-HSH (structures F, G) calculated at MP2/aug-cc-pVTZ level of theory All the values are in kcal/mol

Energy	C	D	E	F	G
ΔE	-4 18	-4 34	-3 90	-3 93	-3 89
BSSE	0 71	0 75	0 76	0 64	0 59
ΔE^{CP}	-3 47	-3 59	-3 14	-3 29	-3 30
ΔE^{ZPE}	-1 78	-1 84	-1 43	-1 85	-1 92
ZPE	24 81	24 87	24 83	24 56	24 50

The vibrational frequencies were calculated for all the optimized geometries The vibrational frequencies for all five minima of Ar-H_2S-H_2O system, calculated at MP2 method using 6-311++G(3df,2p) and aug-cc-pVTZ basis sets, are listed in Table V 9 and Table V 10 The lists include only the frequencies of intramolecular vibrations of H_2S and H_2O The red shifts of the X-H frequencies on hydrogen bonding are very similar to the corresponding dimers

Table V.9. Vibrational frequencies of structures C, D, E, F and G of Ar-H_2S-H_2O at MP2/6-311++G(3df,2p) level of theory All the values are in cm^{-1} Values in parenthesis show the red shift

Modes	C	D	E	F	G	H_2O/H_2S
H_2S bend	1212	1214	1214	1227	1226	1217
H_2O bend	1634	1634	1632	1622	1626	1624
S-H sym Stretch	2772	2771	2771	2734 (42)	2730 (46)	2776
S-H asym Stretch	2790	2790	2790	2788 (7)	2786 (9)	2795
O-H sym Stretch	3792 (69)	3795 (66)	3796 (65)	3849	3850	3861
O-H asym. stretch	3952 (38)	3956 (34)	3956 (34)	3978	3977	3990

Table V.10. Vibrational frequencies of all five minima of Ar-H_2O-H_2S at MP2/aug-cc-pVTZ levels of theory Values in parenthesis show the red shift. All the values are in cm^{-1}

Modes	C	D	E	F	G	H_2O/H_2S
H_2S bend	1207	1208	1209	1218	1218	1212
H_2O bend	1637	1635	1634	1623	1627	1628
S-H sym Stretch	2768	2768	2768	2730 (41)	2728 (43)	2771
S-H asym Stretch	2787	2787	2788	2785 (6)	2784 (7)	2791
O-H sym Stretch	3748 (74)	3752 (70)	3756 (66)	3812	3814	3822
O-H asym stretch	3910 (38)	3913 (35)	3913 (35)	3938	3939	3948

It should be mentioned, here, that for the conformers with H_2O as H-bond donor (for both H_2S-HOH and Ar-H_2S-HOH), one intermolecular bending mode has sufficiently high frequency At MP2/aug-cc-pVTZ level of calculation, it is 446 cm^{-1} for the dimer, and remains almost unchanged in the trimer However, the frequency of the corresponding vibrational mode in the H_2O-HSH (Ar-H_2O-HSH) conformer is 368 cm^{-1} (~372 cm^{-1}, see Table V H) at the same level of calculation Clearly, this mode contributes most to alter the relative stability of the conformers, when zero point vibrational energy is added to the interaction energy

V.5. Preliminary experimental results of Ar-H_2S-H_2O complex

During the search of Ar-$(H_2S)_2$ complex some lines were present which require Ar, H_2S and H_2O to be observed The optimum expansion condition for these lines was similar to that for Ar-$(H_2S)_2$ and the microwave pulse was optimum at 0 3 μs Hence it was thought that those signals could be of Ar-H_2S-H_2O complex Rotational transitions were predicted for this complex and the PNFT microwave spectrometer was scanned in limited frequency region in search of related signals So far six transitions have been

Table V.11. Observed transition frequencies of Ar-H_2S-H_2O and their probable assignment

Probable assignment	Observed Frequency	Probable assignment	Observed Frequency
	5153 691		6738 695
$0_{00} \rightarrow 1_{11}$	5153 565	$1_{10} \rightarrow 2_{11}$	6738 739
	5153 520		6738 786
	5153 447		6738 884
	5500 431		7583 578
$1_{11} \rightarrow 2_{12}$	5500 442	$1_{01} \rightarrow 2_{12}$	7583 694
	5500 475		7583 743
	--		7583 845
	6010.793		10781 350
$1_{01} \rightarrow 2_{02}$	6010 826	$3_{13} \rightarrow 4_{14}$	10781 320
	6010 847		10781 240
	6010 887		10781 200

Table V.12. Rotational constants for different minima found for Ar-H_2O-H_2S at MP2 level using 6-311++G(3df,2p) and aug-cc-pVTZ basis sets

	6-311++G(3df,2p)			aug-cc-pVTZ		
	C	D	E	C	D	E
A	3687 57	4217 36	230392 2	3746 63	4259 27	13267 29
B	1888 77	1705 26	0602 10	1921 06	1783 55	682 08
C	1263 80	1225 26	589 32	1284 83	1268 93	651 87
	F	G	--	F	G	Experiment
A	4131 93	3579 54	--	4170 86	3538 21	3934
B	1608 42	1932 15	--	1636 09	1986 59	1842
C	1167 80	1262 12	--	1185 45	1279 77	1217

observed which are likely to be for Ar-H_2O-H_2S complex Each of these transitions is a set of three/four lines The complete list of the frequencies observed and their probable assignments are given in Table V 11 These assignments give the rotational constants to be A = 3934 MHz, B = 1842 MHz and C = 1217 MHz The rms deviation of the fit with only these six transitions is ~6 MHz Certainly more number of transitions is needed to determine a more reliable set of rotational and distortion constants The rotational constants are comparable to the values (given in Table V 12) calculated for some of the *ab initio* minima found for Ar-H_2O-H_2S Hence, it is likely that the transitions, observed, are for Ar-H_2O-H_2S complex

V.6. Conclusions

Ab initio calculations have been done for H_2S-H_2O and Ar-H_2S-H_2O complexes at MP2 level of theory using 6-311++G(3df,2p) and aug-cc-pVTZ basis set For the dimer, H_2S-HOH (structure A) is more stable on the basis of CP corrected interaction energy However, H_2O-HSH (structure B) becomes marginally more stable on further correction of the interaction energy for zero point vibrational energy These two structures appear to be very close in energy For the trimer, three minima have been found for Ar-H_2S-HOH and two minima have been found for Ar-H_2O-HSH The relative stability of different minima for Ar-H_2S-H_2O also alters on taking zero point vibrational energy into account Some rotational transitions have been observed which are likely to be of Ar-H_2O-H_2S

Table V.A. Optimized structural parameters of H_2O and H_2S at MP2 level The distances are in Å and angles are in degrees

Parameters	H_2O		H_2S	
	6-311++G(3df,2p)	aug-cc-pVTZ	6-311++G(3df,2p)	aug-cc-pVTZ
R(1,2)	0 9587	0 9614	1 3335	1 3366
R(2,3)	0 9587	0 9614	1 3335	1 3366
A(1,2,3)	104 5	104 1	92 3	92 3
ZPE (kcal/mol)	13 55	13 44	9 71	9 68
	1H 2O/S	3H		

Table V.B. Optimized parameters of the two minima for H_2S-H_2O at MP2 level using 6-311++G(3df,2p) and aug-cc-pVTZ basis sets

Parameters	H_2S-HOH (structure A)		H_2O-HSH (structure B)	
	6-311++G(3df,2p)	aug-cc-pVTZ	6-311++G(3df,2p)	aug-cc-pVTZ
R(1,2)	0 9585	0 9611	1 3333	1 336
R(2,3)	0 9634	0 9662	1 3382	1 341
R(3,4)	2 5287	2 5118	2 1891	2 1837
R(3,5)	2 8337	2 8085	2 8056	2 8152
R(3,6)	2 8337	2 8085	2 8056	2 8152
R(4,5)	1 3343	1 3371	0 9595	0 9619
R(4,6)	1 3343	1 3371	0 9595	0 9619
A(1,2,3)	104.7	104 3	92 6	92 6
A(2,3,4)	167.2	167 2	177 8	177 4
A(2,3,5)	142 0	141 7	162 0	162.1
A(2,3,6)	142 0	141 7	162 0	162 1
A(5,3,6)	39 7	40 2	31 5	31 3
A(5,4,6)	92 4	92 3	104 8	104 5
D(1,2,3,4)	180 0	180 0	180 0	180 0
D(1,2,3,5)	-146 5	-146 4	118 8	118 5
D(1,2,3,6)	146 5	146 4	-118 8	-118 5
Rot const (GHz)	120 24037	119 65279	165 08101	165 94570
	3 55255	3 58355	3 33946	3 34019
	3 54093	3 57153	3 32342	3 32451
A: 1H 2O 3H 4S 5H 6H			**B:** 1H 2S 3H 4O 5H 6H	

Table V.C. Optimized parameters for the three minima (structures C, D and E) of Ar-H_2S-HOH at MP2 level using 6-311++G(3df,2p) and aug-cc-pVTZ basis sets

Parameters	Structure D		Structure C		Structure E	
	6-311++G(3df,2p)	aug-cc-pVTZ	6-311++G(3df,2p)	aug-cc-pVTZ	6-311++G(3df,2p)	aug-cc-pVTZ
R(1,3)	0 9588	0 9614	0 9586	0 9612	0 9586	0 9613
R(1,4)	0 9637	0 9666	0 9635	0 9664	0 9634	0 9662
R(1,7)	3 4609	3 4024	3 8118	3 7475	3 6723	3 6454
R(2,4)	2 5252	2 5099	2 5230	2 5075	2 5278	2 5137
R(2,5)	1 3342	1 3372	1 3343	1 3372	1 3342	1 3370
R(2,6)	1 3342	1 3372	1 3343	1 3371	1 3342	1 3370
R(2,7)	4 0308	3 9442	3 7123	3 6916	--	--
R(3,7)	--	--	--	--	2 8424	2 7062
R(4,5)	2 8148	2 7691	2 7485	2 7004	2 8292	2 7946
R(4,6)	2 8148	2 7691	2 9909	2 9817	2 8292	2 7947
R(4,7)	3 4374	3 3794	3 5062	3 4950	--	--
R(5,7)	3 3941	3 2868	3 3789	3 2153	--	--
R(6,7)	3 3941	3 2868	--	--	--	--
A(3,1,4)	104 6	104 2	104 7	104 3	104 8	104 3
A(3,1,7)	--	--	98 2	112 6	--	--
A(5,2,6)	92 2	92 1	92 5	92 4	92 4	92 3
A(6,2,7)	--	--	151 5	146 8	--	--
A(1,4,2)	166 9	165 8	166 3	164 1	166 7	165 7
A(1,4,5)	141 6	140 2	137 5	134 7	141 6	140 3
A(1,4,6)	141 6	140 2	149 8	149 9	141 6	140 3
A(5,4,6)	39 9	40 7	38 9	39.3	39 8	40 4
A(6,4,7)	--	--	98 3	97 1	--	--
A(1,7,2)	54 6	55 5	54 9	55 2	--	--
A(1,7,5)	63 7	64 4	58 2	58 8	--	--
A(1,7,6)	63 7	64 4	--	--	--	--
A(5,7,6)	32 9	34 1	--	--	--	--
A(2,1,7)	--	--	--	--	140 5	125 3
D(3,1,4,2)	180 0	180 0	-160.0	-165 1	180 0	-180 0
D(3,1,4,5)	-146 6	-147 1	-155.8	-165 0	-146 8	-147 3
D(3,1,4,6)	146 6	147 1	138 7	132 5	146 8	147 3
D(3,1,7,2)	--	--	112 9	107 6	--	--
D(3,1,7,5)	--	--	137 9	132 2	--	--
D(6,2,7,1)	--	--	50 8	58 7	--	--

1O 2S 3H 4H 5H 6H 7Ar

Table V.D. Optimized parameters for the three minima (structures C, D and E) of Ar-H_2O-HSH at MP2 level using 6-311++G(3df,2p) and aug-cc-pVTZ basis sets

Parameters	Structure F		Structure G	
	6-311++G(3df,2p)	aug-cc-pVTZ	6-311++G(3df,2p)	aug-cc-pVTZ
R(1,3)	1 3333	1 3361	1 3335	1 3362
R(1,4)	1 3382	1 3411	1 3384	1 3412
R(1,7)	4 1309	4 0940	3 7056	3 6507
R(2,4)	2 1854	2 1821	2 1909	2 1861
R(2,5)	0 9596	0 9622	0 9597	0 9620
R(2,6)	0 9596	0 9619	0 9597	0 9620
R(2,7)	3 4924	3 4693	3 7297	3 7284
R(4,5)	2 7752	2 6827	2 7622	2 7862
R(4,6)	2 8387	2 9176	2 7622	2 7862
R(4,7)	3 5282	3 5894	3 3482	3 3123
R(5,7)	2 9616	2 7738	3 7047	3 7624
R(6,7)	--	--	3 7047	3 7624
A(3,1,4)	92 6	92 6	92 7	92 6
A(3,1,7)	94 5	96 5	156 9	157 5
A(5,2,6)	104 9	104 7	104 7	104 4
A(6,2,7)	152 7	141 1	81 1	84 6
A(1,4,5)	160 2	151 7	160 1	160 6
A(1,4,6)	164 5	169 8	160 1	160 6
A(1,4,7)	107 4	102 5	94 7	93 6
A(1,7,2)	54 3	54 6	56 7	57 1
A(5,4,6)	31 4	31 2	31 9	31 7
A(6,4,7)	54 5	81 1	73 9	75 6
D(3,1,4,5)	115 5	108 0	126 1	124 7
D(3,1,4,6)	-118 3	-154 5	-126 1	-124 7
D(3,1,4,7)	93 7	96 0	0 0	0 0
D(3,1,7,5)	-97 3	-95 0	13 0	12 7
D(3,1,7,6)	-96 2	-96 6	-13 0	-12 7
	1S 2O 3H 4H 5H 6H 7Ar			

Table V.E. Absolute energies of H_2S-HOH and H_2O-HSH and their fragment monomer and the interaction energies

Energy	H_2S-HOH		H_2O-HSH	
(h)	6-311++G(3df,2p)	aug-cc-pVTZ	6-311++G(3df,2p)	aug-cc-pVTZ
E_{Com}	-475 2168719	-475 2430726	-475 2166221	-475 2425634
E_{H2S}*(C)	-398 8940234	-398 9093597	-398 8937818	-398 9090552
E_{H2O}*(C)	-76 3186998	-76 3291814	-76 3188356	-76 3292798
E_{H2S}*(M)	-398 8934122	-398 908817	-398 8933984	-398 9088033
E_{H2O}*(M)	-76 3184301	-76 3289678	-76 3184491	-76 3289878
E_{H2S}(M)	-398 8934133	-398 9088177	-398 8934133	-398 9088177
E_{H2O}(M)	-76 3184531	-76 3289924	-76 3184531	-76 3289924

Table V.F Energies for two minima of Ar-H_2O-HSH

Energy	Structure F		Structure G	
(h)	6-311++G(3df,2p)	aug-cc-pVTZ	6-311++G(3df,2p)	aug-cc-pVQZ
E_{Com}	-1002 2294992	-1002 2683564	-1002 2295744	-1002 2682884
E_{H2S}*(C)	-398 8938826	-398 909105	-398 8939248	-398 9091236
E_{H2O}*(C)	-76 3189193	-76 3293314	-76 3189844	-76 3293294
E_{Ar}*(C)	-527 0118835	-527 0246455	-527 0119059	-527 0245513
E_{H2S}*(M)	-398 8933985	-398 9088029	-398 8933954	-398 9088004
E_{H2O}*(M)	-76 3184468	-76 3289835	-76 3184503	-76 3289885
E_{Ar}*(M)	-527 0115495	-527 0242833	-527 0115495	-527 0242833
E_{H2S}(M)	-398 8934133	-398 9088177	-398 8934133	-398 9088177
E_{H2O}(M)	-76 3184531	-76 3289924	-76 3184531	-76 3289924
E_{Ar}(M)	-527 0115495	-527 0242833	-527 0115495	-527 0242833

Table V.G Energies of different minima of Ar-H_2S-HOH

	MP2/6-311++G(3df,2p)			MP2/aug-cc-pVTZ		
Energy	Structure C	Structure D	Structure E	Structure C	Structure D	Structure E
E_{Com}	-1002 2297337	-1002 2298531	-1002 2291497	-1002 2687555	-1002 269006	-1002 2683106
E_{H2S}*(C)	-398 8941893	-398 8941354	-398 8940351	-398 9094308	-398 9094223	-398 9093718
E_{H2O}*(C)	-76 3187797	-76.3187569	-76 3187689	-76 3292152	-76 3292216	-76 3292826
E_{Ar}*(C)	-527 011876	-527 0118927	-527 0118227	-527 0245568	-527 0246105	-527 0246293
E_{H2S}*(M)	-398 8934113	-398 8934126	-398 8934123	-398 9088158	-398 9088169	-398 9088172
E_{H2O}*(M)	-76 3184292	-76 3184286	-76.3184284	-76 3289661	-76 3289652	-76 328968
E_{Ar}*(M)	-527 0115495	-527 0115495	-527 0115495	-527 0242833	-527 0242833	-527 0242833
E_{H2S}(M)	-398.8934133	-398 8934133	-398 8934133	-398 9088177	-398 9088177	-398 9088177
E_{H2O}(M)	-76 3184531	-76 3184531	-76 3184531	-76 3289924	-76 3289924	-76 3289924
E_{Ar}(M)	-527 0115495	-527 0115495	-527 0115495	-527 0242833	-527 0242833	-527 0242833

Table V.H Vibrational frequencies for all five minima of Ar-H_2S-H_2O at MP2 level using 6-311++G(3df,2p) and aug-cc-pVTZ basis sets All values are in cm^{-1}

MP2/6-311++G(3df,2p)					MP2/aug-cc-pVTZ				
C	D	E	F	G	C	D	E	F	G
26	38	5	29	34	19	43	9	28	17
39	42	21	33	43	36	43	20	41	31
42	43	36	50	49	54	47	51	56	44
73	98	74	87	102	77	99	91	79	73
100	103	95	106	111	101	106	97	95	88
124	127	125	112	121	133	130	135	111	110
145	138	129	127	123	142	138	154	132	115
280	277	280	167	190	291	285	293	164	174
444	446	446	378	394	437	447	447	371	373
1214	1212	1214	1227	1226	1208	1207	1209	1218	1218
1634	1634	1632	1622	1626	1635	1637	1634	1623	1627
2771	2772	2771	2734	2730	2768	2768	2768	2730	2728
2790	2790	2790	2788	2786	2787	2787	2788	2785	2784
3795	3792	3796	3849	3850	3752	3748	3756	3812	3814
3956	3952	3956	3978	3977	3913	3910	3913	3938	3939

References

1 G R Desiraju and T Steiner, *The Weak Hydrogen Bond In Structural Chemistry and Biology*, Oxford University Press, Oxford (1999)

2 G A Jeffrey and W Saenger, *Hydrogen Bonding in Biological Structures*, Springer Verlog, Berlin (1991)

3 G C. Pimental and A L McClellan, *The Hydrogen Bond*, W H Freeman and Company, San Fransisco (1960)

4 B Nelander, *J Chem Phys* **69**, 3870 (1978)

5 A J Barnes, R M Bentwood and M P Wright, *J Mol Struct* **118**, 97 (1984)

6 F J Lovas, *private communication*

7 P Kollman, J McKelvey, A Johanssen and S Rothenberg, *J Am Chem Soc* **97**, 955 (1975)

8 S Chin and T A Ford, *J Mol Struct* THEOCHEM, **133**, 193 (1985)

9 R D Amos, *Chem Phys* **104**, 145 (1986).

10 J. E DelBene, *J Phys Chem* **92**, 2874 (1988)

11 Y B Wang, F M Tao and Y K Pan, *Chem Phys Lett.* **230**, 480 (1994)

12 S F Boys and F Bernardi, *Mol Phys* **19**, 55 (1970)

13 S Simon, M Duran and J J Dannenberg, *J Chem Phys* **105**, 11024 (1996)

14 I. Alkorta, I. Rozas and J. Elguero, *Chem Soc Rev* **27**, 163 (1998)

15 M J Frisch, G W Trucks, H B Schlegel, G E Scuseria, M A Robb, J R Cheeseman, V G Zakrzewski, J A Montgomery, Jr, R E Stratmann, J C Burant, S Dapprich, J M Millam, A D Daniels, K N Kudin, M C Strain, O Farkas, J Tomasi, V Barone, M Cossi, R Cammi, B. Mennucci, C Pomelli, C Adamo, S Clifford, J Ochterski, G A Petersson, P Y Ayala, Q Cui, K Morokuma, N Rega, P Salvador, J J Dannenberg, D K Malick, A D Rabuck, K Raghavachari, J B Foresman, J Cioslowski, J V Ortiz, A G Baboul, B B Stefanov, G Liu, A Liashenko, P Piskorz, I Komaromi, R Gomperts, R L Martin, D J. Fox, T Keith, M A Al-Laham, C Y Peng, A Nanayakkara, M Challacombe, P M W. Gill, B Johnson, W Chen, M W Wong, J L Andres,

C Gonzalez, M Head-Gordon, E S Replogle, and J A Pople, Gaussian 98, Revision A 11 3, Gaussian, Inc , Pittsburgh PA, (2002)

Chapter VI

Hydrogen Bond Radius

VI.1. Introduction

The nature of chemical bonding, the interaction between atoms within a molecule, is fairly well understood [1] Pauling's classic book[1] talks about covalent radii, ionic radii and metallic radii for various atoms which can be used to predict inter-atomic distances between atoms forming a covalent, ionic or metallic bond [1] However, our understanding of intermolecular interactions is still evolving[2] Hydrogen bonding is one of the stronger intermolecular interactions, which has a great relevance in nature [3,4] Hydrogen bonding remains a fascination for many researchers since its discovery in early twentieth century Till today a large number of theoretical and experimental studies are being carried out by several groups and attempts have been made to unravel the actual nature of H-bond interaction

Originally H-bonding was observed between H, covalently bound to an electronegative atom X (N, O, F), and another electronegative atom Y It is usually represented as X-H···Y The intermolecular separations in these complexes have been largely interpreted in terms of the van der Waals radii[1] of the constituent heavy atoms X and Y There are several previous reports where crystallographic data have been analyzed to correlate the internuclear separation with the van der Waals radii of the heavy atoms involved in the hydrogen bond formation [5-7]

Buckingham and Fowler[8] used a model of H-bonding based on electrostatic interactions only The model could explain and predict fairly the radial and angular geometries for a series of hydrogen bonded complexes Gadre and Bhadane[9] have made a different approach They have calculated the molecular electrostatic potential (MESP) for a series of H-bond acceptors, B, and have tried to make a correlation between H-bond distance and van der Waals radius of hydrogen in B---HF complexes

Gadre and Bhadane approach has been extended for several other series of hydrogen bonded, B HX complexes, where X = F, Cl, Br, CN, OH and CCH From this empirical analysis "hydrogen bond radius" has been defined and it has been determined for the above H-bond donors. Such analysis could not be carried out for SH groups as the available experimental data are quite limited Hydrogen bonding by SH groups is

important in the amino acid Cysteine and its derivatives [4] Hence, it was decided to use theoretical calculations to determine the H-bond radius for SH *Ab initio* and DFT calculations have been performed for several B---HX complex (X = F, Cl, OH and SH) at MP2 and B3LYP level using 6-311++G** basis set From these structural data "hydrogen bond radii" have been determined and compared with the empirical values The comparison of the empirical and the *ab initio* results for HF, HCl and H_2O reveals that the *ab initio* results for H_2S should be reliable Hydrogen bond radii calculated for various donors, HX, show a strong inverse correlation with the dipole moment of H-X bond and the electronegativity difference between X and H

VI.2. Buckingham and Fowler Model

Buckingham and Fowler model for the geometries of hydrogen-bonded complexes, B-HX, is solely electrostatic [8] This model considers the monomer charge densities as a collection of different multi-poles centered at different atoms or bond midpoints Their model satisfies most of the structural features of hydrogen bonding An empirical observation of B F distances in B---HF complexes shows that these distances were close to the sum of van der Waals radii of B and F This led Buckingham and Fowler to conclude that H does not contribute to the intermolecular separation and it is inside the van der Waals sphere of X Legon and coworkers obtained structural data for several B---HCl and B---HBr complexes [10]

For some H-bonded complexes B---HX (X = F, Cl and Br), the distance between the heavy atoms taking part in H-bond formation, r(Z X), are compared to the sum of their van der Waals radii ($\sigma(Z)+\sigma(X)$) in Table VI 1 Z is the atom in B, which is H-bonded to HX For B---HF series, r(Z F) are within 0 1 Å of the van der Waals sum

$$r(Z\ X) \approx \sigma(Z) + \sigma(F) \qquad (1)$$

Hence, the assumption made by Buckingham and Fowler that the heavy atoms in H-bond formation are in contact, looks reasonable

However, for B---HCl and B---HBr complexes (Table VI 1), r(Z X) differs by ~0 2 Å from the corresponding van der Waals sum Other than the complexes with H_3N,

the intermolecular distances are longer than the sum of van der Waals radii of the heavy atoms for B---HCl and B---HBr complexes It is likely that the extent of proton transfer in H_3N---HX complexes is significantly more than that in other B---HX complexes Moreover, it should be noted that in both HCN and H_3N, the H-bonded atom is N In HCN---HX complexes, the intermolecular distances are longer than those in H_3N---HX complexes It is clear that not only the H-bonded atom in an acceptor determines the distance, but the acceptor as a whole plays a significant role

Table VI.1. Experimental distances from a reference atom (Z) in Hydrogen-bond acceptor to the heavy atom (X) of the H-bond donor in a B---HX H-bonded complex These distances are compared with the sum of the van der Waals radii [σ(Z)+σ(X)] of the heavy atoms, Z and X. All the values are in Å.

B	B-HF		B-HCl[b]		B-HBr	
	r(Z F)	σ(Z)+σ(F)	r(Z Cl)	σ(Z)+σ(Cl)	r(Z ·Br)	σ(Z)+σ(Br)
H_2O	2 66[a]	2 75[a]	3 215	3 20	3 414[c]	3 35[d]
OC	3 05[a]	3 05[a]	3 710	3 50	3 917[b]	3 65[b]
HCN	2 80[a]	2 85[a]	3 405	3 30	3 610[b]	3 45[b]
NH_3	2 71[b]	2 85[b]	3 136	3 30	3 255[b]	3 45[b]
H_2S	3 246[b]	3 20[b]	3 809	3 65	3 991[b]	3 80[b]

[a]Ref 8, [b]Ref 10, [c]Ref 11, [d]Ref 1

VI.3. Gadre and Bhadane Model

Gadre and Bhadane[9] looked at a series of B---HF complexes Instead of looking at B F distances they concentrated on B H They used a different approach to correlate the hydrogen bond distance, r(Z H), with the van der Waals radius of the H-bond acceptor They have analyzed the Z H distances in about 20 B---HF complexes (for most of them the Z H distances were taken from rotational spectroscopic data) They computed the molecular electrostatic potential (MESP) for the free bases B at the SCF and MP2 levels with 6-31++G** basis set The MESP at a point **r** is defined as

$$V(r) = \sum_{A}^{N} Z_A / |r - R_A| - \int \rho(r') d^3 r' / |r - r'| \qquad (2)$$

where $\{Z_A\}$ is the nuclear charge at $\{R_A\}$ acting on **r** and $\rho(r)$ is the electronic density They noted that the MESP minimum symbolizes the site of electron localization in a molecule, which attracts hydrogen The location of the MESP minima could explain the radial and angular geometry of the B---HF complexes Gadre and Bhadane further noted that the following correlation existed between r(Z H) and r(E), which are defined below

$$r(Z\ H) = [r(E) \times 1\ 04] + 0\ 47 \qquad (3)$$

Here, r(Z H) is the Z H distance in the complex and r(E) is the distance between Z and the MESP minimum, observed in B The results obtained with HF and MP2 methods were very similar It was pointed out that the r(E) was closer to the van der Waals radius of the Z atom Hence, they concluded that 0 47 Å is the van der Waals radius of H It is significantly smaller than the value suggested by Pauling (1 2 Å) and this feature has been noted in the literature [12] The difference is not surprising given the fact that H bonding (electrostatic) interactions are significantly stronger than van der Waals (induction and dispersion) interactions It should be pointed out that the effective radius of 0 47 Å for H in HF is larger than the covalent radius of H atom, 0 3 Å [1]

VI.4. Extension of Gadre and Bhadane approach

In this work Gadre and Bhadane approach has been extended for several other series of B---HX complexes, where X = Cl, Br, CN, CCH and OH This extension is done to look for trends in the radius determined for H in various HX It is hoped that, such an analysis will help in developing reliable distance criteria for identifying hydrogen bonds Table VI 2 lists the H-bond distances, r(Z H), for all six series of B---HX complexes including HF. A few known experimental data for HI and H_2S complexes are also included in the Table along with the r(E) values for the corresponding free bases (B) calculated at HF and MP2 levels using 6-31++G** basis set

The r(E) values for different H-bond acceptors (B) calculated (by Gadre and coworkers) at HF and MP2 methods are quite similar [9] The MP2 values are slightly higher than the HF values for most of the bases Except for CO, C_3H_6 and $(CH_2)_2O$, the

Table VI.2. Experimental r(Z H) values for different B---HX complexes and the r(E) values for the corresponding H-bond acceptors (B) All values are in Å.

B	r(E)[a]		r(Z H)							
	HF	MP2	X = F	Cl	Br	I	CN	OH	CCH	SH
HF	1 27	1 32	1 86[13]	2 08[c]	--	--	--	--	--	--
H_2O	1 27	1 28	1 74[14]	1 93[c]	1 99[11]	2 13[29]	2 08[33]	2 02[48]	2 23[58]	--
HCN	1 36	1 40	1 87[a]	2 13[c]	2 19[c]	2 29[30]	2 24[34]	--	2 42[59]	--
H_3N	1 25	1 27	1 78[a]	1 85[c]	1 83[c]	--	2 16[35]	2 03[49]	2 33[60]	--
OC	1 54	1 49	2 12[a]	2 41[c]	2 49[c]	2 65[31]	2 61[36]	2 41[50]	2 71[61]	--
C_2H_2	1 60	1 62	2 20[a]	2 42[c]	--	--	2 59[37]	--	2 72[62]	--
C_2H_4	1 62	1 63	2 22[a]	2 44[c]	2 49[c]	--	2 64[38]	2 48[51]	2 78[63]	2 89[66]
H_2S	1 79	1 81	2 32[a]	2 53[c]	2 57[c]	--	2 75[39]	--		2 79[67]
CH_3CN	1 34	1 38	1 83[a]	2 01[18]	2 07[18]	--	2.21[40]	2 07[52]	2 37[59]	--
C_3H_6	1 52	1 61	2 10[a]	2 28[c]	--	--	2.41[41]	2 34[53]	--	--
SO_2	1 32	1 33	1 89[a]	2 10[c]	--	--	--	--	--	--
C_6H_6	1 33	1 39	2 65[a]	2 71[c]	2 72[26]	--	2 79[42]	2 65[54]	--	--
B_2H_6	2 08	2 13	2 50[a]	2 69[19]	--	--	--	--	--	--
CO_2	1 46	1 61	1 91[a]	2 15[20]	--	--	2 35[43]	--	--	--
N_2O	1 40	1 44	1 94[a]	2 08[21]	--	--	--	--	--	--
H_2CO	1.26	1 31	1 73[a]	1 97[c]	--	--	2 21[44]	2 01[55]	2 39[64]	--
N_2	1 57	1 58	2 16[a]	2 42[22]	2 52[27]	--	2 55[45]	2 42[56]	2 60[65]	--
PH_3	1 85[b]	1 85[b]	2 38[15]	2 60[23]	2 63[23]	2 76[32]	2 85[32]	--	--	--
$(CH_2)_2S$	1 67[b]	1 67[b]	2 19[16]	2 33[24]	--	--	2 62[46]	--	--	--
$(CH_2)_2O$	1 22[b]	1 30[b]	1 70[17]	1 84[25]	1 89[28]	--	1 97[47]	1 92[57]	--	--

[a]Reference 9, [b]S R Gadre, private communication; [c]Reference 10

differences between HF and MP2 r(E) values are well within 0 05 Å For C_3H_6 and $(CH_2)_2O$ this difference is close to 0 1 Å However, CO is the only acceptor for which the r(E) value at HF level is higher (by 0 05 Å) than that calculated at MP2 level

VI.4.a. r(Z H) vs r(E)

Following Gadre and Bhadane, the experimental r(Z H) values, listed in Table VI 2, have been plotted against r(E) values for all six series of B---HX (X = F, Cl, Br, CN, CCH and H_2O) complexes The HF and MP2 r(E) values were plotted separately The linear fit of the scatter points give rise to an equation similar to equation (3) for every series of complexes Figure VI 1 (a) and VI 1 (b) show the plots of r(Z H) vs r(E) at MP2 level for all six series of complexes The results of the HF and MP2 methods are similar The results of the fits are tabulated in Table VI 3 The correlation coefficients of the fits are within 0 90 to 0 94 at HF level, whereas they are within 0 85 to 0 89 at MP2 level The slopes (m) of the fitted lines are very close to unity for HF, HCl and H_2O at both HF and MP2 level. However, for HBr, HCN and HCCH they are somewhat higher, the values being 1 20, 1.17 and 1 21 respectively in HF level The

Table VI.3. Results of the linear fits of r(Z H) vs r(E) plot for different B---HX complexes 'A' is the intercept and 'm' is the slope for a particular line, and their values are in Å.

Level	Parameters	HF	HCl	HBr	HCN	H_2O	HCCH
HF	A	0 45	0 67	0 49	0 66	0 66	0 78
	m	1 06	1 04	1 20	1 17	1 09	1 21
	R^2	0 94	0 91	0 90	0.92	0.94	0 90
	SD	0 07	0 08	0 11	0 08	0 06	0 07
MP2	A	0 43	0 66	0 46	0 65	0 66	0 66
	m	1 05	1 02	1.20	1 16	1 06	1 28
	R^2	0 89	0 85	0 85	0 84	0 87	0 87
	SD	0.092	0.11	0 13	0 11	0 10	0 08

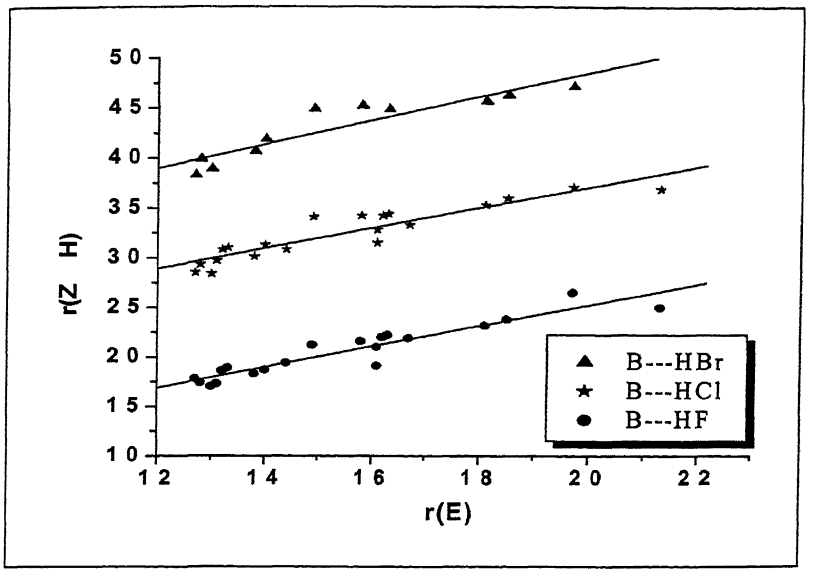

(a)

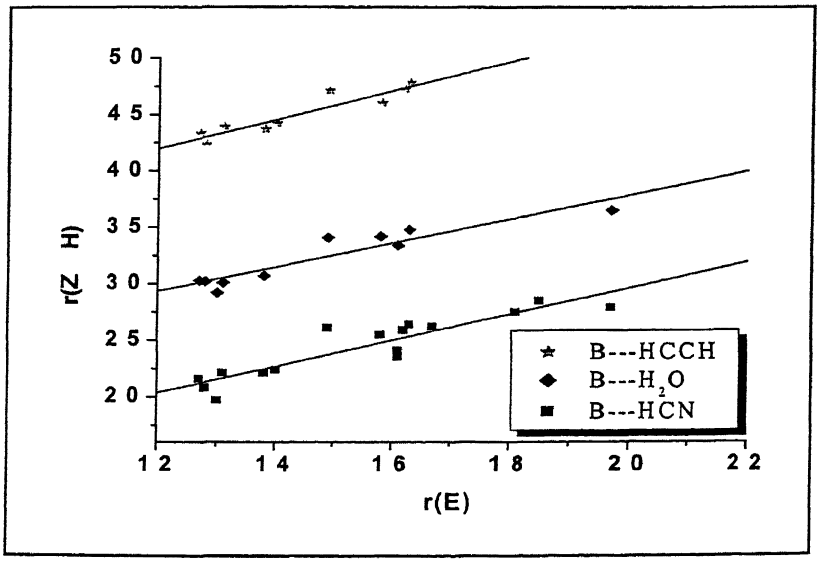

(b)

Figure VI.1 Plots of r(Z H) vs r(E) for B---HX complexes A constant (C) has been added to the Y values of the complexes for clarity; C_{HF} = 0 0, C_{HCl} = 1 0, C_{HBr} = 2.0, C_{H2O}= 0.0, C_{HCN}= 1 0 and C_{HCCH}= 2 0 The line through the points shows the best fit.

MP2 level values are also similar The intercepts (A) vary from a value of 0 45 Å for HF to 0 78 Å for HCCH at HF level, and from 0 43 Å to 0 66 Å at MP2 level According to Gadre and Bhadane interpretation, the effective size of hydrogen varies within the above range

VI.4.b. [r(Z···H) - r(E)] vs r(E) and "Hydrogen Bond Radius"

To obtain a more meaningful effective size of the hydrogen in H-bonded complexes, [r(Z···H) – r(E)] has been plotted as a function of r(E) for all the B---HX complexes The results of the plots at MP2 level are shown in the Figure VI 2 The scattered points for a particular series of complexes were fitted to a straight line The slope was fixed to be zero so that the intercept of the fit could be related to the effective size of the hydrogen of HX in H-bonding The intercepts from Fig VI 2 are quite enlightening They are 0 51 ± 0 09 Å, 0 70 ± 0 10 Å, 0 77 ± 0 13 Å, 0 89 ± 0 12 Å, 0 75 ±0 09 Å and

Table VI.4 'Hydrogen Bond Radii' of different HX. Empirical analysis was carried out for HF, HCl, HBr, HCN, H_2O and HCCH, taking experimental r(Z H) and the r(E) values from calculation at HF and MP2 level For HF, HCl, H_2O and H_2S, the r(H) values have been determined from theoretical (*ab initio*, DFT) analysis as well

	Empirical		*ab initio* (MP2)	DFT (B3LYP)	
r(E)[a]	HF[a]	MP2[a]	MP2[a]	HF[a]	MP2[a]
HF	0 54 ± 0 07	0.51 ± 0 09	0 50 ± 0 06	0 48 ± 0 04	0 46 ± 0 05
HCl	0 73 ± 0 08	0.70 ± 0 10	0.69 ± 0 10	0 67 ± 0 11	0 63 ± 0 10
HBr	0.79 ± 0 11	0 77 ± 0 13	--	--	--
HCN	0 92 ± 0 08	0.89 ± 0 12	--	--	--
H_2O	0 78 ± 0 06	0 75 ± 0 09	0 76 ± 0 08	0 77 ± 0 07	0 75 ± 0 08
HCCH	1 08 ± 0 07	1 07 ± 0 08	--	--	--
H_2S	--	--	1 02 ± 0 10	1 05 ± 0 12	1 03 ± 0 13

[a]The level of theory at which the r(E)'s are calculated

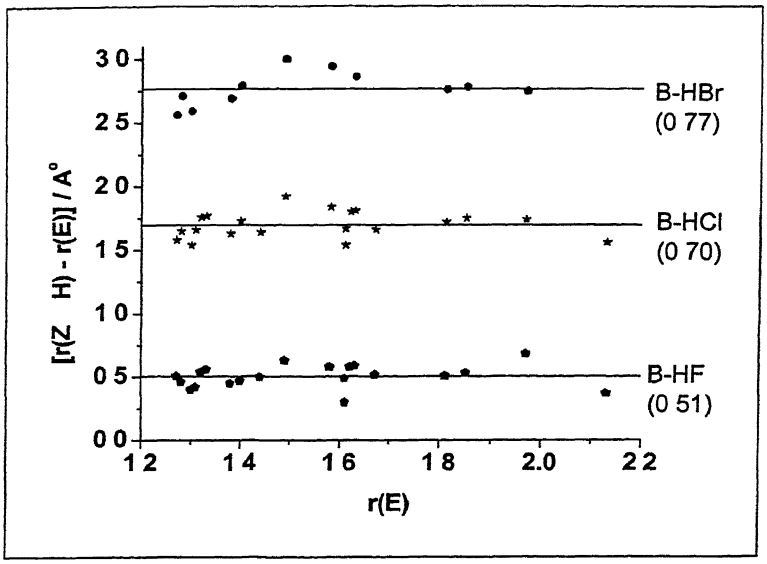

(a)

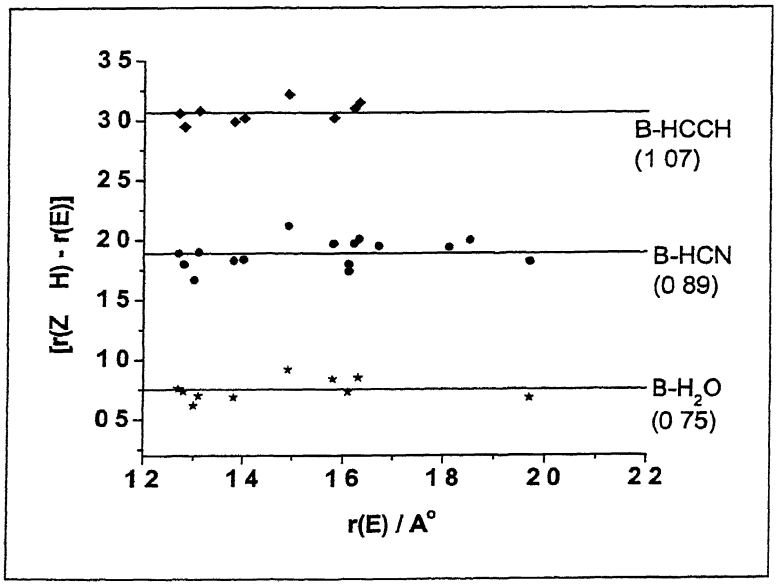

(b)

Figure VI.2. Plots of [r(Z H) - r(E)] vs r(E) at MP2 level for B---HX complexes A constant (C) has been added to the Y values of the complexes for clarity; C_{HF} = 0 0, C_{HCl} = 1.0, C_{HBr} = 2 0, C_{H2O}= 0 0, C_{HCN}= 1.0 and C_{HCCH}= 2 0. The line through the points shows the best fit assuming the slope to be zero The intercepts are shown in parenthesis

1 07 ± 0 08 Å for HF, HCl, HBr, HCN, H_2O and HCCH respectively The HF intercepts are also similar to the MP2 values

As is evident from Fig VI 2, one should be able to get a reasonable estimate for intermolecular separation for B---HX just by adding r(E) for B to the intercept for HX These intercepts are the effective sizes (radii) of Hydrogen of HX in H-bonded complexes, and defined as "Hydrogen Bond Radii (r(H))" of the H-bond donors HX Hence for a particular H-bond donor, the H-bond distance, r(Z ··H) can be estimated within the error limit as

$$r(Z \cdots H) = r(E) + r(H) \qquad . (4)$$

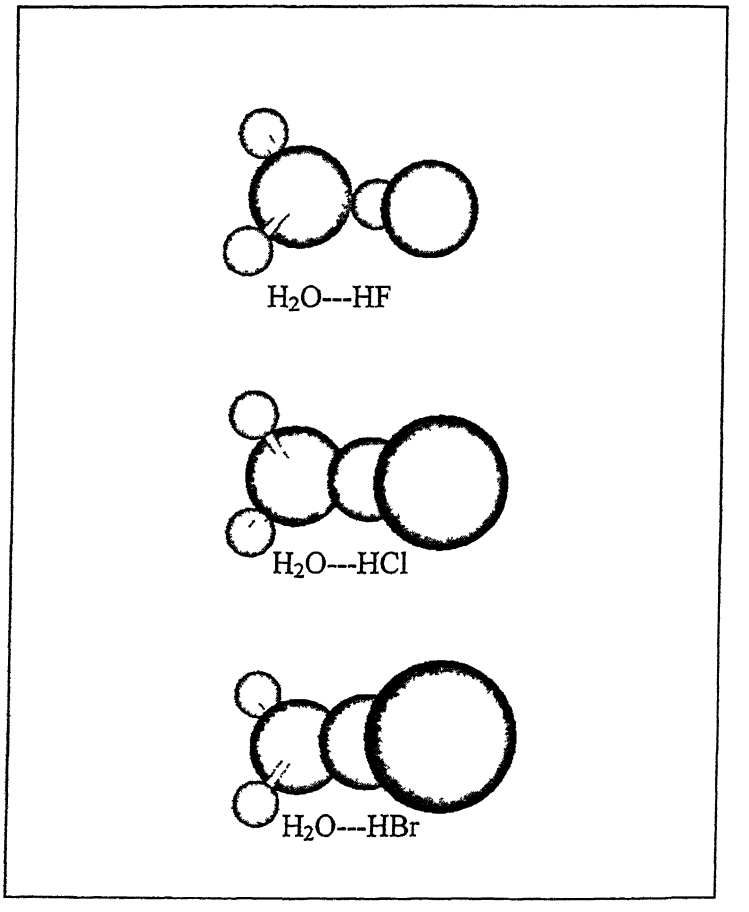

Figure VI.3: Models of H_2O·· HX Hydrogen in HX has certain effective size (r_H) and it changes with HX Here X is F, Cl or Br Figures are not to the scale

The "H-bond radii" for all the H-bond donors, analyzed empirically here, are tabulated in Table VI 4, along with the r(H) values obtained from pure theoretical analysis, which is discussed latter The r(H) values at HF levels are 0 03 Å higher than that at MP2 values for all the H-bond donors except HCCH. However, the differences between the two levels are well within the error limits For HCCH they are 1 08 and 1 07 Å for HF and MP2 level respectively For three hydrogen-halides, the r(H) value increases from HF (0 51 Å) to HCl (0 70 Å) to HBr (0 77 Å) This is shown schematically in Figure VI 3

Hence, it is seen that the effective size (r(H)) of hydrogen of H-bond donor in H-bonding depends on the nature of the donor This analysis shows that a hydrogen bond radius can be defined for each donor and it will be applicable to all acceptors Li Bian has shown that the proton donor plays a dominant role in determining structures and energetics of H-bond formation than the proton acceptor [68] The dependence of r(H) on several properties of HX has been explored too, and they are discussed in latter sections

VI.5. "H-bond radius" of H_2S: *ab initio* analysis

It has been already mentioned that in biological system, hydrogen bonds involving C-H and S-H are very important [3,4] HCCH is treated as the model system for C-H---B H-bonding, and H_2S is taken as the model system for S-H---B H-bonding However, not much experimental data for H_2S complexes are available now to determine its H-bond radius Hence, *ab initio* calculations have been carried out at MP2/6-311++G** and B3LYP/6-311++G** levels of theory for several H_2S complexes From these theoretical structural data, hydrogen bond radius of H_2S has been determined The analysis described in the previous sections regarding "H-bond radius" is based on experimental H-bond distances [r(Z H)] and *ab initio* r(E) values Hence a pure theoretical analysis has been carried out for HF, HCl and H_2O complexes as well, where both r(Z· H) and r(E) are obtained from *ab initio* calculations. The r(H) values obtained from this analysis are compared with the previous analysis It should be mentioned here that our prime interest is obtaining the intermolecular distances from calculations for

determining the hydrogen bond radii Hence, no attempts have been made to correlate the energetics to the distances or the vibrational frequencies, for the above complexes (though they could be obtained from the calculations) However, there are several reports where the interaction energy has been correlated to different properties of H-bond donor and acceptor [69-71]

VI.5.a. Method of calculation

The geometries for almost sixty B---HX complexes (X = F, Cl, OH and SH), ~15 each, have been optimized at MP2 and B3LYP levels using 6-311++G** basis set Though the r(E) values are available at HF level, the intermolecular distances, calculated at this level, were not analyzed The calculations at HF/6-311++G** level for several B---HF and B---HCl complexes have been carried out as well However, the intermolecular distances at this level differs significantly (~0 2 Å or more) from the corresponding experimental values In general HF method is known to produce results (structure and interaction energy), which are far from reality for these kind of weakly bound complexes

Frequency calculation has been done for every optimized complex to confirm the nature of the stationary point For most of the complexes, the H-bonded structure is the global minimum However for some complexes, the H-bonded structure is a local minimum, e g SO_2-H_2O The optimized geometries of the B-HX (X = F and Cl) and B-H_2X (X = O and S) complexes are shown in Figures VI A and VI B respectively The complete lists of the optimized structural parameters are tabulated in Tables VI A and VI B for B-HX and B-H_2X complexes respectively Tables VI C to VI F give the absolute energies of the complexes and the corresponding fragments for HF, HCl, H_2O and H_2S complexes, respectively Tables VI.G and VI H list all the vibrational frequencies, calculated at both levels of theory, for B-HX and B-H_2X series of complexes, respectively Figures VI A and VI B and Tables VI A – VI H are collectively given at the end of this chapter The H-bond distances, r(Z H), obtained from these optimized geometries have been compiled with the r(E)'s of the corresponding bases to

obtain the H-bond radii Gaussian 98 software package[72] was used for all the calculations

VI.5.b. r(Z H) and r(H)

The calculated H-bond distances, r(Z···H), for B---HX (X = F and HCl) are tabulated in Table VI 5 and those for B---H_2X (X = O and S) are listed in the Table VI 6 The H-bond distances for B---HX complexes at B3LYP method are slightly smaller than that in MP2 method and the experimentally observed distances are in

Table VI.5 Hydrogen bond distance [r(Z H)] for B---HX (X = F and Cl) calculated at MP2 and B3LYP method using 6-311++G** basis set All values are in Å.

B	HF		HCl	
	MP2	B3LYP	MP2	B3LYP
HF	1 8708	1 8261	2 0839	2 0271
N_2	2 1364	2 0762	--	--
OC	2 1314	2 0585	2 4314	2 3681
HCN	1 8876	1 8366	2 1035	2 0606
H_2O	1 7312	1 7028	1 9054	1 8552
H_2S	2 3186	2 2709	2 5400	2 4430
H_3N	1 7042	1 6732	1 8196	1 7263
H_3P	2 3899	2 3213	2 6037	2 5016
H_2CO	1 7591	1 7174	1 9440	1 8971
C_2H_2	2 1856	2 1514	2 4375	2 4082
C_2H_4	--	--	2 4388	2 4311
CH_3CN	1 8338	1 7840	2 0348	1 9813
SO_2	--	--	--	--
$(CH_2)_2O$	1 6772	1 6618	1 7874	1 7792
$(CH_2)_2S$	2 1751	2 1541	2 2647	2 2250

Table VI.6 Hydrogen bond distance [r(Z···H)] for B---H_2X (X = O and S) calculated at MP2 and B3LYP method using 6-311++G** basis set All values are in Å.

B	H_2O		H_2S	
	MP2	B3LYP	MP2	B3LYP
HF	--	--	2 3417	2 3133
N_2	2 3869	2 4060	2 6913	2 8109
OC	2 4594	2 4151	2 7809	2 8199
HCN	2 1635	2 1377	2 4238	2 4404
H_2O	1 9500	1 9318	2 1788	2 1569
H_2S	--	--	2 8382	2 8394
H_3N	1 9739	1 9605	2 2266	2 1727
H_3P	2 6478	2 6369	2 9491	2 9575
H_2CO	--	--	2 3101	2 2612
C_2H_2	2 4443	2 4711	2 6741	2 7780
CH_3CN	2 1064	2 0809	2 3537	2 3605
SO_2	2 0602	2 0618	--	--
$(CH_2)_2O$	1 9129	1 9016	2.1482	2 1414
$(CH_2)_2S$	2 4076	2 4221	2.6404	2 6427

between the two However, for B---H_2X complexes, there is no particular trend In most of the cases the distances at both levels are quite close The r(Z H) obtained from MP2 level calculations for HF, HCl, H_2O and H_2S complexes are plotted separately against MP2 level r(E) values These plots and their linear fits are shown in the Figure VI 4 The results of the fits are similar to that of the empirical analysis The slopes of the fitted lines are 1 10, 1 15, 1.14 and 1 15, and the intercepts are 0 36 Å, 0 46 Å, 0 55 Å and 0 80 Å for HF, HCl, H_2O and H_2S complexes respectively Figure VI 5 shows the plots of [r(Z···H) – r(E)] vs r(E) for all four series of complexes The straight lines are their linear fits, forcing the slopes to be zero Thus the H-bond radii determined from this analysis are 0 50 ± 0 06 Å, 0 69 ± 0 10 Å, 0 76 ± 0 08 Å and 1.02 ± 0 10 Å for HF, HCl H_2O and H_2S respectively (Table VI 4)

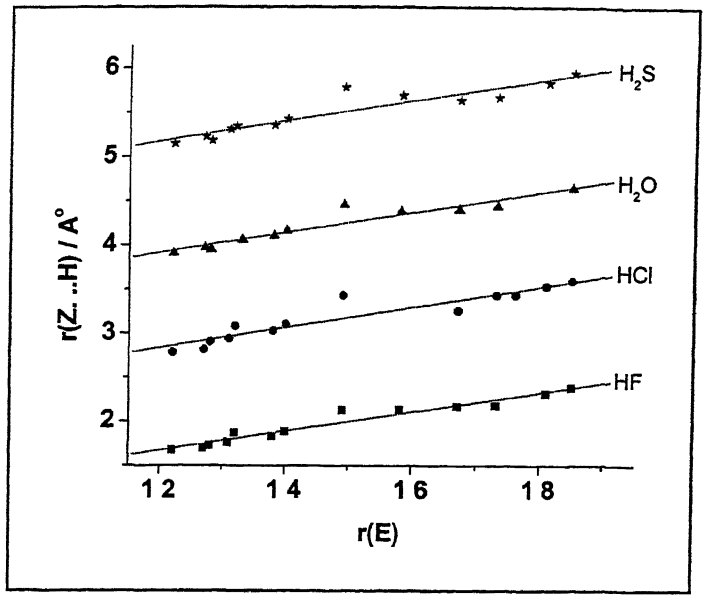

Figure VI.4 Plot of r(Z···H) vs r(E) and their linear fits for HF, HCl, H_2O and H_2S complexes at MP2 level. A constant (C) has been added to the Y values of the four complexes for clarity; $C_{HF} = 0\,0$, $C_{HCl} = 1\,0$, $C_{H2O} = 2\,0$, and $C_{H2S} = 3\,0$

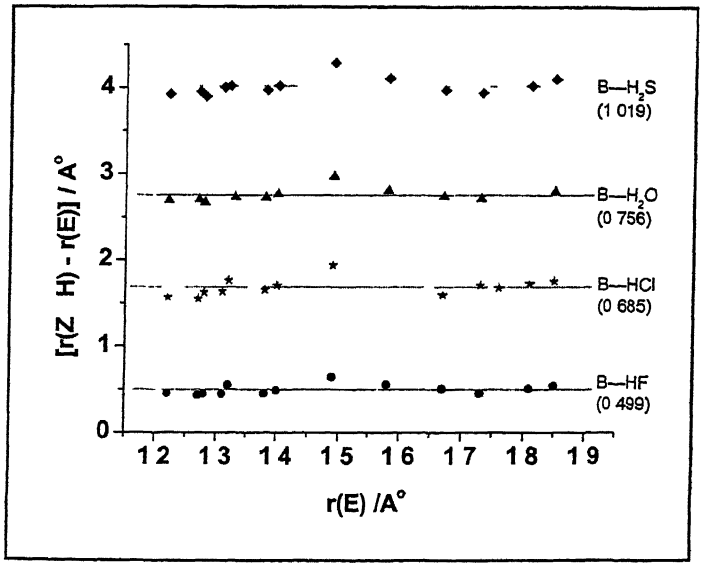

Figure VI.5. Plot of [r(Z···H) – r(E)] vs r(E) and their linear fits, forcing the slopes to be zero, for HF, HCl, H_2O and H_2S complexes at MP2 level. The constants (C) are same as in Figure VI.4 The intercepts are shown in parenthesis

Similar analysis with the structural data from B3LYP calculations produces similar results As the r(E) values are not available at B3LYP level, both HF and MP2 r(E) values were taken separately in the analysis The r(H) values obtained are included in the Table VI 4 The r(H) (from B3LYP calculation) for H_2O and H_2S are similar to that obtained from pure MP2 and empirical analysis whereas for HF and HCl, they are slightly smaller However, the r(H) for HF, HCl and H_2O from this *ab initio* analysis are quite similar to that obtained from empirical analysis The hydrogen bond radius (1 02 ± 0 10 Å) obtained for H_2S is validated by the known experimental data for C_2H_4-H_2S[66] and H_2S-H_2S[67] complexes, the distances being 1 26 Å and 0 98 Å respectively

In both empirical and *ab initio* analysis, it has been seen that CO is a unique H-bond acceptor Regardless of the H-bond donor, it is bonded to, the C H distances are quite larger than the average value for a series of complexes The [r(C H) – r(E)] values for OC--H_2O and OC--H_2S complexes at MP2/6-311++G** level are 0 97 Å and 1 29 Å whereas the average (r(H)) for the corresponding hydrogen bond donors are 0 76 Å and 1 02 Å respectively It is clear from the plot that the deviation in general is very similar for each acceptor Hence, the deviation is not random, but shows the distribution in acceptor properties

VI.6. How does r(H) depend on different properties of the H-bond donor (HX)?

The effective size or radius of hydrogen of HX in H-bonding, r(H), depends on several properties of the H-bond donor Here, attempts have been made to correlate the r(H) of different donors (HX) to the dipole moment and the electronegativity difference of HX The dipole moment of the H-X bond and the difference in electronegativity between H and X for different HX are listed in Table VI 7

The r(H) values obtained from the empirical analysis (r(E) values from MP2 level calculation) for HF, HCl, HBr, H_2O and HCCH, and that of H_2S obtained from pure MP2 analysis, were plotted as a function of the dipole moment of the H-X bond The r(H) for C_2H_4 is also included in the plot A value of 1 33 ± 0 11 Å has been evaluated from

available *ab initio* results, at a sufficiently high level, of four B---C_2H_4 complexes The r(Z H) distances for the complexes of C_2H_4 (C-H B interaction) with NH_3, H_2O, PH_3 and H_2S are 2 608 Å, 2 454 Å, 3 268 Å and 3 187 Å respectively at MP2/6-311++G(3df,2p) level of theory [73]

Table VI.7 Dipole moment of H-X bond and the electronagativity difference between H and X for different H-bond donors (HX)

X	Dipole moment (D)	Reference	E(X) – E(H)[a] (Pauling Scale)	Reference
F	1 82	74	1 9	1
Cl	1 08	74	0 9	1
Br	0 78	74	0 7	1
I	0 45	74	0 4	1
CN	1 13	75	1 66	77
OH	1 51	74	1 32	77
SH	0 70	74	0 4	1
CCH	0 94	76	1 19	78
$HCCH_2$	0 69	76	0 65	78

[a]E(H) = 2 1 in Pauling Scale

The results of the plot are shown in Figure VI.6 As the H-X dipole moment increases, the r(H) decreases The straight line is the linear fit of the scattered points and the bars show the rms deviation of the fit This correlation predicts the r(H) value of HI, having H-X bond moment of 0 448 D, to be 1 19 ± 0 18 Å The extrapolation of this line to zero dipole moment gives a value of 1.40 ± 0 18 Å

A similar inverse correlation is observed between the r(H) of the donors (HX) and the electronegativity difference between H and X (ΔE) Figure VI.7 shows the plot of r(H) as a function of ΔE. On extrapolation of the straight line, the linear fit of the data points, to zero ΔE value produces a radius of 1.18 ± 0 23 Å This correlation predicts the hydrogen bond radius of HI to be 1 07 ± 0 23 Å These predictions are validated by the limited experimental data available on HI complexes The distances observed are 0 86 Å,

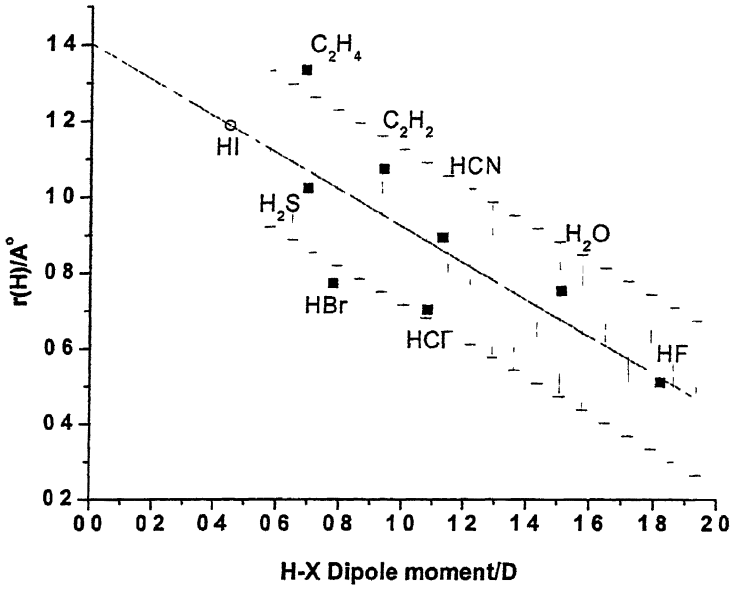

Figure VI.6. Plot of r(H) of different H-bond donors (HX) against the H-X bond moment The solid line is the linear fit The bars show the rms deviation of the fit

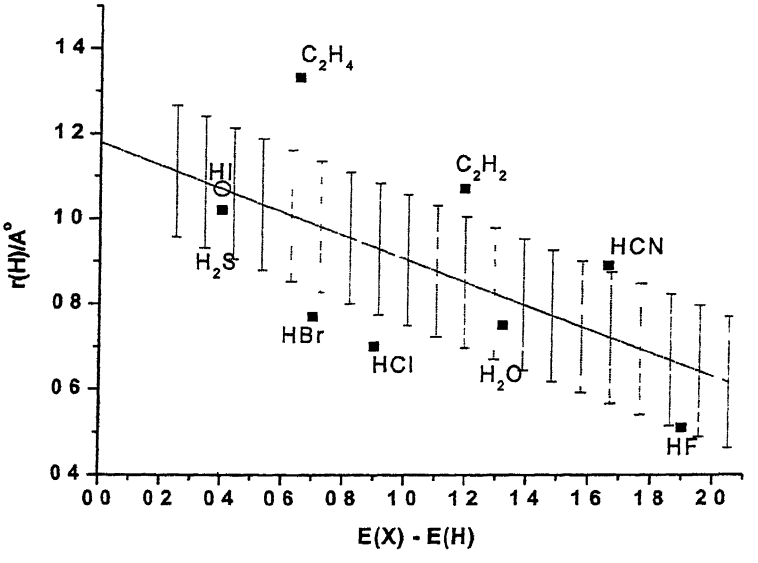

Figure VI.7. Plot of r(H) of different HX against the electronegativity difference between H and X, ΔE The solid line is the linear fit. The bars show the rms deviation of the fit

0 93 Å, 1 11 Å and 0 91 Å for the H_2O[29], HCN[30], OC[31] and PH_3[32] complexes with HI

These extrapolated radii (1 40 and 1 18 Å) can be thought as the radius of Hydrogen when the donor has zero dipole moment, i e H_2 for example Hence, these radii should be similar to the van der Waals radius of Hydrogen It is in very good agreement with Pauling's estimation of 1 20 Å [1] Though it has been tried to establish a linear correlation between r(H) and the H-X dipole moment, there is no particular fundamental basis for that It should be mentioned here that the correlation coefficients (R^2) of the fits are quite small (0 6 for Figure VI 6 and 0 3 for Figure VI 7) The actual correlation could be much complex, and a more detailed analysis is needed to reveal that

VI.7. Distance Criterion for H-bonding

Generally the criteria used for the existence of H-bonding is that the distance between the heavy atoms [r(Z X)] should be less than the sum of their van der Waals radii [σ(Z)+σ(X)] This is the default criterion for H-bonding given in the documentation for the Mercury software in Cambridge Crystal Structure Database [79] However, there have been numerous reports of H-bonding at much longer distances For instance, Desiraju and Steiner[3] point out in their recent book that even a conservative C-O distance threshold of 3 25 or 3 3 Å may still not be long enough to rule out the presence of C-H ·O hydrogen bonds In case of H-bond donors like HCCH or HCN, the distances involved are longer (more than the sum of van der Waals radii) but the interaction energies are quite significant Defining a hydrogen bond radius has shown that the heavy atom distances could be significantly larger than the sum of their van der Waals radii It is suggested that hydrogen bond radii of donor and r(E) for acceptor are used instead of the van der Waals radii of heavy atoms For a particular B---HX complex, the r(Z H) distance should be same as the sum of r(E) of B and r(H) of HX, within the error limit

Recently, a similar analysis has been done for different H-bond donors from the condensed phase structural data available in Cambridge Crystal Structure Database [80] This analysis also resulted in a very similar 'hydrogen bond radii' for OH and C≡CH groups, as found here for H_2O and HCCH After the completion of this work, we have

come across a paper titled "Hydrogen bond radii", published by Wallwork in 1962 [81] He had mentioned the heavy atom distances, r(Z X), as the sum of van der Waals radius of Z and 'hydrogen bond radius' of HX However, he was disappointed not to find a general correlation between his hydrogen bond radius and the hydrogen bond length (Z-X distance)

VI.8. Conclusions

The H-bond distances for different series of complexes have been compiled and analyzed In hydrogen bonding, hydrogen does have some effective size or radius and it has been defined as "hydrogen bond radius", r(H) This radius is the characteristic of the H-bond donors The sum of r(H) of a donor and r(E) (close to van der Waals radius) of an acceptor results into the H-bond distance for a H-bonded complex "Hydrogen bond radii" have been determined for HF, HCl, HBr, HCN, HCCH and H_2O empirically The same have been evaluated for HF, HCl, H_2O and H_2S from pure *ab initio* analysis These values are close to the empirical one The "hydrogen bond radius" has an inverse correlation with the H-X dipole moment and the electronegativity difference between H and X A more reliable distance criterion for H-bonding has evolved from the present analysis

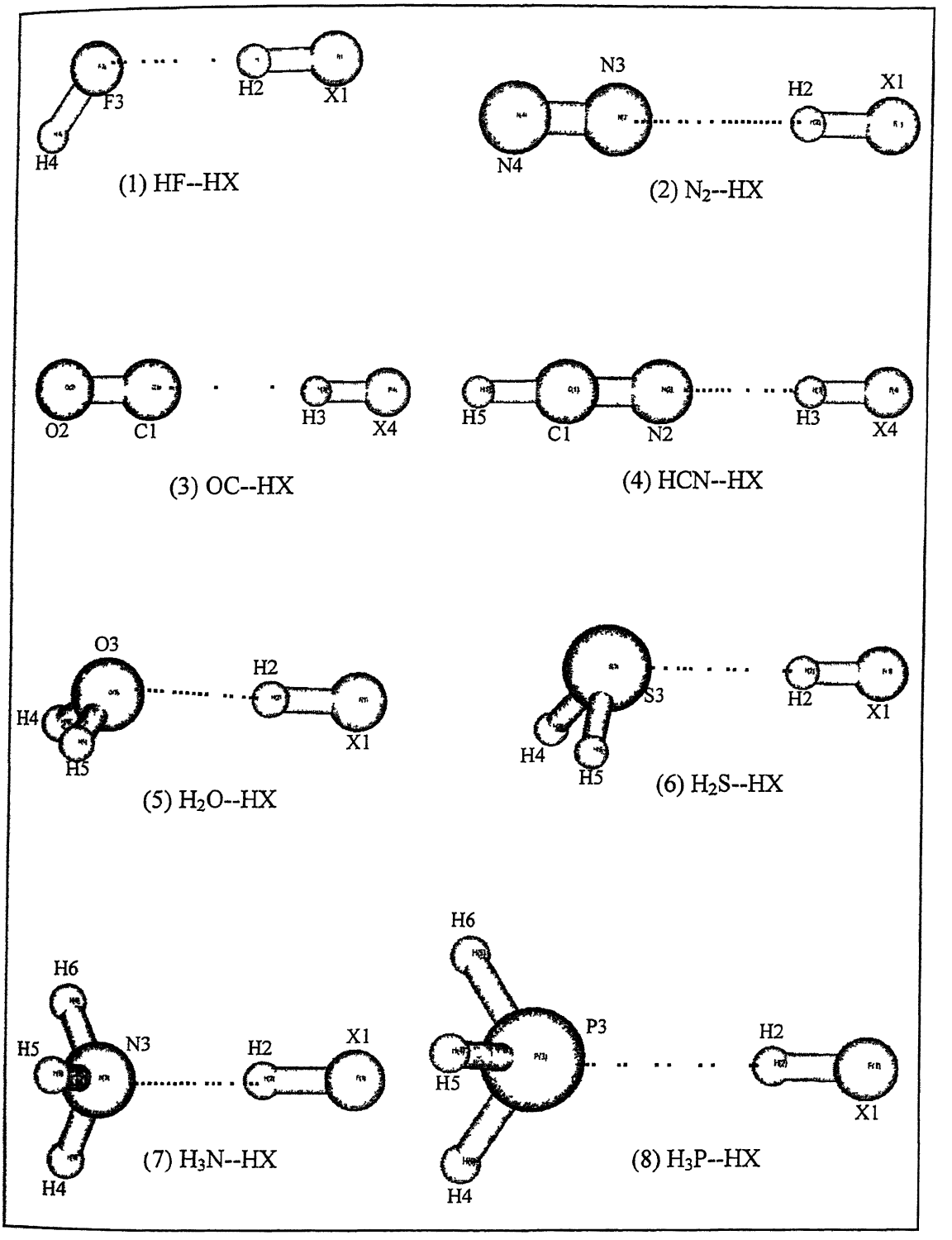

Figure VI.A. Geometries of B---HX complexes optimized at MP2/6-311++G** level of theory

Figure VI A continued

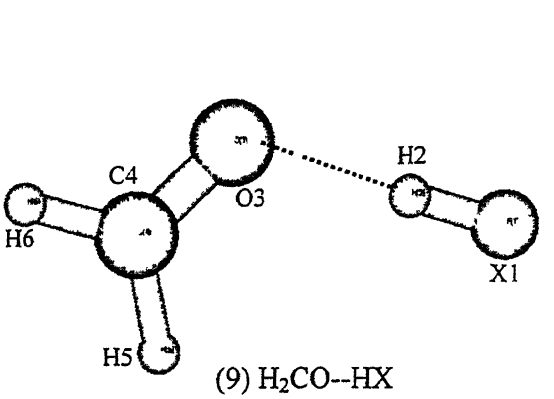

(9) H_2CO--HX

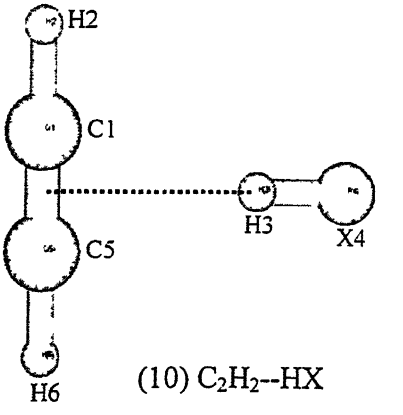

(10) C_2H_2--HX

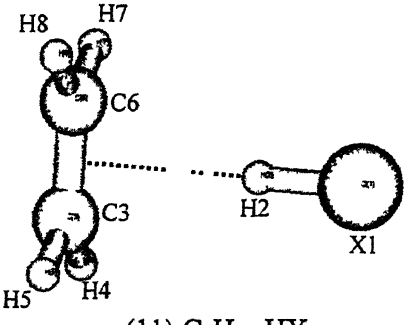

(11) C_2H_4--HX

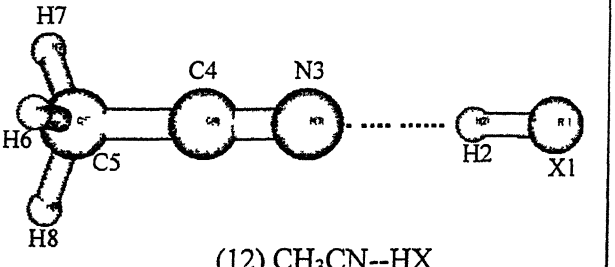

(12) CH_3CN--HX

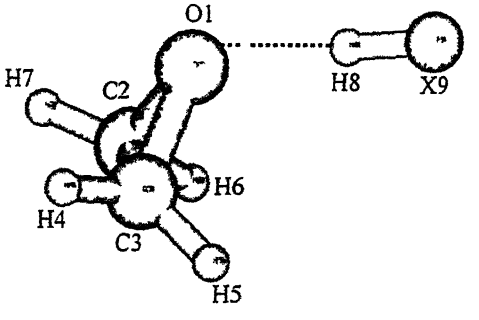

(13) $(CH_2)_2O$--HX

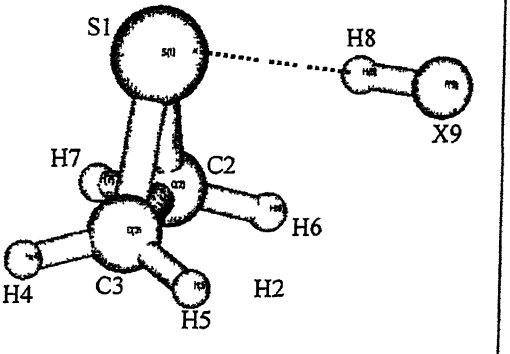

(14) $(CH_2)_2S$--HX

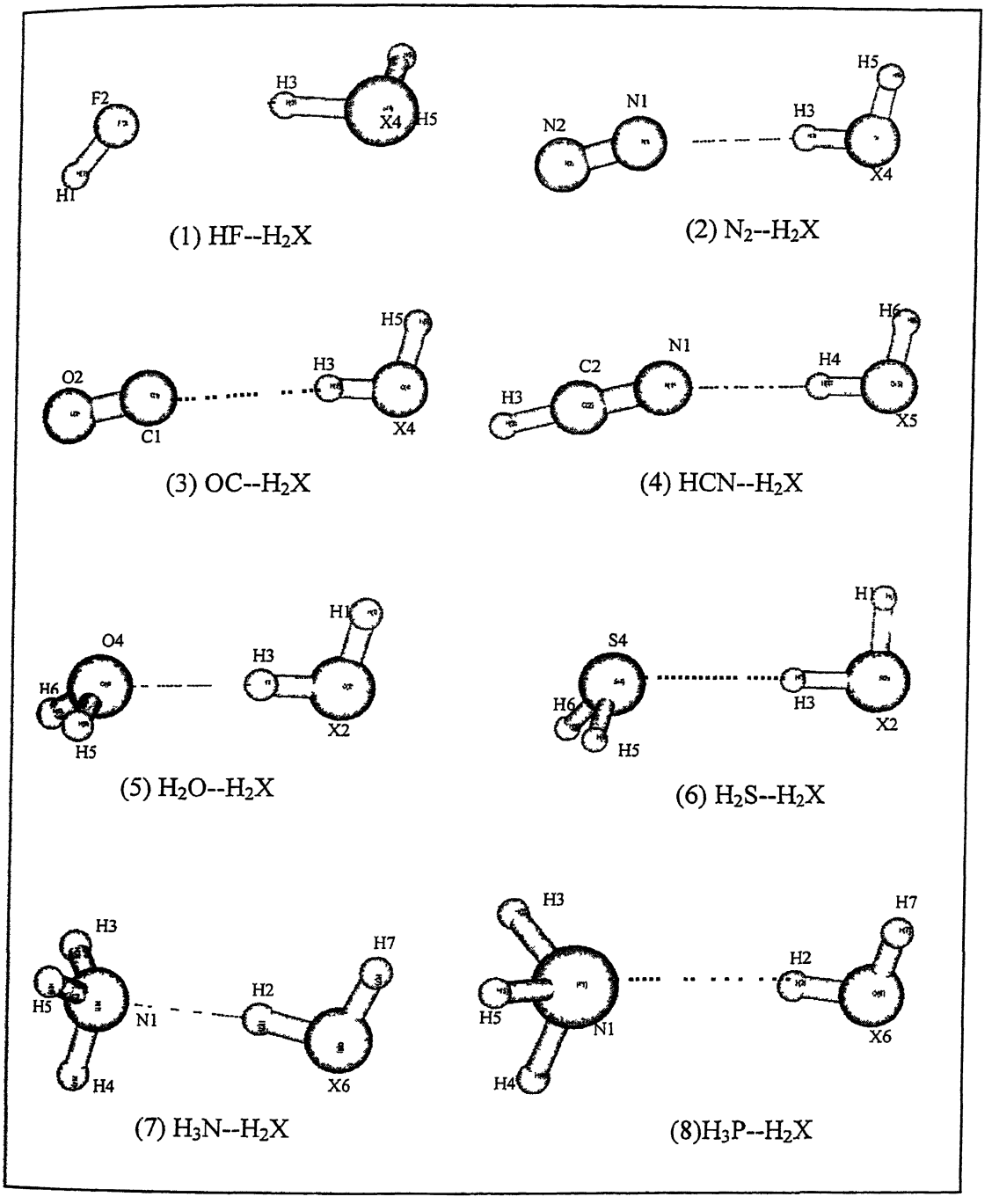

Figure VI.B. Optimized geometries of B---H_2X complexes optimized at MP2/6-311++G** level of theory

Figure VI B continued

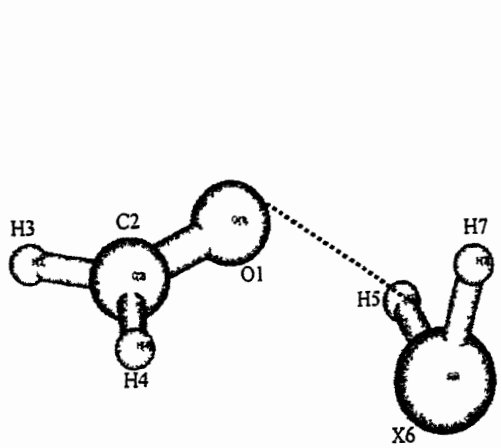

(9) H_2CO--H_2X

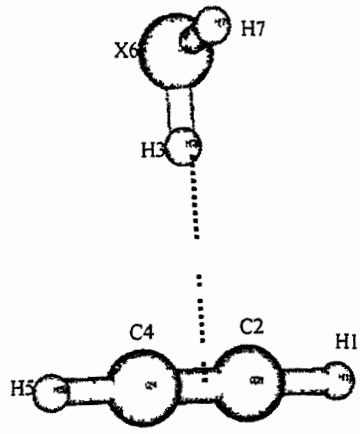

(10) C_2H_2--H_2X

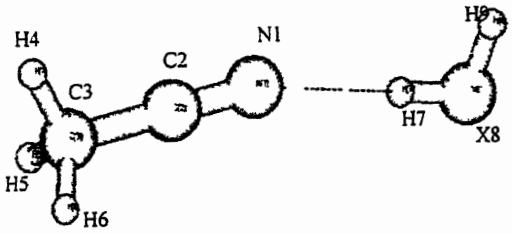

(11) CH_3CN--H_2X

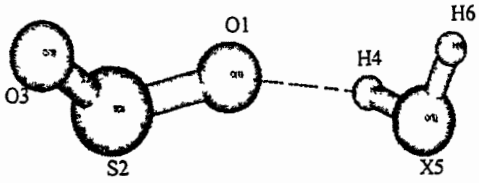

(12) SO_2--H_2X

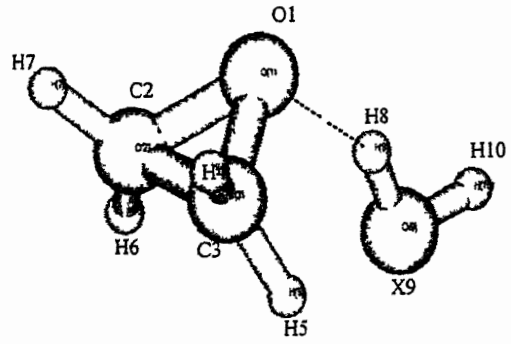

(13) $(CH_2)_2O$--H_2X

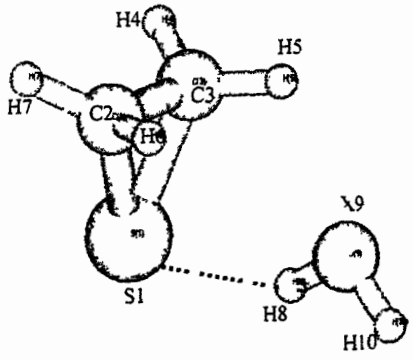

(14) $(CH_2)_2S$--H_2X

VI.A. Optimized Parameters of different B-HX complexes at MP2 and B3LYP methods using 6-311++G** basis set (Figure VI A)

1 HF---HX

Structural Parameters	X = F		X = Cl	
	MP2	B3LYP	MP2	B3LYP
R(1,2)	0 9210	0 9287	1 2761	1 2921
R(2,3)	1 8708	1 8261	2 0839	2 0271
R(3,4)	0 9195	0 9253	0 9185	0 9243
A(1,2,3)	180 0	180 0	180 0	180 0
A(2,3,4)	128 5	125 8	136 8	130 0
D(4,3,2,1)	0 0	0 0	0 0	0.0

X1 H2 F3 H4

2 N_2-HX

Structural Parameters	X = F		X = Cl	
	MP2	B3LYP	MP2	B3LYP
R(1,2)	0 9193	0 926	--	--
R(2,3)	2 1364	2 0762	--	--
R(3,4)	1 1195	1 0946	--	--
A(1,2,3)	180 0	180 0	--	--
A(2,3,4)	180 0	180 0	--	--
D(4,3,2,1)	0 0	0 0	--	--

X1 H2 N3 N4

3. OC-HX

Structural Parameters	X = F		X = Cl	
	MP2	B3LYP	MP2	B3LYP
R(1,2)	1 1371	1 1241	1.1384	1 1255
R(1,3)	2 1314	2.0585	2 4314	2 3681
R(3,4)	0 9222	0 9302	1 2766	1 2921
A(2,1,3)	180 0	180 0	180.0	180.0
A(1,3,4)	180 0	180 0	180.0	180 0
D(4,3,1,2)	0 0	0 0	0 0	0 0

C1 O2 H3 X4

4 HCN-HX

Structural Parameters	X = F		X = Cl	
	MP2	B3LYP	MP2	B3LYP
R(1,2)	1 168	1 1459	1 1697	1 1471
R(1,5)	1 0685	1 0675	1 0686	1 0674
R(2,3)	1 8876	1 8365	2 1035	2 0606
R(3,4)	0 9273	0 9363	1.2826	1 2987

C1 N2 H3 X4 H5

5 H_2O-HX

Structural Parameters	X = F		X = Cl	
	MP2	B3LYP	MP2	B3LYP
R(1,2)	0 932	0 942	1 2876	1 3085
R(2,3)	1 7312	1 7028	1 9054	1 8552
R(3,4)	0 9615	0 9639	0 9615	0 9638
R(3,5)	0 9615	0 9639	0.9615	0 9638
A(1,2,3)	180 0	180 0	180 0	180 0
A(4,3,5)	103 8	105 3	103 2	105 1
A(2,3,4)	114 7	113.3	115 1	113 5
A(2,3,5)	114 7	113.3	115 1	113 5
D(5,3,2,4)	120 0	120.0	120 0	120 0

X1 H2 O3 H4 H5

6 H_2S-HX.

Structural Parameters	X = F		X = Cl	
	MP2	B3LYP	MP2	B3LYP
R(1,2)	0 9256	0 9363	1 2806	1 3032
R(2,3)	2 3185	2 2709	2 54	2 443
R(3,4)	1 3337	1 3493	1 3338	1 3485
R(3,5)	1 3337	1 3493	1 3338	1 3485
A(1,2,3)	179 5	176 8	177 2	177 7
A(4,3,5)	92 7	92 8	92 4	92 8
A(2,3,4)	105 4	98 9	108 4	99 3
A(2,3,5)	105 5	98 4	108 0	99 4
D(4,3,2,1)	100 2	-77 6	141 7	-48 9
D(5,3,2,1)	-162 4	16 6	-119 3	45 6

X1 H2 O3 H4 H5

7 H_3N-HX·

Structural Parameters	X = F		X = Cl	
	MP2	B3LYP	MP2	B3LYP
R(1,2)	0 9477	0 9613	1 3118	1 3497
R(2,3)	1 7042	1 6732	1 8196	1 7263
R(3,4)	1 0155	1 016	1 0157	1 016
R(3,5)	1 0155	1 016	1 0157	1 016
R(3,6)	1 0155	1 016	1 0157	1 016
A(1,2,3)	180 0	180 0	180 0	180 0
A(4,3,2)	112 1	111 2	112 1	110 9
A(5,3,2)	112 1	111 2	112 1	110.9
A(6,3,2)	112 1	111 2	112 1	110 9
D(5,3,2,4)	120 0	120 0	120 0	120 0
D(6,3,2,1)	-120 0	-120 0	-120 0	-120 0

X1 H2 N3 H4 H5 H6

8 H_3P-HX

Structural Parameters	X = F		X = Cl	
	MP2	B3LYP	MP2	B3LYP
R(1,2)	0 9266	0 9371	1.2818	1 3037
R(2,3)	2.3899	2 3213	2 6037	2 5015
R(3,4)	1 4054	1 4174	1 4069	1 419
R(3,5)	1 4054	1 4174	1 4069	1 419
R(3,6)	1 4054	1 4174	1 4069	1 419
A(1,2,3)	180 0	180 0	180 0	180 0
A(4,3,2)	121 0	121 1	121 4	121 5
A(5,3,2)	121 0	121 1	121 4	121 5
A(6,3,2)	121 0	121 1	121 4	121 5
D(5,3,2,4)	120 0	120 0	120 0	120 0
D(6,3,2,1)	-120 0	-120 0	-120 0	-120 0

X1 H2 P3 H4 H5 H6

9 H_2CO---HX

Structural Parameters	X = F		X = Cl	
	MP2	B3LYP	MP2	B3LYP
R(1,2)	0 9304	0 9406	1 2855	1 3052
R(2,3)	1 7591	1 7174	1 944	1 8971
R(3,4)	1 2179	1 208	1 2167	1 2064
R(4,5)	1 1011	1 1034	1 1023	1 1047
R(4,6)	1 1011	1 1034	1 1023	1 1047
A(1,2,3)	180 0	180 0	180 0	180 0
A(4,3,2)	120 2	122 3	120 3	123 0
A(5,4,3)	121 4	121 4	121 5	121 6
A(6,4,3)	121 4	121 4	121 5	121 6
D(4,3,2,1)	0 0	0 0	0.0	0 0
D(5,4,3,2)	0 0	0 0	0 0	0 0
D(6,4,3,2)	180 0	180 0	180 0	180 0

X1 H2 O3 C4 H5 H6

10. C_2H_2---HX.

Structural Parameters	X = F		X = Cl	
	MP2	B3LYP	MP2	B3LYP
R(1,2)	1.0664	1 0645	1 0659	1 0640
R(1,5)	1 2175	1 2008	1 2172	1 2003
R(5,6)	1 0664	1 0645	1 0659	1 0640
R(3,4)	0 9233	0 9322	1 2783	1 2959
R(1,3)	2 2688	2 2336	2 5123	2 4819
R(5,3)	2 2688	2 2336	2 5123	2 4819
A(2,1,3)	105 5	105 5	104 0	103.9
A(3,1,5)	74 4	74 4	75 9	76 0
A(6,5,3)	105 5	105 5	104 0	103 9
A(3,5,1)	74 4	74 4	75 9	76 0
D(4,3,1,2)	0 0	0 0	0 0	0 0
D(4,3,5,6)	0 0	0 0	0.0	0 0

C1 H2 H3 X4 C5 H6

11 C_2H_4---HX

Structural Parameters	X = F		X = Cl	
	MP2	B3LYP	MP2	B3LYP
R(1,2)	--	--	1 2794	1 2971
R(2,3)	--	--	2 5293	2 5143
R(2,4)	--	--	3 0475	2 875
R(2,6)	--	--	2 5301	2 5209
R(2,7)	--	--	3 0485	2 8858
R(3,4)	--	--	1 0855	1 0851
R(3,5)	--	--	1 086	1 085
R(3,6)	--	--	1 3412	1 3315
R(6,7)	--	--	1 0855	1 0851
R(6,8)	--	--	1 086	1 085
A(1,2,3)	--	--	164 1	164 4
A(1,2,4)	--	--	147 5	147 2
A(1,2,6)	--	--	164 2	164 8
A(1,2,7)	--	--	147 5	147 7
A(3,2,7)	--	--	43 4	45.4
A(4,2,6)	--	--	43 4	45.5
A(4,2,7)	--	--	47 8	50 8
A(2,3,5)	--	--	88 5	98 2
A(4,3,5)	--	--	117 2	116 5
A(4,3,6)	--	--	121 3	121 7
A(5,3,6)	--	--	121 4	121 7
A(2,6,8)	--	--	88 5	98 4
A(3,6,7)	--	--	121 3	121 7
A(3,6,8)	--	--	121 4	121 7
A(7,6,8)	--	--	117 2	116 5
D(1,2,3,5)	--	--	70 2	-59.9
D(7,2,3,5)	--	--	-148 8	147 4
D(1,2,6,8)	--	--	-70.3	60 0
D(4,2,6,8)	--	--	148 8	-147 3
D(4,3,6,7)	--	--	-0 0	-0 0
D(4,3,6,8)	--	--	179.2	-179 2
D(5,3,6,7)	--	--	-179 2	179 2
D(5,3,6,8)	--	--	-0 0081	-0 008

X1 H2 C3 H4 H5 C6 H7 H8

12 CH_3CN---HX

Structural Parameters	X = F		X = Cl	
	MP2	B3LYP	MP2	B3LYP
R(1,2)	0 9307	0 9405	1.2854	1 304
R(2,3)	1 8338	1 784	2 0348	1 9813
R(3,4)	1 1702	1 1497	1 1719	1 1508
R(4,5)	1 4609	1 4535	1 4614	1 4545
R(5,6)	1 0913	1 0917	1 0914	1 0917
R(5,7)	1 0913	1 0917	1 0914	1 0917
R(5,8)	1 0913	1 0917	1 0914	1 0917
A(1,2,3)	180 0	180 0	180 0	180 0
A(2,3,4)	180 0	180 0	180 0	180 0
A(3,4,5)	180 0	180 0	180 0	180 0
A(4,5,6)	109 6	109 9	109 7	110 0
A(4,5,7)	109 6	109 9	109.7	110 0
A(4,5,8)	109 6	109 9	109 7	110 0
D(4,3,2,1)	0 0	0 0	0 0	0 0
D(5,4,3,2)	0 0	0 0	0 0	0 0
D(6,5,4,3)	0 0	0 0	0 0	0 0
D(7,5,4,6)	120 0	120 0	120 0	120 0
D(8,5,4,6)	-120 0	-120 0	-120 0	-120 0

X1 H2 N3 C4 C5 H6 H7 H8

13 $(CH_2)_2O$---HX

Structural Parameters	X = F		X = Cl	
	MP2	B3LYP	MP2	B3LYP
R(1,2)	1 4444	1 4432	1 4427	1 4415
R(1,3)	1 4444	1 4432	1 4427	1 4416
R(1,8)	1 6772	1 6618	1 7874	1 7792
R(2,3)	1 4680	1 4664	1.4679	1 4664
R(2,6)	1 0850	1 0855	1 0854	1 0859
R(2,7)	1 0850	1 0849	1 0854	1 0851
R(3,4)	1 0850	1 0848	1.0854	1 0851
R(3,5)	1 0850	1 0854	1 0854	1 0859
R(8,9)	0 9365	0 9466	1 2965	1.3168
A(1,8,9)	175 4	170 9	172 0	171 9
A(2,1,8)	120 0	117 0	118 2	117 0
A(3,1,8)	118 4	116 9	115 9	117 0
A(1,2,6)	114 1	114 5	114 2	114 6
A(1,2,7)	114 1	114 0	114 2	114 2
A(3,2,6)	119 3	119 4	119.3	119.4
A(3,2,7)	119 3	119 7	119 3	119 8
A(6,2,7)	116 8	116 2	116 6	116.1
A(1,3,4)	114 1	114 0	114 2	114 2
A(1,3,5)	114 1	114 5	114 2	114 6
A(2,3,4)	119 3	119 7	119 3	119 8
A(2,3,5)	119 3	119 4	119 3	119 4
A(4,3,5)	116 8	116 2	116 6	116 1
D(8,1,2,6)	-3 0	-3 5	-5 1	-3.3
D(8,1,2,7)	-141 0	-141 0	-143 2	-140.8
D(8,1,3,4)	138 4	140 7	139 5	140 8
D(8,1,3,5)	0 4	3 3	1 4	3 3
D(6,2,3,4)	-155 3	-155 2	-155 0	-154 9
D(6,2,3,5)	0 0	0 0	0 0	0 0
D(7,2,3,4)	0 0	0 0	0 0	0 0
D(7,2,3,5)	155 3	155 2	155 0	154 9
D(2,1,8,9)	-90 0	-36 0	-90 0	-34 7
D(3,1,8,9)	-18 7	33 5	-20 3	34 9

O1 C2 C3 H4 H5 H6 H7 H8 X9

14 $(CH_2)_2S$---HX

Structural Parameters	X = F		X = Cl	
	MP2	B3LYP	MP2	B3LYP
R(1,2)	1 8223	1 8451	1 8204	1 8433
R(1,3)	1 8223	1 8452	1 8204	1 8434
R(1,8)	2 1751	2 1541	2 2647	2 225
R(2,3)	1 4825	1 4758	1 4833	1 4762
R(2,6)	1 0843	1 0833	1 0847	1 0839
R(2,7)	1 0843	1 0832	1 0847	1 0832
R(3,4)	1 0843	1 0832	1 0847	1 0832
R(3,5)	1 0843	1 0833	1 0847	1 0839
R(8,9)	0 9335	0 9458	1 2953	1 3238
A(1,8,9)	175 0	165 4	171 8	166 8
A(2,1,8)	95 0	93 0	88 6	91 9
A(3,1,8)	93 7	92 8	87 2	91 8
A(1,2,6)	114 6	114 4	114 8	114 4
A(1,2,7)	114 6	113 9	114 8	114 1
A(3,2,6)	117 9	118 4	117 9	118 3
A(3,2,7)	117 9	118 6	117 9	118 6
A(6,2,7)	115 9	115 4	115 7	115 3
A(1,3,4)	114 6	113 9	114 8	114 1
A(1,3,5)	114 6	114 3	114 8	114 4
A(2,3,4)	117 9	118 6	117 9	118 6
A(2,3,5)	117 9	118 4	117 9	118 3
A(4,3,5)	115 9	115 4	115 7	115 3
D(8,1,2,6)	-20 6	-20 7	-23 5	-21 0
D(8,1,2,7)	-158 3	-156 6	-161 5	-157 0
D(8,1,3,4)	155 4	156 3	158 2	156 8
D(8,1,3,5)	17 7	20 4	20 3	20 7
D(6,2,3,4)	-147 3	-148 4	-146 9	-148 2
D(6,2,3,5)	0 0	0 0	0 0	0 0
D(7,2,3,4)	0 0	0 0	0 0	0.0
D(7,2,3,5)	147 3	148 4	146 9	148 2
D(2,1,8,9)	-90 0	-23 8	-90.0	-24 0
D(3,1,8,9)	-41 8	23 3	-41 9	23 2

S1 C2 C3 H4 H5 H6 H7 H8 X9

Table VI.B. Optimized structural parameters of different B-H_2X complexes calculated at MP2 and B3LYP levels using 6-311++G** basis set Both H_2O and H_2S complexes have very similar optimized geometries Atom labels are shown in Figure VI B

1 HF---H_2X

Structural Parameters	X = O		X = S	
	MP2	B3LYP	MP2	B3LYP
R(H1-F2)	--	--	0 9177	0 9234
R(F2-H3)	--	--	2 3417	2 3133
R(H3-X4)	--	--	1 3337	1 3489
R(H5-X4)	--	--	1 3334	1 3479
A(H1-F2-H3)	--	--	136 0	125 8
A(F2-H3-X4)	--	--	169 6	167 0
A(H3-X4-H5)	--	--	92 3	92 6
D(H1-F2-H3-X4)	--	--	-22 4	2 4
D(F2-H3-X4-H5)	--	--	138 2	111 8
D(H1-F2-X4-H5)	--	--	116 7	113 5

H1 F2 H3 X4 H5

2 N_2---H_2X

Structural Parameters	X = O		X = S	
	MP2	B3LYP	MP2	B3LYP
R(N1-N2)	1 1200	1 0951	1 1202	1 0954
R(N1-H3)	2 3869	2 406	2 6913	2 8109
R(H3-X4)	0 9601	0 9629	1 3336	1 3479
R(X4-H5)	9594	0 9619	1 3336	1 3481
A(N2-N1-H3)	165 7	169 6	175 8	179 3
A(N1-H3-X4)	176 0	179 0	148 0	166 6
A(H3-X4-H5)	103 4	105 0	92 1	92 5
D(N2-N1-H3-X4)	0 0	0 0	-156 2	0 0
D(N1-H3-X4-H5)	180 0	180 0	-104 8	180 0
D(N2-N1-X4-H5)	180 0	180 0	-117 2	180 0

N1 N2 H3 X4 H5

3 OC---H_2X

Structural Parameters	X = O		X = S	
	MP2	B3LYP	MP2	B3LYP
R(1,2)	1 1385	1 1259	1 1393	1 1268
R(1,3)	2 4594	2 4151	2 7808	2 8199
R(3,4)	0 961	0 9642	1 3339	1 3485
R(4,5)	0 9592	0 9618	1 3336	1 3481
A(2,1,3)	171 2	172 8	167 4	175 1
A(1,3,4)	174 2	174 5	160 6	170 4
A(3,4,5)	103 5	105 2	92 2	92 6
D(2,1,3,4)	42 7	43 7	2.0	9 3
D(1,3,4,5)	135 8	134 5	114 1	178 7

C1 O2 H3 X4 H5

4 HCN---H_2X

Structural Parameters	X = O		X = S	
	MP2	B3LYP	MP2	B3LYP
R(1,2)	1 1698	1 1476	1 1708	1 1484
R(1,4)	2 1634	2 1376	2 4238	2 4404
R(2,3)	1 0684	1 0674	1 0683	1 0672
R(4,5)	0 9633	0 9667	1 3352	1 3500
R(5,6)	0 9589	0 9614	1 3336	1 3480
A(4,5,6)	103 2	104 9	92.5	92 690
A(2,1,4)	166 6	169 8	173 5	174 2
A(1,4,5)	179 2	179 2	166 4	175 7
D(3,2,1,4)	0 7	2 3	3 8	-0 9
D(2,1,4,5)	7 3	175 7	1 4	-0 8
D(1,4,5,6)	172.4	4 3	178 9	-178 9

N1 C2 H3 H4 X5 H6

5 H_2O---H_2X:

Structural Parameters	X = O		X = S	
	MP2	B3LYP	MP2	B3LYP
R(1,2)	0 9586	0 961	1 3334	1 3478
R(2,3)	0 9655	0 9698	1 3367	1 3533

R(3,4)	1 95	1 9318	2 1788	2 1568
R(3,5)	2 5314	2 5023	2 8127	2 7782
R(3,6)	2 5314	2 5023	2 8127	2 7782
R(4,5)	0 9606	0 9628	0 9604	0 9624
R(4,6)	0 9606	0 9628	0 9604	0 9624
A(1,2,3)	103 5	105 1	92 5	92 7
A(2,3,5)	158 6	158 0	161 8	161 5
A(2,3,6)	158 6	158 0	161 8	161 5
A(5,3,6)	34 8	35 7	31 2	32 0
A(5,4,6)	104 0	105 7	103 9	105 7
A(2,3,4)	176 9	176 8	176 6	177 2
D(1,2,3,5)	125 0	124 9	120 8	119 4
D(1,2,3,6)	-125 0	-124 9	-120 8	-119 4
D(1,2,3,4)	180 0	180 0	180 0	180 0
D(2,3,4,5)	-61 9	-62 0	-68 8	-68 4
D(2,3,4,6)	61 9	62 0	68 8	68 4

H1 X2 H3 O4 H5 H6

6 H_2S---H_2X

Structural Parameters	X = O		X = S	
	MP2	B3LYP	MP2	B3LYP
R(1,2)	--	--	1 3337	1 348
R(2,3)	--	--	1 3349	1.3517
R(3,4)	--	--	2 8382	2.8394
R(3,5)	--	--	3 5385	3.3751
R(3,6)	--	--	3 5433	3.3749
R(4,5)	--	--	1 3336	1 3481
R(4,6)	--	--	1 3336	1.3481
A(1,2,3)	--	--	92.3	92 6
A(2,3,5)	--	--	157 9	154 0
A(2,3,6)	--	--	158 1	154 1
A(5,3,6)	--	--	31 5	33 6
A(5,4,6)	--	--	92 3	92 7
A(2,3,4)	--	--	177 8	175 9
D(1,2,3,5)	--	--	-134 9	-140 5
D(1,2,3,6)	--	--	132 2	136 8
D(1,2,3,4)	--	--	-179 8	179 4
D(2,3,4,5)	--	--	48 9	46 2
D(2,3,4,6)	--	--	-52 2	-49 0

H1 X2 H3 S4 H5 H6

7 H_3N---H_2X

Structural Parameters	X = O		X = S	
	MP2	B3LYP	MP2	B3LYP
R(1,2)	1 9739	1 9605	2 2266	2 1727
R(1,3)	1 0151	1 0156	1 0151	1 0156
R(1,4)	1 0155	1 0161	1 0152	1 0158
R(1,5)	1 0151	1 0157	1 0151	1 0156
R(2,3)	2 5997	2 5725	2 8082	2 7361
R(2,4)	2 4129	2 4044	2 7172	2 6745
R(2,5)	2 5866	2 5597	2 7965	2 7288
R(2,6)	0 9716	0 9767	1 3426	1 3627
R(6,7)	0 9584	0 9609	1 3336	1 3479
A(3,1,4)	106 5	107 3	106 5	107 4
A(3,1,5)	106 6	107 5	106 6	107 6
A(4,1,5)	106 6	107 3	106 5	107 4
A(3,2,4)	37 7	38 2	34 2	35 2
A(3,2,5)	36 6	37 2	33 8	34 9
A(3,2,6)	162 5	162 4	164 0	162 1
A(4,2,5)	37.8	38 3	34 3	35 2
A(4,2,6)	146 8	147 3	152 0	154 8
A(5,2,6)	160 9	160 2	161 9	161 1
A(2,6,7)	103 9	105 5	92 7	93 0
A(1,2,6)	171 0	171 6	172 8	175 9
D(3,2,6,7)	84 6	83 5	79 3	68 6
D(4,2,6,7)	176 8	179 3	179 0	178 3
D(5,2,6,7)	-92 9	-88 3	-85 8	-75 0
D(1,2,6,7)	179 7	-175 9	-175 5	-176 3

N1 H2 H3 H4 H5 X6 H7

8 H_3P---H_2X:

Structural Parameters	X = O		X = S	
	MP2	B3LYP	MP2	B3LYP
R(1,2)	2 6478	2 6369	2 9491	2 9575
R(1,3)	1 4074	1 42	1 4084	1 4214

R(1,4)	1 4068	1 4195	1 4082	1 4214
R(1,5)	1 4074	1 42	1 4084	1 4214
R(2,6)	0 9629	0 967	1 3352	1.3514
R(6,7)	0 9593	0 9617	1 3336	1 3481
A(2,1,3)	125 8	126 1	125 6	125 2
A(2,1,4)	113 2	113 3	116 3	117 8
A(2,1,5)	125 0	125 6	123 6	123 6
A(3,1,4)	95 2	94 7	94 7	94 1
A(3,1,5)	95 0	94 6	94 7	94 2
A(4,1,5)	95 2	94 7	94 6	94 1
A(2,6,7)	103 6	105 0	92 2	92 5
A(1,2,6)	171 4	170 7	175 7	177 7
D(3,1,6,7)	65 4	66 6	66 2	62 1
D(4,1,6,7)	179 5	-179 7	-176 7	-179 8
D(5,1,6,7)	-67 2	-66 8	-61.9	-63 8
D(1,2,6,7)	-175 3	-174 4	-165 8	-155 2

P1 H2 H3 H4 H5 X6 H7

9. H_2CO---H_2X

Structural Parameters	X = O		X = S	
	MP2	B3LYP	MP2	B3LYP
R(1,2)	--	--	1 2153	1 2043
R(1,5)	--	--	2 3101	2 2612
R(2,3)	--	--	1 1036	1 1064
R(2,4)	--	--	1 1038	1 1067
R(5,6)	--	--	1 3367	1 3527
R(6,7)	--	--	1 3335	1 348
A(2,1,5)	--	--	104 1	110 9
A(1,2,3)	--	--	121 6	121 6
A(1,2,4)	--	--	121 6	121 8
A(3,2,4)	--	--	116 7	116 5
A(5,6,7)	--	--	92 4	92 7
A(1,5,6)	--	--	149 9	158 6
D(5,1,2,3)	--	--	-179 0	-178 3
D(5,1,2,4)	--	--	0 9	1 6
D(2,1,6,7)	--	--	-107 9	-103 8
D(2,1,5,6)	--	--	1 9	0 4
D(1,5,6,7)	--	--	-111 5	-105 3

O1 C2 H3 H4 H5 X6 H7

10 C_2H_2---H_2X

Structural Parameters	X = O		X = S	
	MP2	B3LYP	MP2	B3LYP
R(1,2)	1 0657	1 0638	1 0655	1 0636
R(1,3)	2 9727	2 9917	3 1609	3 2469
R(2,3)	2 519	2 5431	2 7425	2 8422
R(2,4)	1 2171	1 2001	1 2169	1 1999
R(3,4)	2 5146	2 5358	2 7398	2 8355
R(3,5)	2 9598	2 9728	3 1533	3 2298
R(3,6)	0 9614	0 9652	1 3343	1 3497
R(4,5)	1 0658	1 0639	1 0655	1 0636
R(6,7)	0 9593	0 9618	1 3337	1 3481
A(1,3,4)	48 3	47 4	44 8	43 0
A(1,3,5)	68 7	67 8	64 0	61 8
A(1,3,6)	146 6	146 4	147 5	150 0
A(2,3,5)	48 4	47 6	44 8	43 1
A(2,3,6)	166 9	166 1	165 2	168 6
A(4,3,6)	165 0	165 1	164 3	166 9
A(5,3,6)	144 6	145 2	146 5	148 1
A(3,6,7)	103 4	104 8	92 2	92 5
D(1,3,6,7)	-90 8	-82 0	-103 1	-91 1
D(2,3,6,7)	-92 8	-70 3	-123 1	-93 3
D(4,3,6,7)	93 6	74 4	121 3	93 3
D(5,3,6,7)	92 0	85 1	102 8	91 4

H1 C2 H3 C4 H5 X6 H7

11 CH_3CN-H_2X

Structural Parameters	X = O		X = S	
	MP2	B3LYP	MP2	B3LYP
R(1,2)	1 1722	1 1513	1 1732	1 152
R(1,7)	2 1064	2 0809	2 3537	2 3605
R(2,3)	1 4617	1 4549	1 4622	1 4556

R(3,4)	1 0914	1 0918	1 0915	1 0918
R(3,5)	1 0914	1 0917	1 0915	1 0918
R(3,6)	1 0914	1 0917	1 0915	1 0918
R(7,8)	0 9647	0 9684	1 3365	1 3514
R(8,9)	0 9588	0 9612	1 3336	1 348
A(2,3,4)	109 8	110 0	109 8	110 1
A(2,3,5)	109 7	110 0	109 8	110 1
A(2,3,6)	109 7	110 1	109 8	110 1
A(4,3,5)	109 1	108 8	109 1	108 8
A(4,3,6)	109 1	108 8	109 1	108 8
A(5,3,6)	109 1	108 8	109 1	108 8
A(7,8,9)	103 0	104 7	92 5	92 7
D(4,3,8,9)	-1 0	152 1	-3 4	1 4
D(5,3,8,9)	121 6	-91 1	117 2	122 6
D(6,3,8,9)	-123 3	32 5	-126 7	-119 7

N1 C2 C3 H4 H5 H6 H7 X8 H9

12 SO_2-H_2X

Structural Parameters	X = O		X = S	
	MP2	B3LYP	MP2	B3LYP
R(1,2)	1 4707	1 4619	--	--
R(1,4)	2 0602	2 0618	--	--
R(2,3)	1 4669	1 456	--	--
R(4,5)	0 9615	0 9649	--	--
R(5,6)	0 9591	0 9616	--	--
A(2,1,4)	139 5	141 1	--	--
A(1,2,3)	118 8	118 2	--	--
A(1,4,5)	164 6	164 3	--	--
A(4,5,6)	103 5	105 1	--	--
D(4,1,2,3)	66 6	71 1	--	--
D(2,1,4,5)	34 6	27 6	--	--
D(1,4,5,6)	-148 8	-144 2	--	--

O1 S2 O3 H4 X5 H6

13 $(CH_2)_2O$-H_2X

Structural Parameters	X = O		X = S	
	MP2	B3LYP	MP2	B3LYP
R(1,2)	1 4428	1 4392	1 4387	1 4355
R(1,3)	1 4427	1 4392	1 4381	1 4359
R(1,8)	1 9129	1 9016	2 1482	2 1414
R(2,3)	1 4673	1 4663	1 4674	1 4668
R(2,6)	1 0857	1 0859	1 0865	1 0865
R(2,7)	1 0852	1 0858	1 0855	1 0861
R(3,4)	1 0852	1 0858	1 0856	1 0861
R(3,5)	1 0857	1 0859	1 0865	1 0864
R(8,9)	0 9684	0 9718	1 3398	1 3551
R(9,10)	0 9588	0 9609	1 3338	1 3477
A(2,1,8)	104 9	111 8	106 7	122 6
A(3,1,8)	104 8	111 9	109 6	119.9
A(1,2,6)	114 2	114 6	114 5	115 0
A(1,2,7)	114 2	114 4	114 5	114 7
A(3,2,6)	118 8	119 3	118 8	119 5
A(3,2,7)	119 4	119 7	119 5	119 7
A(6,2,7)	117 0	116 1	116 6	115 7
A(1,3,4)	114 2	114 4	114 5	114 7
A(1,3,5)	114 2	114 6	114 6	114 9
A(2,3,4)	119 4	119 7	119 5	119 6
A(2,3,5)	118 8	119 3	118 8	119 5
A(4,3,5)	117 0	116 1	116 6	115 8
A(1,8,9)	151 5	160 1	150 2	170 6
A(8,9,10)	104 2	105 5	92 3	92 7
D(8,1,2,6)	-11 3	-7 0	-6 5	-1 8
D(8,1,2,7)	-149 8	-144 8	-145 3	-139 8
D(8,1,3,4)	149 7	144 9	150 0	135 6
D(8,1,3,5)	11 3	7 1	11 3	-2 4
D(2,1,8,9)	-32.0	-33 0	-29 3	-50 6
D(3,1,8,9)	31 4	33 5	35 5	22 6
D(6,2,3,4)	-155 0	-154 6	-154 2	-153 9
D(6,2,3,5)	0 0	-0 0	0 0	0 1
D(7,2,3,4)	0.0	0 0	0 0	0 0
D(7,2,3,5)	155.0	154 6	154 2	154 1
D(1,8,9,10)	-178 9	179 4	-102 262	-122 9

O1 C2 C3 H4 H5 H6 H7 H8 X9 H10

15 $(CH_2)_2S$-H_2X

Structural Parameters	X = O		X = S	
	MP2	B3LYP	MP2	B3LYP
R(1,2)	1 8218	1 8447	1 8178	1 8404
R(1,3)	1 8219	1 8446	1 8176	1 8404
R(1,8)	2 4076	2 4221	2 6404	2 6427
R(2,3)	1 4828	1 4761	1 4837	1 4773
R(2,6)	1 0844	1 0835	1 0849	1 0841
R(2,7)	1 0843	1 0835	1 0844	1.0836
R(3,4)	1 0843	1 0835	1 0844	1 0836
R(3,5)	1 0844	1 0835	1.085	1 0841
R(8,9)	0 9672	0 9715	1 3398	1.3574
R(9,10)	0 9595	0 9613	1 3341	1 3479
A(2,1,8)	82 4	84 9	83 3	90 5
A(3,1,8)	82 4	85 1	84 5	91 0
A(1,2,6)	114 7	114 2	115 2	114 8
A(1,2,7)	114 4	114 2	114 8	114 4
A(3,2,6)	117 2	117 9	117 3	118 1
A(3,2,7)	118 1	118 6	118 1	118 5
A(6,2,7)	116 3	115 7	115 8	115 1
A(1,3,4)	114 4	114 2	114 9	114 5
A(1,3,5)	114 7	114 2	115 2	114 8
A(2,3,4)	118 1	118 6	118 1	118 5
A(2,3,5)	117 2	117 9	117 2	118 1
A(4,3,5)	116 3	115 7	115 8	115 2
A(1,8,9)	146 9	148 2	152 8	160 0
A(8,9,10)	103 8	105 5	92 2	92 6
D(8,1,2,6)	-23 71	-23 3	-21.4	-20 5
D(8,1,2,7)	-162 0	-159 8	-160 1	-157 1
D(8,1,3,4)	162 0	160 1	162 8	158 1
D(8,1,3,5)	23 7	23 6	24 1	21 5
D(2,1,8,9)	-24 2	-23 5	-20 1	-23 5
D(3,1,8,9)	24 2	23 8	28 3	23 7
D(6,2,3,4)	-147 4	-148 2	-146 2	-147 2
D(6,2,3,5)	0 0	0 0	0 0	0 0
D(7,2,3,4)	0 0	0 0	0 08	0 0
D(7,2,3,5)	147 4	148 2	146 3	147 3
D(1,8,9,10)	-179 9	179 8	-102 1	-106 0

S1 C2 C3 H4 H5 H6 H7 H8 X9 H10

Table VI.C. Energies of B---HF complexes calculated at MP2 and B3LYP levels using 6-311++G** basis set

B	MP2			B3LYP		
	E_{COM}	E_B	E_{HF}	E_{COM}	E_B	E_{HF}
HF	-200 5652739	-100 2799632	-100 2793465	-200 9726675	-100 4828579	-100 482636
N_2	-209 584443	-109.301838	-100 2795038	-210 0458463	-109 5597858	-100 4827462
OC	-213 3627679	-113 0786194	-100.2794057	-213 8372287	-113 3491598	-100 4826255
HCN	-193 4937085	-93 2036769	-100 27951	-193 9492255	-93 4546414	-100 4826161
H_2O	-176 5692074	-76 2776455	-100 2794139	-176 9568723	-76 4598754	-100 4824291
H_2S	-499 1354638	-398 85022	-100 2792375	-499 9140192	-399 4231829	-100 4824306
H_3N	-156 7157276	-56 4182012	-100 2786674	-157 0878567	-56 5839789	-100 4813175
H_3P	-442 9013193	-342 6155169	-100 2792196	-443 6645911	-343 1735682	-100 482422
H_2CO	-214 5329691	-114 2432033	-100 2794759	-215 0372789	-114 5420294	-100 4825139
C_2H_2	-177 3992082	-77 1147219	-100 2794281	-177.8458465	-77 3567681	-100 4826386
C_2H_4	--	--	--	-179 1050219	-78 6156178	-100 4827202
CH_3CN	-232 704101	-132 4116781	-100 2795842	-233 2938675	-132 7963338	-100 4825766
$(CH_2)_2O$	-253 7007971	-153 4081199	-100 2796897	-254 3348566	-153 8367105	-100 4825292
$(CH_2)_2S$	-576 3127319	-476 0241988	-100 2793951	-577 3289862	-476 8339621	-100 4823475

Table VI.D. Energies of B---HCl complexes, calculated at MP2 and B3LYP levels using 6-311++G** basis set

B	MP2			B3LYP		
	E_{COM}	E_B	E_{HCl}	E_{COM}	E_B	E_{Hcl}
HF	-560 5287024	-100 2794598	-460 2455652	-561 3212615	-100 4826358	-460 8343239
OC	-573 3266815	-113 0783707	-460 245705	-574 1859224	-113 3491133	-460 8344349
HCN	-553 4560732	-93 2035056	-460 2460718	-554 2959447	-93 4546276	-460 8345209
H_2O	-536 5300276	-76 2766874	-460 2459899	-537 3028488	-76 4594799	-460 8342827
H_2S	-859 0984062	-398 8496611	-460 245494	-860 2622513	-399 423162	-460 8341953
H_3N	-516 6752021	-56 4175564	-460 2455046	-517 4329633	-56 5838075	-460 8326043
H_3P	-802.8640734	-342 6149655	-460 2455076	-804 0127841	-343 1736384	-460 8342679
H_2CO	-574 49489	-114 2426022	-460 2460856	-575.3840275	-114 5419902	-460 8344104
C_2H_2	-537 3632308	-77 1143019	-460 2458704	-538 1944785	-77.3567406	-460 8344172
C_2H_4	-538 5966858	-78 3472326	-460 246255	-539 4535584	-78 6155963	-460 8344459
CH_3CN	-592 6659442	-132 4115025	-460 246336	-593 6398313	-132 7963419	-460 8345528
$(CH_2)_2O$	-613.6627761	-153.4073417	-460 2469128	-614 6809447	-153 8365248	-460 8343068
$(CH_2)_2S$	-936 2760062	-476 0235909	-460 2465582	-937 6767715	-476 8339563	-460 8339567

Table VI.E Energies of B---H_2O complexes, calculated at MP2 and B3LYP levels using 6-311++G** basis set

B	MP2			B3LYP		
	E_{COM}	E_B	E_{H2O}	E_{COM}	E_B	E_{H2O}
N_2	-185 5787417	-109 3018305	-76 2753319	-186 0197635	-109 5597645	-76 4587158
OC	-189 3560077	-113 0784322	-76 2752275	-189 8099142	-113 3491133	-76 4586487
HCN	-169 4846151	-93 2035563	-76.2754236	-169 9190716	-93 4545786	-76 4587315
H_2O	-152 5595249	-76 276954	-76 2754293	-152 9263439	-76 4595785	-76 4586986
H_2S	-475 1277583	-398 8499812	-76 27516	--	--	--
H_3N	-132 7021562	-56 4174246	-76 2753535	-133 0528374	-56 5836842	-76 458529
H_3P	-418 8934162	-342 6151333	-76 2751637	-419 6358858	-343 1737161	-76.4586209
C_2H_2	-153 392698	-77 114471	-76 2753485	-153 8184388	-77 3566858	-76 4587365
CH_3CN	-208 6940737	-132 4115602	-76.2756152	-209 2624037	-132 7962365	-76 4588072
SO_2	-624 0692597	-547 7902893	-76 2754497	-625 1284406	-548 6658427	-76 4587422
$(CH_2)_2O$	-229 6916568	-153 407126	-76 2760844	-230 3040331	-153 8365749	-76 4588753
$(CH_2)_2S$	-552 3061384	-476 0235208	-76 2759158	-553 2998707	-476 8339693	-76 4587624

Table VI.F. Energies of the B---H_2S complexes, calculated at MP2 and B3LYP levels using 6-311++G** basis set

B	MP2			B3LYP		
	E_{COM}	E_B	E_{H2S}	E_{COM}	E_B	E_{H2S}
HF	-499 1294953	-100 2793398	-398 8483317	-499 9074646	-100 4825614	-399 4228081
N_2	-508 151402	-109 3017374	-398 8490924	-508 9830258	-109 5597331	-399 4229342
OC	-511 9278837	-113 078308	-398 8485196	-512 7725984	-113 3490581	-399 4228582
HCN	-492 05521	-93 2034402	-398 8487601	-492 880222	-93 4545463	-399 4229011
H_2O	-475 1284889	-76 2760554	-398 8487036	-475 8862546	-76 4591078	-399 4228897
H_2S	-797 6989884	-398 8492869	-398 8483033	-798 8476365	-399 4231007	-399 4228392
H_3N	-455 2700869	-56 4166508	-398 8487681	-456 0118475	-56 5833513	-399 4228233
H_3P	-741 4642769	-342 6145352	-398 8482835	-742 598012	-343 1736807	-399 4228028
H_2CO	-513 094574	-114 2423088	-398 8491854	-513 9681245	-114 5418958	-399 4229294
C_2H_2	-475 9644406	-77 1141276	-398 8487179	-476 7809017	-77 3566628	-399 4228988
CH_3CN	-531 2641414	-132 4114305	-398 8489041	-532 2229243	-132 7962265	-399 4229723
$(CH_2)_2O$	-552 2609012	-153 406505	-398 8504162	-553 2634066	-153 8363497	-399 4230603
$(CH_2)_2S$	-874 8761311	-476 0229345	-398 8500895	-876 2601004	-476 8339602	-399 4230244

Table VI.G Frequency of B---HX complexes calculated at MP2 and B3LYP method using 6-311++G** basis set

B	HF		HCl	
	MP2	B3LYP	MP2	B3LYP
HF	151	162	104	112
	208	204	130	159
	425	432	232	288
	529	543	314	362
	4108	3961	3060	2870
	4162	4057	4172	4068
N_2	53	64	--	--
	53	64	--	--
	105	117	--	--
	272	329	--	--
	272	329	--	--
	2183	2455	--	--
	4141	4012	--	--
OC	92	94	45	64
	92	94	45	64
	118	135	79	79
	460	475	221	283
	460	475	221	283
	2148	2245	2136	2231
	4067	3906	3043	2854
HCN	77	83	59	61
	77	83	59	61
	167	185	115	118
	598	634	318	423
	598	634	318	423
	736	779	738	778

Table VI G continued

	736	779	738	778
	2048	2224	2031	2212
	3481	3452	2968	2774
	3957	3788	3478	3451
	--	240	158	168
	--	263	186	213
	--	331	277	287
	--	751	512	534
H_2O	--	890	596	646
	--	1628	1649	1622
	--	3661	2887	2646
	--	3808	3867	3804
	--	3900	3975	3901
	131	147	85	97
	181	208	141	162
	227	223	173	178
	574	576	376	420
H_2S	609	612	419	444
	1221	1206	1226	1205
	2817	2672	2816	2672
	2836	2688	2835	2689
	3979	3767	2976	2695
H_3N	264	277	180	194
	281	289	235	266
	281	289	235	266
	987	1010	739	841
	987	1010	739	841
	1190	1144	1169	1121
	1644	1662	1637	1660
	1644	1662	1637	1660

Table VI G continued

	3485	3247	2525	2130
	3524	3476	3515	3473
	3657	3592	3655	3593
	3657	3592	3655	3593
H_3P	129	145	83	93
	157	151	108	112
	157	151	108	112
	592	568	386	409
	592	568	386	409
	1054	1013	1054	1010
	1151	1137	1144	1137
	1151	1137	1144	1137
	2537	2419	2527	2412
	2547	2431	2537	2423
	2547	2431	2537	2423
	3955	3748	2955	2685
H_2CO	--	70	32	49
	--	196	135	159
	--	234	147	159
	--	680	370	479
	--	715	448	509
	--	1211	1210	1208
	--	1265	1282	1261
	--	1528	1557	1528
	--	1794	1753	1797
	--	2934	2909	2676
	--	3016	3004	2922
	--	3687	3087	2997
C_2H_2	101	99	76	74
	121	137	88	87

Table VI G continued

	375	417	205	260
	471	498	313	340
	541	662	532	660
	581	706	534	685
	770	778	768	776
	785	801	774	793
	1957	2055	1958	2057
	3444	3408	3016	2801
	3534	3511	3448	3411
	4039	3866	3538	3515
C_2H_4	--	--	73	63
	--	--	87	86
	--	--	98	110
	--	--	286	303
	--	--	322	312
	--	--	829	835
	--	--	881	973
	--	--	977	993
	--	--	1070	1063
	--	--	1238	1239
	--	--	1381	1376
	--	--	1482	1473
	--	--	1669	1677
	--	--	2997	2779
	--	--	3173	3124
	--	--	3189	3139
	--	--	3264	3198
	--	--	3290	3226
CH_3CN	--	49	28	37
	--	49	28	37

Table VI G continued

	--	186	112	117
	--	389	348	385
	--	389	348	385
	--	698	376	491
	--	698	376	491
	--	939	938	935
	--	1060	1069	1061
	--	1060	1069	1061
	--	1411	1424	1411
	--	1470	1496	1471
	--	1470	1496	1471
	--	2387	2225	2376
	--	3049	2923	2701
	--	3122	3101	3049
	--	3122	3197	3121
	--	3694	3197	3121
$(CH_2)_2O$	65	72	44	54
	83	81	65	65
	242	255	177	181
	813	805	552	594
	821	810	569	601
	843	829	838	821
	843	835	841	823
	902	880	898	877
	1073	1050	1072	1048
	1178	1147	1177	1143
	1192	1171	1190	1167
	1193	1174	1191	1171
	1202	1180	1200	1178
	1320	1298	1319	1297

Table VI G continued

	1527	1500	1528	1499
	1560	1533	1560	1532
	3166	3106	2750	2530
	3173	3111	3161	3101
	3271	3196	3168	3107
	3284	3210	3264	3190
	3743	3559	3277	3204
$(CH_2)_2S$	40	58	42	52
	74	75	71	69
	174	191	128	141
	665	614	487	526
	676	637	514	569
	677	658	667	615
	702	693	698	644
	848	840	846	839
	954	918	951	915
	1000	962	997	960
	1089	1055	1085	1054
	1137	1088	1138	1087
	1175	1150	1174	1149
	1208	1201	1205	1199
	1500	1474	1500	1473
	1529	1501	1529	1499
	3177	3130	2742	2431
	3180	3131	3172	3126
	3274	3215	3175	3127
	3286	3229	3268	3210
	3789	3561	3280	3225

Table VI.H Frequencies of B---H_2X complexes calculated at MP2 and B3LYP methods using 6-311++G** basis set

B	H_2O		H_2S	
	MP2	B3LYP	MP2	B3LYP
HF	--	--	69	69
	--	--	81	91
	--	--	92	105
	--	--	124	129
	--	--	228	260
	--	--	1247	1214
	--	--	2820	2676
	--	--	2839	2691
	--	--	4183	4081
N_2	21	25	28	38
	51	40	56	42
	85	76	70	45
	108	116	97	108
	148	211	187	162
	1635	1607	1240	1216
	2178	2449	2175	2446
	3884	3815	2818	2677
	3998	3917	2837	2694
OC	52	52	304	33
	61	60	41	38
	86	87	63	46
	180	186	90	98
	298	309	197	156
	1636	1605	1242	1214
	2135	2228	2128	2219
	3874	3797	2815	2674
	3991	3906	2834	2690
HCN	45	55	26	36
	56	62	43	38
	125	128	85	75
	227	248	162	138
	416	455	169	273
	735	774	732	771
	738	775	734	771
	1652	1624	1254	1217
	2031	2208	2021	2201
	3480	3450	2806	2663

Table VI H continued

	3849	3767	2829	2683
	3979	3897	3480	3451
H_2O	135	130	87	78
	170	157	108	113
	176	169	115	119
	202	193	131	121
	385	362	195	187
	669	671	395	418
	1638	1612	1252	1220
	1664	1630	1633	1610
	3807	3708	2790	2628
	3877	3816	2828	2682
	3973	3893	3875	3815
	3990	3917	3992	3920
H_2S	38	--	49	60
	101	--	68	71
	145	--	76	94
	173	--	122	98
	305	--	231	197
	454	--	272	304
	1227	--	1230	1205
	1654	--	1256	1218
	2815	--	2806	2636
	2835	--	2817	2673
	3853	--	2829	2684
	3980	--	2836	2690
H_3N	42	17	25	42
	173	180	121	128
	201	205	122	163
	207	215	142	166
	470	476	305	330
	733	738	441	502
	1143	1091	1120	1063
	1644	1636	1268	1239
	1648	1664	1641	1663
	1673	1665	1644	1664
	3518	3474	2706	2503
	3658	3564	2823	2684
	3661	3591	3517	3472
	3680	3594	3660	3593
	3965	3887	3662	3594
H_3P	38	20	17	54
	90	84	60	59

Table VI H continued

	111	89	63	64
	116	107	82	80
	273	254	170	158
	450	402	269	256
	1057	1015	1056	1017
	1149	1138	1143	1139
	1154	1139	1145	1139
	1647	1612	1249	1215
	2525	2406	2518	2398
	2533	2414	2526	2406
	2536	2418	2527	2409
	3841	3746	2801	2639
	3976	3892	2828	2685
	--	--	67	42
	--	--	98	80
	--	--	109	110
	--	--	114	113
	--	--	173	183
	--	--	291	325
	--	--	1210	1206
H_2CO	--	--	1244	1218
	--	--	1282	1261
	--	--	1557	1528
	--	--	1755	1804
	--	--	2789	2631
	--	--	2828	2681
	--	--	2987	2901
	--	--	3067	2969
C_2H_2	42	39	51	39
	98	95	73	56
	119	114	82	85
	154	162	118	98
	370	367	240	230
	533	658	529	659
	542	679	536	669
	767	776	763	776
	770	786	767	781
	1636	1609	1244	1208
	1958	2058	1959	2059
	3450	3413	2812	2661
	3540	3516	2831	2685
	3865	3782	3452	3415

Table VI H continued

	3985	3899	3541	3518
	6	16	7	20
	25	31	8	21
	43	47	19	54
	128	132	84	76
	252	272	129	160
	356	384	181	315
	360	388	357	385
	466	512	358	386
	937	934	935	931
	1069	1060	1069	1061
CH_3CN	1070	1061	1069	1061
	1424	1411	1251	1219
	1497	1472	1424	1411
	1498	1472	1498	1473
	1662	1632	1498	1473
	2223	2373	2214	2367
	3101	3048	2794	2648
	3196	3119	2827	2685
	3196	3120	3100	3047
	3829	3740	3195	3118
	3974	3894	3195	3118
	28	25	--	--
	40	38	--	--
	75	76	--	--
	140	136	--	--
	242	236	--	--
	429	425	--	--
SO_2	498	509	--	--
	1078	1133	--	--
	1284	1306	--	--
	1651	1618	--	--
	3870	3793	--	--
	3988	3904	--	--
$(CH_2)_2O$	67	47	49	20
	69	50	61	40
	138	92	103	69
	203	199	134	112
	389	385	190	210
	608	602	357	360
	839	823	838	820
	843	826	845	831

Table VI H continued

	899	880	901	881
	1075	1048	1072	1044
	1177	1145	1175	1142
	1190	1165	1184	1159
	1191	1170	1186	1167
	1202	1178	1195	1174
	1320	1298	1249	1228
	1524	1499	1320	1298
	1558	1532	1524	1501
	1656	1633	1557	1535
	3160	3096	2751	2603
	3166	3102	2823	2687
	3263	3184	3153	3090
	3277	3198	3159	3097
	3745	3664	3254	3175
	3966	3894	3267	3190
$(CH_2)_2S$	85	53	63	40
	97	70	72	46
	142	84	94	88
	148	148	104	98
	306	328	179	191
	509	481	326	332
	665	614	669	618
	696	643	699	648
	854	844	847	839
	960	918	948	909
	1004	964	998	958
	1092	1056	1081	1049
	1143	1089	1136	1082
	1175	1150	1172	1147
	1212	1203	1201	1196
	1494	1470	1241	1216
	1525	1497	1492	1473
	1645	1617	1521	1498
	3175	3126	2744	2564
	3177	3126	2822	2685
	3274	3211	3172	3121
	3286	3225	3173	3122
	3761	3660	3267	3203
	3960	3889	3278	3218

References

1 Pauling, L *The Nature of the Chemical Bond*, Cornell University Press, Ithaca, New York, (1960)

2 K Muller-Dethlefs, and P Hobza, *Chem Rev* **100,** 143 (2000)

3 G R Desiraju and T Steiner, *The Weak Hydrogen Bond In Structural Chemistry and Biology*, Oxford University Press, Oxford (1999)

4 G A Jeffrey and W Saenger, *Hydrogen Bonding in Biological Structures*, Springer Verlog, Berlin (1991)

5 L. N Kuleshova and P M Zorkii, *Acta Cryst* B, **37**, 1363 (1981)

6. S. C Nyburg, C. H Faerman and L. Prasad, *Acta Cryst* B, **43**, 106 (1987)

7 Z Rahim and B N Barman, *Acta Cryst* A, **34**, 761 (1978)

8 A. D Buckingham and P W Fowler, *Can J Chem* **63**, 2018 (1985)

9 S R Gadre and P. K. Bhadane, *J Chem Phys* **107**, 5625 (1997) and references cited therein

10 A C Legon, *Angew Chem Int Ed* **38**, 2686 (1999) and references cited therein

11 A C Legon and A P Suckley, *Chep Phys Lett* **150**, 153 (1988).

12 G J B Hurst, P. W Fowler, A J Stone and A D Buckingham, *Int J Quantum Chem* **29**, 1223 (1986).

13 T R Dyke, B J. Howard, and W Klemperer, *J Chem Phys* **56**, 2442 (1972)

14 J. W Bevan, Z. Kisiel, A C Legon, D J Millen, and S C Rogers, *Proc R Soc London, Ser A*, **372**, 441 (1980)

15. A C Legon and L C. Willoughby, *Chem Phys* **74**, 127 (1983)

16. M J. Atkins, A C Legon and H E Warner, *Chem Phys Lett* **229**, 267 (1994).

17. A. C. Legon and A L Wallwork, *Chem Phys Lett* **178**, 279 (1991)

18 A C Legon, D J. Millen, and H M North, *J Phys Chem* **91**, 5210 (1987)

19 C Chuang, T D. Klots, R S. Ruoff, T Emilsson, and H S Gutowsky, *J Chem Phys.* **95**, 1552 (1991)

20 S W. Sharpe, Y. P. Zeng, C Wittig, and R A Beaudet, *J Chem Phys* **92**, 943 (1990).

21 Y P Zeng, S W Sharpe, D Reifschneider, C Wittig, and R A Beaudet, *J Chem Phys* **93**, 183 (1990)

22 R S Altman, M D Marshall, and W Klemperer, *J Chem Phys* **79**, 57 (1983)

23 Legon, A C and Willoughby, L C , *J Chem Soc Chem Comm* 1982, 997

24 C M Evans and A C Legon, *Chem Phys* **198**, 119 (1995)

25 A C Legon, C A Rego and A L Wallwork, *J Chem Phys* **97**, 3050 (1992)

26 S A Cooke, G K Corlett, C M Evans, and A C Legon, *Chem Phys Lett* **272**, 61 (1997)

27 N W Howard and A C Legon, *J Chem Phys* **90**, 672 (1989)

28 A C Legon and A L Wallwork, *J Chem Soc , Faraday Trans* , **86**, 3975 (1990)

29 A McIntosh, R R Lucchese, J W Bevan, R D Suenram and A C Legon, *Chem Phys Lett* **314**, 57 (1999)

30 P W Fowler, A C Legon and S A Peebles, *Chem Phys Lett* **226**, 501 (1994)

31 Z Wang, R R Lucchese, J W Bevan, A P Suckley, C. A. Rego and A C Legon, *J Chem Phys* **98**, 1761 (1993)

32 A C Legon and L C Willoughby, *Chem Phys* **85**, 443 (1984)

33 A J Fillery, A C Legon, and L C Willoughby, *Chem Phys Lett* **98**, 369 (1983)

34 K Georgiou, A C Legon, D J Millen, and P J Mjoberg, *Proc R Soc London, A,* **399**, 377 (1985)

35 G T Fraser, K R. Leopold, D D Nelson, A Tung, and W Klemperer, *J Chem Phys* **80**, 307 (1984)

36 E J Goodwin and A C. Legon, *Chem Phys* **87**, 81 (1984)

37 P D. Aldrich, S G Kukolich, and E J Campbell, *J Chem Phys* **78**, 3521 (1983)

38 S G Kukolich, W G Read, and P D. Aldrich, *J Chem Phys* **78**, 3552 (1983)

39 E J. Goodwin and A C Legon, *J Chem Soc Faraday Trans II,* **80**, 1669 (1984)

40 N. W Howard and A. C. Legon, *J Chem Soc Faraday Trans II,* **83**, 991 (1987)

41 S G Kukolich, *J Chem Phys* **78**, 4832 (1983)

42. H S. Gutowsky, E Arunan, T Emilsson, S L. Tschopp, and C E Dykstra, *J Chem Phys* **103**, 3917 (1995)

43. T D Klots, R S Ruoff, and H S. Gutowsky , *J Chem Phys.* **90**, 4216 (1989)

44 E J Goodwin and A C Legon, *J Chem Phys* **87**, 2426 (1987)

45 E J Goodwin and A C Legon, *J Chem Phys* **82**, 4434 (1985)

46 J Cosleou, D J Lister and A C Legon, *Chem Phys Lett* **231**, 151 (1994)

47 E J Goodwin, A C Legon and D J Millen, *J Chem Phys* **85**, 676 (1986)

48 T R. Dyke, J S Muenter, *J Chem Phys,* **60**, 2929 (1974)

49 P. Herbine and T R Dyke, *J Chem Phys* **83**, 3768 (1985)

50 D Yaron, K I Peterson, D Zolandz, W Klemperer, F J Lovas and R D Suenram, *J Chem Phys* **92**, 7095 (1990)

51. K I Peterson and W Klemperer, *J Chem Phys* **85**, 725 (1986)

52. F J Lovas and J Sobhanadri, Proc Ohio State Spectroscopy Symposium, TC 12 (1994)

53. A M Andrews, K W Hilling II and R L Kuczkowski, *J Am Chem Soc.* **114**, 6765 (1992)

54. H S Gutowsky, T Emilsson and E Arunan, *J Chem Phys* **99**, 4883 (1993)

55 F J. Lovas and C L. Lugez, *J Mol Spectrosc.* **179**, 320 (1996)

56 H O. Leung, M D Marshall, R D Suenram and F J Lovas, *J Chem Phys.* **90**, 700 (1989)

57 W Caminati, P Moreschini, I Rossi and P. G. Favero, *J Am Chem Soc* **120**, 11144 (1998)

58 K I Peterson and W Klemperer, *J Chem Phys* **81**, 3842 (1984)

59 N W Howard and A C Legon, *J Chem Phys* **85**, 6898 (1986)

60 G T Fraser, K R Leopold and W. Klemperer, *J Chem Phys.* **80**, 1423 (1984)

61. M A. Rochrig and S G Kukolich, *Chem Phys Lett.* **188**, 232 (1992).

62 D J. Prichard, R. N. Nandi and J S Muenter, *J Chem Phys* **89**, 115 (1988)

63 G T Fraser, F J Lovas, R D Suenram, J. Z Gillies and C W Gillies, *Chem Phys* **163**, 91 (1992)

64 N W. Howard and A. C Legon, *J Chem Phys.* **88**, 6793 (1988)

65 A C Legon, A L. Wallwork and P W. Fowler, *Chem Phys Lett.* **184**, 175 (1991)

66 M Goswami, P K Mandal, D J Ramdass and E Arunan, *Chem Phys Lett* **393**, 22 (2004)

67 F J Lovas, private communication, Chapter IV of this Thesis

68 L Bian, *J Phys Chem A*, **107**, 11517 (2003)

69 P Kollman, J McKelvy, A Johansson and S Rothenberg, *J Am Chem Soc* **97**, 955 (1975)

70 S D Wetmore, R Schofield, D M Smith and L Radom, *J Phys Chem A*, **105**, 8718 (2001)

71 S J Grabowski, *J Phys Chem A*, **105**, 10739 (2001)

72 M J Frisch, G W Trucks, H B Schlegel, G. E Scuseria, M A Robb, J R Cheeseman, V G Zakrzewski, J A Montgomery, Jr, R E Stratmann, J C Burant, S Dapprich, J M Millam, A D Daniels, K N Kudin, M C Strain, O Farkas, J Tomasi, V Barone, M Cossi, R Cammi, B Mennucci, C Pomelli, C Adamo, S Clifford, J Ochterski, G A Petersson, P Y Ayala, Q Cui, K Morokuma, N Rega, P Salvador, J J Dannenberg, D K Malick, A D Rabuck, K Raghavachari, J B Foresman, J Cioslowski, J V Ortiz, A G. Baboul, B B Stefanov, G Liu, A Liashenko, P Piskorz, I Komaromi, R Gomperts, R L Martin, D J Fox, T Keith, M A Al-Laham, C Y Peng, A Nanayakkara, M Challacombe, P M W Gill, B Johnson, W. Chen, M W Wong, J L Andres, C Gonzalez, M Head-Gordon, E S Replogle, and J A Pople, Gaussian 98, Revision A 11 3, Gaussian, Inc , Pittsburgh PA, (2002).

73 M Hartmann, S. D. Wetmore and L Radom, *J Phys Chem A*, **105**, 4470 (2001)

74 *CRC Handbook of Chemistry and Physics*, **80th Edition**, 9-42 to 9-50 (1999-2000)

75 G E Hyde and D F Hornig, *J Chem Phys* **20**, 647 (1952)

76 L M Sverdlov, *Optika i Spektroskopya*, **11**, 35 (1961)

77. J E Huhee, E. A Keitter and R L Keiter, *Inorganic Chemistry Principles of Structure and Reactivity*, Harper Collins College Publishers, New York, **4th Edition**, p 197 (1993)

78 L C Allen, *J Amer Chem Soc.*, **111** (1989) 9003, D F Shriver, P W Atkins, C H Langford, *Inorganic Chemistry*, p640

79 I J Bruno, J C Cole, P R Edgington, M K Kessler, C F Macrae, P McCabe, J Pearson and R Taylor, *Acta Crystallgr , Sect B*, **B58**, 389 (2002) Available at the website http //www ccdc cam ac uk/support/documentation/#mercury

80 B Lakshmi, A G Samuelson, K V J Jose, S R Gadre and E Arunan, *New J Chem* **29**, 371 (2005)

81 S C Wallwork, *Acta Cryst* **15**, 758 (1962)

Chapter VII

Conclusions and Future Directions

VII.1. Conclusions

A pulsed nozzle Fourier transform microwave spectrometer has been fabricated in our laboratory successfully This spectrometer is being used routinely to study the weakly bound complexes Several weakly bound H_2S complexes have been studied Theoretical calculations have also been performed along with the experiment to enhance our understanding

The first system studied using the spectrometer, Ar_2-H_2S complex, is an asymmetric top with C_{2v} symmetric heavy atom geometry Only one set of rotational transitions have been observed, though two sets of transitions are expected corresponding to *ortho* and *para* H_2S in the complex. Several *a*-dipole transitions are observed for Ar_2-H_2S, Ar_2-HDS and Ar_2-D_2S complexes Due to the presence of C_2 symmetry axis interchanging two identical Ar nuclei (I = 0), transitions are observed only between rotational levels $J_{Kp,Ko}$, which have K_p and K_o either *ee* or *eo* The Ar-Ar distance in the complex is 3 820 Å, which is almost identical to that in free Ar_2 dimer The Ar-c m(H_2S) separation is 4 105 Å, which is in between the Ar-c m(H_2S) distances in Ar-H_2S and Ar_3-H_2S. H_2S undergoes a large amplitude internal motion in the complex A Potential energy surface scan starting from a C_{2v} symmetric geometry has been performed at MP2/6-311++G(3df,2p) level for internal rotation of H_2S about its three principal inertial axes. It has a very floppy potential energy surface The zero point energy is comparable to the barrier height for the internal rotation, making H_2S virtually a free rotor

Rotational spectra for Ar-$(H_2S)_2$ and Ar-$(D_2S)_2$ have been observed Both *a* and *b*-dipole transitions are observed The *b*-dipole transitions are relatively stronger suggesting that the dipole moment on '*b*' axis, the H_2S-H_2S axis, is more For both isotopomers two sets of transitions have been observed, which correspond to two tunneling/internal rotor states Both sets of transitions could be fitted into a rigid rotor Hamiltonian. The splitting in (A+B)/2 between the two states is ~12 3 MHz for Ar-$(H_2S)_2$ and ~45 kHz for Ar-$(D_2S)_2$. A similar two states pattern in rotational spectra has been observed for $(H_2S)_2$ also, but the splitting is very different [1] It is unlikely that the dimer states and the trimer states have 1·1 correlation The distortion constants for the

two states of Ar-$(H_2S)_2$ are very different whereas those for the two states of Ar-$(D_2S)_2$ are very close The Ar-$(H_2S)_2$ trimer has a T-shaped heavy atom geometry The Ar-H_2S distance is 4 09 Å, and the c m separation between the two H_2S units is 4 05 Å, which is 0 07 Å shorter than that in $(H_2S)_2$ dimer This is attributed to the third body effect *Ab initio* calculations at several levels of theory predict three minima, including a pseudo linear one, for the trimer The other two minima have T-shaped heavy atom geometry and are very close in energy Both of them could be correlated to the rotational spectra observed

Ab initio calculations were performed for H_2O-H_2S dimer and Ar-H_2O-H_2S trimer H_2O-H_2S can have two structures H_2S-HOH and H_2O-HSH Most recent theoretical results predict H_2S-HOH (H_2S acceptor and H_2O donor) to be the global minima [2] It was assumed that the zero point correction of the energy would not alter the relative stability of the minima. Calculations at MP2 level using 6-311++G(3df,2p) and aug-cc-pVTZ basis sets show that H_2O-HSH becomes slightly more stable than H_2S-HOH, on zero point energy correction However, the energy difference between the two structures is quite small Total five minima could be optimized for Ar-H_2O-H_2S trimer Three of them having Ar attached to H_2S-HOH and the other two have Ar bound to H_2O-HSH Without zero point correction, one minima of Ar-H_2S-HOH is most stable However, correcting for the zero point energy, predicts Ar-H_2O-HSH to be more stable It shows similar results as H_2O-H_2S dimer The zero point correction is very important for such weakly bound complexes Some rotational transitions have been observed which are likely to be for Ar-H_2O-H_2S

Hydrogen bond radii have been defined and determined for several hydrogen bond donors HX (HF, HCl, HBr, HCN, HCCH and H_2O) The experimental data available for different series of complexes (B-HX) were compiled and analyzed to determine an effective size of hydrogen in these complexes This radius is characteristic of the hydrogen bond donor Sum of the hydrogen bond radius of a donor and the r(E) of an acceptor results into the hydrogen bond distance (B H distance) for a H-bonded complex B-HX. The r(E) is the distance between center or atom in B which is bonded to H and the minimum in molecular electrostatic potential of B. As the experimental data

on H_2S complexes are scarce, hydrogen bond radius for H_2S has been determined from the *ab initio* structural parameters The hydrogen bond radius shows a inverse correlation with both the dipole moment and the electronegativity difference of HX

VII.2. Future Directions

The future directions of this research could be many-fold Firstly, a stark cage can be incorporated to the spectrometer so that the stark effect could be observed Measuring stark effect would give the dipole moment of the system directly From the exact dipole moment data, important structural features could be obtained

For Ar_2-H_2S and Ar-$(H_2S)_2$ complexes rotational spectra of the isotopomers with ^{34}S isotope should be pursued The experimental data on ^{34}S species would again produce valuable structural information of the complexes Extensive theoretical studies are necessary to explain the difference in distortion constants between Ar_2-H_2S and Ar_2-D_2S, and between the two states of Ar-$(H_2S)_2$. Preliminary data for Ar-H_2O-H_2S complex are obtained in this work The predictions for the rotational transitions could be refined on the basis of those data By solving the complete rotational spectra, valuable structural and dynamical information could be obtained for the trimer The splitting of each transition into 3/4 lines is enough indications for a complicated dynamic nature of the complex. As mentioned, the experimental data on H_2S complexes are rare Already, a systematic study on several H_2S complexes has been started in our laboratory[3] Generating sufficient experimental data would lead to successful determination of hydrogen bond radius of H_2S from the experimental distances

References

1. F J. Lovas, *private communication*
2. Y. B. Wang, F M Tao and Y K. Pan, *Chem Phys Lett* **230**, 480 (1994)
3. M. Goswami, P K. Mandal, D J. Ramdass and E Arunan, *Chem Phys Lett* **393**, 22 (2004).